# Cerebellar supervision of action

Small brother is watching you

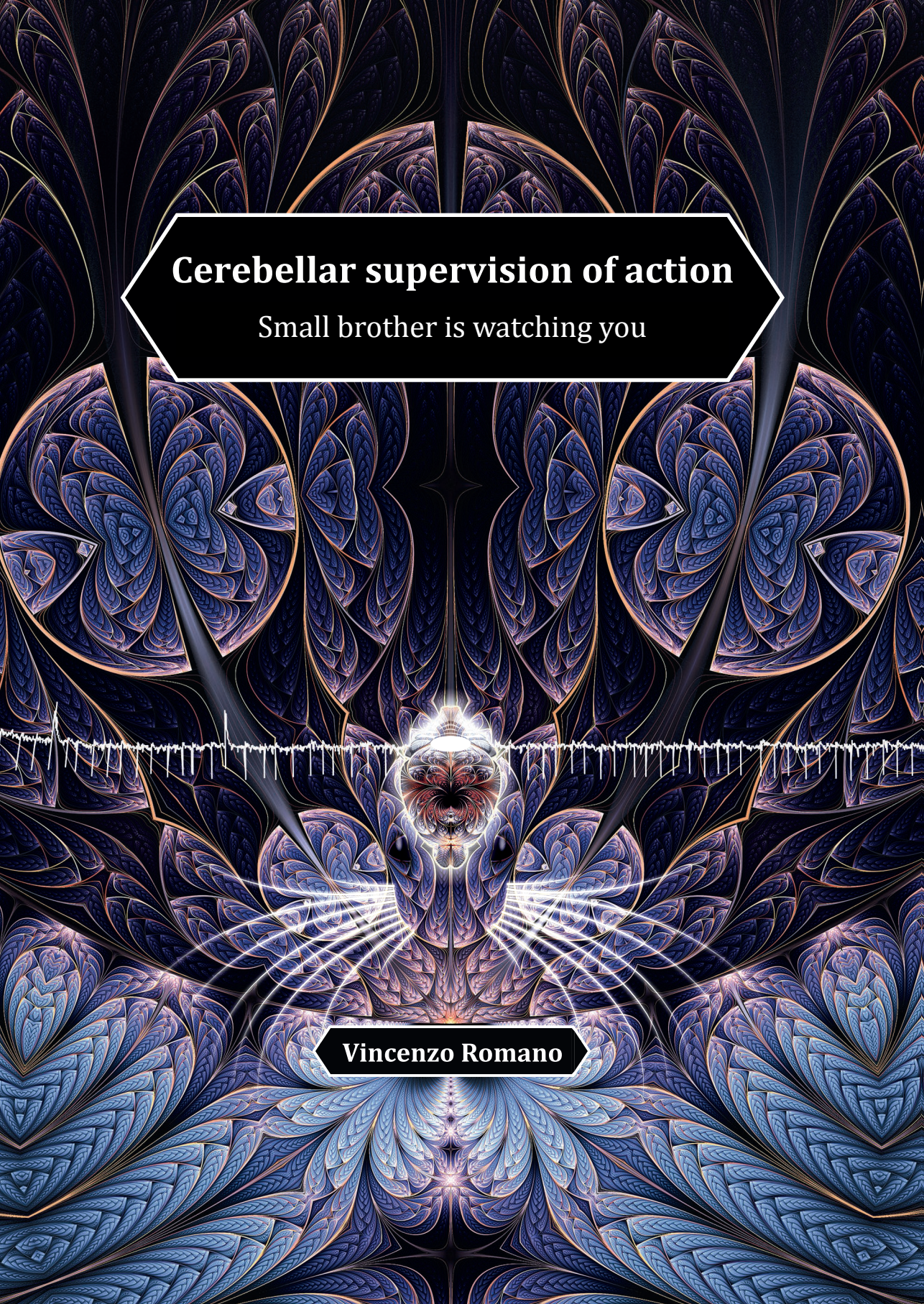

Vincenzo Romano

# Cerebellar supervision of action
# Small brother is watching you

Vincenzo Romano

ISBN: 978-94-6361-423-8
Layout and printing: Optima Grafische Communicatie, Rotterdam, The Netherlands

# Cerebellar Supervision of Action

## Small brother is watching you

Cerebellair toezicht op actie

Kleine broer houdt je in de gaten

**Proefschrift**

ter verkrijging van de graad van doctor aan de
Erasmus Universiteit Rotterdam
op gezag van de rector magnificus
Prof.dr. R.C.M.E. Engels
en volgens het besluit van het College voor Promoties.
De openbare verdediging zal plaatsvinden op

woensdag 3 juni 2020 om 11.30 uur

**Vincenzo Romano**
geboren te Cariati, Italië

**Erasmus University Rotterdam**

**promotor**

Prof. dr. C.I. de Zeeuw

**Other members:**

- Dr. M. Schonewille
- Prof. dr. M.A. Frens
- Prof. dr. T. Celikel

**copromotor**

Dr. L.W.J. Bosman

## ABSTRACT

Synaptic plasticity has been historically considered the primary neural correlate of learning and memory.

Initially, depression at the parallel fiber to Purkinje cell synapse was considered the sole cellular mechanism underlying cerebellar motor learning. In line with other findings of the past decade, this thesis shows the importance of other forms of cerebellar plasticity, in particular that of Purkinje cell potentiation. More specifically, we show the relevance of this form of postsynaptic plasticity during adjustments of whisker protraction, licking and respiration. Based upon these findings, I suggest that intrinsic excitability and potentiation of the parallel fiber to Purkinje cell synapse result in increased simple spike activity, which in turn leads to faster sensorimotor integration. These results imply that deficits in such neuronal mechanisms can contribute to impairments in the acquisition and execution of faster reflexes in cerebellar patients.

To my family
Assunta, Bina, mamma e papà

## TABLE OF CONTENTS


| | | |
|---|---|---|
| 1. | Introduction | 11 |
| 2. | Cerebellar potentiation and learning a whisker-based object localization task with a time response window | 29 |
| 3. | Potentiation of cerebellar Purkinje cells facilitates whisker reflex adaptation through increased simple spike activity | 59 |
| 4. | Quasiperiodic rhythms of the inferior olive | 113 |
| 5. | Functional convergence of autonomic and sensorimotor processing in the lateral cerebellum | 161 |
| 6. | Cerebellar Purkinje cells can differentially modulate coherence between sensory and motor cortex depending on region and behavior | 201 |
| 7. | General discussion | 237 |
| Appendices | | 249 |

# 1

# Introduction

## CEREBELLAR SURVEILLANCE AND CORRECTION OF ACTIONS

Life is a continuum of receiving environmental information and formulation of responses for survival, satisfaction, and, in the best-case scenario, also happiness. The central nervous system is specialized in processing information conveyed by the sensory organs and elaborates reactions effectuated by the muscles and the endocrine system.

The process of reacting to environmental stimuli can be very simple, like the knee-jerk reflex in which the touch of the knee causes the movement of the leg. In everyday life, however, reacting to environmental stimuli can be incredibly complex. When a person is playing soccer or when a prey runs away from a predator, the sensory information, from multiple modalities, flows into the nervous system as a continuum, and it is continually used to adjust the ongoing movements. The complexity of this process is further increased by the possibility of moving some of the sensory organs to optimize the collection of information. The process by which sensory and motor systems communicate and coordinate with each other to couple perception and action is called sensory-motor integration. While simple reflexes, like the knee-jerk reflex, are mediated by the spinal cord (McHenry, 1969), more complex forms of sensory-motor integration involve several brain structures, including the cerebellum (Devi & Reddy, 1972; Doba

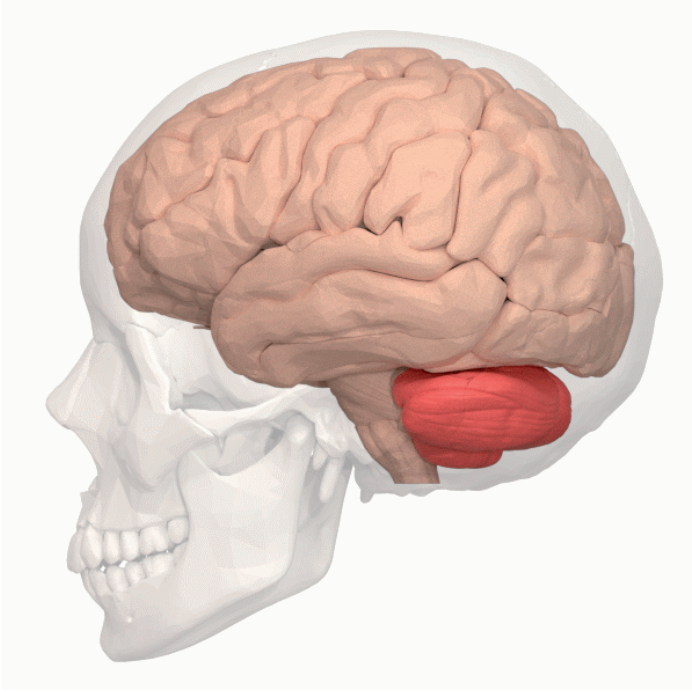

**Figure 1.** The human brain has three main parts: the cerebrum, brainstem, and cerebellum, the latter of which is highlighted in red. Image from Wikimedia Commons, created by DBCLS and distributed under Creative Commons Attribution.

& Reis, 1972; Fujita, 1982; Higgins, 1987; Mnukhina, 1951; Pellegrini & Evinger, 1997; Shinoda & Yoshida, 1974). The cerebellum is an essential part of the central nervous system that integrates the inputs coming from the sensory organs and several parts of the brain, to control the spatial accuracy and the temporal coordination of the muscles during movements (for a review see (Fine, Ionita, & Lohr, 2002). This structure was named cerebellum, which in Latin means "small-brain" because, in almost all vertebrates, its volume is far smaller than the volume of the cerebrum, the "big-brain" (Figure 1), (Sultan & Glickstein, 2007). Despite the cerebellar volume being approximately one-tenth of the volume of the cerebrum, it contains the majority of the neurons of the whole central nervous system (Williams & Herrup, 1988). However, cases of severe deficiencies in the development of the cerebellum suggest that this structure is not required for human survival (Glickstein, 1994). For instance, in a recent and well-described case of complete cerebellar agenesis, "...only mild to moderate motor deficiency, dysarthria and ataxia" were reported (Yu, Jiang, Sun, & Zhang, 2015), (Figure 2). The fact that the person without the cerebellum was only diagnosed when she was 24-year-old, already married, and gave birth to a daughter suggests that the cerebellum is dispensable for many body functions.

Nevertheless, even though there was initially no critical need to have a clinical diagnosis, even in this patient, many suboptimal sensorimotor functions were already present during early life (Yu et al., 2015). Accordingly, the cerebellum has been found to play many roles in a great number of processes that range from sensorimotor to autonomic and cognitive functions (Fine et al., 2002). This seeming contradiction between contributing to many things and being dispensable for many others suggests that the cerebellum is an auxiliary structure that gets involved specifically in optimizing the acquisition and the execution of functions that could still take place, but with less accuracy. This hypothesis could explain why the abovementioned person without cerebellum did start to walk and speak only around the age of 7-years-old. A similar conception has also emerged in a very different context, including experimental settings. For instance, a genetically modified mouse line, in which the activity of the majority of cerebellar

**Figure 2.** Sagittal MRI of a case of cerebellar agenesis. Adapted from (Yu et al., 2015).

neurons was suppressed, showed impairments in learning but not in the execution of classical behavioral tests (Galliano et al., 2013). It is known that compensatory mechanisms are likely to occur in the cases of human cerebellar agenesis, as well as in cerebellar specific mouse models (Jin et al., 2019). However, it was surprising that symptoms associated with spinocerebellar ataxia such as intention tremor, dystonia and ataxia were absent also in many other cerebellar specific knockout mice (Schonewille et al., 2010; Schonewille et al., 2011). In these mouse mutants, the intact cerebellum is essential only for the acquisition of new complex actions like the more challenging adaption of the oculomotor activity (Galliano et al., 2013; Galliano et al., 2018). The cerebellum, however, modulates its activity along with several types of basic movement (Becker & Person, 2019; Cerminara, Apps, & Marple-Horvat, 2009; Chen, Augustine, & Chadderton, 2017; Krauzlis & Lisberger, 1991; Sarnaik & Raman, 2018). For example, experiments on mouse whisker movements have shown that, even though the cerebellar neuronal activity encodes the execution of simple motor behaviors, it does not clearly show the temporal features required to drive the movement (Chen, Augustine, & Chadderton, 2016; Chen et al., 2017). Anatomical studies suggest that the modulation of the cerebellar activity during movements could be driven by proprioceptive reafferent inputs coming from large part of the body (G. Sengul, Y. H. Fu, Y. Yu, & G. Paxinos, 2015). During movement, the cerebellum also receives an efferent copy of inputs that from the motor areas, such as the primary motor cortex, target primary motor neurons (Wolpert, Ghahramani, & Jordan, 1995). According to this scenario, the cerebellum receives information about ongoing movements but does not necessarily always contribute to its execution. Therefore, the fact that the cerebellum continually keeps an eye on the ongoing motor performance could serve to adapt rapidly, compensate, and correct for any unforeseen circumstance or perturbation. To adjust ongoing movements rapidly, it has been proposed that the cerebellum generates an internal representation (i.e., neuronal model) of the sensory-motor consequences of the motor command (Wolpert et al., 1995). Whether the cerebellum generates predictions or bases the adaptation of the ongoing motor program just on the somatosensory feedback, the existing body of literature lets us envision a scenario in which the cerebellum oversees our actions - a bit like the big brother that George Orwell described in 1984. In his marvelous novel, Orwell recounts the omnipresent government surveillance in the imaginary super-state of Oceania. Anytime anything would deviate from the desires of Big Brother, the leader of the single-party of Oceania, the Thought Police would intervene to correct anything related to that deviation. If we imagine our body as the super-state of Oceania, then indeed, we would have the cerebellum as the Big Brother of Orwell's novel, which controls the execution of all our actions. Whenever correction is required, the "observer" goes into action, outputting the specific spike patterns that can be read out by the downstream pre-motor nuclei. Before going into detail about the aim of my research, I will briefly introduce some basic anatomical and physiological background.

# CEREBELLAR ANATOMY, CIRCUITRY, AND FUNCTIONS

## Gross anatomy

In all mammals, the cerebellum can be subdivided into three main lobes. The primary fissure separates the anterior and posterior lobes. The posterolateral fissure, instead, divides the posterior from the flocculonodular lobe. Phylogenetically, the flocculonodular lobe is the most primitive, and it is also named "vestibulocerebellum." Later the medial portion of both the anterior and the posterior lobes developed (which includes the vermis and medial part of the hemispheres), which is named "spinocerebellum." Finally, the lateral hemispheres or "cerebrocerebellum" developed (Kandel, 2013). The three lobes can be further subdivided into ten lobules indicated by the roman numbers (Larsell, 1952) or using an alternative nomenclature that emphasizes the relative independence of the vermis and hemispheres (Bolk, 1906). In Bolk's nomenclature, the hemispheres corresponding to lobules six and seven are named Simplex, Crus 1, and Crus 2 (Figure 3). In rodents, these lobules receive sensory inputs from the whisker system (Bosman et al., 2010; S. T. Brown & Raman, 2018; Kleinfeld, Berg, & O'Connor, 1999; Shambes, Gibson, & Welker, 1978), and their stimulation can elicit whisker movement (Esakov & Pronichev, 2001; Lang, Sugihara, & Llinas, 2006). Since the whisker system is the model that we have selected to study the cerebellar functions, in this thesis, we investigated the neural activity of Simplex, Crus 1, and Crus 2 lobules.

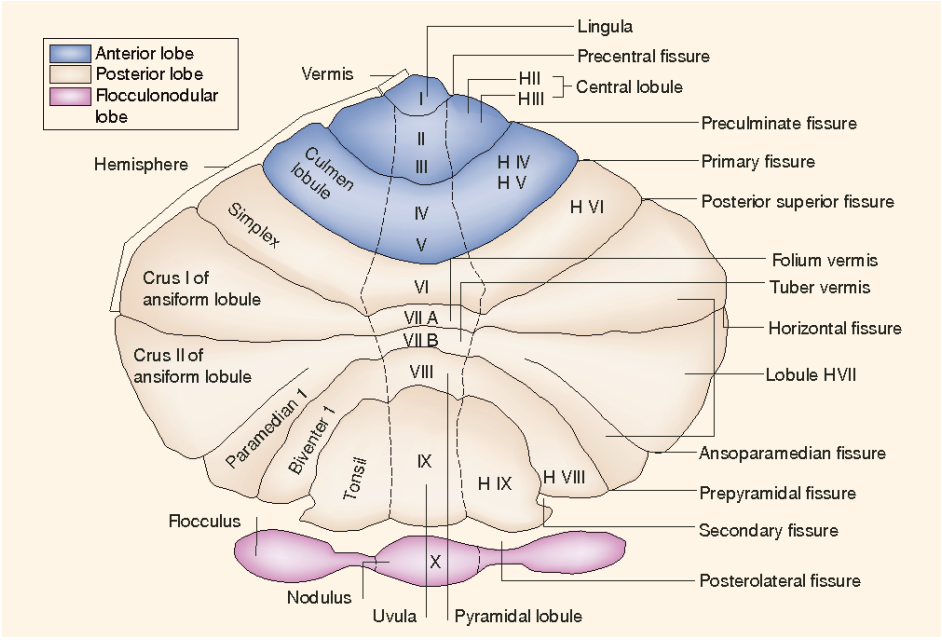


**Figure 3.** Representation of the cerebellar lobules. From (Manni & Petrosini, 2004) with permission.

## Cytoarchitecture of the cerebellar cortex

Despite some minute differences that have been recently discovered (Cerminara, Lang, Sillitoe, & Apps, 2015), the cytoarchitecture of the cerebellar cortex is highly homogeneous (Kandel, 2013). It constitutes of three layers throughout all lobules. The granular cell layer represents the input layer of the cerebellar cortex and the mossy fiber system innervates it. The mossy fiber afferences provide excitatory glutamatergic inputs coming from many areas of the central and peripheral nervous system (Berretta, Perciavalle, & Poppele, 1991; Schafer & Hoebeek, 2018; G. Sengul, Y. Fu, Y. Yu, & G. Paxinos, 2015) to granular and Golgi cells in a particular structure called the glomerulus. The climbing fiber system, instead, targets Purkinje cells forming one of the strongest excitatory synapses of the whole brain (De Zeeuw et al., 2011). These fibers contact the proximal part of the dendrites of the Purkinje cells, which are extended up to the peripheral end of the molecular layer. The molecular layer forms the outmost portion of the cerebellar cortex; this layer contains the parallel fibers, which originate from granular cells and provide direct excitatory glutamatergic input to Purkinje cells and inhibit Purkinje cells via the molecular layer interneurons (stellate and basket cells), (Figure 4). Thus, the Purkinje cells integrate the inputs from the mossy fiber – parallel fiber system with those carried by the climbing fibers (De Zeeuw et al., 2011). These inputs control the spike activity of the Purkinje cells, which consist of relatively rare complex spikes (1-2Hz) and more frequent simple spike (30-150 Hz) (De Zeeuw et al., 2011). While parallel fibers modulate the simple spike firing, the climbing fibers elicit complex spikes whose calcium transients regulate several plasticity mechanisms in a synergistic fashion (Gao, van Beugen, & De Zeeuw, 2012).

## Neuronal activity and information processing by Purkinje cells

Within a Purkinje cell, a very high level of input integration takes place. Their primary input source is represented by the granular cells. These cells are more numerous than all the other neurons of the brain taken together. In humans, for instance, there are an estimated 70 billion granular cells (Williams & Herrup, 1988). Each granular cell has an ascending axon that reaches the molecular layer where it bifurcates to form two parallel fibers running orthogonally for several millimeters and potentially reaching up to hundreds of Purkinje cells dendritic trees (Palkovits, Magyar, & Szentagothai, 1971). Thus, the inputs coming from thousands of mossy fibers are conveyed into granular cells with a high level of divergence, and with billions of parallel fibers, these inputs converge onto the massive Purkinje cell dendritic tree (which is one of the, if not the, largest of all neurons), (Kandel, 2013). Since the Purkinje cells form the sole output station of the cerebellar cortex, the activity of all cerebellar cortical neurons is eventually integrated into the Purkinje cells. Due to these Purkinje cell peculiarities, the axonal spiking of the Purkinje cells represents the final output of all cerebellar cortex computations. Thus, given that Purkinje cells can be considered to be the main computational unit of the cerebellar cortex (An et al., 2019; A. M. Brown et al., 2019), I have taken their electrical activity as the main outcome measure of this thesis.

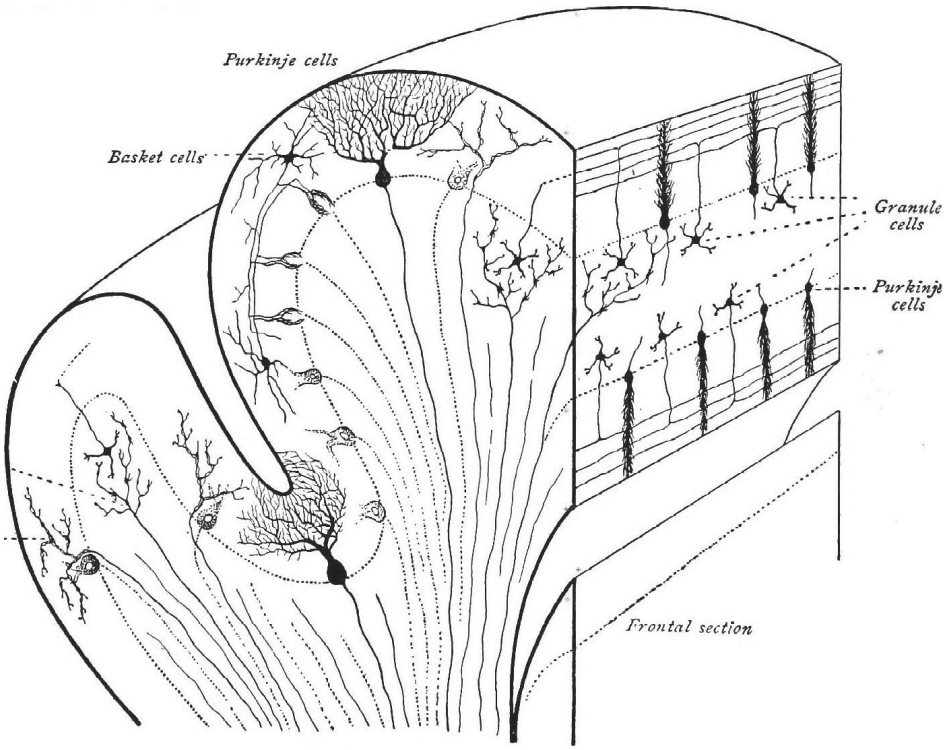


**Figure 4.** Cytoarchitecture of the cerebellar cortex. From (Villiger & Piersol, 1912) via Wikimedia Commons.

## Anatomical pathway of the olivo-cerebellar system

Besides the cerebellar cortical circuit, discussed in the previous paragraph, the activity of Purkinje cells gets integrated within a series of other circuits that involve several areas of the central nervous system. The inputs from the Purkinje cells provide a powerful convergent inhibition onto the vestibular and cerebellar nuclei (Figure 5). The cerebellar nuclei neurons, together with axons of the Purkinje cells that target the vestibular nuclei, constitute the sole output of the entire cerebellum (Kandel, 2013). The cerebellar output then targets downstream pre-motor neurons located in the brainstem (Teune, van der Burg, van der Moer, Voogd, & Ruigrok, 2000), the spinal cord (Berretta et al., 1991) and, several portions of the cerebral cortex via the thalamus (Kelly & Strick, 2003). Some of those brainstem nuclei, in turn, project back to the cerebellum generating a series of feedback loops. The most remarkable loops are represented by the projections from the cerebellar nuclei to the inferior olive that can provide direct mono-synaptic inhibition or indirect di-synaptic excitation via the nuclei of the meso-diencephalic junction (De Zeeuw & Ruigrok, 1994). The olivo-cerebellar loops are organized in parasagittal modules (Ruigrok, 2011). Purkinje cells of a longitudinal zone of the cerebellar cortex, via the corresponding part of cerebellar nuclei, target the portion of the inferior olive from which originate their own climbing fibers (Voogd, 2011). The cerebellar nuclei also project

to the cerebral cortex via the thalamus. In turn, projections from the cerebral cortex go directly or indirectly to the cerebellum via the pontine nuclei and inferior olive, from which mossy fibers and climbing fibers originate, respectively (Schafer & Hoebeek, 2018). The presence of these recurrent connectivities implies that the cerebellum operates in close relationship with other brain areas and that behavior is likely to emerge by their reciprocal influence. Some pieces of evidence in this respect are presented in chapter 6 of this thesis. In particular, we tested the impact of the Purkinje cell stimulation onto the primary somatosensory and motor cortex and on whisker movements. The whisker system has been used as a model to study the cerebellar functions throughout all the experiments presented in this thesis.

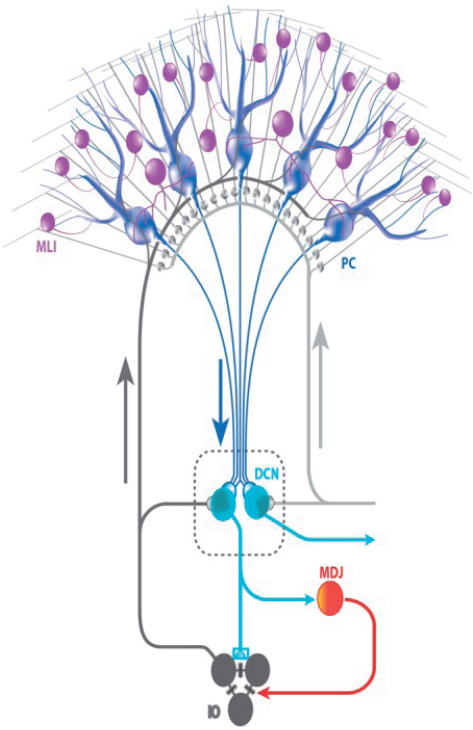


**Figure 5.** Schematic representation of the Olivo-cerebellar loops

## The whisker system as a model to study the cerebellar function

The whisker system has been proposed as an ideal model to study sensory-motor integration (Bosman et al., 2011; Bosman et al., 2010; Kleinfeld, Ahissar, & Diamond, 2006). Among mammals, mice are preferably used in neuroscience, mostly because specific genes can be easily inserted or knocked out from their genome, increasing the possibility of manipulating a certain system dramatically. The main sensory modality by which mice explore their environment is represented by tactile sensory information coming from the facial whiskers (Ahl, 1986;

Prescott, Diamond, & Wing, 2011). Thus the whisker system is highly ethologically relevant for mice, and mice are highly relevant for neuroscience studies. The whisker system combines the movements of the mystacial vibrissae with direct sensory feedback. The cerebellum receives whisker inputs via both the mossy fiber and climbing fiber pathways. From the trigeminal nuclei, whisker inputs go directly to the cerebellar cortex (via the mossy fibers) and indirectly via the inferior olive (Bosman et al., 2011; Kleinfeld et al., 1999), where the climbing fibers originate (Torvik, 1956). Other trigeminal nuclei projections reach the mossy fiber system via the pontine nuclei and a thalamo-cerebro-pontine loop (Kleinfeld et al., 1999). It was proposed that the cerebellar output reach the portion of the facial nucleus responsible for whisker movements via the motor cortex (Lang et al., 2006). Recently, connections from the cerebellar nuclei to the whisker related pre-motor nuclei in the reticular formation have been proposed as a more direct pathway for the cerebellar control of whisker movements (S. T. Brown & Raman, 2018). Thus, whiskers and cerebellum are reciprocally connected via multiple sensory and motor pathways as expected for a system performing sensory-motor integration processes. For this reason, the whisker system can be used as a model to study how cerebellar neurons convert sensory inputs to motor commands. The whisker system can be also be used to study the neural control of its coordination with other motor domains. For instance, in chapter 5, we used the knowledge that the whisker movement can be phase-locked with breathing (Moore et al., 2013) to explore whether the same cerebellar area controls multiple motor domains. Besides, the whisker system is likely to be plastic and undergo adaptation upon specific training. Whether this is indeed the case and whether the cerebellum plays any possible role in whisker adaptation was completely unknown. This motivated us to study the cerebellar contribution to whisker sensory-motor integration and to the adaptation of the whisker system in chapter 3. In fact, if the whisker system undergoes cerebellar-mediated plastic changes, it could be used as a new model for the study of the neural correlates of cerebellar learning.

## Neuronal correlates of cerebellar learning

In general terms, the cellular substrate of learning and memory is the neuronal plasticity. Neuronal plasticity is the capability of neurons to adapt their morphology and/or their functioning based on their antecedent activity. During the last fifty years, a great number of cellular mechanisms underlying neural adaptation have been discovered (for a review see (Gao et al., 2012)). Among these many forms of neuronal plasticity, the modification of the synaptic strength has been historically proposed as the main mechanism underlying learning and memory (Bliss & Collingridge, 1993; Hawkins, Abrams, Carew, & Kandel, 1983; Hebb, 1949; Shaw, 1986). For a few decades, the depression at parallel fiber to Purkinje cell synapses (PF-LTD) has been considered to be the main mechanism underlying cerebellar learning (Gilbert & Thach, 1977; Ito, 1972, 1982; Koekkoek et al., 2003; Medina & Lisberger, 2008; Simpson & Alley, 1974). The original cerebellar learning theory, proposed by David Marr in 1969, foresaw the facilitation of the parallel fiber to Purkinje cell synapses (PF-LTP) rather than their

depression (Marr, 1969). Two years later, this original hypothesis has been changed because James S. Albus, in his legendary article, stated that "the learning process to be stable must be accomplished principally by weakening synaptic weights rather than by strengthening them" (Albus, 1971). This last theory hypothesizes that the cerebellar motor learning is supervised by the activity of the climbing fibers that act as a teaching signal. Within the Purkinje cells, the signal representing the ongoing movement is compared with the signal representing the desired movement, and the teaching signal (i.e., the complex spike activity) adjusts the cerebellar output to correct the movement. James S. Albus's prediction received strong support from the Masao Ito's experimental results about the capability of the climbing fiber activity to induce PF-LTD (Ito, 1982). Consequently, the possible role of parallel fiber to Purkinje cells facilitation in learning processes was relatively diminished while the Marr-Albus-Ito's theory with PF-LTD as main neuronal correlates of learning has constituted one of the main milestones of the cerebellar doctrine. In this thesis, however, I will focus on the importance of the facilitation of Purkinje cells, as originally proposed by David Marr exactly fifty years ago. In this respect, this can be seen as my modest tribute to David Marr for the fiftieth anniversary of his "A theory of cerebellar cortex."

## Multiple forms of plasticity underlying motor learning

Beside the PF-LTD (Konnerth, Dreessen, & Augustine, 1992), long term potentiation at the parallel fiber to Purkinje cell synapses (PF-LTP) was demonstrated to exist (Hansel, Linden, & D'Angelo, 2001), and the directionality of these competing forms of plasticity depends on the climbing fiber activity (Coesmans, Weber, De Zeeuw, & Hansel, 2004; Hirano, 1990; Linden & Ahn, 1999; Shibuki & Okada, 1992). Further studies showed that many other cerebellar neuron types undergo plastic changes of their structure, intrinsic excitability, and synaptic strength (for a review see (Gao et al., 2012)). In this scenario, multiple types of plasticity act together at several levels of the cerebellar circuitry in a synergistic manner to more efficiently adapt the computation and so the behavior. Among all these plasticity mechanisms, PF-LTD has been the most extensively studied in association with learning paradigms such as eye-blink conditioning and saccadic eye movements adaptation (Herzfeld, Kojima, Soetedjo, & Shadmehr, 2018; Koekkoek et al., 2003; Medina & Lisberger, 2008; ten Brinke et al., 2015; Ten Brinke et al., 2017; Voges, Wu, Post, Schonewille, & De Zeeuw, 2017). However, increased simple spike activity was observed during saccadic eye movement adaptation and acquisition of VOR gain-increase (Herzfeld et al., 2018; Medina & Lisberger, 2008; Voges et al., 2017). Thus, during this type of learning, the increased simple spike activity could be caused by cellular mechanisms such as the potentiation of Purkinje cell-intrinsic excitability and parallel fiber to Purkinje cell synapses (*for simplicity I will refer to the combination of these two mechanisms as Purkinje cells potentiation, while considering Purkinje cell depression as the opposite mechanism*). This also emerged with learning deficits reported in Purkinje cell potentiation-deficient mutant mice (Schonewille et al., 2010; Schonewille et al., 2011). Conversely, no cerebellar learning deficit could be detected

in three independent mutant mouse lines with impaired PF-LTD (Schonewille et al., 2011). Thus, the specific plasticity mechanisms that sustain the different types of cerebellar learning are still not well understood. To test whether a learning-induced simple spike's facilitation requires Purkinje cell potentiation, in chapter 3 of this thesis, we developed a new training paradigm for the adaptation of whisker reflexive protraction and applied it to two independent PF-LTP deficient mouse lines.

## Differential prevalence of Purkinje cell potentiation or suppression in cerebellar lobules encoding for different forms of cerebellar dependent learning

The fact that LTP deficient mice showed more severe learning deficits than LTD deficient mice suggested that some types of cerebellar motor learning could require Purkinje cell potentiation more than Purkinje cell depression (De Zeeuw & Ten Brinke, 2015; Galliano et al., 2013; Galliano et al., 2018; Schonewille et al., 2011). It has also been shown that the instructive climbing fiber signal, by which Purkinje cell depression is induced, is not required for one of the most classical cerebellar dependent learning paradigm (Ke, Guo, & Raymond, 2009). The group of Jennifer Raymond induced the vestibular ocular reflex adaptation using a training paradigm in which the "instructive" climbing fiber signal was absent. The induction of learning in absence of climbing fiber signal suggested that "other neural instructive signals make a substantial and independent contribution to motor learning." However, experiments involving other forms of cerebellar dependent learning, such as saccade adaptation and eyeblink conditioning, have shown to be dependent on climbing fiber activity and consequent Purkinje cell simple spike suppression (Attwell, Ivarsson, Millar, & Yeo, 2002; Herzfeld et al., 2018; Koekkoek et al., 2003; Medina & Lisberger, 2008). Importantly, these different types of cerebellar learning depend on different lobules of the cerebellum. Therefore, it has been proposed that in some cerebellar lobules, memory formation is predominantly sustained by suppression mechanism while potentiation mechanisms prevail in other cerebellar zones (De Zeeuw & Ten Brinke, 2015). More specifically, in Purkinje cells located at the floor of the primary cerebellar fissure, which is the area linked to conditioned eyelid behavior, suppression of simple spike activity, and not facilitation, appears to be the most prominent correlate of learning (ten Brinke et al., 2015). Conversely, the main neural correlate of learning in Purkinje cells located in the flocculus, which instead is an area associated with VOR adaptation, appears to be potentiation and simple spike facilitation (Voges et al., 2017). Therefore, we know which plasticity mechanisms are likely to sustain specific types of cerebellar learning only for a few specific parts of the cerebellar cortex. Conversely, we do not know which plasticity mechanisms may prevail in other parts of the cerebellar cortex and what are their ultimately impact on behavioral functions. For instance, even if we know that the adaptation of locomotion is cerebellar dependent and, we know which portion of the cerebellar cortex is more related with this particular type of behaviour (Darmohray, Jacobs, Marques, & Carey, 2019), we still don't know which are the main plasticity mechanisms underlying its

adaptation. Similarly, while we know that, in mice, large parts of Crus 1 and Crus2 lobules are anatomically and functionally related to the whisker system (Bosman et al., 2010; S. T. Brown & Raman, 2018; Chen et al., 2016; Kleinfeld et al., 1999; Lang et al., 2006; Shambes et al., 1978), we do not know which is the cerebellar contribution to whisker movement and which particular forms of plasticity in these areas are responsible for the adaptation of whisker kinematic. In this respect, the research reported in this thesis predominantly aimed to elucidate the relatively unknown contribution of the spike activity of Purkinje cells of Crus 1 and Crus 2 lobules on whisker movement and the plasticity mechanisms underlying its adaptation.

## SCOPE OF THE THESIS

Continuing on the efforts of this laboratory, which provided pioneering evidence on the importance of parallel fiber to Purkinje cell potentiation in cerebellar motor learning, this thesis aspires to elucidate further the role of Purkinje cell potentiation and simple spike facilitation in several behavioral circumstances.

After the brief introduction of **Chapter 1**, we want to address the following questions:

- **Chapter 2:** To what extent does the discrimination between two object positions depend on potentiation at parallel fiber to Purkinje cell synapses? Is Purkinje cells potentiation particularly relevant when a whisker-based discrimination task has to be performed in a shorter time interval?
- **Chapter 3:** Can sensory stimulation induce long term increase of simple spike activity and associated plastic changes in the whisker system? Is Purkinje cells potentiation a required mechanism for such an increase of simple spike and its ultimate impact at the behavioral level?
- **Chapter 4:** To what extent can the rhythmicity of climbing fiber discharges be induced by applying external stimuli to behaving mice or to a realistic tissue-scale computational model?
- **Chapter 5:** Can the Purkinje cells of the same cerebellar area contribute to the synergistic control of breathing and whisking?
- **Chapter 6:** How does the cerebellar output affect the interplay between primary motor and somatosensory cortex during sensory-motor processing?

Finally, in **Chapter 7**, the main results of all the chapters are summarized and discussed, highlighting the significance of these findings and the future direction of our research.

## REFERENCES


Ahl, A. S. (1986). The role of vibrissae in behavior: a status review. *Vet Res Commun, 10*(4), 245-268. doi:10.1007/bf02213989

Albus, J. S. (1971). A theory of cerebellar function. *Mathematical Biosciences, 10*(1), 25-61. doi:https://doi.org/10.1016/0025-5564(71)90051-4

An, L. L., Tang, Y. H., Wang, Q., Pei, Q. Q., Wei, R., Duan, H. Y., & Liu, J. K. (2019). Coding Capacity of Purkinje Cells With Different Schemes of Morphological Reduction. *Frontiers in Computational Neuroscience, 13*. doi:ARTN 29 10.3389/fncom.2019.00029

Attwell, P. J., Ivarsson, M., Millar, L., & Yeo, C. H. (2002). Cerebellar mechanisms in eyeblink conditioning. *Ann N Y Acad Sci, 978*, 79-92. doi:10.1111/j.1749-6632.2002.tb07557.x

Becker, M. I., & Person, A. L. (2019). Cerebellar Control of Reach Kinematics for Endpoint Precision. *Neuron, 103*(2), 335-348 e335. doi:10.1016/j.neuron.2019.05.007

Berretta, S., Perciavalle, V., & Poppele, R. E. (1991). Origin of spinal projections to the anterior and posterior lobes of the rat cerebellum. *J Comp Neurol, 305*(2), 273-281. doi:10.1002/cne.903050208

Bliss, T. V., & Collingridge, G. L. (1993). A synaptic model of memory: long-term potentiation in the hippocampus. *Nature, 361*(6407), 31-39. doi:10.1038/361031a0

Bolk, L. (1906). *Das Cerebellum der Säugetiere. Eine vergleichend anatomische Untersuchung*. Jena: Fischer.

Bosman, L. W., Houweling, A. R., Owens, C. B., Tanke, N., Shevchouk, O. T., Rahmati, N., . . . De Zeeuw, C. I. (2011). Anatomical pathways involved in generating and sensing rhythmic whisker movements. *Front Integr Neurosci, 5*, 53. doi:10.3389/fnint.2011.00053

Bosman, L. W., Koekkoek, S. K., Shapiro, J., Rijken, B. F., Zandstra, F., van der Ende, B., . . . De Zeeuw, C. I. (2010). Encoding of whisker input by cerebellar Purkinje cells. *J Physiol, 588*(Pt 19), 3757-3783. doi:10.1113/jphysiol.2010.195180

Brown, A. M., Arancillo, M., Lin, T., Catt, D. R., Zhou, J., Lackey, E. P., . . . Sillitoe, R. V. (2019). Molecular layer interneurons shape the spike activity of cerebellar Purkinje cells. *Sci Rep, 9*(1), 1742. doi:10.1038/s41598-018-38264-1

Brown, S. T., & Raman, I. M. (2018). Sensorimotor integration and amplification of reflexive whisking by well-timed spiking in the cerebellar corticonuclear circuit. *Neuron, 99*(3), 564-575. doi:10.1016/j.neuron.2018.06.028

Cerminara, N. L., Apps, R., & Marple-Horvat, D. E. (2009). An internal model of a moving visual target in the lateral cerebellum. *J Physiol, 587*(2), 429-442. doi:10.1113/jphysiol.2008.163337

Cerminara, N. L., Lang, E. J., Sillitoe, R. V., & Apps, R. (2015). Redefining the cerebellar cortex as an assembly of non-uniform Purkinje cell microcircuits. *Nat Rev Neurosci, 16*(2), 79-93. doi:10.1038/nrn3886

Chen, S., Augustine, G. J., & Chadderton, P. (2016). The cerebellum linearly encodes whisker position during voluntary movement. *Elife, 5*, e10509. doi:10.7554/eLife.10509

Chen, S., Augustine, G. J., & Chadderton, P. (2017). Serial processing of kinematic signals by cerebellar circuitry during voluntary whisking. *Nat Commun, 8*(1), 232. doi:10.1038/s41467-017-00312-1

Coesmans, M., Weber, J. T., De Zeeuw, C. I., & Hansel, C. (2004). Bidirectional parallel fiber plasticity in the cerebellum under climbing fiber control. *Neuron, 44*(4), 691-700. doi:10.1016/j.neuron.2004.10.031

Darmohray, D. M., Jacobs, J. R., Marques, H. G., & Carey, M. R. (2019). Spatial and Temporal Locomotor Learning in Mouse Cerebellum. *Neuron, 102*(1), 217-231 e214. doi:10.1016/j.neuron.2019.01.038

De Zeeuw, C. I., Hoebeek, F. E., Bosman, L. W., Schonewille, M., Witter, L., & Koekkoek, S. K. (2011). Spatiotemporal firing patterns in the cerebellum. *Nat Rev Neurosci, 12*(6), 327-344. doi:10.1038/nrn3011

De Zeeuw, C. I., & Ruigrok, T. J. H. (1994). Olivary projecting neurons in the nucleus of Darkschewitsch in the cat receive excitatory monosynaptic input from the cerebellar nuclei. *Brain Res, 653*(1-2), 345-350. doi:10.1016/0006-8993(94)90411-1

De Zeeuw, C. I., & Ten Brinke, M. M. (2015). Motor Learning and the Cerebellum. *Cold Spring Harb Perspect Biol, 7*(9), a021683. doi:10.1101/cshperspect.a021683

Devi, K. S., & Reddy, K. S. (1972). Cerebellum and carotid sinus reflex activity. *Indian J Med Res, 60*(7), 1107-1110. Retrieved from https://www.ncbi.nlm.nih.gov/pubmed/4661459

Doba, N., & Reis, D. J. (1972). Cerebellum: role in reflex cardiovascular adjustment to posture. *Brain Res, 39*(2), 495-500. doi:10.1016/0006-8993(72)90451-9

Esakov, S. A., & Pronichev, I. V. (2001). [Movement representation of facial muscles and vibration in the brain of white mice Mus musculus]. *Zh Evol Biokhim Fiziol, 37*(6), 492-495. Retrieved from https://www.ncbi.nlm.nih.gov/pubmed/11898599

Fine, E. J., Ionita, C. C., & Lohr, L. (2002). The history of the development of the cerebellar examination. *Semin Neurol, 22*(4), 375-384. doi:10.1055/s-2002-36759

Fujita, M. (1982). Simulation of adaptive modification of the vestibulo-ocular reflex with an adaptive filter model of the cerebellum. *Biological Cybernetics, 45*(3), 207-214. doi:10.1007/bf00336193

Galliano, E., Gao, Z., Schonewille, M., Todorov, B., Simons, E., Pop, A. S., . . . De Zeeuw, C. I. (2013). Silencing the majority of cerebellar granule cells uncovers their essential role in motor learning and consolidation. *Cell Rep, 3*(4), 1239-1251. doi:10.1016/j.celrep.2013.03.023

Galliano, E., Schonewille, M., Peter, S., Rutteman, M., Houtman, S., Jaarsma, D., . . . De Zeeuw, C. I. (2018). Impact of NMDA Receptor Overexpression on Cerebellar Purkinje Cell Activity and Motor Learning. *eNeuro, 5*(1). doi:10.1523/ENEURO.0270-17.2018

Gao, Z., van Beugen, B. J., & De Zeeuw, C. I. (2012). Distributed synergistic plasticity and cerebellar learning. *Nat Rev Neurosci, 13*(9), 619-635. doi:10.1038/nrn3312

Gilbert, P. F., & Thach, W. T. (1977). Purkinje cell activity during motor learning. *Brain Res, 128*(2), 309-328. doi:10.1016/0006-8993(77)90997-0

Glickstein, M. (1994). Cerebellar agenesis. *Brain, 117 ( Pt 5)*, 1209-1212. doi:10.1093/brain/117.5.1209

Hansel, C., Linden, D. J., & D'Angelo, E. (2001). Beyond parallel fiber LTD: the diversity of synaptic and non-synaptic plasticity in the cerebellum. *Nat Neurosci, 4*(5), 467-475. doi:10.1038/87419

Hawkins, R. D., Abrams, T. W., Carew, T. J., & Kandel, E. R. (1983). A cellular mechanism of classical conditioning in Aplysia: activity-dependent amplification of presynaptic facilitation. *Science, 219*(4583), 400-405. doi:10.1126/science.6294833

Hebb, D. O. (1949). *The Organization of Behavior: A Neuropsychological Theory*: Wiley.

Herzfeld, D. J., Kojima, Y., Soetedjo, R., & Shadmehr, R. (2018). Encoding of error and learning to correct that error by the Purkinje cells of the cerebellum. *Nat Neurosci, 21*(5), 736-743. doi:10.1038/s41593-018-0136-y

Higgins, D. C. (1987). The cerebellum and initiation of movement: the stretch reflex. *Yale J Biol Med, 60*(2), 123-131. Retrieved from https://www.ncbi.nlm.nih.gov/pubmed/3577209

Hirano, T. (1990). Depression and potentiation of the synaptic transmission between a granule cell and a Purkinje cell in rat cerebellar culture. *Neurosci Lett, 119*(2), 141-144. doi:10.1016/0304-3940(90)90818-t

Ito, M. (1972). Neural design of the cerebellar motor control system. *Brain Res, 40*(1), 81-84. doi:10.1016/0006-8993(72)90110-2

Ito, M. (1982). Experimental verification of Marr-Albus' plasticity assumption for the cerebellum. *Acta Biol Acad Sci Hung, 33*(2-3), 189-199. Retrieved from https://www.ncbi.nlm.nih.gov/pubmed/6129762

Jin, C., Kang, H. R., Kang, H., Zhang, Y., Lee, Y., Kim, Y., & Han, K. (2019). Unexpected Compensatory Increase in Shank3 Transcripts in Shank3 Knock-Out Mice Having Partial Deletions of Exons. *Front Mol Neurosci, 12*, 228. doi:10.3389/fnmol.2019.00228

Kandel, E. R. (2013). *Principles of neural science*.

Ke, M. C., Guo, C. C., & Raymond, J. L. (2009). Elimination of climbing fiber instructive signals during motor learning. *Nat Neurosci, 12*(9), 1171-1179. doi:nn.2366 [pii] 10.1038/nn.2366

Kelly, R. M., & Strick, P. L. (2003). Cerebellar loops with motor cortex and prefrontal cortex of a nonhuman primate. *J Neurosci, 23*(23), 8432-8444. Retrieved from https://www.ncbi.nlm.nih.gov/pubmed/12968006

Kleinfeld, D., Ahissar, E., & Diamond, M. E. (2006). Active sensation: insights from the rodent vibrissa sensorimotor system. *Curr Opin Neurobiol, 16*(4), 435-444. doi:10.1016/j.conb.2006.06.009

Kleinfeld, D., Berg, R. W., & O'Connor, S. M. (1999). Anatomical loops and their electrical dynamics in relation to whisking by rat. *Somatosens Mot Res, 16*(2), 69-88. doi:10.1080/08990229970528

Koekkoek, S. K., Hulscher, H. C., Dortland, B. R., Hensbroek, R. A., Elgersma, Y., Ruigrok, T. J., & De Zeeuw, C. I. (2003). Cerebellar LTD and learning-dependent timing of conditioned eyelid responses. *Science, 301*(5640), 1736-1739. doi:10.1126/science.1088383

Konnerth, A., Dreessen, J., & Augustine, G. J. (1992). Brief dendritic calcium signals initiate long-lasting synaptic depression in cerebellar Purkinje cells. *Proc Natl Acad Sci U S A, 89*(15), 7051-7055. doi:10.1073/pnas.89.15.7051

Krauzlis, R. J., & Lisberger, S. G. (1991). Visual motion commands for pursuit eye movements in the cerebellum. *Science, 253*(5019), 568-571. doi:10.1126/science.1907026

Lang, E. J., Sugihara, I., & Llinas, R. (2006). Olivocerebellar modulation of motor cortex ability to generate vibrissal movements in rat. *J Physiol, 571*(Pt 1), 101-120. doi:10.1113/jphysiol.2005.102764

Larsell, O. (1952). The morphogenesis and adult pattern of the lobules and fissures of the cerebellum of the white rat. *J Comp Neurol, 97*(2), 281-356. doi:10.1002/cne.900970204

Linden, D. J., & Ahn, S. (1999). Activation of presynaptic cAMP-dependent protein kinase is required for induction of cerebellar long-term potentiation. *J Neurosci, 19*(23), 10221-10227. Retrieved from https://www.ncbi.nlm.nih.gov/pubmed/10575019

Manni, E., & Petrosini, L. (2004). A century of cerebellar somatotopy: a debated representation. *Nat Rev Neurosci, 5*(3), 241-249. doi:10.1038/nrn1347

Marr, D. (1969). A theory of cerebellar cortex. *J Physiol, 202*(2), 437-470. doi:10.1113/jphysiol.1969.sp008820

McHenry, L. C. (1969). Garrison's History of Neurology. Retrieved from http://public.ebookcentral.proquest.com/choice/publicfullrecord.aspx?p=1589725

Medina, J. F., & Lisberger, S. G. (2008). Links from complex spikes to local plasticity and motor learning in the cerebellum of awake-behaving monkeys. *Nat Neurosci, 11*(10), 1185-1192. doi:10.1038/nn.2197

Mnukhina, R. S. (1951). [Role of the cerebellum in processes of reflex coordination of the spinal cord]. *Fiziol Zh SSSR Im I M Sechenova, 37*(1), 52-58. Retrieved from https://www.ncbi.nlm.nih.gov/pubmed/14831658

Moore, J. D., Deschenes, M., Furuta, T., Huber, D., Smear, M. C., Demers, M., & Kleinfeld, D. (2013). Hierarchy of orofacial rhythms revealed through whisking and breathing. *Nature, 497*(7448), 205-+. doi:10.1038/nature12076

Palkovits, M., Magyar, P., & Szentagothai, J. (1971). Quantitative histological analysis of the cerebellar cortex in the cat. II. Cell numbers and densities in the granular layer. *Brain Res, 32*(1), 15-30. doi:10.1016/0006-8993(71)90152-1

Pellegrini, J. J., & Evinger, C. (1997). Role of cerebellum in adaptive modification of reflex blinks. *Learn Mem, 4*(1), 77-87. doi:10.1101/lm.4.1.77

Prescott, T. J., Diamond, M. E., & Wing, A. M. (2011). Active touch sensing. *Philos Trans R Soc Lond B Biol Sci, 366*(1581), 2989-2995. doi:10.1098/rstb.2011.0167

Ruigrok, T. J. H. (2011). Ins and outs of cerebellar modules. *Cerebellum, 10*(3), 464-474. doi:10.1007/s12311-010-0164-y

Sarnaik, R., & Raman, I. M. (2018). Control of voluntary and optogenetically perturbed locomotion by spike rate and timing of neurons of the mouse cerebellar nuclei. *Elife, 7*. doi:10.7554/eLife.29546

Schafer, C. B., & Hoebeek, F. E. (2018). Convergence of primary sensory cortex and cerebellar nuclei pathways in the whisker system. *Neuroscience, 368*, 229-239. doi:10.1016/j.neuroscience.2017.07.036

Schonewille, M., Belmeguenai, A., Koekkoek, S. K., Houtman, S. H., Boele, H. J., van Beugen, B. J., . . . De Zeeuw, C. I. (2010). Purkinje cell-specific knockout of the protein phosphatase PP2B impairs potentiation and cerebellar motor learning. *Neuron, 67*(4), 618-628. doi:10.1016/j.neuron.2010.07.009

Schonewille, M., Gao, Z., Boele, H. J., Veloz, M. F., Amerika, W. E., Simek, A. A., . . . De Zeeuw, C. I. (2011). Reevaluating the role of LTD in cerebellar motor learning. *Neuron, 70*(1), 43-50. doi:10.1016/j.neuron.2011.02.044

Sengul, G., Fu, Y., Yu, Y., & Paxinos, G. (2015). Spinal cord projections to the cerebellum in the mouse. *Brain Struct Funct, 220*(5), 2997-3009. doi:10.1007/s00429-014-0840-7

Sengul, G., Fu, Y. H., Yu, Y., & Paxinos, G. (2015). Spinal cord projections to the cerebellum in the mouse. *Brain Structure & Function, 220*(5), 2997-3009. doi:10.1007/s00429-014-0840-7

Shambes, G. M., Gibson, J. M., & Welker, W. (1978). Fractured somatotopy in granule cell tactile areas of rat cerebellar hemispheres revealed by micromapping. *Brain Behav Evol, 15*(2), 94-140. Retrieved from http://www.ncbi.nlm.nih.gov/entrez/query.fcgi?cmd=Retrieve&db=PubMed&dopt=Citation&list_uids=638731

Shaw, G. L. (1986). *Donald Hebb: The Organization of Behavior*, Berlin, Heidelberg.

Shibuki, K., & Okada, D. (1992). Cerebellar long-term potentiation under suppressed postsynaptic Ca2+ activity. *Neuroreport, 3*(3), 231-234. doi:10.1097/00001756-199203000-00003

Shinoda, Y., & Yoshida, K. (1974). [Proceedings: Effect of cerebellum and brain stem on the vestibular oculomotor reflex system in cats]. *Nihon Seirigaku Zasshi, 36*(8-9), 272. Retrieved from https://www.ncbi.nlm.nih.gov/pubmed/4377425

Simpson, J. I., & Alley, K. E. (1974). Visual climbing fiber input to rabbit vestibulo-cerebellum: a source of direction-specific information. *Brain Res, 82*(2), 302-308. doi:10.1016/0006-8993(74)90610-6

Sultan, F., & Glickstein, M. (2007). The cerebellum: Comparative and animal studies. *Cerebellum, 6*(3), 168-176. doi:10.1080/14734220701332486

ten Brinke, M. M., Boele, H. J., Spanke, J. K., Potters, J. W., Kornysheva, K., Wulff, P., . . . De Zeeuw, C. I. (2015). Evolving Models of Pavlovian Conditioning: Cerebellar Cortical Dynamics in Awake Behaving Mice. *Cell Rep, 13*(9), 1977-1988. doi:10.1016/j.celrep.2015.10.057

Ten Brinke, M. M., Heiney, S. A., Wang, X., Proietti-Onori, M., Boele, H. J., Bakermans, J., . . . De Zeeuw, C. I. (2017). Dynamic modulation of activity in cerebellar nuclei neurons during pavlovian eyeblink conditioning in mice. *Elife, 6*. doi:10.7554/eLife.28132

Teune, T. M., van der Burg, J., van der Moer, J., Voogd, J., & Ruigrok, T. J. (2000). Topography of cerebellar nuclear projections to the brain stem in the rat. *Prog Brain Res, 124*, 141-172. doi:10.1016/S0079-6123(00)24014-4

Torvik, A. (1956). Transneuronal changes in the inferior olive and pontine nuclei in kittens. *J Neuropathol Exp Neurol, 15*(2), 119-145. doi:10.1097/00005072-195604000-00001

Villiger, E., & Piersol, G. A. (1912). *Brain and Spinal Cord: A Manual for the Study of the Morphology and Fibre-tracts of the Central Nervous System*: J. B. Lippincott Company.

Voges, K., Wu, B., Post, L., Schonewille, M., & De Zeeuw, C. I. (2017). Mechanisms underlying vestibulo-cerebellar motor learning in mice depend on movement direction. *J Physiol, 595*(15), 5301-5326. doi:10.1113/JP274346

Voogd, J. (2011). Cerebellar zones: a personal history. *Cerebellum, 10*(3), 334-350. doi:10.1007/s12311-010-0221-6

Williams, R. W., & Herrup, K. (1988). The control of neuron number. *Annu Rev Neurosci, 11*, 423-453. doi:10.1146/annurev.ne.11.030188.002231

Wolpert, D. M., Ghahramani, Z., & Jordan, M. I. (1995). An internal model for sensorimotor integration. *Science, 269*(5232), 1880-1882. doi:10.1126/science.7569931

Yu, F., Jiang, Q. J., Sun, X. Y., & Zhang, R. W. (2015). A new case of complete primary cerebellar agenesis: clinical and imaging findings in a living patient. *Brain, 138*(Pt 6), e353. doi:10.1093/brain/awu239

# 2

# Cerebellar Potentiation and Learning a Whisker-Based Object Localization Task with a Time Response Window

Negah Rahmati[1*], Cullen B. Owens[1*], Laurens W.J. Bosman[1*], Jochen K. Spanke[1,2*], Sander Lindeman[1], Wei Gong[1], Jan-Willem Potters[1], Vincenzo Romano[1], Kai Voges[1], Letizia Moscato[1], Sebastiaan K.E. Koekkoek[1], Mario Negrello[1], and Chris I. De Zeeuw[1,2]

[*] These authors contributed equally to this work.

[1] Department of Neuroscience, Erasmus MC, 3000 CA Rotterdam, The Netherlands

[2] Netherlands Institute for Neuroscience, Royal Academy of Arts & Sciences, 1105 BA Amsterdam, The Netherlands

Corresponding author: c.dezeeuw@erasmusmc.nl

## ABSTRACT

Whisker-based object localization requires activation and plasticity of somatosensory and motor cortex. These parts of the cerebral cortex receive strong projections from the cerebellum via the thalamus, but it is unclear whether and to what extent cerebellar processing may contribute to such sensorimotor task. Here, we subjected knockout mice, which suffer from impaired intrinsic plasticity in their Purkinje cells and long-term potentiation (LTP) at their parallel fiber-to-Purkinje cell synapses (L7-PP2B), to an object localization task with a time-response window. Water deprived animals had to learn to localize an object with their whiskers, and based upon this location they were trained to lick within a particular period ("go" trial) or refrain from licking ("no-go" trial). L7-PP2B mice were not ataxic and showed proper basic motor performance during whisking and licking, but learning this task was severely impaired compared to wild-type littermates. Significantly less L7-PP2B mice were able to learn the task at long response windows. Those L7-PP2B mice that eventually learned the task made unstable progress, were significantly slower in learning, and showed deficiencies in temporal tuning. These differences became greater as the response window became narrower. Trained wild-type, but not L7-PP2B mice, showed a net increase in simple spikes and complex spikes of their Purkinje cells during the task. We conclude that cerebellar processing and potentiation in particular can contribute to learning a whisker-based object localization task when timing is relevant. This study points towards a relevant role of cerebello-cerebral interaction in a sophisticated cognitive task requiring strict temporal processing.

## INTRODUCTION

Active touch by mystacial vibrissae forms a major source of sensory information for rodents (Carvell and Simons, 1990; Hartmann, 2009). Head-fixed mice can be trained to exploit such active exploration to associate the position of a stimulation bar in their whisker field with the availability of a water reward (O'Connor et al., 2010ab). Whisker-based object localization has been shown to involve correlated neuronal activity in the barrel cortex (S1) and the whisker motor cortex (M1) (Xu et al., 2012). However, it is unclear whether other brain regions also contribute to such tasks. Given the numerous brain regions involved in whisker control and given their intricate connections (Bosman et al., 2011; Kleinfeld and Deschênes, 2011), one may expect other areas to also play a role in whisker-based object localization. Here we focus on the cerebellum, a region important for sensorimotor integration, central to the whisker system, and required for procedural learning and accurate timing of fine movements (Grodd et al., 2001; Bosman et al., 2010; De Zeeuw et al., 2011).

Purkinje cells form the sole output neurons of the cerebellar cortex. Their activity depends on both synaptic and intrinsic plasticity (Hansel et al., 2001; Ito, 2001; Gao et al., 2012). In the absence of calmodulin-activated protein phosphatase 2B (PP2B) both enhancement of intrinsic excitability of Purkinje cells and long-term potentiation (LTP) at the parallel fiber-to-Purkinje cell synapses are impaired, resulting in increased simple spike firing regularity (Schonewille et al., 2010). Purkinje cell-specific PP2B knock-out (L7-PP2B) mice show deficits in motor learning and consolidation, as demonstrated during adaptation of the vestibulo-ocular reflex and eyeblink conditioning (Schonewille et al., 2010). To date, of all currently available cell-specific cerebellar mouse mutants that are not ataxic the L7-PP2B mutant shows the most prominent deficits in procedural learning (De Zeeuw et al., 2011; Gao et al., 2012). Yet, when subjected to standard non-motor tasks like the Morris water maze, fear conditioning or social interaction task in which no fine temporal control is required, the L7-PP2B mutants do not show abnormal performance (Galliano et al., 2013).

The primary objective of this study was to investigate whether, and if so to what extent, potentiation of intrinsic activity and synaptic strength of Purkinje cells in the cerebellum is required for a localization task in which the response has to be given within an allotted response period following the insertion of a bar into the whisker field. To this end we tested L7-PP2B mice using a modified version of the object localization task introduced by O'Connor et al. (2010b) while subsequently tightening temporal constraints of the response. We demonstrate that L7-PP2B mutants are severely impaired in learning this whisker-based object localization task. The cerebellar contribution to this learning task was further corroborated by electrophysiological recordings showing a net upregulation of Purkinje cell activity during trials in wild type, but not in L7-PP2B mice. Thus we show for the first time that this learning task can depend in part on plasticity and/or processing in the cerebellum when response timing is relevant.

## MATERIALS AND METHODS

The generation of mice lacking functional PP2B in their Purkinje cells has been described previously (Schonewille et al., 2010). Briefly, we used crossings of mice in which the gene for the regulatory subunit (CNB1) of PP2B was flanked by loxP sites (Zeng et al., 2001) with transgenic mice expressing Cre under control of the L7 promoter (Barski et al., 2000). L7-Cre$^{+/-}$-*cnb1*$^{f/f}$ mice ("L7-PP2B mice") were compared with littermate controls ("WT mice") consisting of L7-Cre$^{-/-}$-*cnb1*$^{f/f}$ and L7-Cre$^{-/-}$-*cnb1*$^{+/+}$ mice. All experimental procedures were approved by the institutional animal welfare committee as required by Dutch law.

### Licking behavior

Since licking behavior was used as the behavioral read out of the localization task (see below), we first assessed the overall performance during baseline licking in 10 female L7- PP2B mice

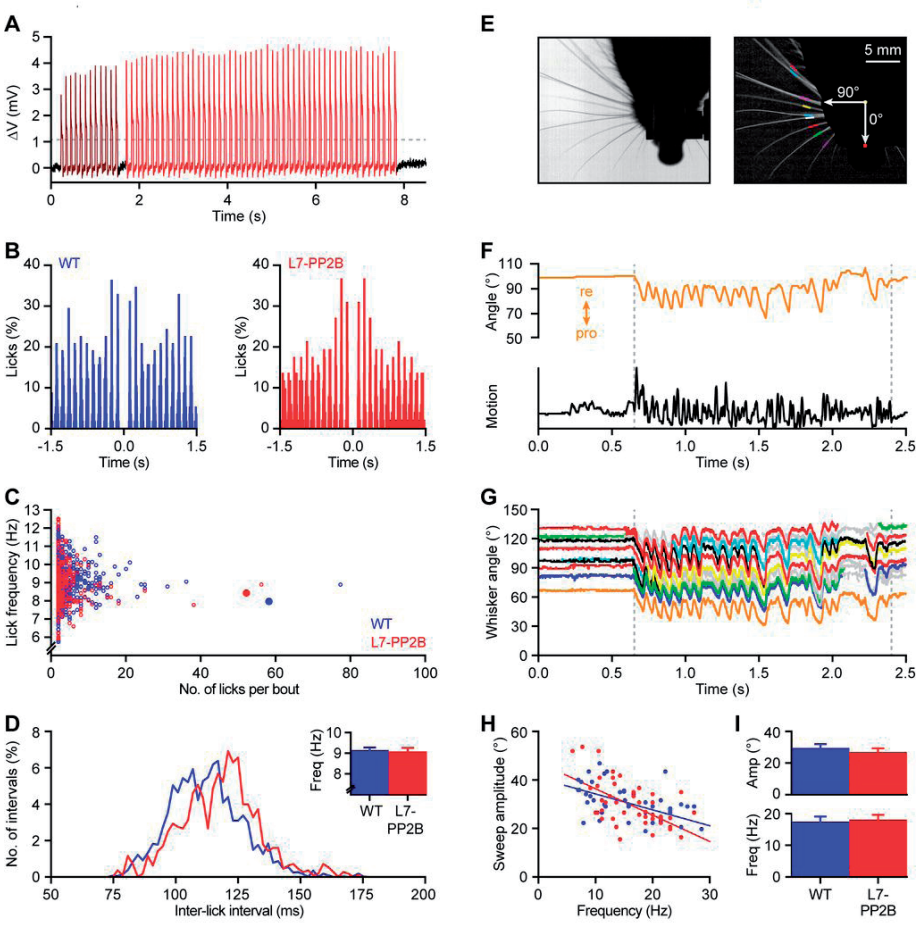

and 9 female WT littermates of 20-25 weeks old. Baseline licking was measured in the home-cages of naïve mice by measuring threshold crossings in the junction potential between an aluminum floor plate and the spout of a normal drinking bottle with the use of an AD converter operating at a sample rate of 6 kHz (RZ2, Tucker-Davis Technologies, Alachua, FL) (Fig. 1*A*). Our experimental design was based on that of Hayar et al. (2006). Since mice normally lick very sparsely, they were deprived of water for 20 h prior to the period of experimental testing, which lasted approximately 1 h. We restricted our analysis of baseline performance to bouts of rhythmic licking, which were defined by the occurrence of at least two licks with a maximal inter-lick interval of 175 ms (Fig. 1*A*). Licking during the training paradigm was detected by laser beam crossings at the lick-port. In order to avoid double detections, we used a dead time of 20 ms.

Auto-correlograms with a bin width of 5 ms were made of the lick times in the home cage as well as during the association task and the object localization task (see below). Side peaks were normalized to the center peak and detected as local maxima. The amplitude of these first side peaks was considered to be the strength of the rhythmicity. Rhythmic licking predominantly occurred at frequencies between 6 and 12 Hz. Further quantitative analysis was done in this frequency band. Licking was considered to be rhythmic if the first side peak exceeded the average + 3 SD of the period between 1000 and 800 ms before each lick.

## Whisking behavior

Since whisking behavior was used as the critical sensory detection mechanism for the localization task (see below), we also assessed the overall performance during free whisking in 11

**Figure 1.** L7-PP2B mice do not have motor deficits preventing normal, rhythmic licking and whisking
**A** – A period of rhythmic licking in a freely moving L7-PP2B mouse. Licks can be seen as positive deflections of the junction potential between the spout of the drinking bottle and an aluminum floor plate in the home cage. This licking period consists of 2 individual licking bouts as indicated with two colors. Dashed line indicates the threshold used for automated lick detection. **B** – Auto-correlograms of licking bouts in a WT (*left*) and a L7-PP2B mouse (*right*). The right panel is the auto-correlogram of the second licking bout (depicted in red) in panel **A**. The center bin was removed to improve visibility. **C** – Both WT and L7-PP2B mice displayed short and long licking bouts with lick frequencies predominantly between 6 and 12 Hz. Shorter licking bouts tended to vary more in lick frequency than long bouts in both genotypes. The auto-correlograms shown in **B** are taken from the bouts that are indicated with larger, filled symbols. **D** – Histograms of all inter-lick intervals within licking bouts showed similar distributions in WT and L7-PP2B mice, indicating that L7-PP2B had no motor deficits preventing them to lick rhythmically. The histograms were made with a bin size of 2 ms and the area under the plot was normalized to 100%. *Inset:* Average licking frequency ± SEM per mouse ($n$ = 9 WT and 10 L7-PP2B mice; $p$ – 0.773). **E** – Whisker movements were quantified from high-speed video recordings. In each frame, the proximal parts of the whiskers were tracked with small line segments (colored lines in the right plot). Whisker angles were measured relative to the body axis. **F** – Whisker motion during a whisking bout was tracked manually (*top*) and characterized using the motion detection algorithm (*bottom*; see Methods). It can be seen that the motion detection reliably captured the duration of the whisker movements. **G** – The same fragment was subsequently analyzed using automated line detection and subsequent post-processing to detect movements of individual whiskers (see Methods); tracks with > 500 data points are shown with randomly assigned colors, while shorter tracks are shown in grey. The orange trace refers to the same whisker that had been tracked manually (top trace in **F**). **H** – There is a clear negative correlation between the frequency and amplitude of a whisker bout: the higher the frequency the smaller the movements. Linear regression lines of WT ($n$ = 47 bouts from 10 mice) and L7-PP2B ($n$ = 46 bouts from 11 mice) data were not significantly different from each other ($z$ = 1.579; $p$ = 0.114). **I** – Neither the amplitude nor the frequency of whisker bouts was significantly different between WT and L7-PP2B mice ($p$ = 0.378 and $p$ = 0.784, respectively).

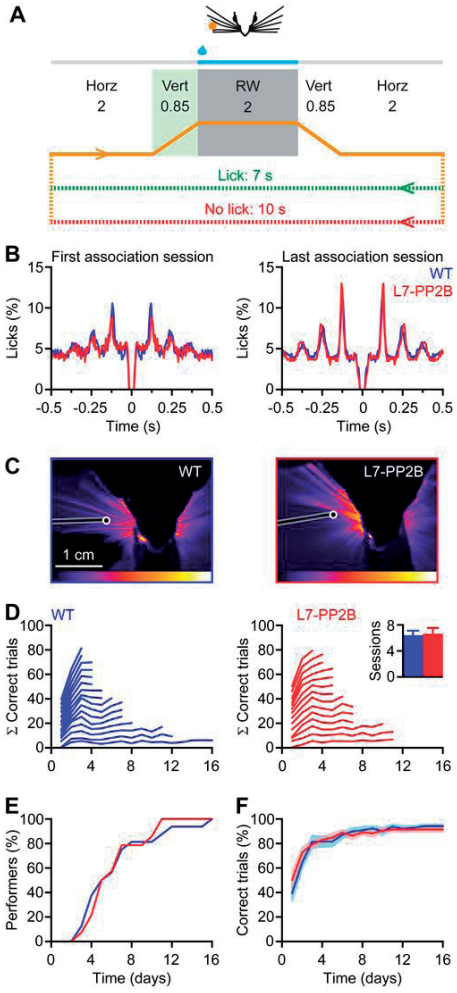


**Figure 2.** Mice learn to lick after feeling a stimulus bar in their whisker field

**A** – Learning paradigm. During the association task mice were only subjected to go trials and learned to lick following whisker contact with a metal bar (orange dot) within a 2000 ms response window (RW). Once the stimulation bar completed the horizontal movement from the (neutral) resting position to the go position, it moved vertically into the whisker field. Whisker contact with the stimulation bar became possible roughly around half way the time interval allotted for the vertical movement. To indicate this we marked the time period of the vertical movement with a green shading. The RW started after the completion of the vertical movement and is indicated with a grey shading. Correct responses triggered a water reward; incorrect responses postponed the next trial. **B** – Mice licked rhythmically during the RW of the association phase. Over the sessions the mice increased their licking rhythmicity as demonstrated by the increase of the amplitudes of the side peaks around 125 ms (corresponding to a dominant lick frequency of 8 Hz; cf. naïve mice (during the first association session) in *left panel* and trained mice (during the last association session) in *right panel*). The auto-correlograms were made with a bin size of 5 ms and were normalized to the center peak (which is not shown to improve clarity). **C** - Standard deviation projection plot showing a representative example of whisker movement during the RW. The color bar at the bottom indicates the amount of movement (black = no change; white = maximal change). It can be seen that both mice moved their whiskers actively during the RW and touched the stimulus bar. **D** – Summed learning curves during the association phase (see Methods section). The inset shows the average number of sessions required to reach criterion. Error bars indicate SD. **E** – Cumulative histogram of the percentage of mice that reached criterion showing that WT and L7-PP2B mice learned the association task at a similar rate. **F** – The fraction of correct trials over the sessions. *Dark lines* show the averages and the shaded areas cover the average ± SEM.

adult female L7-PP2B and 10 adult female WT littermates (Fig. 1*E-I*). We decided to keep all whiskers intact. Spontaneous whisker movements in head-restrained mice were recorded with high-speed videos (full frame rate 1000 Hz; A504k camera, Basler Vision Technologies, Ahrensburg, Germany) using a red LED panel (λ = 640 nm) as backlight. In addition, videos were made during selected sessions of the training paradigm (see below; Figs. 2-4). The latter videos were recorded with a full frame rate of 160 Hz (piA640-210gm camera, Basler Vision Technologies) and infrared lighting to avoid luminance of the training environment (λ > 900 nm).

In order to establish the periods during which the mice actively moved their whiskers we estimated whisker motion using the BlockMatcher function in Matlab (Mathworks, Natick, MA). First, we selected a rectangular region of interest containing the proximal part of the whiskers. This region was sliced into a grid with rectangular blocks. Across contiguous frames, each block was transformed by a rotation and translation, such that the distance between the blocks in consecutive frames was minimized. The whisker motion was calculated as the Pythagorean addition of the translation and the rotation of all blocks (Fig. 1*F*). To validate the automated algorithms for both whisker motion periods and for whisker angle and position tracking, we also tracked individual whiskers manually in 25 video fragments. This was done by marking in each frame the position of the follicle and the intersection of the whisker with a line parallel to the body axis at approximately 2.5 cm lateral to the whisker pad. It turned out that the motion detection could reliably detect periods during which whisker movements occurred. The extent of whisker movements was further illustrated using standard deviation (SD) projection plots of video fragments (ImageJ, NIH). During the training paradigms, each video fragment reflected the activity during a single response window (RW; see below). Here we used pseudo-colored SD projection plots to illustrate the whisker movements over time.

The outcome of the motion estimation algorithm was used to truncate the video files in time in order to process only those periods of the video files that show whisker motion (see below). To this end the variability in the motion estimation result was evaluated with a sliding window approach that calculated the local standard deviation of the signal. In a second step this local standard deviation signal was thresholded to identify periods of motion. During the periods in which the whisker moved we tracked them automatically using the Biotact Whisker Tracking Tool with the sdGeneric, stShapeSpaceKalman, ppBigExtractionAndFiltering and wdIgorMeanAngle plugins (http://bwtt.sourceforge.net; for details see Perkon et al., 2011). Briefly, we first determined in each frame the position of the snout semi-automatically by fitting a template to the snout. After masking the snout and subtracting the unmoved background from each frame, the whiskers themselves were traced in a radial approach. The algorithm detected edges in the frame in consecutive concentric snout-shaped masks around the actual snout mask. Ultimately, we detected the start and end nodes of the fitted line segments and calculated the angles of the whiskers from these values.

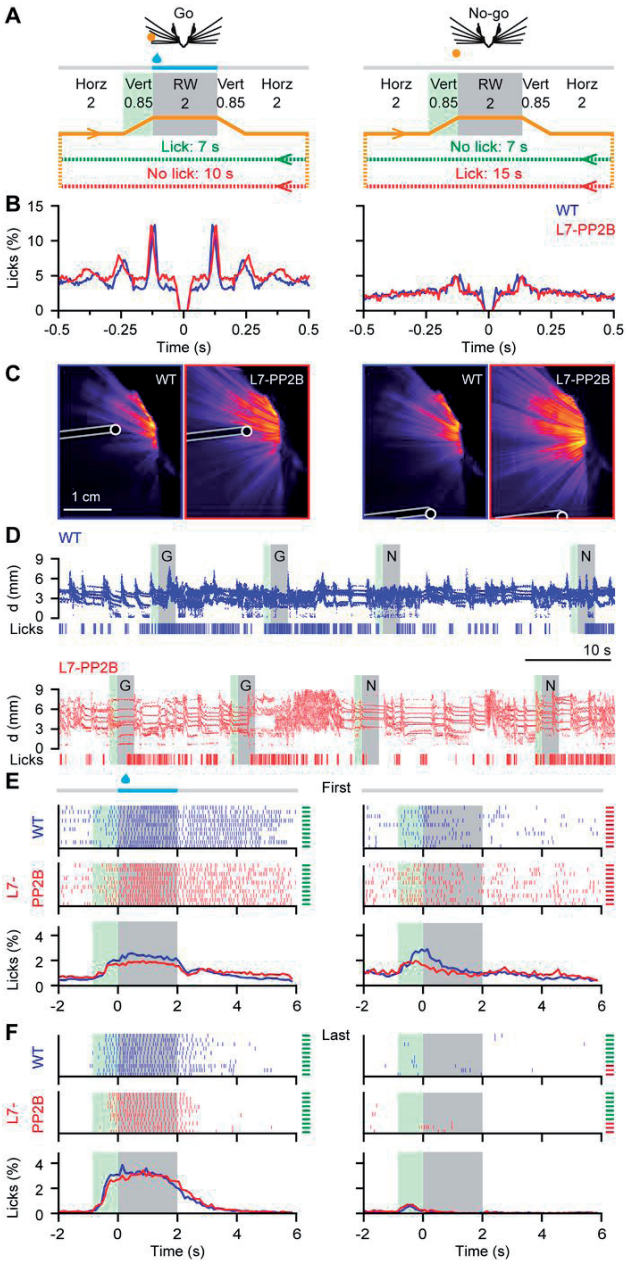


**Figure 3.** Motor behavior during the object localization task with a RW of 2000 ms

**A** – Learning paradigm. During the object localization task mice were subjected not only to go trials, but also to no-go trials. The mice had to learn to lick during the response window (RW) of the go, but not during that of the no-go trials. Once the stimulation bar completed the horizontal movement from the (neutral) resting position to the go or the no-go position, it moved vertically into (go) or just in front of (no-go) the whisker field. Whisker contact with the stimulation bar became possible roughly around half way the time interval allotted for the vertical movement. To indicate this we marked the time period of the vertical movement with a green shading. The RW started after the completion of the vertical movement and is indicated with a grey shading. Licks during the RW of go trials triggered a water reward; incorrect responses postponed the next trial. **B** – Mice licked rhythmically during the RW. Rhythmic licking was more prevalent during the go trials, when there was water, than during no-go trials, when there was no water. **C** – Standard deviation projection plots showing representative examples of whisker movement during the RW. It can be seen that both mice moved their whiskers actively during the RW and touched the stimulus bar, both in the go and in the no-go trials. **D** – Whisker movements during the first association phase illustrating that mice of both genotypes whisk often during the task. Plotted are the rostro-caudal positions of the center whiskers at approx. 3 mm from the snout. Grey areas indicate the RW and green areas the periods of the preceding vertical movement. Go trials are indicated with a "G", no- go trials with a "N". Longer inter-trial intervals indicate incorrect responses. **E** – Raster plots of lick times showing the first 10 go (*left*) and no-go trials (*right*) of representative experiments during the first session of the 2000 ms object localization task. The two top panels show raster plots for a single individual per genotype. The lines at the right border of the plot indicate whether the trial was performed correctly (green) or incorrectly (red). The bottom panel shows the histograms of the relative timing of the licks over all trials averaged for all performers. The green area (850 ms) refers to the interval during which the stimulation bar moved vertically, either into (go trials) or in front of (no-go trials) the resting position of the whisker field. The grey area indicates the response window (2000 ms). **F** – Idem for the last session of the 2000 ms.

The final BWTT result provided us with the angles of all detected whiskers per video frame. In order to relate the angles across frames to the tracks we wrote an algorithm that predicts track values in consecutive frames based on the position and velocity in the angular value as well as the y-position of the last video frames. The predicted track values for the next frame were compared with the detected values in the next frame and assigned according to a minimum deviation approach between them (within reasonable bounds) (see whisker in Fig. 1*G*).

Frequency and amplitudes of individual whisking bouts were derived from the automatically tracked whisker movements. We defined a whisking bout as a period of at least three consecutive sweeps with a minimal amplitude of 10°. The frequency was always derived from the first three sweeps and the amplitude was defined as the difference between the rostral-most and caudal-most position during these three sweeps. The tracked whisker was taken from the caudal half of all whisker tracks, preferably the caudal-most full track. The traces in Fig. 3*D* and 4*D* were made from videos with a lower frame rate (160 Hz) and infrared illumination. To account for changes in the number of visible whiskers across frames (for example, because of overlapping or merging with the snout mask during a retraction), we discarded the whiskers with positions larger than 75% and smaller than 25% of the position distribution, which tend to disappear from the frame, thereby keeping the ones close to the center of the whisker field. In each frame, the whisker position distributions were calculated from the cumulative distribution of whisker positions derived from 10 frames pre and post the frame of interest.

## Habituation and association stage

We prepared 14 female L7-PP2B mice and 16 female WT littermate controls, all of which were 20-25 weeks of age and carried a body weight of 22-25 g, for behavioral testing. These mice received a magnetic pedestal that was attached to the skull above bregma using Optibond adhesive (Kerr Corporation, Orange, CA) under isoflurane anesthesia (2-4% V/V in $O_2$). Post-surgical pain was treated with 5 mg/kg carprofen ("Rimadyl", Pfizer, New York, NY) and 5 mg lidocaine (Braun, Meisingen, Germany). After two days of recovery, mice were put on water restriction (1 ml/day), while food was available *ad libitum*. On the fourth, fifth and sixth day of water restriction mice were put in a head-fixed position using the magnetic pedestal and habituated to the experimental set-up for one 15 min session per day. During these sessions water drops (~20 µl/lick) were triggered upon breaking the laser beam of the lick port. The mice did not receive extra water after the habituation sessions.

Upon completion of the habituation phase, the mice progressed to the association task to ensure that the L7-PP2B mutants and WT mice had similar levels of motor and sensory performance at the onset of localization training. In this respect our protocol deviated from that in the study by O'Connor et al. (2010b), which was designed to describe correlates with cerebral cortical activity rather than to compare cerebellar phenotypes. During the association task the mice learned to associate the rising of a bar (~1 mm diameter) into their right whisker field with the availability of water at the lick-port. The association trials started with a

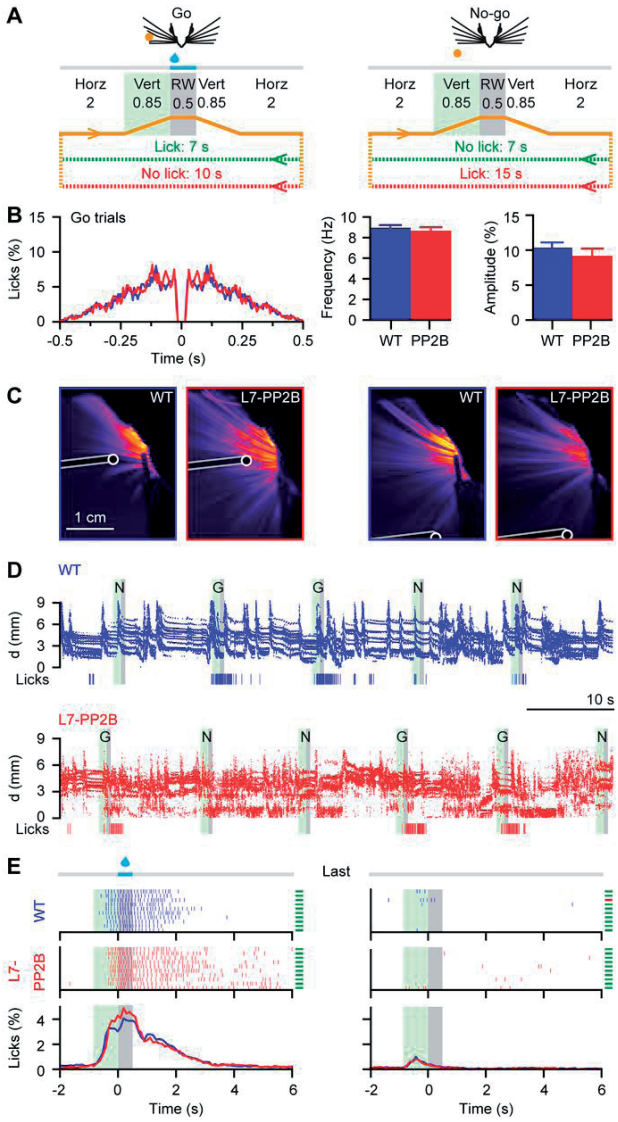


**Figure 4.** Motor behavior during the object localization task with a RW of 500 ms

**A** – Learning paradigm. Once the stimulation bar completed the horizontal movement from the (neutral) resting position to the go or the no-go position, it moved vertically into (go) or just in front of (no-go) the whisker field. Whisker contact with the stimulation bar became possible roughly around half way the time interval allotted for the vertical movement. To indicate this we marked the time period of the vertical movement with a green shading. The RW started after the completion of the vertical movement and is indicated with a grey shading. Licks during the RW of go trials triggered a water reward; incorrect responses postponed the next trial. **B** – Mice licked rhythmically during the RW of go trials of the last 500 ms object localization session. At this stage, the mice performed so well that licking during no-go trials was really sparse and that there were not enough licks during the RW of no-go trials to permit quantitative analysis. **C** – Standard deviation projection plot showing a representative example of whisker movement during the RW. It can be seen that both mice moved their whiskers actively during the RW and touched the stimulus bar, both in the go and in the no-go trials. **D** – Example traces of whisker movements during the last session of the 500 ms object localization task illustrating that mice of both genotypes whisk often during the task. Plotted are the rostro-caudal positions of the center whiskers at approx. 3 mm from the snout. Inter-trial whisking occurs less often in trained mice than in naïve mice (cf. Fig. 3*D*). Licks are indicated in the bottom rows Go trials are indicated with a "G", no-go trials with a "N". A longer inter-trial interval indicates an incorrect response. **E** – Raster plots of lick times showing the last 10 go (*left*) and no-go trials (*right*) of representative experiments during the first session of the 500 ms object localization task. The two top panels show raster plots for a single individual per genotype. The lines at the right border of the plot indicate whether the trial was performed correctly (green) or incorrectly (red). The bottom panel shows the histograms of the relative timing of the licks over all trials averaged for all performers. The green area (850 ms) refers to the interval during which the stimulation bar moved vertically, either into (go trials) or in front of (no-go trials) the resting position of the whisker field. The grey area indicates the response window (500 ms).

horizontal movement below the reach of their whiskers (lasting for 2 s) of the stimulation bar, followed by a vertical movement (lasting for 850 ms) that placed the bar inside the whisker field (approximately 5 mm posterior and 10 mm lateral to the tip of the nose) (Fig. 2*A*). Mice were able to touch the stimulation bar at some point during vertical rise of the stimulation bar. The exact moment of touch depended on the length and position of the whiskers at that time. To indicate the point in time in which the whisker could touch the bar during vertical rise prior to onset of the response window (RW), we indicated the period of upward movement with green shading in Fig. 2-4. Once the bar reached its highest position, the RW opened. A water droplet was triggerted at the onset of the fist lick in this window during correct go trials (see RW indicated with grey shading in Fig. 2-4). The droplet remained at the lick-port for the duration of the RW until all remaining water was sucked out of the lick-port and the bar moved downwards returning to its starting position via the same route and at the same speed. When the animal did not respond to the stimulation during the RW during a go trial, the next trial was postponed by an extra 3 s delaying the possibility of reinforcement at the next trial. Licking outside the RW did not have any positive or negative consequences, except for the absence of water outside the RW. Each mouse was trained for one daily session consisting of 100 trials. The association task was completed as soon as a mouse licked at least once within the RW in at least 80% of the trials for at least two consecutive sessions. To minimize visual cues, the entire task took place in complete darkness, except for some sessions in which we made a video of the whisker movements using infrared illumination; these videos were recorded with a full frame rate of 160 Hz using infrared lighting at $\lambda > 900$ nm.

## Localization learning

Following completion of the association task mice continued with the object localization task consisting of “go” and “no-go” trials on the following day. During a go trial, the stimulation bar moved horizontally in the caudal direction from the neutral position below the right whisker field to approximately 5 mm posterior to the nose and then vertically into the whisker field as described above. During a no-go trial the stimulation bar moved horizontally from the neutral position into the rostral direction below the whisker field to approximately 5 mm anterior to the nose, and then vertically into the whisker field. The no-go position was outside the whisker field at rest, but could be reached during active whisking. The actual distance between the go and the no-go position depended on the size of the head and varied between 8 and 11 mm. A trial always began from and ended with the stimulation bar at rest in the neutral position, which was in the middle between the go and the no-go position, to ensure that the timing of any possible auditory cues during go and no-go trials was identical. During rest at the neutral position and during the horizontal movements, the stimulation bar was well below reach of the whiskers. For both types of trials the RW started as soon as the vertical movement of the bar was completed, but only during the go trials the mice were rewarded with a drop of water when they licked the lick-port within the RW. The total duration of a trial was approximately

6.2-7.2 s depending on the duration of the RW, followed by an inter-trial interval of 7 s in correct trials. An incorrect response (not licking) during a go trial resulted in an extra inter-trial interval of 3 s, whereas an erroneous response (licking) during a no-go trial resulted in an extra inter-trial interval of 8 s (Fig. 3*A*). Each (daily) session consisted of 100 pseudo-randomized trials (50% go and 50% no-go trials) or until the mouse discontinued licking, which was defined as not showing any responses for 10 consecutive go trials. For each session, we calculated the percentage of correct trials, taking both the go and the no-go sessions into account. Once the mice performed at ≥ 80% correct during two consecutive sessions of the localization task with a RW of 2000 ms, the RW was decreased to 500 ms (via an intermediate step using a RW of 1000 ms) (Figs. 3-5). Mice that did not learn the 2000 ms localization task within 35 sessions

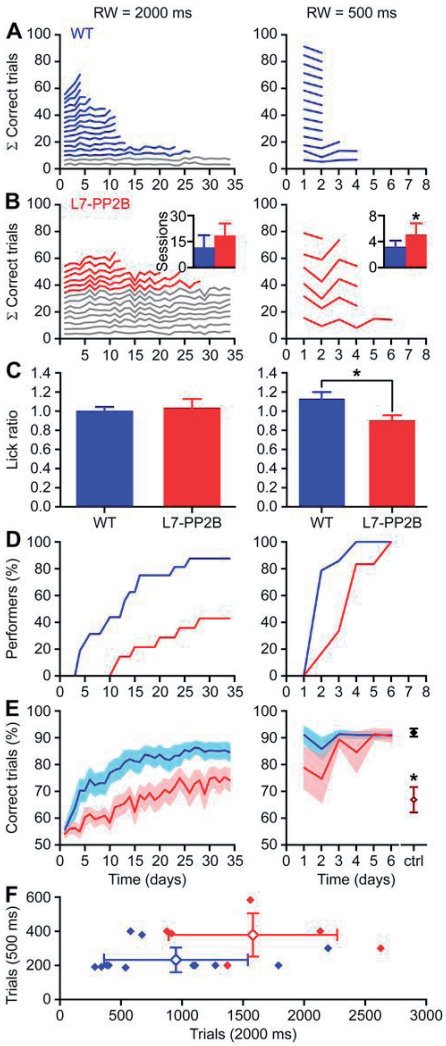


**Figure 5.** Absence of PP2B in cerebellar Purkinje cells impairs learning of a whisker- based object localization task

**A** – Summed learning curves of WT mice during the 2000 ms (*left panel*) and the 500 ms (*right panel*) object localization task across consecutive sessions (x-axis). The number of trials per session was normalized to 100% (see Methods section for details). Upon reaching a success rate of ≥ 80% during two consecutive sessions mice continued to the next phase. Performers and non-performers are indicated in blue and grey, respectively. **B** – Idem for L7- PP2B mice (performers indicated in red). *Insets:* Averaged number of sessions ± SD that performers needed to complete the complete object localization task; * $p < 0.017$ (*t* test). **C** – The fine timing of the lick responses at the end of the 100 ms period preceding the RW and at the first 100 ms period of the RW suggests a cerebellar role in the timing of the decision process to lick. We compared the number of licks during the first 100 ms of the RW and the 100 ms prior to the start of the RW, thus the ratio of licks just after the availability of water and the licks just before the availability of water. This ratio equaled 1 during the last session of the 2000 ms object localization task (*left*), but was increased in trained WT mice (but not in L7-PP2B mice) during the last 500 ms object localization task (*right*); * $p < 0.02$. **D** – Cumulative histograms of the percentage of mice that reached criterion showing that more WT mice were able to learn the object localization task than L7-PP2B and that WT performers were faster than L7-PP2B performers. **E** – The fraction of correct trials over the sessions. *Dark lines* show the averages and the shaded areas cover the average ± SEM. For control, we clipped the whiskers of 10 mice (8 WT + 2 L7-PP2B mice) following successful completion of the 500 ms object localization task. Their performance level during the subsequent session (dark red open symbol) was comparable to that of naïve mice and much lower than that during the last session with intact whiskers (black closed symbol); * $p < 0.001$ (paired *t* test). **F** – The average numbers of trials the L7-PP2B mice needed to learn the 500 ms and 2000 ms object localization tasks were significantly greater than those in WTs ($p < 0.05$).

were considered non-performers and they were not tested any further. For control, we cut all whiskers in 10 mice (under isoflurane anesthesia) following completion of the 500 ms localization task and we tested their performance again on the next day.

## Constructing learning trajectories

For each session, we plotted the average hit rate and average false alarm rate of all mice per group (Fig. 6). To this end we calculated for each mouse and for each session the hit rate, i.e. the fraction of correct responses (licks) during the go trials relative to all go trials, and the false alarm rate, i.e. the fraction of incorrect responses (licks) during the no-go trials relative to all no-go trials. Linear regression lines were fitted to the group averages and the deviation from the linear regression was calculated as the least squared difference (SigmaPlot, Systat Software, Chicago, IL). The sensitivity index (d') was calculated using the *z* transformations of the hit rate and the false alarm rates (d'= *z*(hit rate) – *z*(false alarm rate)), assuming a Gaussian distribution. The 80% correct level corresponded to a d' score of approximately 1.7 (cf. Huber et al. 2012).

## Electrophysiology

Electrophysiological recordings were performed in awake mice as described previously (Bosman et al., 2010). Briefly, mice first received a craniotomy of the occipital bone under isoflurane (4% V/V in $O_2$). Post-surgical pain was treated with carprofen ("Rimadyl", Pfizer, New York, NY, 5 mg/kg, injected subcutaneously) and lidocaine (~1 µg applied to the wound). After surgery, mice were allowed to recover at least three days prior to retraining and electrophysiological recordings. Single-unit recordings were made using quartz-coated platinum/tungsten electrodes (2-5 MΩ, outer diameter = 80 µm, Thomas Recording, Giessen, Germany). The electrodes were placed in an 8x4 matrix (Thomas Recording), with an inter- electrode distance of 305 µm over crus 1 and crus 2 ipsilateral to the whisker stimulation bar. All recordings were made at a minimal depth of 500 µm. The electrophysiological signal was digitized at 25 kHz, using a 30-6,000 Hz band-pass filter, 22x pre-amplified and stored using a RZ2 multi-channel workstation (Tucker-Davis Technologies, Alachua, FL). Spikes were detected offline using SpikeTrain (Neurasmus, Rotterdam, The Netherlands) or a custom program written in Labview (National Instruments, Austin, TX). We identified Purkinje cell activity by the presence of both complex spikes and simple spikes. Complex spikes were recognized based on the presence of spikelets following the initial spike. For each recording we constructed a histogram of simple spike time stamps triggered by complex spike time stamps. We accepted a recording as a single unit if the 7 ms following a characteristic complex spike were devoid of simple spikes. Further analysis was exclusively done on single unit Purkinje cell recordings that had a clear signal-to-noise ratio. The recording was split into "inter-trial" and "trial" periods and further analyzed only if we had at least 50 s of each period. The trial period consisted of the time during vertical rise of the bar, the RW, and the complete time of the vertical decent of the bar following the RW. The inter-trial interval was defined as the period between the end of the (second) horizontal

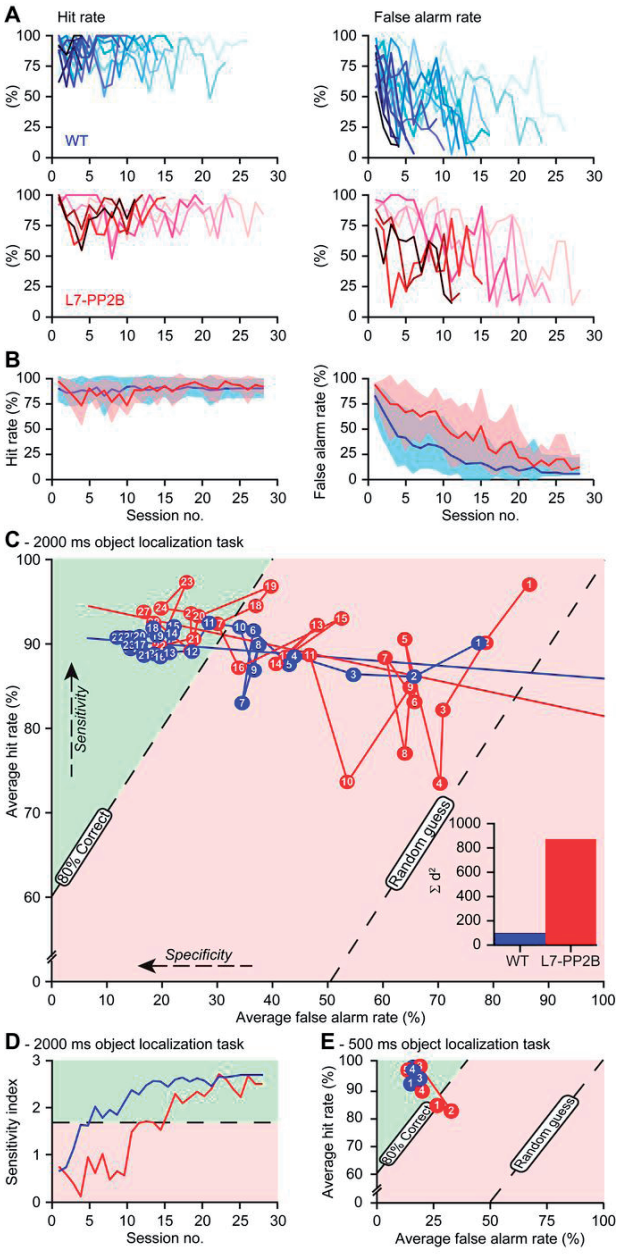


**Figure 6.** WT mice have more efficient learning trajectories than L7-PP2B mice

**A** –The hit rates (licking during the RW of go trials; *left*) and the false alarm rates (licking during the RW of no-go trials; *right*) of all WT (*top*) and L7-PP2B (*bottom*) performers over the sessions of the 2000 ms object localization task. **B** – Averaged hit (*left*) and false alarm (*right*) rate of all performers. Dark lines indicate the average and the shaded area the average ± SD. **C** -Average false alarm rates versus average hit rates in receiver operating characteristic (ROC) space during the 2000 ms object localization task. Perfect classification of both the go trials and the no-go trials would be 0% false alarms and 100% hits. Successful trials (≥ 80% correct) can be found in the green area. Plotted are the averages of all WT (blue) and L7- PP2B (red) performers for 28 sessions (session no. indicated on each symbol), which was the maximum number of sessions required to master the 2000 ms object localization task. Linear regression lines are indicated. Note that the WT mice decrease the number of false alarms from the beginning on, while the L7-PP2B mice first generally reduce the licking responses, irrespective of the trial type. The linear regression lines of WT and L7-PP2B are not significantly different ($z = 1.498$; $p = 0.134$). Inset: Summed least squared differences between the first 28 sessions and the linear regression lines for WT and L7-PP2B performers during the 2000 ms object localization task. **D** – The sensitivity index (d') of all animals (0 = chance performance; 1.68 = 80% correct trials). **E** – The same plot as **C**, but for the 500 ms object localization task. Note that the WT mice are in the green area from the start on, while the L7-PP2B mice initially show a decreased performance relative to the previous phases of the object localization tasks.

movement of one trial and the start of the (first) horizontal movement of the next trial. The local variation in simple spike firing (CV2) was calculated as $CV2 = 2\ |ISI_{n+1} - ISI_n|\ /\ (ISI_{n+1}+ISI_n)$, with ISI = inter-spike interval (Shin et al., 2007).

### Data analysis

Summed learning curves were made for both the association stage and the object localization task. First, we calculated for each mouse and each session the percentage of correct responses and divided that by the number of mice in that group. For example, if the group size was 14 mice, each individual mouse had a normalized success rate between 0% and 100%/14 = 7.14%. Next, we sorted the mice per group based on the number of sessions they required to reach criterion. The lowest line represents the normalized learning curve for the mouse that needed the most sessions. The second line from below is the sum of the normalized success rate of the first mouse plus that of the second mouse and so on. Each additional line is the sum of the normalized success rates of that mouse and of the mice represented by the lines below that line. As a consequence, the top line represents the group average. Unless stated otherwise, data are represented as means ± SEM and statistical testing was performed using Student's *t* test. For unrelated tests we used a level of significance of 5%. For repeated tests the level of significance was corrected using Bonferroni correction ($\alpha_{corr} = \alpha / n$ with $\alpha = 0.05$ and $n$ = number of tests). Where Bonferroni correction was applied, $\alpha_{corr}$ is mentioned in the text.

## RESULTS

### Licking in freely moving mice is comparable across genotype

Since we are using licks as the read-out parameter of learning capabilities during the object localization task, putative deficits in motor aspects of licking could in principle create a bias in the learning performance. Therefore, we first studied the licking behavior of WT and L7- PP2B mice in their home cages. Both WT (n = 9) and L7-PP2B mice (n = 10) licked during multiple periods. Such licking periods often consisted of a few bouts of uninterrupted licking, each of which consisted of a series of rhythmic licks (Fig. 1*A*-*B*). Neither the licking frequency (9.15 ± 0.13 Hz for WT versus 9.08 ± 0.18 Hz for L7-PP2B mice) nor the number of licks per bout (5.7 ± 0.6 and 5.4 ± 1.1) differed significantly among genotypes ($p = 0.773$ and $p = 0.841$, respectively; Fig. 1*C*, *D*). In addition, the distributions of inter-lick intervals within bouts were similar between WT and L7-PP2B mice ($p = 0.693$; Kolmogorov-Smirnov test; Fig. 1*D*). These data indicate that the baseline licking performance of freely moving L7- PP2B mice is intact.

### Free whisking in head-restrained mice

Putative abnormal whisker use could be a cause for deficits in the results of our whisker-based object localization task. Therefore, we quantified the spontaneous whisker movements of 10

untrained WT mice and 11 L7-PP2B littermates during recording sessions in which no whisker stimulation took place (Fig. 1*E*). To facilitate automated detection of whisker movements, we first quantified whisker motion (see Methods). The whisker motion algorithm reliably identified periods with whisker movements as verified by manual tracking (see Methods; Fig. 1*F*). The video fragments containing whisker movement were further analyzed quantitatively using BWTT (Perkon et al., 2011) and post-processed to track traces of individual whiskers over time (Fig. 1*G*). We confirmed the accuracy of automatically traced tracks with manually traced ones (see e.g. orange trace in Fig. 1*F*, which is derived from the same whisker as the orange (bottom) trace in Fig. 1*G*, but made from a more distal location accounting for the sharper peaks). We found that all mice showed repetitive periods of whisking. We quantified the movements of individual whiskers during bouts of rhythmic whisking. Within such bouts, neither the amplitude (WT: 29.5 ± 2.5°; L7-PP2B: 26.9 ± 2.4°; $p = 0.378$) nor the frequency (WT: 17.5 ± 1.6 Hz; L7-PP2B: 18.1 ± 1.5 Hz; $p = 0.784$) differed significantly between the two groups of mice (Fig. 1*G-I*). There was a clear inverse correlation between the amplitude and the frequency of a whisker bout (WT: R = 0.503; $p < 0.001$; L7-PP2B: R = 0.606; $p < 0.001$; linear regression; Fig. 1*H*). The regression lines of the WT and the L7-PP2B mice were not significantly different from each other ($z = 1.579$; $p = 0.114$). We conclude that WT and L7-PP2B mice are similar in their range and frequency of free whisking.

## General motor performance during the association stage

Since the frequency of licking can depend on the ease of access to water (Weijnen, 1998), we also compared the licking behavior in head-restrained mice during the association task when water was available during the 2000 ms RW. Overall, the average number of licks per minute – as calculated over the whole first association session – was comparable between head- restrained WT ($n = 16$) and L7-PP2B ($n = 14$) mice (WT: 96 ± 18 licks/min; L7-PP2B: 120 ± 24 licks/min; $p = 0.535$; data not shown). Most mice (14 out of 16 (87.5%) WT and 14 out of 14 (100%) L7-PP2B mice; $p = 0.485$; Fisher's exact test) licked rhythmically during the RW of the first association session. WT mice had a slightly different licking frequency, but the difference with L7-PP2B mice was not significant (f = 8.3 ± 0.1 Hz and 7.9 ± 0.1 Hz, respectively; $p = 0.06$). The strength of the rhythmicity was similar (13.0 ± 0.8% and 11.8 ± 0.7%; $p = 0.306$; Fig. 2*B*). As the association training proceeded, rhythmic licking during the RW increased; at the end, the strength of the rhythmicity was 15.1 ± 1.0% and 14.3 ± 0.9% for WT and L7-PP2B mice, respectively ($p = 0.576$). The frequency remained around 8 Hz for both groups (7.9 ± 0.1 Hz and 7.8 ± 0.1 Hz, respectively; $p = 0.624$). Moreover, video analyses of the whisker movements showed that WT and L7-PP2B mice were both actively whisking during the association trials. Fig. 2*C* shows an example of whisker movements in a video of a WT and a L7-PP2B mouse during the first session of the association task. Both mice whisked actively and contacted the stimulation bar during the RW of the association task. Thus, as in naïve mice both WT and L7-PP2B mice

had similar lick responses and active whisker exploration behavior while being head-restrained during the RWs of the association task.

## Association learning

Next, we analyzed the performance of the mice during the association training. We identified a trial as correct when a mouse licked at least once within the RW independent from its activity outside the RW. On average both groups had similar percentages of correct trials during the first session when the rod was elevated inside the whisker field (WT: 39.4 ± 24.6%; L7-PP2B: 50.1 ± 24.2%; mean ± SD; $p$ = 0.241). In addition, both genotypes learned equally well during the association task (last session: WT: 93.8 ± 5.4%; L7-PP2B: 91.4 ± 7.1%; mean ± SD; $p$ = 0.238). WT and L7-PP2B mice required a similar number of sessions to reach criterion (6.6 ± 3.6 and 6.4 ± 2.6 sessions, respectively; mean ± SD; $p$ = 0.865) (Fig. 2*D*; see also Table 1). The rate at which they mastered the task was very similar for WT and L7-PP2B mice ($p$ = 0.458; paired $t$-test; Fig. 2*E*). Also the learning curve represented as percentage of correct trials per session was highly comparable for both types of mice ($p$ = 0.963; repeated measures ANOVA; Fig. 2*F*). Thus, all mice – irrespective of their genotype – learned to lick during the RW of the association test at a similar pace.

## General motor performance during localization training

Following completion of the association stage, during which mice only received go trials, they were subjected to the localization learning task, wherein they received both go and no-go trials. During the go trials the pole was positioned inside the whisker field (as in the association stage), whereas during the no-go trials the pole was raised just in front of their baseline whisker field so they could only detect the rod by means of active forward exploration (Fig. 3*A*). In contrast to the go trials when the mice were encouraged to lick, they had to withhold their licking during no-go trials in order to prevent a long delay for the next trial postponing potential reinforcement.

First, we subjected the animals to trials with a RW of 2000 ms and we analyzed the licking pattern during the RWs of the first localization session. Licking was more rhythmic during the RW of go trials, when the mice received water, than during that of no-go trials, when the mice did not receive water (Fig. 3*B*). During go trials, the lick rhythm was again around 8 Hz for both genotypes (WT: 8.2 ± 0.1 Hz and L7-PP2B: 7.9 ± 0.1 Hz; $p$ = 0.085) and both genotypes had similar strength of rhythmic licking (15.6 ± 1.0% and 14.4 ± 0.6%, respectively; $p$ = 0.304; $t$ test). During no-go trials, the lick rhythm was 8.1 ± 0.2 Hz for WT and 7.4 ± 0.2 Hz for mutants ($p$ = 0.072), and the amplitude was 7.9 ± 1.0% and 7.4 ± 0.9%, respectively ($p$ = 0.710). Likewise when we analyzed the whisking behavior during the localization task (from 5 WT and 5 L7-PP2B mice), we found active whisking during both go and no-go trials, irrespective of the genotype of the mouse (Fig. 3*C*-*D*). For this reason, we concluded that, at least initially, the mice were localizing both stimulus positions rather than simply detecting the stimulus during the go trials.

Note that the mice could already sense the stimulation bar before it reached the top position. The moment of contact could vary per trial and depended on the actual position of the whiskers. Since mice could contact the stimulation bar as it moved upward into the whisker field we indicated this period with green shading in Figs. 2-4. On average there were 13.3 ± 5.9 times as many licks during the "green period" of go trials than during that of no-go trials in expert mice ($p < 0.001$; paired *t* test; Fig. 3*F*). The ratio was higher in WT mice (17.2 ± 7.8) than in L7-PP2B mice (4.3 ± 1.1), but this difference was not significant ($p = 0.147$). Together this indicates that although there were licks before the start of the RW, these early licks were mainly related to go trials, indicating presence of whisker contact just prior to the start of the RW. We found a tendency that WT mice were better able to categorize trials in an early phase of the trial than L7-PP2B mice, since especially WT mice showed many more licks during the early onset of go trials than during that of no-go trials.

The mice that performed well during the 2000 ms object localization task were ultimately tested with the same test with a RW of 500 ms (Fig. 4*A*). During the 500 ms RW of the go trials, mice licked again rhythmically around 8 Hz (frequency: WT: 8.8 ± 0.4 Hz; L7- PP2B: 8.5 ± 0.3 Hz; $p = 0.514$; amplitude: WT: 10.3 ± 0.8%; L7-PP2B: 9.2 ± 1.0%; $p = 0.385$). During this task, high-frequency tongue movements were relatively abundant in both WT and L7-PP2B mice, leading to a similar shape of the auto-correlograms ($p = 0.795$; Kolmogorov-Smirnov test; Fig. 4*B*). This high frequency licking was probably due to the shorter time period of the presence of water at the lick-port (500 ms instead of 2 s). Licking during the RW of no-go trials was very sparse in both trained WT and mutant mice (see Fig. 4*E*), precluding a meaningful quantification of lick rhythmicity during the no-go trials. During the last session of the 500 ms object localization task both WT and L7-PP2B mice whisked actively during both go and no-go trials (Fig. 4*C*), but in comparison to naïve mice both genotypes whisked less during inter-trial intervals (compare Fig. 3*D* and 4*D*).

## More WT than L7-PP2B mice learned the localization task

Contrary to the association phase, which could be mastered by all mice, the object localization task with a 2000 ms RW was not learned by all mice. Of the 16 WT mice, 14 reached a success rate of more than 80% correct trials during two consecutive sessions within 35 daily sessions. Significantly less L7-PP2B mice were able to learn this task: only 6 out of 14 mice succeeded in obtaining the same criteria (87.5% vs. 42.9%; $p = 0.019$; Fisher's exact test; left panels in Fig. 5*A*-*B*). The mice that did not manage to learn the object localization task with a RW of 2000 ms were considered as non-performers and not tested any further. Mice that did obtain the necessary criteria were considered perfomers and moved to the short RW phase paradigm.

## WT performers learned the localization task faster than L7-PP2B performers

WT performers were faster learners than L7-PP2B mice. For example, the fastest WT mouse took four sessions to master the 2000 ms localization task, whereas the fastest L7-PP2B mouse

needed eleven sessions. The complete task including both the 2000 ms and 500 ms localization tasks was learned significantly faster by WTs than by L7-PP2B performers (genotype: WT ($n$ = 14) 17.4 ± 8.7 vs. L7-PP2B ($n$ = 6) 24.8 ± 7.7 sessions; mean ± SD; $F_{1,54}$ = 4.395; $p$ = 0.041; two-way ANOVA; Fig. 5*A-B*; see also Table 1 for the number of trials involved). With regard to the 2000 ms object localization task only, it took the L7-PP2B mice longer to learn the task than the WT mice, but this difference did not reach statistical significance (WT: 11.6 ± 7.0 versus L7-PP2B: 18.5 ± 6.9 sessions; mean ± SD; $p$ = 0.090 (not significant: $\alpha_{corr}$ = 0.017 (see Methods)); Mann-Whitney test; Fig. 5*A-B*, *D*). The reduced learning efficiency of the L7-PP2B mice was also reflected in the slower increase of correct responses during the 2000 ms task (genotype: $F_{1,27}$ = 5.098; $p$ = 0.032; repeated measures ANOVA; Fig. 5*E*).

**Table 1.** Number of trials for each phase of the learning paradigm

| | Association | 2000 ms RW non-performers | 2000 ms RW performers | 500 ms RW performers |
|---|---|---|---|---|
| WT | 511 ± 303 ($n$=16) | 2918 ± 532 ($n$=2) | 950 ± 589 ($n$=14) | 232 ± 72 ($n$=14) |
| L7-PP2B | 535 ± 253 ($n$=14) | 3041 ± 283 ($n$=8) | 1581 ± 690 ($n$=6) | 378 ± 127 ($n$=6) |
| $p$-value | 0.810 | 0.799 | 0.086 | 0.036* |

Each session consisted of up to 100 trials. On average, WT and L7-PP2B mice required a similar number of trials to master the association phase. Non-performers (at the 2000 ms RW test) also received comparable numbers of trials. However, those L7-PP2B mice that were able to learn the object localization task needed more trials than their WT littermates. This was especially true for the 500 ms RW test. Significance tested with two-way ANOVA (genotype: $p < 0.001$) and subsequent $t$ tests.

## WTs learned to fine-tune the timing of their lick responses better than L7-PP2B mice

When we reduced the RW from 2000 ms to 500 ms, the L7-PP2B mice required on average significantly more sessions than their WT littermates to reach criterion (WT: 2.4 ± 0.7 vs. L7- PP2B: 3.8 ± 1.3 sessions; $p$ = 0.010 (significant: $\alpha_{corr}$ = 0.017; Mann-Whitney test; Fig. 5*A-B*; see also Table 1 for the number of trials involved). Thus, while the L7-PP2B mice in general had more difficulties learning the object localization task, the difference with WT mice was especially clear when fast response timing was required.

Further evidence for this claim is indicated in the differences in precise timing of the licks between WT and L7-PP2B mice. We compared the number of licks just before the RW to the number of licks just after the start of the RW. Note that the water reward became available at the start of the RW. The ratio of the licks between 100 ms after and 100 ms before the start of the RW was not significantly different between WT and L7-PP2B mice at the end of the training with the 2000 ms RW (WT: ratio = 1.01 ± 0.04; L7-PP2B: 1.04 ± 0.09; $p$ =

0.758). This indicates that the mice did not time their licks very precisely around the onset of the RW. However, at the end of the training with the 500 ms RW, the WT mice showed a clear increase in licking just at the onset of the RW. In contrast, the L7-PP2B mice did not do so (WT: ratio = 1.13 ± 0.07; L7-PP2B: 0.91 ± 0.05; $p$ = 0.019; Fig. 5*C*). These data point at reduced

sensorimotor timing abilities in L7-PP2B mice that become only apparent under strict timing restraints.

Importantly, whisker clipping following training with a RW of 500 ms significantly affected the performance during the object localization task ($n$ = 10 mice; $p < 0.001$; paired $t$ test (right panel in Fig. 5*E*)) confirming that mice use their whiskers to detect the stimulus bar and respond accordingly. Since not all sessions had an equal number of trials, we also compared the number of trials per individual required for the 2000 and 500 ms task. This confirmed that WT mice were in general faster in learning than L7-PP2B mice (Fig. 5*F*; Table 1). Moreover, together with the more accurate timing of the licks in WT mice (Fig. 5*C*), these data indicated that the differences among WT and L7-PP2B mice are more prominent with shorter RWs.

## WT mice show a better learning trajectory than L7-PP2B mice

Since we found that the WT and L7-PP2B mice differed in their learning skills during the object localization task, we further investigated the relative contributions of their licks during the go trials and the withholding of their licking during the no-go trials to the overall learning process. First, we plotted for all performers the individual learning curves of the hit rates (i.e., the percentages of go trials during which the mice licked during the RW) and the false alarm rates (i.e., the percentages of no-go trials during which the mice licked during the RW) (Fig. 6*A-B*). It can be seen that mice started the object localization training with both high hit rates and false alarm rates, and gradually learned to refrain from licking during the no-go trials. This behavior was further analyzed by plotting the "false alarm" rates vs. the "hit" rates for each session of the object localization task. Separate plots of the learning trajectories were constructed in receiver operating characteristic (ROC) space (Fig. 6*C*). As mentioned before, the mice were trained during the preceding association phase to lick during all trials. Consequently, during the first object localization session (with a 2000 ms RW) they licked very often irrespective of the trial type. As a result, they performed close to guess rate.

During the subsequent sessions, the WT performers markedly and consistently increased accuracy, moving almost along a straight line towards our defined criteria: the green area in Fig. 6*C*. They continued to lick during the go trials, but decreased their licking during no-go trials. Thus, they maintained a high level of sensitivity to go trials, but specifically reduced their response to no-go trials. The WT mouse with the fastest learning capability reached criterion after four sessions, whereas the fastest L7-PP2B mouse reached criterion only after 11 sessions (see Fig. 5*A-B*). In contrast to WT mice, the L7-PP2B mice reduced their licking during the first four sessions in a random fashion: they stayed close to guess rate. The difference between the WT and L7-PP2B mice during these first four sessions was striking: the WT mice kept licking at the same rate during the go trials, but reduced their licking during the no-go trials. In contrast, the L7-PP2B mice initially did not discriminate between go and no-go trials.

In the subsequent sessions also the six L7-PP2B performers increased their successful licks, but their learning trajectories remained noisier than those of the WT performers. This differ-

ence in learning trajectories was particularly evident when comparing the deviations from the linear regression between the WT and L7-PP2B performers (Fig. 6*C* inset). The linear regression lines themselves were not significantly different ($z$ = 1.498; $p$ = 0.134), but the much larger deviations from the regression line in the L7-PP2B mice in combination with the longer time required to reach high-performance levels clearly confirmed that learning was affected in L7-PP2B mice. The differences in learning strategies were characterized by the changes in the sensitivity index (d') (WT vs. L7-PP2B: $p$ = 0.001; Fig. 6*D*). These curves illustrated the superior ability of WT mice in comparison to L7-PP2B mutants to discriminate between go and no-go trials and act accordingly. When the same analysis was done for the 500 ms localization task, which was rapidly learned, the averages of the WT and L7-PP2B performers were already mostly in the "green area", indicating good performance, from the first session onwards (Fig. 6*E*). Still, here too, the L7-PP2B performers showed a clear drop in performance during the second session of the 500 ms task.

## Purkinje cell activity during object localization

If the differences in learning ability for whisker-based object localization between WT and L7-PP2B are indeed due to differences in intrinsic and synaptic potentiation of Purkinje cells, one can expect differences in the activity of these cells among the two genotypes. We therefore recorded at the end of the localization task single-unit activity of Purkinje cells in ipsilateral crus 1 and crus 2, which are involved in both whisking (Axelrad and Crepel, 1977; Bosman et al., 2010) and licking (Bryant et al., 2010). In order to compare Purkinje cell activity during the trial with baseline activity we divided the recordings in trial and inter-trial periods. We considered the interval between the end of the (second) horizontal movement and the start of the (first) horizontal movement of the next trial the inter-trial period and the interval between the start of the upward vertical movement until the end of the downward vertical movement the trial period (see also Fig. 3*A*).

First, we characterized the simple spike and complex spike firing during the inter-trial periods. In line with the findings by Schonewille and colleagues (2010) for the vestibulocerebellum, the rate of simple spike firing was similar between WT and L7-PP2B Purkinje cells (WT ($n$ = 24): 60.23 ± 4.65 Hz vs. L7-PP2B ($n$ = 25): 55.36 ± 3.31 Hz; $p$ = 0.398), but the local variation in simple spike firing (CV2 WT vs L7-PP2B: 0.490 ± 0.027 vs. 0.275 ± 0.026; $p < 0.001$) as well as the complex spike firing rate (CS FF WT vs L7-PP2B: 1.35 ± 0.06 vs. 1.00 ± 0.08 Hz; $p$ = 0.002) were significantly reduced in L7-PP2B Purkinje cells (left panels of Fig 7*C*, *D* and *E*).

Next, we compared Purkinje cell activity between trial and inter-trial periods. WT Purkinje cells showed a moderate, but consistent net increase in simple spike firing (inter- trial: 60.23 ± 4.66 Hz vs. trial: 62.72 ± 4.74 Hz; $p$ = 0.004 Wilcoxon matched pairs test) (Fig 7*C* top panel). In contrast, L7-PP2B Purkinje cells did not show such an increased simple spike firing (inter-trial: 55.36 ± 3.31 Hz vs. trial: 55.54 ± 3.32 Hz; $p$ = 0.853; Wilcoxon matched pairs test; Fig 7*C* bottom panel). Thus as might be predicted, the net increase in simple spike firing observed in WT

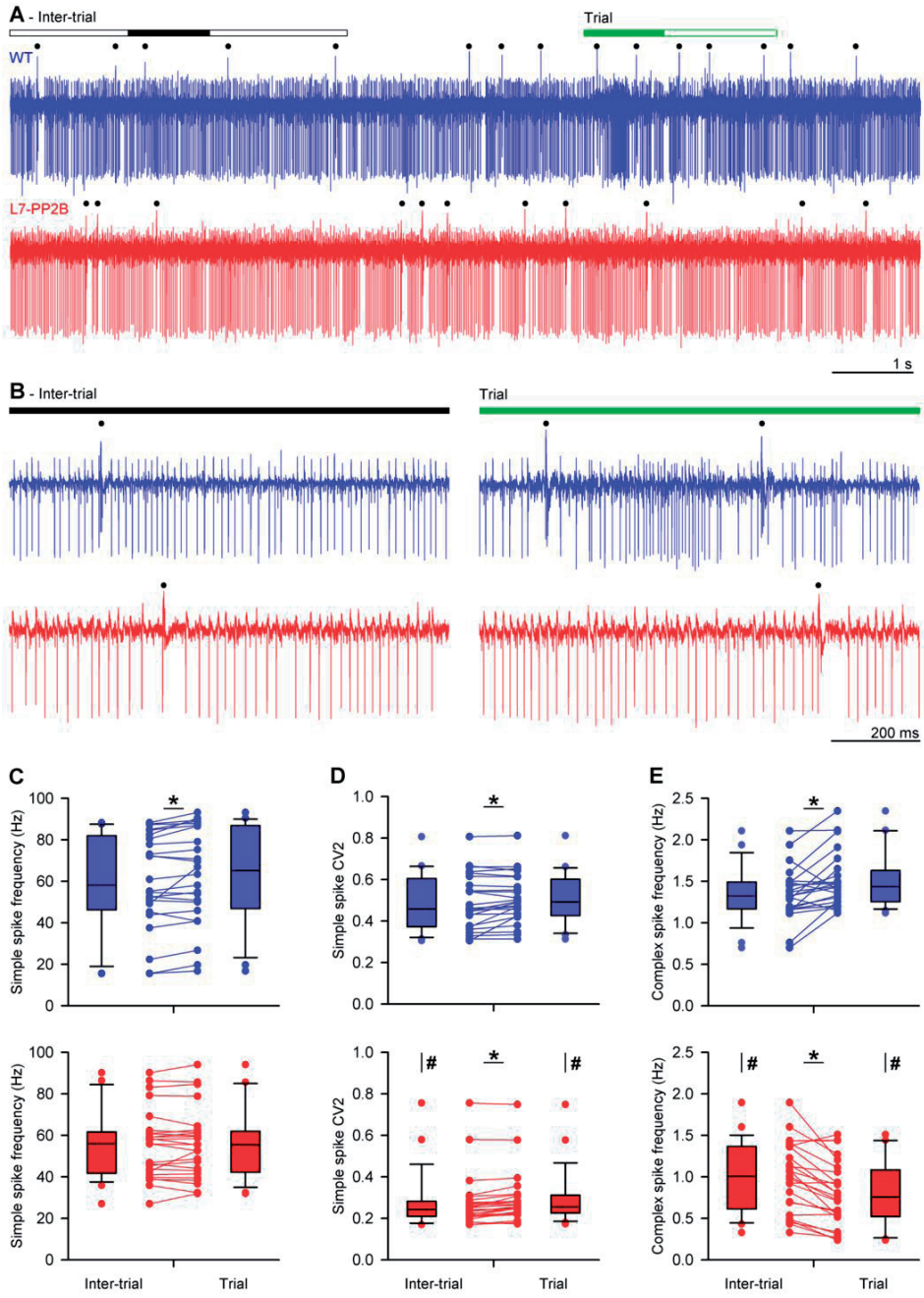


**Figure 7.** Differential Purkinje cell activity during the object localization task

**A** – Example single-unit traces of a WT (top) and a L7-PP2B (bottom) Purkinje cell in crus 1/crus 2 area of the cerebellum ipsilateral to the stimulus location in trained mice. The recording was divided into a trial period (consisting of the RW and the flanking periods of vertical movement of the stimulation bar) and an inter-trial period (excluding the trial period and the flanking periods of horizontal movement of the stimulation bar; see Fig. 3A). The filled lines indicate the periods that

mice is not observed in trained mice in the absence of intrinsic and synaptic potentiation of their Purkinje cells. In line with the occurrence of sensory input, the simple spike CV2 was increased both in WT and in L7-PP2B Purkinje cells, indicating that these Purkinje cells were indeed involved in the behavioral task (WT: inter-trial: 0.490 ± 0.027 vs. trial: 0.507 ± 0.024; $p$ = 0.021; L7-PP2B: inter-trial: 0.275 ± 0.026 vs. trial: 0.292 ± 0.025; $p < 0.001$; Wilcoxon matched pairs tests). The complex spike activity of WTs and L7-PP2B mutants also both showed prominent changes between trial and inter-trial periods, but these changes moved into opposite directions (Fig. 7*E*). In WT complex spike firing rate increased (intertrial vs. trial: 1.35 ± 0.06 vs. 1.50 ± 0.07 Hz; $p$ = 0.001), whereas in L7-PP2B it decreased (inter-trial vs. trial: 1.00 ± 0.08 vs. 0.79 ± 0.08 Hz; $p$ = 1.000 one-sided Wilcoxon matched pairs tests). We conclude that Purkinje cells in both WT and L7-PP2B mice were probably involved in the object localization task, since both groups of Purkinje cells showed an increased variability in simple spike firing. Yet, trained WT mice reacted with a net increase in both simple spike and complex spike firing, whereas the L7- PP2B mice did not. We expect that such a difference in Purkinje cell activity may cause changes in the output of the cerebellar nuclei that can in turn affect cerebral cortical processing via the thalamus.

## DISCUSSION

In the current study we showed that L7-PP2B mice, which suffer from impaired intrinsic plasticity and synaptic potentiation of their Purkinje cells (Schonewille et al., 2010), exhibited learning deficits during a whisker-based object localization task. Not only were fewer L7- PP2B mice able to learn the task at long response windows, the ones that did, needed more time and the fine-tuning of the precise timing of their learned responses was especially deficient at short response windows. Moreover, L7-PP2B mice showed deficits in maintaining hit rate while reducing false alarms and their learning trajectory was considerably noisier. Finally, we showed that Purkinje cells in WT, but not L7-PP2B, showed a net increase in firing during trials in trained mice, which further substantiates the possibility that the cerebellum is involved in learning of this whisker-based object localization task.

are enlarged in **B**. Complex spikes are indicated with a black dot above the trace. The other downward deflections are the simple spikes. The firing characteristics of 24 WT and 25 L7-PP2B Purkinje cells are summarized with box plots for the simple spike frequency (**C**), simple spike CV2 (**D**) and complex spike frequency (**E**). Recordings were made after finishing the object localization training. The simple spike frequency was not significantly different between WT and L7-PP2B Purkinje cells. Only in WT Purkinje cells there was a modest but significant increase in simple spike frequency during the trial periods compared to the inter-trial periods. The local variation (CV2) in simple spike firing was reduced in L7-PP2B compared to WT Purkinje cells. Yet, in both types of Purkinje cells the CV2 was increased during the trial periods. The complex spike frequency was reduced in L7-PP2B compared to WT Purkinje cells. The WT Purkinje cells showed an increase in complex spike firing during trial periods, whereas the L7-PP2B Purkinje cells showed a decrease during trial periods. # $p < 0.05$ (WT vs. L7-PP2B); * $p < 0.05$ (trial vs. inter-trial)

## Can the observed learning deficits be explained by motor, sensory and/or developmental aberrations?

Even though L7-PP2B mice do not show overt signs of motor ataxia (Schonewille et al., 2010), in principle they might suffer from small deficits in motor performance during licking and/or whisking behavior, since both types of behavior have neural correlates in the cerebellum (Lang et al., 2006; Bosman et al., 2010; Bryant et al., 2010). We therefore first investigated licking and whisking behavior of freely moving and head-fixed WT and L7- PP2B mice. In line with the literature (Horowitz et al. 1977; Wiesenfeld et al. 1977; Yamamoto et al. 1982), the licking behavior was dominated by ~8Hz rhythmic tongue movements for both WT and L7-PP2B. Moreover, the variations in lick rhythmicity, which can depend on contextual parameters (Weijnen, 1998) such as those associated with the various stages of learning employed here, occurred at an equal level in WT and L7-PP2B mice. Likewise, we recorded free whisking behavior in head-restrained mice and found that WT and L7-PP2B mice showed bouts of rhythmic whisking at comparable frequencies, that both WT and L7-PP2B mice scanned the whole area within reach of their whiskers, and that they both actively whisked during the insertion and presence of the stimulus bar in all trials tested. These control data are particularly relevant as object localization in the horizontal dimension requires active whisking (Knutsen et al., 2006) and exploratory whisking in healthy mice typically occurs at frequencies 5-15Hz (Berg and Kleinfeld, 2003; Cao et al., 2012).

It is also possible that deficits in cerebellar sensory processing occur in L7-PP2B mice rather than motor deficits (Hartmann and Bower, 2001). We adapted our paradigm by beginning training of both genotypes with an association phase. This allowed a baseline performance measure to test whether both groups not only whisked equally well, but also responded well to sensory stimulation. We found these initial learning curves and responses to stimuli to be similar in both genotypes in this phase. Moreover, at the subsequent go and no- go trial testing (see Fig. 4), L7-PP2B performers were able to reach criteria (albeit more slowly) and showed similar performance levels indicating an ability to carry out the necessary responses to sensory stimuli.

Finally, since PP2B- and Cre-expressions are affected from early on in the L7-PP2B mutants, it is possible that their learning deficits in the whisker-based localization task result from aberrations in development rather than acute ongoing defects in cerebellar plasticity. If present at all, these potentially negative effects are probably relatively mild, since developmental compensation usually rescues negative confounders (Wulff et al., 2009) and since our electrophysiological recordings showed that the acute deficits in Purkinje cell activity of adult L7-PP2B mutants are in line with their putative deficits in potentiation and thereby learning deficits. Taken together, we conclude that L7-PP2B mice do not show overt abnormalities in rhythmicity, frequency or amplitude of either licking or whisker movements and that their learning deficits in the current whisker-based localization task are in line with the abnormalities in intrinsic plasticity and synaptic plasticity of their Purkinje cells.

## Potential role of the cerebellum in cognitive tasks

Over the past decade an active debate has emerged on the potential role of the cerebellum in cognition. Supportive evidence was not only obtained in neuropsychological studies of cerebellar patients, functional imaging studies of human subjects and tracing experiments in monkeys (Strick et al., 2009; Schmahmann, 2010; Timmann et al., 2010; Onuki et al., 2013), but also in behavioral studies of cerebellar cell-specific mutant mice, in which specific aspects of spatial navigation or repetitive behavior were affected (Burguiere et al., 2005; Rochefort et al., 2011; Tsai et al., 2012). Yet, it is not directly clear how to neutralize the argument that most of these so-called cognitive effects reflect small aberrations in sensorimotor activity such as the planning of eye movements (Glickstein et al., 2009). Moreover, we recently subjected four different cerebellar cell-specific mouse mutants, including L7-PP2B mice, to various cognitive tasks such as a sociability test, Morris watermaze, contextual and cued fear conditioning, and open-field anxiety test, and none of the mutants showed a consistent deficit in any cognitive function (Galliano et al., 2013). However, none of these cognitive tasks included a response window or demanded precise processing in the temporal domain with a resolution of tens to hundreds of milliseconds. Given that the role of cerebellar processing in motor control has been shown to be particularly relevant when precise temporal accuracy is required (De Zeeuw et al., 2011; Onuki et al., 2013), we reasoned that this facet might be paramount also for its control in cognitive function. We therefore undertook the current whisker-based localization study in which the temporal constraints play a prominent role, while the essential role of cerebral cortex in this task has been established (Brecht, 2007; Aronoff et al., 2010; O'Connor et al., 2010ab; Huber et al., 2012; Petreanu et al., 2012; Xu et al., 2012). Several of the present findings support the possibility that the cerebellum contributes to cognitive processing when temporal demands are critical. First, the findings that fewer L7-PP2B mice were able to learn the whisker-based localization task, that they needed more time and that their learning trajectories were considerably noisier than in WTs support the possibility of a general contribution of cerebellar processing in this particular cognitive task. Second, the findings that fine-tuning of the precise timing of learned responses of L7-PP2B mutants was especially deficient at short response windows and that the trained WT, but not L7-PP2B, mice showed a well-timed increase in licking just at the onset of the 500 ms RW, corroborate our hypothesis that the cerebellum contributes to cognitive processing in particular when temporal demands are engaged.

## How may the cerebellum contribute to temporal precision in cognitive functions?

Different parts of the cerebellar cortex may engage different coding schemes varying from pure rate coding to temporal coding (Heck et al., 2013). Given that we observed during trials an increase in both firing rate and variability (CV2) in the simple spike activity of WT Purkinje cells, while the firing rate of their complex spike was also increased, it is likely that both coding mechanisms play a role (De Zeeuw et al., 2011). Indeed, in L7-PP2B animals we did not observe

an increase in simple spike or complex spike firing frequency in the transition from inter-trial to trial periods, and the irregularity of their simple spike firing was consistently lower than that in WTs. While changes in rate coding might directly translate into differences in modulation amplitude and thereby rate activity of downstream targets (De Zeeuw et al., 1995), those in temporal coding may have a prominent impact on the precise timing of the activity of downstream targets (De Zeeuw et al., 2008; De Zeeuw et al., 2011). Pauses in simple spike activity, which are reflected in the irregularity of firing, can translate into prominent rebound firing in the cerebellar nuclei, which in turn can trigger the initiation of movements (Witter et al., 2013). Likewise, one could imagine that rebound firing in the nuclei affects well-timed initiation of activity in areas downstream of the thalamus that are involved in cognitive tasks. For the whisker-based localization task, these may include not only the barrel cortex and whisker motor cortex (Popa et al., 2013ab), but also the striatum (Hoshi et al., 2005; Bostan et al., 2010). Conditional discrimination tasks that require goal- directed acts are typically thought to involve the basal ganglia (Nishizawa et al., 2012; Hallock et al., 2012), which may process stop cues for cancelling actions such as during no-go trials (Schmidt et al., 2013). One could hypothesize that the differences in activity in the cerebellar microzones that employ rate coding (Heck et al., 2013; Zhou et al., 2013) explain the significant difference between the number of L7-PP2B and WT mice that exhibit successful learning at the long response window phase, whereas those in the cerebellar zones that employ predominantly temporal coding may explain the differences and deficits seen at the shorter response window phase and no-go trials.

## Acknowledgements

The authors wish to thank Dr. Karel Svoboda for help with the behavioral training and related apparatus, Kees Donkersloot, Froukje Zandstra and Alex Brouwer for excellent technical support and Dr. Jos van der Geest for advice on statistical analysis. We gratefully used the BIOTACT Whisker Tracking Tool (http://bwtt.sourceforge.net) for tracking whisker movements. This work was supported by funds for C.I.D.Z. from the Dutch Organization for Medical Sciences (ZonMw), Life Sciences (ALW), Senter (Neuro-Basic), and ERC-adv, CEREBNET, and C7 programs of the European Community.

The authors declare no competing financial interests.

## REFERENCES


Aronoff R, Matyas F, Mateo C, Ciron C, Schneider B, Petersen CC. (2010) Long-range connectivity of mouse primary somatosensory barrel cortex. Eur J Neurosci. 31(12):2221-33. Review.

Axelrad H, Crepel F (1977) Représentation sélective des vibrisses mystaciales au niveau des cellules de Purkinje du cervelet par la voie de fibres grimpantes chez le rat. C R Acad Sci Hebd Seances Acad Sci D 284: 1321-1324.

Barski JJ, Dethleffsen K, Meyer M (2000) Cre recombinase expression in cerebellar Purkinje cells. Genesis 28:93-98.

Berg RW, Kleinfeld D (2003) Rhythmic whisking by rat: retraction as well as protraction of the vibrissae is under active muscular control. J Neurophysiol 89:104-117.

Bosman LWJ, Koekkoek SKE, Shapiro J, Rijken BFM, Zandstra F, van der Ende B, Owens CB, Potters JW, de Gruijl JR, Ruigrok TJH, De Zeeuw CI (2010) Encoding of whisker input by cerebellar Purkinje cells. J Physiol 588:3757-3783.

Bosman LWJ, Houweling AR, Owens CB, Tanke N, Shevchouk OT, Rahmati N, Teunissen WHT, Ju C, Gong W, Koekkoek SKE, De Zeeuw CI (2011) Anatomical pathways involved in generating and sensing rhythmic whisker movements. Front Integr Neurosci 5:53.

Brecht M. (2007) Barrel cortex and whisker-mediated behaviors. Curr Opin Neurobiol. 17(4):408-16. Review.

Bryant JL, Boughter JD, Gong S, Ledoux MS, Heck DH (2010) Cerebellar cortical output encodes temporal aspects of rhythmic licking movements and is necessary for normal licking frequency. European Journal of Neuroscience 32:41-52.

Burguière E, Arleo A, Hojjati M, Elgersma Y, De Zeeuw CI, Berthoz A, Rondi-Reig L (2005) Spatial navigation impairment in mice lacking cerebellar LTD: a motor adaptation deficit? Nat Neurosci 8:1292-1294.

Cao Y, Roy S, Sachdev RN, Heck DH (2012) Dynamic correlation between whisking and breathing rhythms in mice. J Neurosci 32:1653-1659.

Carvell GE, Simons DJ (1990) Biometric analyses of vibrissal tactile discrimination in the rat. J Neurosci 10:2638-2648.

De Zeeuw CI, Wylie DR, Stahl JS, Simpson JI. (1995) Phase relations of Purkinje cells in the rabbit flocculus during compensatory eye movements. J Neurophysiol. 74(5):2051-64.

De Zeeuw CI, Hoebeek FE, Schonewille M. (2008) Causes and consequences of oscillations in the cerebellar cortex. Neuron. 58(5):655-8.

De Zeeuw CI, Hoebeek FE, Bosman LWJ, Schonewille M, Witter L, Koekkoek SK (2011) Spatiotemporal firing patterns in the cerebellum. Nat Rev Neurosci 12:327-344.

Fukabori R, Okada K, Nishizawa K, Kai N, Kobayashi K, Uchigashima M, Watanabe M, Tsutsui Y, Kobayashi K. (2012) Striatal direct pathway modulates response time in execution of visual discrimination. Eur J Neurosci 35: 784-797.

Galliano E, Potters JW, Elgersma Y, Wisden W, Kushner SA, De Zeeuw CI, Hoebeek FE (2013) Synaptic transmission and plasticity at inputs to murine cerebellar Purkinje cells are largely dispensable for standard non-motor tasks. J Neurosci 33:12599-12618.

Gao Z, Van Beugen BJ, De Zeeuw CI (2012) Distributed synergistic plasticity and cerebellar learning. Nat Rev Neurosci 13:619-635.

Grodd W, Hülsmann E, Lotze M, Wildgruber D, Erb M (2001) Sensorimotor mapping of the human cerebellum: fMRI evidence of somatotopic organization. Hum Brain Mapp 13:55-73.

Hallock HL, Arreola AC, Shaw CL, Griffin AL (2012) Dissociable roles of the dorsal striatum and dorsal hippocampus in conditional discrimination and spatial alternation T-maze tasks. Neurobiol Learn Mem 100:108-116.

Hansel C, Linden DJ, D'Angelo E (2001) Beyond parallel fiber LTD: the diversity of synaptic and non-synaptic plasticity in the cerebellum. Nat Neurosci 4:467-475.

Hartmann MJ, Bower JM (2001) Tactile responses in the granule cell layer of cerebellar folium crus IIa of freely behaving rats. J Neurosci. 21:3549-63.

Hartmann MJZ (2009) Active touch, exploratory movements, and sensory prediction. Integr Comp Biol 49:681-690.

Hayar A, Bryant JL, Boughter JD, Heck DH (2006) A low-cost solution to measure mouse licking in an electrophysiological setup with a standard analog-to-digital converter. J Neurosci Methods 153:203-207.

Heck DH, De Zeeuw CI, Jaeger D, Khodakhah K, Person AL. (2013) The Neuronal Code(s) of the Cerebellum. J Neurosci. 33(45):17603-9.

Hoshi E, Tremblay L, Féger J, Carras PL, Strick PL (2005) The cerebellum communicates with the basal ganglia. Nat Neurosci 8:1491–1493.

Horowitz GP, Stephan FK, Smith JC, Whitney G (1977) Genetic and environmental variability in lick rates of mice. Physiol Behav 19:493-496.

Huber D, Gutnisky DA, Peron S, O'Connor DH, Wiegert JS, Tian L, Oertner TG, Looger LL, Svoboda K (2012) Multiple dynamic representations in the motor cortex during sensorimotor learning. Nature 484:473-478.

Ito M (2001) Cerebellar long-term depression: characterization, signal transduction, and functional roles. Physiol Rev 81:1143-1195.

Kleinfeld D, Deschênes M (2011) Neuronal basis for object location in the vibrissa scanning sensorimotor system. Neuron 72:455-468.

Knutsen PM, Pietr M, Ahissar E (2006) Haptic object localization in the vibrissal system:behavior and performance. J Neurosci 26:8451-8464.

Koekkoek SKE, Hulscher HC, Dortland BR, Hensbroek RA, Elgersma Y, Ruigrok TJH, De Zeeuw CI (2003) Cerebellar LTD and learning-dependent timing of conditioned eyelid responses. Science 301:1736-1739.

Krupa DJ, Matell MS, Brisben AJ, Oliveira LM, Nicolelis MAL (2001) Behavioral properties of the trigeminal somatosensory system in rats performing whisker-dependent tactile discriminations. J Neurosci 21:5752-5763.

Lang EJ, Sugihara I, Llinás R (2006) Olivocerebellar modulation of motor cortex ability to generate vibrissal movements in rat. J Physiol 571:101-120.

Moore JD, Deschênes M, Furuta T, Huber D, Smear MC, Demers M, Kleinfeld D (2013) Hierarchy of orofacial rhythms revealed through whisking and breathing. Nature 497:205-210.

O'Connor DH, Peron SP, Huber D, Svoboda K (2010a) Neural activity in barrel cortex underlying vibrissa-based object localization in mice. Neuron 67:1048-1061.

O'Connor DH, Clack NG, Huber D, Komiyama T, Myers EW, Svoboda K (2010b) Vibrissa- based object localization in head-fixed mice. J Neurosci 30:1947-1967.

Okamoto T, Shirao T, Shutoh F, Suzuki T, Nagao S (2011) Post-training cerebellar cortical activity plays an important role for consolidation of memory of cerebellum-dependent motor learning. Neurosci Lett 504:53-56.

Onuki Y, Van Someren EJ, De Zeeuw CI, Van der Werf YD (2013) Hippocampal-cerebellar interaction during spatio-temporal prediction. Cereb Cortex 2013. In Press.

Perkon I, Kosir A, Itskov PM, Tasic J, Diamond ME (2011) Unsupervised quantification of whisking and head movement in freely moving rodents. J Neurophysiol 105:1950-1962.

Petreanu L, Gutnisky DA, Huber D, Xu NL, O'Connor DH, Tian L, Looger L, Svoboda K (2012) Activity in motor-sensory projections reveals distributed coding in somatosensation. Nature 489:299-303.

Popa D, Spolidoro M, Proville RD, Guyon N, Belliveau L, Léna C (2013a) Functional role of the cerebellum in gamma-band synchronization of the sensory and motor cortices. J Neurosci 33:6552-6556.

Popa T, Velayudhan B, Hubsch C, Pradeep S, Roze E, Vidailhet M, Meunier S, Kishore A (2013b) Cerebellar processing of sensory inputs primes motor cortex plasticity. Cereb Cortex 23:305-314.

Schmahmann JD (2010) The role of the cerebellum in cognition and emotion: personal reflections since 1982 on the dysmetria of thought hypothesis, and its historical evolution from theory to therapy. Neuropsychol Rev 20:236-260.

Schonewille M, Belmeguenai A, Koekkoek SK, Houtman SH, Boele HJ, van Beugen BJ, Gao Z, Badura A, Ohtsuki G, Amerika WE, Hosy E, Hoebeek FE, Elgersma Y, Hansel C, De Zeeuw CI (2010) Purkinje cell-specific knockout of the protein phosphatase PP2B impairs potentiation and cerebellar motor learning. Neuron 67:618-628.

Shin SL, Hoebeek FE, Schonewille M, De Zeeuw CI, Aertsen A, De Schutter E (2007) Regular patterns in cerebellar Purkinje cell simple spike trains. PLoS One 2:e485.

Strick PL, Dum RP, Fiez JA (2009) Cerebellum and nonmotor function. Ann Rev Neurosci 32:413-434.

Timmann D, Drepper J, Frings M, Maschke M, Richter S, Gerwig M, Kolb FP (2010) The human cerebellum contributes to motor, emotional and cognitive associative learning. A review. Cortex 46:845-857.

Tsai PT, Hull C, Chu Y, Greene-Colozzi E, Sadowski AR, Leech JM, Steinberg J, Crawley JN, Regehr WG, Sahin M (2012) Autistic-like behaviour and cerebellar dysfunction in Purkinje cell *Tsc1* mutant mice. Nature 488:647-651.

Weijnen JAWM (1998) Licking behavior in the rat: measurement and situational control of licking frequency. Neurosci Biobehav Rev 22:751-760.

Wiesenfeld Z, Halpern BP, Tapper DN (1977) Licking behavior: evidence of hypoglossal oscillator. Science 196:1122-1124.

Witter L, Canto CB, Hoogland TM, de Gruijl JR, De Zeeuw CI. (2013) Strength and timing of motor responses mediated by rebound firing in the cerebellar nuclei after Purkinje cell activation. Front Neural Circuits. 7:133.

Wulff P, Schonewille M, Renzi M, Viltono L, Sassoè-Pognetto M, Badura A, Gao Z, Hoebeek FE, van Dorp S, Wisden W, Farrant M, De Zeeuw CI. (2009) Synaptic inhibition of Purkinje cells mediates consolidation of vestibulo-cerebellar motor learning. Nat Neurosci. 12:1042-9.

Xu NL, Harnett MT, Williams SR, Huber D, O'Connor DH, Svoboda K, Magee JC (2012) Nonlinear dendritic integration of sensory and motor input during an active sensing task. Nature 492:247-251.

Yamamoto T, Matsuo R, Fujiwara T, Kawamura Y (1982) EMG activities of masticatory muscles during licking in rats. Physiol Behav 29:905-913.

Zeng H, Chattarji S, Barbarosie M, Rondi-Reig L, Philpot BD, Miyakawa T, Bear MF, Tonegawa S (2001) Forebrain-specific calcineurin knockout selectively impairs bidirectional synaptic plasticity and working/episodic-like memory. Cell 107:617-629.

Zhou H, Lin Z, Voges K, Gao Z, Ruigrok TJ, Hoebeek FE, De Zeeuw CI, Schonewille M (2013) Cerebellar modules operate at different frequencies. Abstract, Gordon Conference on Cerebellum, Aug. 11–16, 2013, New London, NH.

# 3

# Potentiation of cerebellar Purkinje cells facilitates whisker reflex adaptation through increased simple spike activity

Vincenzo Romano[1,5], Licia De Propris[1,2,5], Laurens W.J. Bosman[1,5,*], Pascal Warnaar[1], Michiel M. ten Brinke[1], Sander Lindeman[1], Chiheng Ju[1], Arthiha Velauthapillai[1], Jochen K. Spanke[1], Emily Middendorp Guerra[1], Tycho M. Hoogland[1,2], Mario Negrello[1], Egidio D'Angelo[3,4] and Chris I. De Zeeuw[1,2,*]

[1]Department of Neuroscience, Erasmus MC, Rotterdam, 3000 CA, the Netherlands
[2]Netherlands Institute for Neuroscience, Royal Academy of Arts and Sciences, Amsterdam, 1105 BA, the Netherlands
[3]Department of Brain and Behavioral Sciences, University of Pavia, Pavia, 27100, Italy
[4]Brain Connectivity Center, Instituto Fondazione C. Mondino, Pavia, 27100, Italy
[5]These authors contributed equally.
[*]Correspondence to: Chris I. De Zeeuw, Department of Neuroscience, PO Box 2040, 3000 CA Rotterdam, the Netherlands, c.dezeeuw@erasmusmc.nl or Laurens W.J. Bosman, Department of Neuroscience, PO Box 2040, 3000 CA Rotterdam, the Netherlands, l.bosman@erasmusmc.nl

## SUMMARY

Cerebellar plasticity underlies motor learning. However, how the cerebellum operates to enable learned changes in motor output is largely unknown. We developed a sensory-driven adaptation protocol for reflexive whisker protraction and recorded Purkinje cell activity from crus 1 and 2 of awake mice. Before training, simple spikes of individual Purkinje cells correlated during reflexive protraction with the whisker position without lead or lag. After training, simple spikes and whisker protractions were both enhanced with the spiking activity now leading behavioral responses. Neuronal and behavioral changes did not occur in two cell-specific mouse models with impaired long-term potentiation at their parallel fiber to Purkinje cell synapses. Consistent with cerebellar plasticity rules, increased simple spike activity was prominent in cells with low complex spike response probability. Thus, potentiation at parallel fiber to Purkinje cell synapses may contribute to reflex adaptation and enable expression of cerebellar learning through increases in simple spike activity.

## IMPACT STATEMENT

Physiological and behavioral analyses show that expression of cerebellar whisker learning can be mediated by increased simple spike activity, depending on LTP induction at parallel fiber to Purkinje cell synapses.

## INTRODUCTION

Active touch is important for exploring our environment, allowing us to assess the shape, substance and movements of objects and organisms around us (Prescott et al., 2011). Throughout the animal kingdom, various systems have evolved for this purpose; these include for example the antennae of insects, the fingertips of primates and the well-developed whisker systems of rodents and sea mammals (Ahl, 1986, Dehnhardt et al., 2001, Staudacher et al., 2005, Dere et al., 2007, Anjum and Brecht, 2012). Activation of these sensory organs can provoke reactive movements, often occurring as a reflex (Nguyen and Kleinfeld, 2005, Bellavance et al., 2017, Brown and Raman, 2018, Staudacher et al., 2005). For survival it is important to maintain optimal control of such reflexes in daily life and to be able to adapt these movements (Voigts et al., 2015, Anjum and Brecht, 2012, Arkley et al., 2017).



Given the impact of cerebellar plasticity on a wide variety of motor learning tasks (Herzfeld et al., 2015, Herzfeld et al., 2018, Medina and Lisberger, 2008, Ten Brinke et al., 2015, Thier et al., 2002, Voges et al., 2017, Yang and Lisberger, 2017), it can be anticipated that adaptation of reflexive whisker movements is also partly controlled by plastic processes in the cerebellum. Historically, most studies on cerebellar learning have suggested that long-term depression (LTD) at the parallel fiber to Purkinje cell (PC) synapse may act as the main cellular mechanism underlying induction of cerebellar motor learning (Albus, 1971, Konnerth et al., 1992, Ito, 2003, Koekkoek et al., 2003, Medina and Lisberger, 2008, Boele et al., 2018, Narain et al., 2018). However, parallel fiber LTD is unlikely to be the sole cellular mechanism underlying cerebellar learning (Gao et al., 2012, Hansel et al., 2001, D'Angelo et al., 2016). Short-term forms of plasticity probably also contribute, as some forms of behavioral adaptation can be linked to changes in PC activity during the previous trial (Yang and Lisberger, 2014, Herzfeld et al., 2018). Moreover, long-term potentiation (LTP) of parallel fiber to PC synapses may also be relevant, as various PC-specific mutants with impaired LTP show deficits in cerebellar learning (Schonewille et al., 2010, Schonewille et al., 2011, Rahmati et al., 2014, Gutierrez-Castellanos et al., 2017). Possibly, different cerebellar cellular mechanisms dominate the induction of different forms of learning, dependent on the requirements of the downstream circuitries involved (De Zeeuw and Ten Brinke, 2015, Suvrathan et al., 2016).

While many studies have focused on the synaptic mechanism(s) that may induce cerebellar motor learning, the spiking mechanisms that are responsible for the expression thereof remain relatively unexplored. To date, whereas evidence is emerging that the expression of conditioned eyeblink responses is mediated by a long-lasting *suppression* of simple spikes of PCs in the deep fissure of lobule simplex (Heiney et al., 2014, Halverson et al., 2015, Ten Brinke et al., 2015), it is unclear to what extent enduring *increases* in simple spike activity can also contribute to the expression of cerebellar learning, and if so for what forms of learning. Here, we developed a novel whisker training paradigm that is likely to generate plasticity in the cerebellar cortex and to produce increases in simple spike activity at the PC level following

induction of LTP at the parallel fiber to PC synapse (D'Angelo et al., 2001, Lev-Ram et al., 2002, Lev-Ram et al., 2003, Coesmans et al., 2004, Ramakrishnan et al., 2016, van Beugen et al., 2013). Indeed, we show that a brief period of 4 Hz air-puff stimulation of the whiskers can enhance touch-induced whisker protraction as well as PC simple spike firing for tens of minutes. Moreover, these behavioral and neuronal changes are both absent in two independent mouse mutant lines deficient for parallel fiber to PC LTP, bridging the putative mechanism of memory expression with that of memory induction.

## RESULTS

### Touch-induced whisker protraction

The large facial whiskers are a prime source of sensory information for many mammals, in particular for rodents that can make elaborate movements with their large facial whiskers (Arkley et al., 2017, Brecht, 2007, Welker, 1964, Bosman et al., 2011, Vincent, 1913). It has been noted that passive touch can trigger active whisker movements in mice (Bellavance et al., 2017, Brown and Raman, 2018, Nguyen and Kleinfeld, 2005, Ferezou et al., 2007), but this behavior has not been described in great detail yet. Here, we studied whisker movements following rostro-caudal air-puff stimulation of the whisker pad in 16 awake, head-restrained mice (Figure 1A-C). The air-puffer was placed in such a way that most, if not all, large mystacial whiskers were affected by the air flow from the front. The mice made active whisker protractions following the retractions induced by the air flow in the large majority (82%) of stimulus trials (Figure 1D-E; Figure 1 – figure supplement 1C). Because of the systematic full-field air-flow from the front, the touch-induced protraction was typically performed by all whiskers simultaneously (*data not shown*), which is in line with the presumed reflexive nature of this movement (Bellavance et al., 2017, Brown and Raman, 2018, Nguyen and Kleinfeld, 2005). Moreover, as reported previously (Ferezou et al., 2007), the touch-induced whisker protraction was followed in about half the trials (51%) by extended periods of active whisker movements during the subsequent 200 ms interval (Figure 1D; Figure 1 – figure supplement 1A-C). However, under our experimental conditions with a 2 s inter-trial interval, spontaneous whisking in between the stimuli was relatively rare. Across all 16 mice measured, we found spontaneous movements (with an amplitude exceeding 10°) only in 12% of the 100 trials per mouse during the 200 ms interval prior to stimulus onset.

To find out whether touch-induced whisker protraction can indeed be described as a reflex (Bellavance et al., 2017, Brown and Raman, 2018, Nguyen and Kleinfeld, 2005), we wanted to know to what extent the movements also show signs characteristic of startle responses or voluntary events, which have a different identity. A startle response would be expected to be not only highly stereotypic, but to also show relatively little direction-specificity, and to reveal signs of pre-pulse inhibition (Gogan, 1970, Swerdlow et al., 1992, Moreno-Paublete et al.,

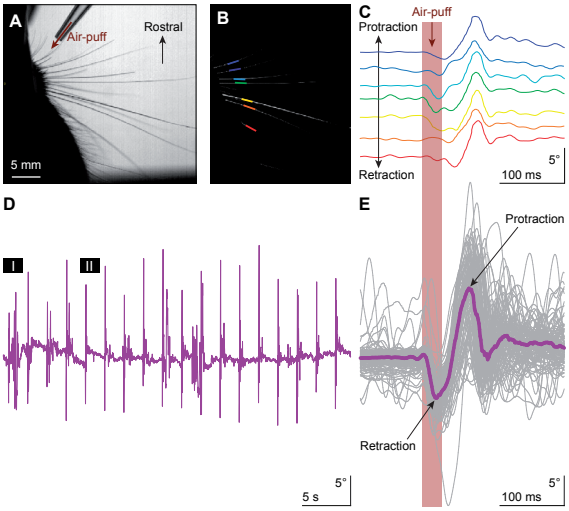


**Figure 1.** Touch-induced whisker protraction

A brief (30 ms) air-puff to the whisker pad induces a reflexive protraction of all large mystacial whiskers. Our experiments were performed in awake, head-restrained mice that had all whiskers intact. **A.** Photograph showing a part of the mouse head with the large facial whiskers and the location and direction of the air-puffer (top). **B.** The large facial whiskers were recognized in high-speed videos (1 kHz full-frame rate) by a tracking algorithm and individual whiskers are color-coded. **C.** Air-puff stimulation triggered stereotypic whisker movements consisting of an initial backward movement followed by active protraction. Deflection angles of individually tracked whiskers are denoted in distinct colors (same color scheme as in **B**). **D.** The mean whisker angle during 0.5 Hz air-puff stimulation of the whisker pad from a representative mouse. During approximately half the trials, the active protraction was only a single sweep; in the other traces multiple sweeps were observed. Prolonged periods of active whisking were rare. The periods marked "I" and "II" are enlarged in Figure 1 – figure supplement 1A. **E.** To indicate the variability in whisker behavior, 100 trials of the same experiment were superimposed. The thick colored line indicates the median. The retraction due to the air-puff is followed by an active protraction.

The following supplements are available for Figure 1:

Figure supplement 1. Whisker movements are largely restricted to the period after the air-puff

Figure supplement 2. Air-puffs induce reflexive whisker movements

2017). Instead, if the air-puff triggered a conscious, explorative movement, the animal would most likely make spontaneous movements towards the source of the air-puff, dependent on its specific position. To explore these possibilities, we placed a second air-puffer at the caudal side of the whisker field and a third air-puffer at the front of the contralateral whisker field, and we provided air-puffs from the three different orientations, intermingling trials with and without brief pre-pulses in random order (Figure 1 – figure supplement 2A). An air-puff from the front on the ipsilateral side induced a retraction prior to the active protraction. Such a retraction was mostly absent when stimulating from the back. Contralateral stimulation also evoked a slight retraction, followed by a much larger forward sweep (Figure 1 – figure supplement 2B-E; Table S1). Thus, applying the air-puff from different angles produced different retractions and different subsequent protractions, arguing against a stereotypical startle behavior that occurs independent from the stimulus conditions. Moreover, we did not observe a diminishing effect of the weaker pre-pulse on the reaction to the stronger pulse ($p$ = 0.268; Dunn's

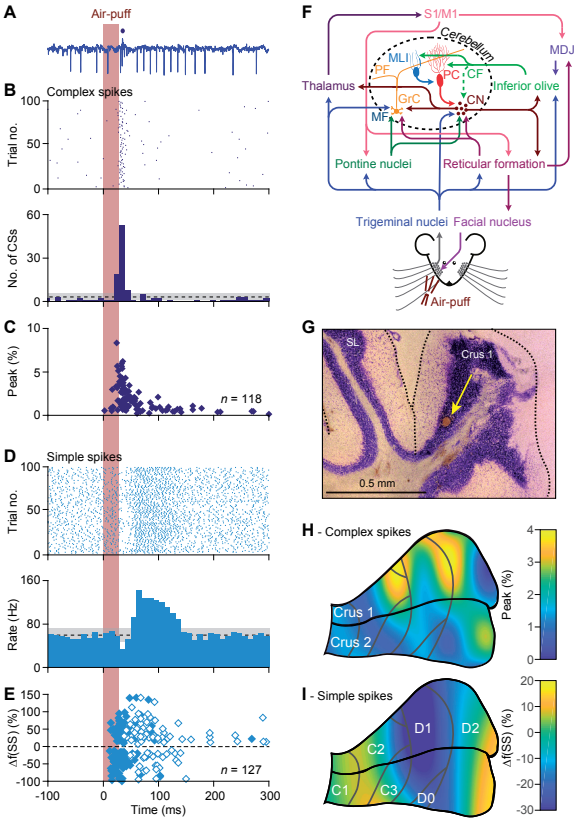


**Figure 2.** Anatomical distribution of Purkinje cell responses to whisker pad stimulation

**A.** Representative extracellular recording of a cerebellar Purkinje cell (PC) in an awake mouse showing multiple simple spikes (vertical deflections) and a single complex spike that is indicated by a blue dot above the trace. **B.** Scatter plot and histogram of complex spike firing around the moment of air-puff stimulation of the whisker pad (applied at 0.5 Hz) of the same PC. **C.** The latencies vs. the peak of the complex spike responses of all 118 PCs with a significant complex spike response. Note that a minority of the PCs showed relatively long latency times. **D.** Simple spike responses of the same PC showing a bi-phasic response: first inhibition, then facilitation. Note that the simple spike firing frequency of this PC at rest is about 60-70 Hz. **E.** Peak amplitudes and peak latency times of simple spike responses of all 127 PCs showing a significant simple spike response to whisker pad stimulation. As simple spike responses were often found to be bi-phasic, we represented the first phase with closed and the second phase with open symbols. Non-significant responses are omitted. **F.** Simplified scheme of the somatosensory pathways from the whisker pad to the PCs and of the motor pathways directing whisker movement. The information flows from the whisker pad via the trigeminal nuclei and the thalamus to the primary somatosensory (S1) and motor cortex (M1). S1 and M1 project to the inferior olive via the nuclei of the meso-diencephalic junction (MDJ) and to the pontine nuclei. Both the inferior olive and the pontine nuclei also receive direct inputs from the trigeminal nuclei. The mossy fibers (MF) from the pontine nuclei converge with direct trigeminal MF and those of the reticular formation on the cerebellar granule cells (GrC) that send parallel fibers (PF) to the PCs. The inferior olive provides climbing fibers (CF) that form extraordinarily strong synaptic connections with the PCs. Both the PFs and the CFs also drive feedforward inhibition to PCs via molecular layer interneurons (MLI). The GABAergic PCs provide the sole output of the cerebellar cortex that is directed to the cerebellar nuclei (CN). The CN sends the cerebellar output both upstream via the thalamus back to the cerebral cortex and downstream to motor areas in the brainstem and spinal cord. The whisker pad muscles are under control of the facial nucleus which is mainly innervated via the reticular formation. Several feedback loops complement these connections. For references, see main text. **G.** For most of the PC recordings in this study, the anatomical locations were defined by a combination of surface photographs and electrolytic lesions made after completion of the recordings. An example of such a lesion in crus 1 is shown here in combination with a Nissl staining. SL = simple lobule. **H**. Heat map showing the anatomical distribution of the strength

pairwise post-hoc test after Friedman's ANOVA; $p = 0.003$; Fr = 13.933; df = 3). Finally, we also did not observe distinct explorative movements linked to the puff sources, which might have suggested dominant voluntary components (Figure 1 - figure supplement 2B-C). Altogether, the reactive nature of the touch-induced whisker movements in the absence of characteristic signs of startle or voluntary responses indicates that the air-puff induced protraction is indeed a reflexive movement.



## Anatomical distribution of Purkinje cell responses to whisker pad stimulation

In line with the fact that PCs receive sensory whisker input not only directly from the brainstem but also indirectly from thalamo-cortical pathways (Figure 2F) (Kleinfeld et al., 1999, McElvain et al., 2018, Bosman et al., 2011, Brown and Raman, 2018, Kubo et al., 2018), the dynamics of their responses upon whisker stimulation are heterogeneous (Brown and Bower, 2001, Loewenstein et al., 2005, Bosman et al., 2010, Chu et al., 2011). To study the anatomical distribution of these responses within cerebellar lobules crus 1 and crus 2 we mapped the complex spike and simple spike firing of their PCs following ipsilateral whisker pad stimulation with air-puffs in awake mice. Of the 132 single-unit PCs from which we recorded, 118 (89%) showed significant complex spike responses, albeit with large variations in latency and amplitude (Figure 2A-C, Figure 2 – figure supplement 1A-B). We considered a response to be significant if it passed the threshold of 3 s.d. above the average of the pre-stimulus interval. Cluster analysis revealed that in terms of complex spike modulation PCs can better be considered as two separate clusters rather than a continuum spectrum (indicated by the lowest absolute BIC value for two components (437, compared to 490 and 442 for one and three components, respectively; Figure 2 – figure supplement 1D). We refer to the cells of the cluster with the higher complex spike response probability as "strong" (34%, with a peak response above 1.98%; see Methods) and the other as "weak" (66%) responders (Figure 2 – figure supplement 1D-F). Similarly, of the 132 recorded PCs 127 (96%) showed a significant simple spike response. Simple spike responses were often bi-phasic, consisting of a period of inhibition followed by one of excitation, or vice versa (Figure 2D-E, Figure 2 – figure supplement 1C). The trough of the simple spike responses typically correlated in a reciprocal fashion with the peak of the complex spike responses (Figure 2A-E; Figure 2 – figure supplement 1A-C) (De Zeeuw et al., 2011, Zhou et al., 2014, Badura et al., 2013). Only 2 PCs, out of the 132, did not show any significant modulation (i.e. for neither complex spikes nor simple spikes). To chart the spatial distribution of the PCs with different

of the complex spike responses projected on the surface of crus 1 and crus 2. The locations of all 132 recorded PCs were attributed to a rectangular grid. The average complex spike response strength was calculated per grid position and averaged between each grid position and its neighbor. The grey lines indicate the borders to the cerebellar zones (see Figure 2 - figure supplement 2D). **I.** The same for the variation in the first phase of the simple spike responses. Note that for the simple spikes the blue colors indicate suppression of firing rather than the absence of a response.

The following supplements are available for Figure 2:

Figure supplement 1. Diversity in Purkinje cell responses

Figure supplement 2. Anatomy of the whisker region in the cerebellar hemispheres

response kinetics upon whisker stimulation we first combined electrolytic lesions (Figure 2G) with reconstructions of the electrode entry points, generating a map of the locations of the PCs from which we recorded with the quartz/platinum electrodes ($n$ = 132). Complex spike responses to whisker stimulation were found to be especially strong in parts of crus 1 overlapping with large areas of the C2, D1 and D2 zones (Figure 2H), whereas the primary simple spike responses were predominantly facilitating in adjacent areas in the medial and lateral parts of crus 1 and crus 2, as predicted by the overall tendency for reciprocity (Figure 2H-I; Figure 2 – figure supplement 1G-H). This distribution was verified using double-barrel glass pipettes with which we injected the neural tracer, BDA 3000, at the recording spot after recording complex spike responses. Following identification of the source of the climbing fibers in the inferior olive and the projection area in the cerebellar nuclei (Figure 2 – figure supplement 2A-C), we defined the cerebellar area in which the recorded PC was located (Apps and Hawkes, 2009, Voogd and Glickstein, 1998). These experiments confirmed that the PCs with strong complex spike responses were situated most prominently in centro-lateral parts of crus 1, whereas the PCs with weak complex spike responses were predominant in adjacent areas in crus 1 and crus 2 (Figure 2 – figure supplement 2D).

## Large reflexive whisker protractions are preceded by complex spikes

As complex spikes have been reported to be able to encode, at the start of a movement, the destination of arm movements (Kitazawa et al., 1998), we wondered whether a similar association could be found for whisker movements. Therefore, we asked whether trials that started with a complex spike involved larger or smaller protractions. To this end, we separated all trials of a session based upon the presence or absence of a complex spike during the first 100 ms after stimulus onset in a single PC. It turned out that during the trials with a complex spike, the protraction was significantly larger (see Figure 3A for a single PC; Figure 3B for the population of 55 PCs of which we had electrophysiological recordings during whisker tracking and that responded to air-puff stimulation). A direct comparison between the timing of the complex spike response and the difference in whisker position between trials with and without a complex spike revealed that the peak in complex spike activity preceded the moment of maximal difference in position by 63 ± 4 ms (mean ± SEM; $n$ = 55; Figure 3C-D). The maximal difference in protraction in trials with a complex spike equaled 0.80° (median, with IQR of 2.80°; $p < 0.001$), whereas this was only 0.28° (0.92°) for retraction ($p$ = 0.002; Wilcoxon matched pairs tests, significant after Bonferroni correction for multiple comparisons: $\alpha = 0.05/3 = 0.017$) (Figure 3E). These findings imply that trials that started with a complex spike showed bigger whisker protractions than those without a complex spike.

We next questioned whether there was a correlation between the strength of the complex spike response and the difference in maximal protraction. This did not seem to be the case (R = 0.119; $p$ = 0.386; Pearson correlation; Figure 3 – figure supplement 1A). Thus, in general, the complex spike of any PC showing whisker-related complex spike activity could have a similar

predictive power for the amplitude of the subsequent protraction. In line with this, a map showing the distribution of the PCs based upon the correlation of their complex spikes with whisker protraction was fairly homogeneous. Only in an area overlapping with the rostral part of crus 1, a small cluster of PCs was observed whose complex spikes correlated with an unusually large difference in protraction (Figure 3 – figure supplement 1B). However, since sensory-induced complex spikes were typically more frequent in lateral crus 1, PCs in this area appeared to have overall a stronger correlation with increased touch-induced whisker protraction than the PCs in the surrounding areas (Figure 3 – figure supplement 1C).



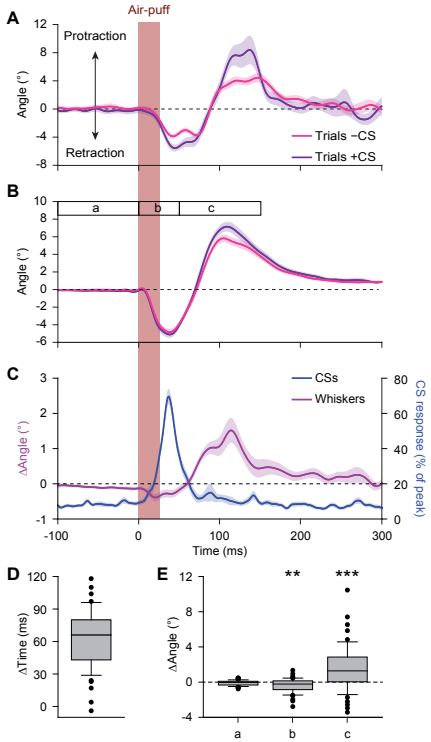


**Figure 3.** Large reflexive whisker protractions are preceded by complex spikes

**A.** Upon sorting the whisker traces based on the presence (violet) or absence (magenta) of a complex spike (CS) produced by a simultaneously recorded PC in the first 100 ms after stimulus onset, it is apparent that the trials with a complex spike tended to have a stronger protraction. **B.** This observation was confirmed in the population of PCs with a significant complex spike response to air-puff stimulation ($n$ = 55). **C.** Averaged convolved peri-stimulus time histograms of complex spikes (*blue*) and the averaged difference in whisker position (*purple*) between trials with and without complex spikes. Complex spikes precede the observed differences in movement. Shaded areas indicate s.d. (**A**) or SEM (**B** and **C**). **D.** Time intervals between the peak of the complex spike response and the moment of maximal difference in whisker position between trials with and without complex spikes, indicating that the complex spikes lead the whisker movement by approximately 60 ms. **E.** Changes in average whisker angle before stimulation (period a; see time bar in panel **B**), in maximal retraction (period b) and in maximal protraction (period c) between trials with and without a complex spike in the 100 ms after an air-puff. * $p > 0.05$; ** $p < 0.01$; *** $p < 0.001$ (Wilcoxon matched pairs tests (with Bonferroni correction for multiple comparisons in **E**)). See also Source Data file.

The following supplements are available for Figure 3:

Figure supplement 1. Correlation between complex spike firing and whisker protraction especially strong in the D2 zone

Figure supplement 2. Coherent complex spike firing is specifically enhanced by whisker pad stimulation

Previous studies showed that motor control can be related to the coherence of complex spike firing of adjacent PCs (Mukamel et al., 2009, Hoogland et al., 2015). We therefore expected to observe also increased coherence at the trial onsets in our experiments. To test this, we performed two-photon $Ca^{2+}$ imaging to study the behavior of adjacent groups of PCs in crus 1 around the moment of whisker pad air-puff stimulation in awake mice. After injection of the $Ca^{2+}$-sensitive dye Cal-520 we could recognize the dendrites of PCs as parasagittal stripes, each of which showed fluorescent transients at irregular intervals (Figure 3 – figure supplement 2A-B). Previous studies identified these transients as the result of PC complex spike firing (Ozden et al., 2008, Tsutsumi et al., 2015, Schultz et al., 2009, De Gruijl et al., 2014). Occasionally, signals could be found that were shared by many PCs, even in the absence of sensory stimulation (Figure 3 – figure supplement 2B) in line with earlier reports (Ozden et al., 2009, De Gruijl et al., 2014, Mukamel et al., 2009, Schultz et al., 2009). Upon whisker pad stimulation, however, complex spike firing occurred much more often collectively in multiple Purkinje cells (Figure 3 – figure supplement 2C). To quantify this form of coherent firing, we counted the number of complex spikes fired per frame (of 40 ms) and determined the level of coherence using cross-correlation analyses (Figure 3 – figure supplement 2D) (see also Ju et al., (2018)). The levels of coherence increased to such strength that they were extremely unlikely to have occurred by the increase in firing frequency alone (compared to a re-distribution of all events based on a Poisson distribution; Figure 3 – figure supplement 2E). In other words, firing of a single or a few PCs was the dominant mode of activity in the absence of stimulation, and this changed towards the involvement of multiple PCs upon stimulation, firing coherently as can be seen in the change in distribution of coherently active PCs (Figure 3 – figure supplement 2F-G). We conclude that groups of adjacent PCs respond to whisker pad stimulation by increased complex spike firing with an enhanced level of coherence, which is likely to further facilitate the occurrence of bigger whisker reflexes (see above).

## Instantaneous simple spike firing correlates with whisker protraction during reflex

The firing rate of simple spikes has been shown to correlate with whisker position: in the large majority of PCs, simple spike firing is correlated with protraction and in a minority it correlates with retraction (Brown and Raman, 2018, Chen et al., 2016). This led us to study the correlation in simple spike firing during touch-induced whisker protraction. At first sight, variation in simple spike firing roughly correlated to periods with whisker movement (Figure 4A-B). To study this in more detail, we made use of the inter-trial variations in simple spike rate and whisker position, allowing us to make a correlation matrix between these two variables on a trial-by-trial basis (see Ten Brinke et al., 2015). In a representative example (Figure 4C), the whisker protraction and peak in simple spike firing were roughly simultaneous. In the correlation matrix, this is visualized by the yellow color along the 45° line. This turned out to be the general pattern in 25 of the 56 PCs (45%) of which we had electrophysiological recordings during whisker tracking

(Figure 4D). In all of these 25 PCs, there was a positive correlation between instantaneous simple spike firing and whisker protraction that occurred relatively late during the movement,

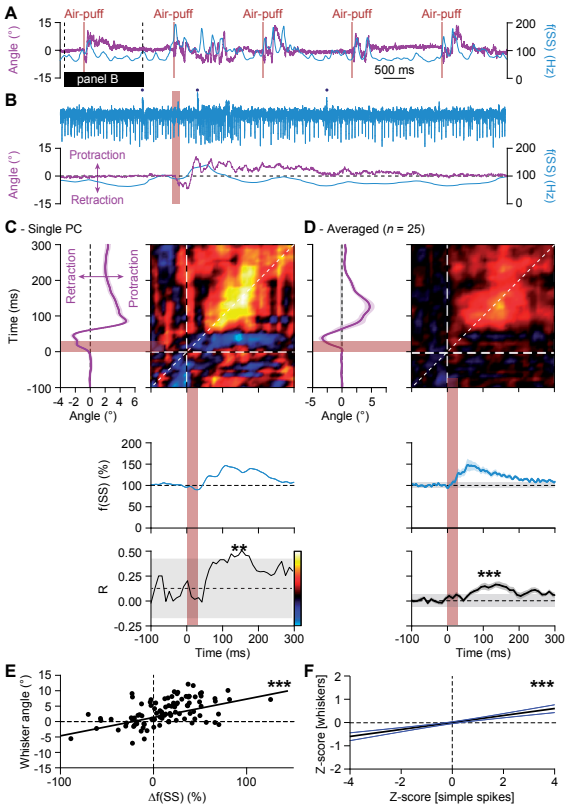


**Figure 4.** Instantaneous simple spike firing correlates with whisker protraction during reflex

**A.** Changes in the instantaneous simple spike (SS) firing rate (convolved with a 6 ms Gaussian kernel; *blue*) correlate roughly with whisker movement (*purple*). This is illustrated with a representative recording of a PC. Vertical brown lines indicate the moments of air-puff stimulation to the (ipsilateral) whisker pad. The horizontal black line designates the interval expanded in **B**. Blue dots mark complex spikes. **C.** Correlation matrix showing a clear positive correlation of simple spike firing (blue trace at the bottom shows convolved peri-stimulus time histogram triggered on air-puff stimulation) and whisker protraction (red trace at the left; indicated is the mean ± SEM of the whisker position) based on a trial-by-trial analysis. The correlation coefficient (R) over the dashed 45° line is shown at the bottom, together with the 99% confidence interval (*grey area*). These data correspond to the example PC shown in **A-B**. Averaged data from all 25 PCs that displayed a significant correlation between simple spike rate and whisker position is shown in **D**. **E.** Scatter plots with linear regression lines show a positive correlation between whisker protraction and instantaneous simple spike firing as illustrated here for the Purkinje cell represented in **C** ($R = 0.517$; $p < 0.001$; Pearson's correlation). Data are taken from the moment with the strongest correlation (150-160 ms after the onset of the air-puff for both parameters). **F.** For all PCs with a significant correlation between whisker angle and simple spike rate, this correlation turned out to be positive when evaluating 100 trials for each of the 25 Purkinje cells ($R = 0.199$; $p < 0.001$; Pearson's correlation). Shown is the linear regression line (*black*) and the 95% confidence intervals (*blue*). The experiments are normalized based upon their Z-score. Data are taken from the moment with the strongest correlation (120-130 ms (whiskers) vs. 140-150 ms (simple spikes)). Thus, increased simple spike firing correlates with whisker protraction. ** $p < 0.01$; *** $p < 0.001$.

The following supplement is available for Figure 4:

Figure supplement 1. Simple spike firing is predominantly associated with protraction

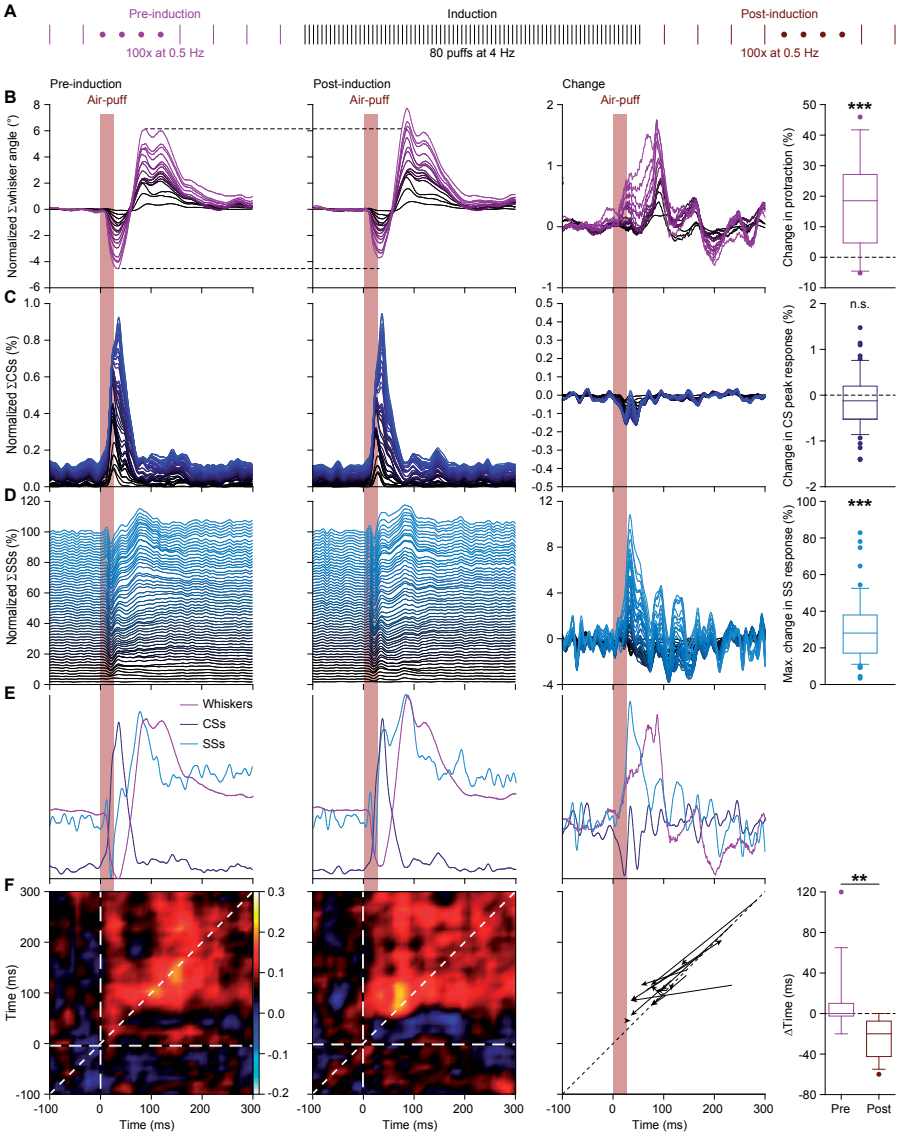


**Figure 5.** 4 Hz air-puff stimulation leads to acceleration of the simple spike response and to stronger protraction of the whiskers

**A.** Induction protocol: air-puff stimulation at 0.5 Hz is used to characterize the impact of a brief period (20 s) of 4 Hz air-puff stimulation. **B.** Stacked line plots showing the averaged whisker responses before (1st column) and after (2nd column) 4 Hz air-puff stimulation. The plots are sorted by the increase of the touch-induced whisker protraction (3rd column). Each color depicts one mouse. Plots are normalized so that the most intense color represents the average of 16 mice. 4 Hz air-puff stimulation leads to a stronger touch-induced whisker protraction (4th column). Similar plots for complex spikes (**C**, showing little change) and simple spikes (**D**, showing a clear increase in firing, especially during the early phase of the response). For comparison, the averages are superimposed in **E** (for y-scaling and variations refer to **B**-**D**). Trial-by-trial analysis of 14 Purkinje cells before and after 4 Hz air-puff stimulation (cf. Figure 4C-D) highlighting the anticipation of simple spike firing (**F**). The x-axis is based upon the instantaneous simple spike firing frequency and the y-axis upon the whisker angle. The moment of maximal correlation between simple spike firing and whisker movement anticipated after induction, as can be seen by

in particular between 80 and 200 ms after the start of the stimulus (Figure 4C-D; Figure 4 – figure supplement 1A-C), thus well after the complex spike responses occurred (Figure 3C). In the 31 remaining PCs, i.e. the ones that did not display a significant correlation when evaluated at the level of individual cells, we still observed a slight, yet significant, correlation at the population level. Remarkably, this correlation was slightly negative, i.e. possibly reflecting a correlation between simple spike firing and retraction (Figure 4 – figure supplement 1). We conclude that during the touch-induced whisker reflex simple spikes predominantly correlate with whisker protraction and that this correlation is maximal without a clear time lead or lag, unlike the complex spikes, the occurrence of which tended to precede the reflexive protraction.



## 4 Hz air-puff stimulation leads to acceleration of simple spike response and to stronger protraction of whiskers

Next, we investigated whether sensory experience could modulate the touch-induced whisker protraction, the frequency of simple spike firing and the relation between them. We hypothesized that whisker movements might be enhanced following air-puff stimulation at 4 Hz, as this frequency has been shown to be particularly effective in inducing potentiation at the parallel fiber-to-PC synapse (Coesmans et al., 2004, D'Angelo et al., 2001, Lev-Ram et al., 2002, Ramakrishnan et al., 2016). Indeed, application of this 4 Hz air-puff stimulation to the whisker pad for only 20 seconds was sufficient to induce an increase in the maximal protraction (average increase 17.9 ± 3.9%; mean ± SEM; $p < 0.001$; Wilcoxon-matched pairs test; $n = 16$ mice) (Figure 5A-B; Table S2).

This change in the amplitude of the touch-induced whisker protraction was not accompanied by any substantial change in the complex spike response to whisker pad stimulation ($p = 0.163$; Wilcoxon matched pairs test; $n = 55$ PCs) (Figure 5C; Table S2). However, the rate of simple spike firing upon air-puff stimulation was markedly increased after 20 s of 4 Hz air-puff stimulation. This was especially clear during the first 60 ms after the air-puff ($p = 0.003$; Wilcoxon matched pairs test; $n = 55$ PCs) (Figure 5D; Table S2). Overlaying the averaged whisker traces and PC activity profiles highlighted the earlier occurrence of facilitation in simple spike firing after the 4 Hz air-puff stimulation protocol (Figure 5E). To study this timing effect in more

the change in position of the yellow spot between the correlation plots in the 1st and 2nd column (see also Figure 5 – figure supplement 1A-B). After induction, the maximal correlation implied a lead of the simple spikes, as illustrated for each PC in the graph of the 3rd column. Every arrow indicates the shift of the position of the maximal correlation between before and after induction. Overall, the difference in timing between the maximal correlation changed from around 0 ms pre-induction to an approximate lead of 20 ms of the simple spikes after induction (4th column). ** $p < 0.01$; *** $p < 0.001$. See also Table S2 and Source Data File.

The following supplements are available for Figure 5:

Figure supplement 1. Simple spike response anticipates after 4 Hz air-puff stimulation

Figure supplement 2. Purkinje cell responses during 4 Hz air-puff stimulation

Figure supplement 3. Contralateral whisker pad stimulation induces stronger whisker protraction and stronger simple spike responses

Figure supplement 4. Optogenetic stimulation of Purkinje cells increases whisker protraction following air-puff stimulation

detail, we repeated the trial-based correlation analysis (cf. Figure 4C-D). The short period of 4 Hz air-puff stimulation caused an anticipation of the moment of maximal correlation between simple spike firing and whisker position. Along the 45° line – thus regarding only the zero-lag correlation between simple spike firing and whisker position – this changed from 152.1 ± 18.1 ms to 90.7 ± 9.4 ms (means ± SEM); $p$ = 0.020; $t$ = 2.664; df = 13; paired $t$ test; $n$ = 14 PCs) (Figure 5 – figure supplement 1A-B). The slope of the correlation between the instantaneous simple spike frequency and the whisker position remained unaltered ($p$ = 0.197, $t$ = 1.360, df = 13, $n$ = 14, paired $t$ test) (Figure 5 – figure supplement 1C-D). However, the point of maximal correlation was no longer with a zero-lag, but after induction the simple spikes led the whisker position (pre-induction: Δtime = 0 ± 10 ms; post-induction: Δtime = 20 ± 30 ms; medians ± IQR; $n$ = 14; $p$ = 0.001; Wilcoxon matched-pairs test) (Figure 5F). Thus, not only the simple spike rate increased, but also its relative timing to the touch-induced whisker protraction, now preceding the likewise increased touch-induced whisker protraction.

During the entrainment itself (i.e., during the 20 s period with 4 Hz air-puff stimulation), the whisker responses as well as the complex spike and the simple spike responses to each air-puff were weakened compared to the pre-induction period during which we used 0.5 Hz stimulation. More specifically, the touch-induced whisker protraction decreased by 62.2% (median; IQR = 37.5%). The maximum response of the complex spikes significantly decreased from a median of 1.27% (with an IQR of 1.89%) during pre-induction to 0.52% (with an IQR of 0.43%) during induction ($p$ < 0.001; Wilcoxon matched pairs tests, $n$ = 55 PCs), and the average modulation of the simple spikes in the first 200 ms after the puff decreased from a median of 5.9% (with an IQR of 18.2%) during pre-induction to -0.3% (IQR = 3.13) during induction ($p$ = 0.039, Wilcoxon matched-pairs test) (Figure 5 – figure supplement 2). Thus, during the 4 Hz training stage, all responses – both at the behavioral and neuronal level – diminished compared to the preceding 0.5 Hz stimulation stage.

Given the correlation between instantaneous simple spike rate and whisker position described above, one would expect that contralateral air-puff stimulation – which triggers a stronger protraction (Figure 1 – figure supplement 2) – also triggers a stronger simple spike response. To test this hypothesis we recorded PC activity while stimulating the ipsi- and contralateral whiskers in a random sequence (Figure 5 – figure supplement 3A-B). The change in maximal protraction was considerable (difference in maximal protraction: 7.30 ± 1.24° (mean ± SEM); $n$ = 9 mice) (Figure 5 – figure supplement 3C; cf. Figure 1 – figure supplement 2E). Possibly, the absence of the direct mechanical retraction on the ipsilateral side during contralateral air-puff stimulation can explain part of this difference, which is also in line with the earlier onset of the protraction during contralateral stimulation (Figure 5 – figure supplement 3C). However, in addition a change in simple spikes may contribute to this difference as well, as the simple spikes increased significantly more during contralateral stimulation (increase during first 60 ms after air-puff onset for contra- vs. ipsilateral stimulation: 13.7 ± 5.3%; mean ± SEM; $p$ = 0.023; $t$ = 2.413; df = 26; paired $t$ test; $n$ = 27 PCs) (Figure 5 – figure supplement 3E). Such a contribution

is compatible with the fact that most mossy fiber pathways related to whisker movement are bilateral with a contralateral preponderance (Bosman et al., 2011). Instead, the complex spikes were less activated during contralateral stimulation (complex spike peak response: ipsilateral: 1.40% (1.25%); contralateral: 0.71% (0.81%); medians (IQR); $p < 0.001$; Wilcoxon matched-pairs test; $n = 27$ PCs) (Figure 5 – figure supplement 3D). This response is in line with a bilateral component of the projection from the trigeminal nucleus to the olive (De Zeeuw et al., 1996).

To establish a causal link between increases in simple spike firing and whisker protraction, artificial PC stimulation would also have to affect whisker movement. Previously, it has been shown that simple spikes modulate ongoing whisker movements rather than initiate them (Brown and Raman, 2018, Chen et al., 2016, Proville et al., 2014). To find out whether simple spike firing could modulate touch-induced whisker protraction under our recording conditions, we investigated the impact of activation of PCs by optogenetic stimulation. To this end we used *Pcp2-Ai27* mice, which express channelrhodopsin-2 exclusively in their PCs and which respond with a strong increase in their simple spike firing upon stimulation with blue light (Witter et al., 2013). We placed an optic fiber with a diameter of 400 µm over the border between crus 1 and crus 2 and compared air-puff induced whisker movements among randomly intermingled trials with and without optogenetic PC stimulation. The period of optogenetic stimulation (i.e. 100 ms) was chosen to mimic preparatory activity of PCs and thus corresponded well to the period during which we observed increased simple spike firing after 4 Hz air-puff stimulation (Figure 5D). As expected, the whisker protraction was substantially bigger during the period of optogenetic stimulation ($p < 0.001$; $t = 4.411$; df = 12; paired $t$ test; $n = 13$ mice; Figure 5 – figure supplement 4). Thus, even though optogenetic stimulation of PCs can also trigger secondary feedback mechanisms that may influence the outcome (Witter et al., 2013, Chaumont et al., 2013), we conclude that increases in simple spike firing can cause stronger whisker protraction.

## Complex spikes inhibit increased simple spike firing

As cerebellar plasticity is bi-directional and under control of climbing fiber activity (Ohtsuki et al., 2009, Lev-Ram et al., 2003, Coesmans et al., 2004), we wanted to find out to what extent plastic changes in simple spike activity can be related to the strength of the complex spike response generated by climbing fibers. To this end we compared for each PC the strengths of the complex spike and simple spike responses before, during and after the 4 Hz air-puff stimulation. As expected, we found a significant negative correlation between the strength of the complex spike response, as measured by the peak of the PSTH before the 4 Hz air-puff stimulation, and the change in simple spike response following this 4 Hz stimulation ($R = 0.311$; $p = 0.021$; Pearson correlation $n = 55$ PCs) (Figure 6A). We further substantiated these findings by looking separately at the average complex spike firing frequency of the strong and weak responders (cf. Figure 2 – figure supplement 1E). The correlation found between the frequency of complex spike firing and the change in simple spike activity after 4 Hz air-puff stimulation proved to be present only in the weak responders, taking the firing rate during the pre-induction and induc-

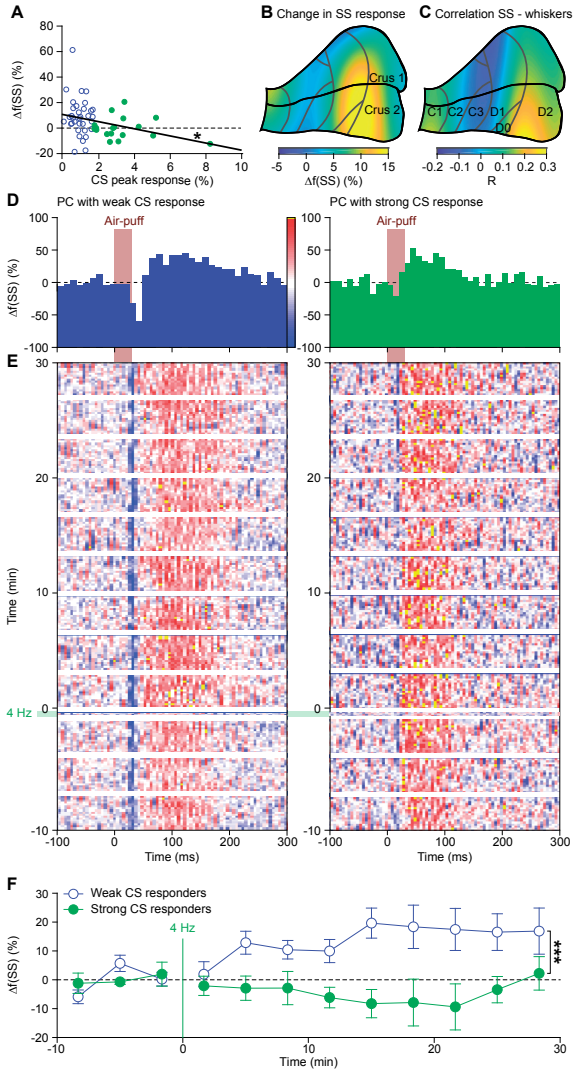


**Figure 6.** Complex spikes inhibit increased simple spike firing

**A.** Repeated sensory stimulation induced an increase in simple spike (SS) response to whisker pad stimulation (see Figure 5). This increase in simple spike responses was, however, not observed in all PCs: there was a clear negative correlation between the strength of the complex spike (CS) response and the potentiation of the simple spike response. Overall, the simple spike potentiation was larger in the PCs with a weak complex spike response than in those with a strong complex spike response (cf. Figure 2 – figure supplement 1). **B.** Heat map showing the anatomical distribution of the strength of the simple spike increase projected on the surface of crus 1 and crus 2. The 55 PCs were attributed to a rectangular grid. The average simple spike response strength was calculated per grid position and averaged between each grid position and its neighbor. The grey lines indicate the borders to the cerebellar zones (see Figure 2 - figure supplement 2D). **C.** Heat map of the distribution of PCs cells based upon the correlation of their simple spike rate and whisker position (cf. Figure 4D). Note that the strongest increase of simple spike responses after 4 Hz air-puff stimulation occurred in the region that also displayed the strongest correlation between instantaneous simple spike rate and whisker position. **D.** Example PSTHs of the simple spike response to whisker pad air-puff stimulation of representative PCs and how they changed over time, depicted as heat maps of the instantaneous simple spike frequency (**E**; see scale bar in **D**). The left column displays the data from a PC with a weak complex spike response, the right column of one with a strong complex spike response. The induction period is indicated with "4 Hz". **F.** The number of simple spikes following an air-puff stimulation increased in weakly responding Purkinje cells and this increase remained elevated until the end of the recording (at least 30 min). In contrast, this increase was not found in Purkinje cells with strong complex spike responses. * $p < 0.05$; ** $p < 0.01$; *** $p < 0.001$.

The following supplements are available for Figure 6:

Figure supplement 1. Complex spike rates are negatively correlated with sensory-induced potentiation

Figure supplement 2. 4 Hz air-puff stimulation enhances stereotypic whisker protraction for at least 30 minutes

tion period into account (Figure 6 – figure supplement 1). This is again in line with the notion that parallel fiber activity in the absence of climbing fiber activity promotes parallel fiber to PC LTP (Coesmans et al., 2004, Lev-Ram et al., 2002, Ramakrishnan et al., 2016). The PCs with the strongest effect of 4 Hz air-puff stimulation on simple spike firing were mainly located in the lateral part of crus 2 (Figure 6B), posterior to the crus 1 area with the strongest complex spike responses (Figure 2H). We compared the location of this lateral crus 2 area to that of the PCs with the strongest correlations between simple spike firing and whisker protraction and we found these two crus 2 locations to match well (Figure 6B-C).

The impact of 4 Hz air-puff stimulation on the simple spike activity of PCs with a weak complex spike response lasted as long as our recordings lasted (i.e. at least 30 min), whereas that on PCs with a strong complex spike response was not detectable during this period (Figure 6D-F). Indeed, the weak responders differed significantly from the strong responders in this respect (weak vs. strong responders: $p$ = 0.005; $F$ = 3.961; df = 4.424; two-way repeated measures ANOVA with Greenhouse-Geyser correction; $n$ = 8 weak and $n$ = 6 strong responders; Fig. 6F). Likewise, the impact of the 4 Hz air-puff stimulation on touch-induced whisker protraction also lasted throughout the recording in that the protraction sustained (Figure 6 – Figure supplement 2). Thus, both simple spikes and whisker muscles remained affected by the 4 Hz air-puff stimulation for as long as our recordings lasted.

## Expression of PP2B in Purkinje cells is required for increased protraction and simple spike firing following 4 Hz air-puff stimulation

In reduced preparations, 4 Hz stimulation of the parallel fiber inputs leads to LTP of parallel fiber to PC synapses (Coesmans et al., 2004, Lev-Ram et al., 2002, Ramakrishnan et al., 2016). At the same time, parallel fiber LTP is inhibited by climbing fiber activity (Coesmans et al., 2004, Lev-Ram et al., 2003, Ohtsuki et al., 2009). Hence, our data appear in line with a role for parallel fiber LTP as a potential mechanism underlying the observed increase in simple spike firing upon a brief period of 4 Hz stimulation. To further test a potential role for LTP, we repeated our 4 Hz air-puff stimulation experiments in *Pcp2-Ppp3r1* mice, which lack the PP2B protein specifically in their PCs, rendering them deficient of parallel fiber-to-PC LTP (Schonewille et al., 2010) (Figure 7A). The impact of 4 Hz air-puff stimulation on the maximal protraction was significantly less in the *Pcp2-Ppp3r1* mutant mice compared to wild types ($p$ = 0.044, $t$ = 2.162, df = 19, $t$ test; Figure 7B-D). Accordingly, in contrast to those in their wild type (WT) littermates ($p$ < 0.001, $t$ = 4.122, df = 15, $t$ test), the maximal touch-induced whisker protraction before and after induction was not significantly different in *Pcp2-Ppp3r1* mice ($p$ = 0.647, $t$ = 0.470, df = 12, $t$ test; Fig. 7E). Thus, *Pcp2-Ppp3r1* mice do not show increased touch-induced whisker protraction after 4 Hz air-puff stimulation.

In line with the absence of increased touch-induced whisker protraction, also the increase in simple spike firing observed in wild type mice was absent in *Pcp2-Ppp3r1* mice. As the strong complex spike responders in WTs did not show changes in simple spike activity (cf. Figure 6), we

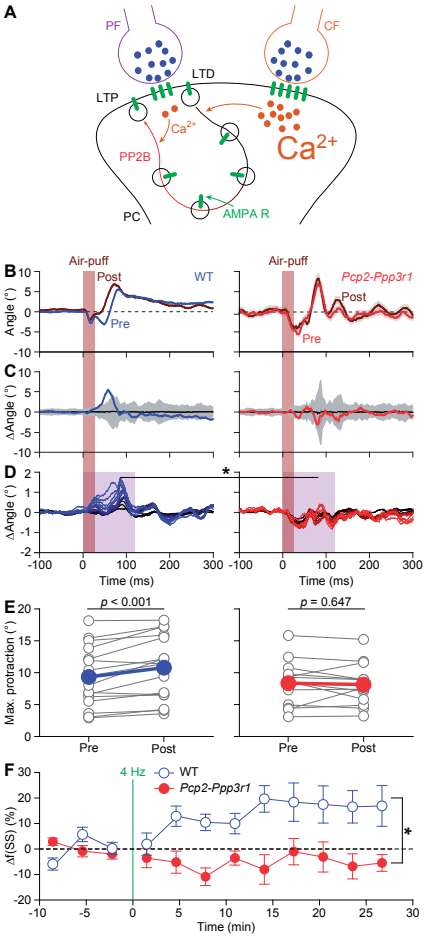


**Figure 7.** Expression of PP2B in Purkinje cells is required for increased protraction and simple spike firing following 4 Hz air-puff stimulation

**A.** Schematic representation of the principal pathways regulating bidirectional plasticity at the parallel fiber (PF) to Purkinje cell (PC) synapses. The direction of PF-PC plasticity depends on the intracellular $Ca^{2+}$ concentration ($[Ca^{2+}]_i$) that is largely determined by climbing fiber (CF) activity. Following CF activity, $[Ca^{2+}]_i$ raises rapidly and activates a phosphorylation cascade involving α-$Ca^{2+}$/calmodulin-dependent protein kinase II (CaMKIIA) and several other proteins eventually leading to internalization of AMPA receptors and consequently to long-term depression (LTD). PF volleys in the absence of CF activity, on the other hand, result in a moderate increase in $[Ca^{2+}]_i$, activating a protein cascade involving protein phosphatase 2B (PP2B, encoded by *Ppp3r1*) that promotes the insertion of new AMPA receptors into the postsynaptic density, thereby leading to long-term potentiation (LTP) of the PF-PC synapse. GluA3 subunits are part of the postsynaptic AMPA receptors. **B.** Example of a representative mouse with the averaged whisker movements before and after theta sensory stimulation, showing a stronger protraction afterwards, as evidenced by the differences between post- and pre-induction compared to a bootstrap analysis on the normal variation in whisker movements (**C**; shade: 99% confidence interval). Variations in whisker protraction in *Pcp2-Ppp3r1* mutants did generally not exceed the expected variability (right). **D.** Stacked line plots of whisker movement differences between post- and pre-induction for all mice highlighting the absence of increased touch-induced whisker protraction in *Pcp2-Ppp3r1* mutant mice. The plots are normalized so that the brightest line indicates the average per genotype ($n$ = 16 WT and $n$ = 13 *Pcp2-Ppp3r1* KO mice). **E.** The average maximal protraction before and after induction for each mouse confirms the increase in WT, but not in *Pcp2-Ppp3r1* mutant mice. The colored symbols indicate the average per genotype. **F.** In contrast to simple spike responses in WT mice, those in *Pcp2-Ppp3r1* KO mice could not be potentiated by our 4 Hz air-puff stimulation protocol. This effect was stable, also during longer recordings. For this analysis, we selected those with weak complex spike responses, as the PCs with a strong complex spike response did not show increased simple spike firing after 4 air-puff stimulation (see Figure 6A). * $p < 0.05$; ** $p < 0.01$; *** $p < 0.001$

The following supplement is available for Figure 7:

Figure supplement 1. Also in *Pcp2-Ppp3r1* KO mice, complex spike rates are negatively correlated with sensory-induced potentiation

compared weak complex spike responders of both genotypes. Simple spike responses were stably increased in WT PCs with a weak complex spike response following 4 Hz air-puff stimulation (as shown in Figure 6F), but not in those of *Pcp2-Ppp3r1* mice (effect of genotype: $p = 0.003$, $F = 4.361$, df = 4.137, two-way repeated measures ANOVA with Greenhouse-Geyser correction; $n = 8$ WT and $n = 9$ *Pcp2-Ppp3r1* PCs) (Figure 7F). Despite the lack of potentiation, we found that the *Pcp2-Ppp3r1* mice still had a significant correlation between the complex spike frequency during the induction block and changes in simple spike activity (R = 0.489, $p = 0.013$, Pearson correlation; Figure 7 – figure supplement 1A); this correlation may result from other forms of

plasticity that are still intact in *Pcp2-Ppp3r1* mice (Schonewille et al., 2010). Yet, in line with the absence of increased simple spike responsiveness, the correlation between changes in simple spike firing during the induction block and the impact of 4 Hz air-puff stimulation, as present in the WT PCs, was absent in the *Pcp2-Ppp3r1* mice (Figure 7 - figure supplement 1B). Thus, in the absence of the PP2B protein in PCs, the impact of 4 Hz air-puff stimulation on touch-induced whisker protraction as well as on the simple spike responsiveness was not detectable. These correlations between complex spike and simple spike firing on the one hand and modification of the simple spike response to whisker pad stimulation on the other hand further strengthen our hypothesis that parallel fiber to PC LTP is one of the main mechanisms that underlies the long-term changes that can be observed at both the level of simple spike activity and whisker protraction after 4 Hz air-puff stimulation.

## Expression of AMPA receptor GluA3 subunits in Purkinje cells is required for increased protraction and simple spike firing following 4 Hz air-puff stimulation

To control for compensatory mechanisms specific for *Pcp2-Ppp3r1* mice we used a second, independent, yet also PC-specific, mutant mouse line deficient in parallel fiber LTP. In these mice (*Pcp2-Gria3*), PCs lack the AMPA receptor GluA3 subunit (Gutierrez-Castellanos et al., 2017). As in the *Pcp2-Ppp3r1* mice, we did not find evidence for increased whisker protraction after 4 Hz air-puff stimulation (e.g., change in whisker angle during the first 120 ms after air-puff onset: WT vs. *Pcp2-Gria3* mice: $p = 0.007$, Tukey's post-hoc test after ANOVA ($p = 0.001$, $F = 9.111$, df = 2), $n = 16$ WT and $n = 6$ *Gria3* deficient mice) (Figure 8A-C). Moreover, as in the *Pcp2-Ppp3r1* mice, also the increase in simple spike responsiveness after 4 Hz stimulation was absent in *Pcp2-Gria3* mice (change in simple spike count between WT and *Pcp2-Gria3* PCs during the first 60 ms after air-puff onset: $p = 0.004$; Tukey's post-hoc test after ANOVA ($p = 0.002$, $F = 6.681$, df = 2), $n = 35$ WT PCs and $n = 13$ *Gria3* KO PCs, next to $n = 23$ *Pcp2-Ppp3r1* KO PCs, all with weak complex spike responses) (Figure 8D-F). Thus an independent line of evidence supports the findings made in the *Pcp2-Ppp3r1* mice.

For control we compared the basic electrophysiological profiles of PCs in the three genotypes used in this study. When averaged over the entire period with episodes of stimulation, the overall complex spike rate, simple spike rate and simple spike CV2 value (i.e. parameter for level of irregularity) of PCs in the *Pcp2-Ppp3r1* KO mice were moderately, but significantly, reduced compared to those in WTs (Figure 8 – figure supplement 1A-D; Table S3). However, as the *Pcp2-Gria3* mice did not show any significant deviations in these overall firing properties (Figure 8 – figure supplement 1A-D; Table S3), it is unlikely that the aberrant firing properties of *Pcp2-Ppp3r1* mice could explain the lack of adaptation at both the behavioral and electrophysiological level. Comparing the response probabilities to whisker pad stimulation we found that both the number of complex spikes and simple spikes after the air-puff were reduced in *Pcp2-Ppp3r1* mice (Figure 8 – figure supplement 1E-J; Table S3). The predominantly suppressive

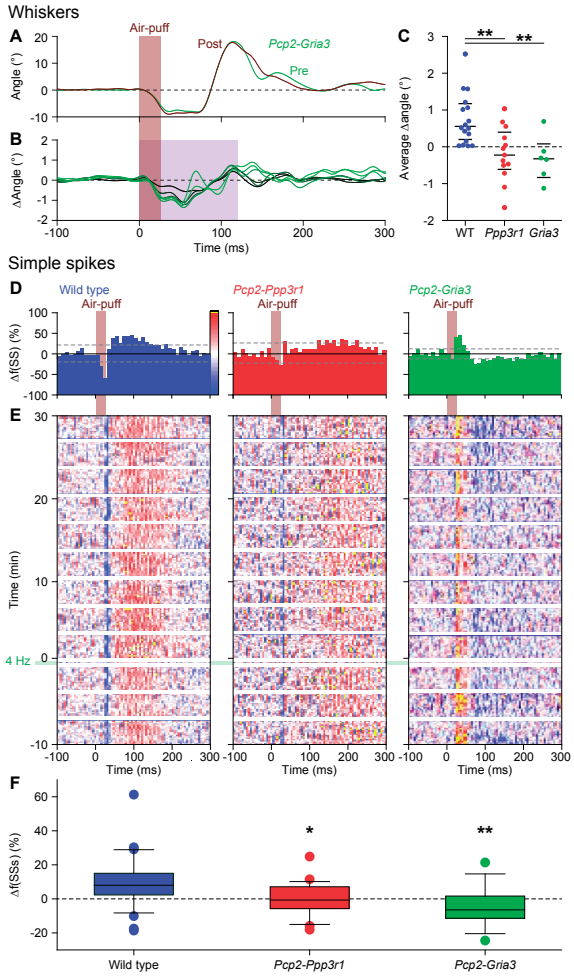


**Figure 8.** Expression of AMPA receptor GluA3 subunits in Purkinje cells is required for increased protraction and simple spike firing following 4 Hz air-puff stimulation

**A.** Example of a representative *Pcp2-Gria3* mutant mouse that is deficient for the GluA3 subunit with the averaged whisker movements before and after 4 Hz air-puff stimulation, showing similar degrees of protraction. **B.** Overall, 4 Hz air-puff stimulation did not result in stronger whisker protraction in *Pcp2-Gria3* mutant mice as observed in WT mice (see Figure 7). This is illustrated with a stacked line plot. **C.** Comparison of the average change in whisker angle over the 120 ms following the onset of the air-puff shows enhanced protraction in WT ($n$ = 16), but not in LTP-deficient mice - neither in *Pcp2-Ppp3r1* ($n$ = 13) nor in *Pcp2-Gria3* ($n$ = 6) mutants, pointing towards a central role for parallel fiber-to-Purkinje cell LTP for the enhanced protraction in WT mice following a brief period of 4 Hz air-puff stimulation. The horizontal lines indicate the medians and the 1st and 3rd quartiles. The lack of change in whisker protraction following 4 Hz air-puff stimulation was reflected in the lack of change in simple spike responses as illustrated in three representative PCs (cf. Figure 6D-E). On top are the peri-stimulus time histograms (**D**) followed by heat maps illustrating the instantaneous firing rate over time (**E**). The induction period is indicated with "4 Hz". F. Overall, WT PCs ($n$ = 35) showed increased simple spike firing after 4 Hz stimulation, while those in *Pcp2-Ppp3r1* ($n$ = 21) or *Pcp2-Gria3* ($n$ = 13) mutant mice did not. For this analysis, we restricted ourselves to the PCs with weak complex spike responses as the PCs with strong complex spike responses did not show potentiation in the WT mice (see Figure 6A) and to the first 100 trials after induction. * $p < 0.05$; ** $p < 0.01$. See also Source Data File.

The following supplements are available for Figure 8:

Figure supplement 1. Purkinje cell responses to whisker pad stimulation in *Pcp2-Ppp3r1* and *Pcp2-Gria3* mice

Figure supplement 2. Before induction, touch-induced whisker protraction is not affected by *Pcp2-Ppp3r1* and *Pcp2-Gria3* mutations

simple spike responses were not found in *Pcp2-Gria3* mice, but the latter also had a reduced complex spike response to air-puff stimulation. Since a reduced complex spike response acts permissive for the adaptive increase in the simple spike response, it is unlikely that the observed reduction in complex spike firing would be the cause of the observed lack of simple spike enhancement in both mutant mouse lines. Moreover, the amplitudes of the touch-induced whisker protraction as measured before the induction phase were similar between the WT and the mutant mice (Figure 8 – figure supplement 2). We therefore conclude that the absence of simple spike potentiation and the concomitant increase in touch-induced whisker protraction is likely due to the absence of parallel fiber LTP caused by the genetic mutations rather than to altered firing patterns of the PCs involved.



## DISCUSSION

In this study we show for the first time that a brief period of intense sensory stimulation can evoke adaptation of reflexive whisker protraction. Extracellular recordings revealed that the simple spike activity of the PCs that modulate during whisker movements is congruently increased when the adapted behavior is expressed. These PCs, which are predominantly located in the crus 2 region, show a present but weak complex spike response to whisker stimulation, which appears to act permissive for the occurrence of parallel fiber to PC LTP. This form of plasticity is likely to be one of the main mechanisms underlying this whisker reflex adaptation, as two independent cell-specific mouse models, both of which lack LTP induction at their parallel fiber to PC synapses, did not show any alteration in their whisker protraction or simple spike response following the training protocol with 4 Hz air-puff stimulation. By contrast, the PCs that show a strong complex spike response to whisker stimulation and that are mainly located in crus 1 did not manifest a prominent regulatory role to enhance the simple spike responses or whisker movements in the long-term. Our study highlights how moderate climbing fiber activity may permit induction of PC LTP in a behaviorally relevant context and how this induction may lead to an increase in simple spike modulation when the adapted motor output is expressed.

### Control of whisker movements

Although most mammals have whiskers, only few species use their whiskers to actively explore their environment by making fast, rhythmic whisker movements (Vincent, 1913, Ahl, 1986, Welker, 1964, Woolsey et al., 1975). In “whisking” animals, such as mice and rats, both whisker protraction and retraction are under direct muscle control, while especially whisker retraction can additionally reflect a passive process involving skin elasticity (Berg and Kleinfeld, 2003, Simony et al., 2010, Haidarliu et al., 2015, Moore et al., 2013, Deschênes et al., 2017). Animals can modify the pattern of whisker movements upon sensory feedback during natural behavior, as has been demonstrated for example during gap crossing and prey capture (Anjum and

Brecht, 2012, Voigts et al., 2015). The neural control of adaptation of reflexive whisker movements is still largely unknown. Given the widespread networks in the brain controlling whisker movements (Bosman et al., 2011, Kleinfeld et al., 1999), it is likely that multiple brain regions contribute. We show here, at least for a specific reproducible form of whisker adaptation, that parallel fiber to PC LTP and enhancement in PC simple spike activity may contribute to the induction and expression of this form of motor learning, respectively.

## Simple spike firing during normal and adapted whisker movements

Our electrophysiological recordings indicate that the simple spike activity correlates well with whisker protraction, especially in PCs located in crus 2, and that this relation is context-dependent. Under the baseline condition of our paradigm, during the 0.5 Hz whisker pad stimulation, simple spikes correlate positively with the position of the whiskers during protraction on a single trial basis. The correlation between the rate of simple spikes and that of protraction was also found when comparing the impact of contralateral vs. ipsilateral whisker pad stimulation. The absence of a clear time lag or lead between simple spike activity and whisker movements under this condition suggests that during normal motor performance without sensorimotor mismatch signaling the simple spikes predominantly represent ongoing movement. Our data under baseline conditions are compatible with those obtained by the labs of Chadderton and Léna (Chen et al., 2016, Proville et al., 2014). In their studies on online motor performance, the simple spike activity of most PCs in the lateral crus 1 and/or crus 2 regions correlated best with protraction of the set point, defined as the slowly varying midpoint between maximal protraction and maximal retraction.

During and after training with 4 Hz air-puff stimulation the temporal dynamics of the simple spikes shifted in that the simple spikes were found to precede the whisker movement and to predict the magnitude of the protraction, suggesting the emergence of an instructive motor signal. Optogenetic stimulation experiments confirmed that increased simple spike firing during the early phase of touch-induced whisker protraction can promote whisker protraction. Thus, the current dataset confirms and expands on previous studies, highlighting a role of the cerebellar PCs injecting additional accelerating and amplifying signals into the cerebellar nuclei during entrainment (De Zeeuw et al., 1995).

## Cerebellar plasticity

Synaptic plasticity in the cerebellar cortex has, next to that in the cerebellar and vestibular nuclei (Lisberger and Miles, 1980, Lisberger, 1998, Zhang and Linden, 2006, McElvain et al., 2010), generally been recognized as one of the major mechanisms underlying motor learning (Ito, 2001, Ito, 2003). For forms of motor learning that require a decrease in simple spike activity for expression of the memory, such as eyeblink conditioning (Halverson et al., 2015, Ten Brinke et al., 2015, Jirenhed et al., 2007), long-term depression (LTD) of the parallel fiber to PC synapse may play a role during the initial induction stage (Ito, 2003, Koekkoek et al., 2003). In LTD-

deficient mouse models the potential contribution of LTD is most apparent when compensatory mechanisms that involve activation of the molecular layer interneurons are blocked (Boele et al., 2018). However, for forms of motor learning that require an increase in simple spike activity for expression of the procedural memory it is less clear which forms of cerebellar cortical plasticity may contribute. Here, we show that increasing whisker protraction by repetitive sensory stimulation requires an increase in simple spike activity and that blocking induction of parallel fiber to PC LTP prevents changes in both spiking and motor activity following the same training paradigm. Possibly, adaptation of the vestibulo-ocular reflex (VOR) follows partly similar learning rules in that various genetic mouse models with impaired induction of parallel fiber to PC LTP show reduced VOR learning (Gutierrez-Castellanos et al., 2017, Rahmati et al., 2014, Schonewille et al., 2010, Ly et al., 2013, Peter et al., 2016) and that optogenetic stimulation of PCs in the flocculus of the vestibulocerebellum can increase VOR gain (Voges et al., 2017). In this respect it will be interesting to find out to what extent increases in simple spike activity in the flocculus can also be correlated with an entrained increase in VOR gain on a trial-by-trial basis, as we show here for whisker learning.

The differential learning rules highlighted above indicate that different forms of cerebellar plasticity may dominate the induction of different forms of learning (Hansel et al., 2001, Gao et al., 2012, D'Angelo et al., 2016, De Zeeuw and Ten Brinke, 2015). The engagement of these rules may depend on the requirements of the downstream circuitries involved (Suvrathan et al., 2016, De Zeeuw and Ten Brinke, 2015). Indeed, whereas the eyeblink circuitry downstream of the cerebellar nuclei comprises purely excitatory connections and hence requires a simple spike suppression of the inhibitory PCs to mediate closure of the eyelids, the VOR circuitry comprises an additional inhibitory connection and hence requires a simple spike enhancement so as to increase the compensatory eye movement (De Zeeuw and Ten Brinke, 2015, Voges et al., 2017). The circuitry downstream of the cerebellum that mediates control of whisker movements is complex (Bosman et al., 2011). Possibly, the cerebellar nuclei may modulate the trigemino-facial feedback loop in the brainstem that controls the touch-induced whisker protraction (Bellavance et al., 2017). This could be done via the intermediate reticular formation, which receives a direct input from the cerebellar nuclei (Teune et al., 2000) and projects to the facial nucleus where the whisker motor neurons reside (Zerari-Mailly et al., 2001, Herfst and Brecht, 2008). As the latter projection is inhibitory (Deschênes et al., 2016), the same configuration may hold as described for the VOR pathways (De Zeeuw and Ten Brinke, 2015) in that adaptive enhancement of the whisker reflex may require induction of parallel fiber to PC LTP and increases in simple spike activity. Thus, given the current findings and the known neuro-anatomical connections in the brainstem, the picture emerges that cerebellar control of whisker movements follows the general pattern which suggests that the predominant forms of PC plasticity and concomitant changes in simple spike activity align with the requirements downstream in the cerebellar circuitry (De Zeeuw and Ten Brinke, 2015).

## Heterogeneous pools of PCs with differential complex spike responses to whisker stimulation

A minority of the PCs we recorded had a high complex spike response probability upon air-puff stimulation of the whisker pad. These PCs were predominantly located in the centro-lateral part of crus 1. Most of the other PCs, in particular those in the medial part of crus 1 and in crus 2, showed a low, yet significant, complex spike response probability to sensory whisker stimulation. In these cells the absence of a strong complex spike response to air-puff stimulation probably acted as a permissive gate to increase the simple spike response following training, which is in line with current theories on cerebellar plasticity (Coesmans et al., 2004, Ito, 2001, Lev-Ram et al., 2002, Ohtsuki et al., 2009). The PCs with a relatively high complex spike response probability were not prone for increases in simple spike activity following our training protocol. Instead, they may dynamically enhance reflexive whisker protraction through increases in their coherent complex spike firing, likely engaging ensemble encoding (Hoogland et al., 2015, Mukamel et al., 2009, Ozden et al., 2009, Schultz et al., 2009). This enhancement does not require a repetitive training protocol and also occurs during single trial stimulation. Indeed, these complex spike responses, which tended to precede the active whisker movement, could be correlated to the strength of the touch-induced whisker protraction under baseline conditions. This is in line with previous studies showing that complex spikes can facilitate the initiation of movements and define their amplitude (Hoogland et al., 2015, Kitazawa et al., 1998, Welsh et al., 1995). Thus, PCs with strong complex spike responses to whisker stimulation – especially those located in the D2 zone of crus 1 – show poor simple spike enhancement to mediate whisker adaptation, but they might facilitate execution of touch-induced whisker protraction under baseline conditions by relaying coherent patterns of complex spikes onto the cerebellar nuclei neurons.

## Conclusion

Based on a known form of reflexive whisker movements, we introduced a novel adaptation paradigm and investigated the underlying cerebellar plasticity mechanism and spiking learning rules. A brief period of increased sensory input appeared to be sufficient to induce a lasting impact on touch-induced whisker protraction: the whisker reflex started earlier and had a bigger amplitude. This motor adaptation probably requires induction of parallel fiber LTP in PCs that can be identified by their weak but present complex spike response to sensory stimulation. The resultant increased simple spike firing of these PCs may affect the brainstem loop controlling touch-induced whisker protraction via the reticular formation in the brainstem, in line with optogenetic stimulation experiments. Thus, our study proposes induction of parallel fiber to PC LTP as a cellular mechanism for enhancing PC simple spike responsiveness that facilitates the expression of the entrained whisker protraction.

## ACKNOWLEDGEMENTS

Financial support was provided by the Netherlands Organization for Scientific Research (NWO-ALW; C.I.D.Z.), the Dutch Organization for Medical Sciences (ZonMW; C.I.D.Z.), Life Sciences (C.I.D.Z.), ERC-adv and ERC-POC (C.I.D.Z.) and the China Scholarship Council (No. 2010623033; C.J.). We thank E. Haasdijk, E. Goedknegt, M. Rutteman, and A.C.H.G. IJpelaar for technical assistance and Drs. T.J.H. Ruigrok, S.K.E. Koekkoek, J.J. White and M. Schonewille of the Neuroscience Department at the Erasmus Medical Center for their input and scientific discussions, as well as Dr. D. Rizopoulos of the Biostatistics Department at the Erasmus Medical Center and Dr. D. Vidotto from Tilburg University for statistical consulting regarding the cluster analysis.



## COMPETING FINANCIAL INTERESTS

The authors declare no competing financial interests.

## MATERIALS AND METHODS

### Key Resource Table

| Reagent type (species) or resource | Designation | Source or reference | Identifiers | Additional information |
|---|---|---|---|---|
| strain, strain background (*Mus musculus*) | *Tg*(*Pcp2-cre*)*2Mpin; Ppp3r1*$^{tm1Stl}$ | (Schonewille et al., 2010) | | C57Bl6/J background |
| strain, strain background (*M. musculus*) | *Tg*(*Pcp2-cre*)*2MPin; Gria3*$^{tm2Rsp}$ | (Gutierrez-Castellanos et al., 2017) | | C57Bl6/J background |
| strain, strain background (*M. musculus*) | C57Bl6J mice | Charles Rivers | IMSR_JAX: 000664 | |
| strain, strain background (*M. musculus*) | *Tg*(*Pcp2-cre*)*2Mpin:: Gt*(*ROSA*)*26Sor*$^{tm27.1(CAG-OP4*H134R/tdTomato)Hze}$ | (Witter et al., 2013) | | C57Bl6/J background |
| chemical compound, drug | Dextran, Biotin, 3000 MW, Lysine Fixable (BDA-3000) | Thermo Fisher Scientific | D7135 | |
| chemical compound, drug | Paraformaldehyde | Merck | 1.040005.1000 | |
| chemical compound, drug | Thionine | Sigma | T-3387 | |
| chemical compound, drug | Gelatin | J.T.Baker | 2124-01 | |
| software, algorithm | MATLAB v2012a-v2017a | Mathworks | | |
| software, algorithm | LabVIEW (for video acquisition) | National Instruments | | |
| software, algorithm | BWTT Toolbox (for whisker tracking) | http://bwtt.sourceforge.net https://github.com/MRIO/BWTT_PP | | |

## Animals

For most of the experiments in this study, we used two different mutant mouse lines on a C57Bl/6J background. Comparisons of electrophysiological parameters were always made between the mutant mice and their respective wild-type (WT) littermates, although for easier visualization the WTs were sometimes grouped as indicated in the figure legends. Both mouse lines had been used before and details on their generation have been published. Briefly, *Pcp2-Ppp3r1* mice (*Tg*(*Pcp2-cre*)*2Mpin;Ppp3r1*$^{tm1Stl}$) lacked functional phosphatase 2B (PP2B) specifically in their PCs. They were created by crossing mice in which the gene for the regulatory subunit (Cnbl1) of PP2B was flanked by loxP sites (Zeng et al., 2001) with transgenic mice expressing Cre-recombinase under control of the *Pcp2* (*L7*) promoter (Barski et al., 2000) as described in Schonewille et al. (2010). *Pcp2-cre*$^{+/-}$*-Ppp3r1*$^{f/f}$ mice ("*Pcp2-Ppp3r1* mice") were compared with *Pcp2-cre*$^{-/-}$*-Ppp3r1*$^{f/f}$ littermate controls. We used 35 WT mice (17 males and 18 females of 21 ± 9 weeks of age (average ± s.d.)) and 22 *Pcp2-Ppp3r1* mice (6 males and 16 females of 18 ± 10 weeks of age (average ± s.d.)). *Pcp2-Gria3* mice (*Tg*(*Pcp2-cre*)*2MPin;Gria3*$^{tm2Rsp}$) lacked the AMPA receptor GluA3 subunit specifically in their PCs. They were created by crossing mice in which the *Gria3* gene was flanked by loxP sites (Sanchis-Segura et al., 2006) with transgenic mice expressing Cre-recombinase under control of the *Pcp2* promoter (Barski et al., 2000) as described in Gutierrez-Castellanos et al. (2017). We used *Pcp2-cre*$^{+/-}$*-Gria3*$^{f/f}$ mice ("*Pcp2-Gria3* mice") and *Pcp2-cre*$^{-/-}$*-Gria3*$^{f/f}$ as littermate controls. We used 5 WT male mice (25 ± 3 weeks of age (average ± s.d.)) and 9 *Pcp2-Gria3* mice (6 males and 3 females of 26 ± 4 weeks of age (average ± s.d.)). Mutants and wild-types were measured in random sequence. For the two-photon $Ca^{2+}$ imaging experiments, we used 6 male C57Bl/6J mice (Charles Rivers, Leiden, the Netherlands) of 4-12 weeks of age. The photostimulation experiments were performed on 7 mice (3 males and 4 females of 25 ± 1 weeks of age (average ± s.d.)) expressing Channelrhodopsin-2 exclusively in their PCs (*Tg*(*Pcp2-cre*)*2Mpin;Gt*(*ROSA*)*26Sor*$^{tm27.1(CAG-COP4*H134R/tdTomato)Hze}$) as described previously (Witter et al., 2013). All mice were socially housed until surgery and single-housed afterwards. The mice were kept at a 12/12 h light/dark cycle and had not been used for any invasive procedure (except genotyping shortly after birth) before the start of the experiment. All mice used were specific-pathogen free (SPF). All experimental procedures were approved a priori by an independent animal ethical committee (DEC-Consult, Soest, The Netherlands) as required by Dutch law and conform the relevant institutional regulations of the Erasmus MC and Dutch legislation on animal experimentation. Permissions were obtained under the following license numbers: EMC2656, EMC2933, EMC2998, EMC3001, EMC3168 and AVD101002015273.

## Surgery

All mice that were used for electrophysiology received a magnetic pedestal that was attached to the skull above bregma using Optibond adhesive (Kerr Corporation, Orange, CA) and a craniotomy was made on top of crus 1 and crus 2. The surgical procedures were performed

under isoflurane anesthesia (2-4% V/V in $O_2$). Post-surgical pain was treated with 5 mg/kg carprofen ("Rimadyl", Pfizer, New York, NY, USA), 1 µg lidocaine (Braun, Meisingen, Germany), 1 µg bupivacaine (Actavis, Parsippany-Troy Hills, NJ, USA) and 50 µg/kg buprenorphine ("Temgesic", Indivior, Richmond, VA, USA). After three days of recovery, mice were habituated to the recording setup during at least 2 daily sessions of approximately 45 min. In the recording setup they were head-fixed using the magnetic pedestal. The mice used for two-photon imaging received a head plate with a sparing on the location of the craniotomy instead of a pedestal. The head plate was attached to the skull with dental cement (Superbond C&B, Sun Medical Co., Moriyama City, Japan). To prevent the growth of scar tissue, which could affect image quality, two-photon recordings were made on the day of the surgery (recording started at least 1 h after the termination of anesthesia).



## Whisker stimulation and tracking

Air-puff stimulation to the whisker pad was applied with a frequency of 0.5 Hz s at a distance of approximately 3 mm at an angle of approximately 35° (relative to the body axis). The puffs were delivered using a tube with a diameter of approximately 1 mm with a pressure of ~2 bar and a duration of 30 ms. During the induction period, the stimulation frequency was increased to 4 Hz and 80 puffs were given. In a subset of experiments, a 2 ms air-puff (pre-pulse) was delivered 100 ms prior to the 30 ms puff. Videos of the whiskers were made from above using a bright LED panel as backlight (λ = 640 nm) at a frame rate of 1,000 Hz (480x500 pixels using an A504k camera from Basler Vision Technologies, Ahrensburg, Germany). The whiskers were not trimmed or cut.

## Electrophysiology

Electrophysiological recordings were performed in awake *Pcp2-Ppp3r1* WT mice using either glass pipettes (3-6 MΩ) or quartz-coated platinum/tungsten electrodes (2-5 MΩ, outer diameter = 80 µm, Thomas Recording, Giessen, Germany). The latter electrodes were placed in an 8x4 matrix (Thomas Recording), with an inter-electrode distance of 305 µm. Prior to the recordings, the mice were lightly anesthetized with isoflurane to remove the dura, bring them in the setup and adjust all manipulators. Recordings started at least 60 min after termination of anesthesia and were made in crus 1 and crus 2 ipsilateral to the side of the whisker pad stimulation at a minimal depth of 500 µm. The electrophysiological signal was digitized at 25 kHz, using a 1-6,000 Hz band-pass filter, 22x pre-amplified and stored using a RZ2 multi-channel workstation (Tucker-Davis Technologies, Alachua, FL).

## Neural tracing & electrolytic lesions

For the neural tracing experiments, we used glass electrodes filled with 2 M NaCl for juxtacellular recordings. After a successful recording of a PC, neural tracer was pressure injected (3 x 10 ms with a pressure of 0.7 bar) either from the same pipette re-inserted at the same

location or from the second barrel or a double barrel pipette. We used a gold-lectin conjugate has described previously (Ruigrok et al., 1995) (*n* = 3) or biotinylated dextran amine (BDA) 3000 (10 mg/ml in 0.9% NaCl; ThermoFisher Scientific, Waltham, MA, USA) (*n* = 7). Five days after the tracer injection, the mice were anesthetized with pentobarbital (80 mg/kg intraperitoneal) and fixated by transcardial perfusion with 4% paraformaldehyde. The brains were removed and sliced (40 µm thick). The slices were processed by Nissl staining. Experiments were included in the analysis if the electrophysiology fulfilled the requirements mentioned above with a recording duration of at least 50 s and if the tracer was clearly visible. For BDA 3000 this implied that it was taken up by the PCs at the injection spot and transported to the axonal boutons a single subgroup in the cerebellar nuclei. BDA 3000 was also found in the inferior olive. For the gold-lectin conjugate the subnucleus of the inferior olive was considered. Based upon the subnuclei of the cerebellar nuclei and/or the inferior olive, the sagittal zone of the recording site was identified according to the scheme published in Apps and Hawkes (2009).

After the recordings made with the quartz/platinum electrodes, electrolytic lesions were applied to selected electrodes in order to retrieve the recording locations. To this end, we applied a DC current of 20 µA for 20 s. This typically resulted in a lesion that could be visualized after Nissl staining of 40 µm thick slices made of perfused brains. We accepted a spot as a true lesion if it was visible in at least 2 consecutive slices at the same location. In total, we could retrieve 16 successful lesions. Recording locations were approximated using pictures of the entry points of the electrodes in combination with the locations of the lesions.

## Two-photon $Ca^{2+}$ imaging

After the surgery (see above) with the dura mater intact, the surface of the cerebellar cortex was rinsed with extracellular solution composed of (in mM) 150 NaCl, 2.5 KCl, 2 $CaCl_2$, 1 $MgCl_2$ and 10 HEPES (pH 7.4, adjusted with NaOH). After a 30 minute recovery period from anesthesia animals were head-fixed in the recording setup and received a bolus-loading of the cell-permeant fluorescent $Ca^{2+}$ indicator Cal-520 AM (0.2 mM; AAT Bioquest, Sunnyvale, CA, USA). The dye was first dissolved with 10% w/V Pluronic F-127 in DMSO (Invitrogen) and diluted 20x in the extracellular solution. The dye solution was pressure injected into the molecular layer (50–80 µm below the surface) at 0.35 bar for 5 min. After dye loading, the brain surface was covered with 2% agarose dissolved in saline (0.9% NaCl) in order to reduce motion artefacts and prevent dehydration.

Starting at least 30 min after dye injection, *in vivo* two-photon $Ca^{2+}$ imaging was performed of the molecular layer using a setup consisting of a titanium sapphire laser (Chameleon Ultra, Coherent, Santa Clara, CA), a TriM Scope II system (LaVisionBioTec, Bielefeld, Germany) mounted on a BX51 microscope with a 20x 1.0 NA water immersion objective (Olympus, Tokyo, Japan) and GaAsP photomultiplier detectors (Hamamatsu, Iwata City, Japan). A typical recording sampled 40 x 200 µm with a frame rate of approximately 25 Hz.

## Data inclusion

We included all mice measured during this study, with the exception of one mouse where video-analysis revealed that the air-puff was delivered more to the nose than to the whisker pad. Single-unit data was included if the recording was of sufficient quality and reflected the activity of a single PC according to the rules defined below (see section *Electrophysiological analysis*).



## Whisker tracking

Whisker movements were tracked offline as described previously (Rahmati et al., 2014) using a method based on the BIOTACT Whisker Tracking Tool (Perkon et al., 2011). We used the average angle of all trackable large facial whiskers for further quantification of whisker behavior. The impact of 4 Hz air-puff stimulation on air-puff-triggered whisker movement was quantified using a bootstrap method. First, we took the last 100 trials before induction and divided these randomly in two series of 50. We calculated the differences in whisker position between these two series, and repeated this 1000 times. From this distribution we derived the expected variation after whisker pad air-puff stimulation. We took the 99% confidence interval as the threshold to which we compared the difference between 50 randomly chosen trials after and 50 randomly chosen trials before induction.

## Electrophysiological analysis

Spikes were detected offline using SpikeTrain (Neurasmus, Rotterdam, The Netherlands). A recording was considered to originate from a single PC when it contained both complex spikes (identified by the presence of stereotypic spikelets) and simple spikes, when the minimal inter-spike interval of simple spikes was 3 ms and when each complex spike was followed by a pause in simple spike firing of at least 8 ms. The regularity of simple spike firing was expressed as the local variation (CV2) and calculated as $2|ISI_{n+1}-ISI_n|/(ISI_{n+1}+ISI_n)$ with ISI = inter-simple spike interval (Shin et al., 2007). Only single-unit recordings of PCs with a minimum recording duration of 200 s were selected for further analysis. However, for the neural tracing experiments (see below), on which no quantitative analysis was performed, we accepted a minimum recording duration of 50 s.

## Two-photon $Ca^{2+}$ imaging analysis

Image analysis was performed offline using custom made software as described and validated previously (Ozden et al., 2008, Ozden et al., 2012, De Gruijl et al., 2014). In short, we performed independent component analysis to define the areas of individual Purkinje cell dendrites (Figure 3 – figure supplement 2A). The fluorescent values of all pixels in each region of interest were averaged per frame. These averages were plotted over time using a high-pass filter. A 8% rolling baseline was subtracted with a time window of 0.5 ms (Ozden et al., 2012). $Ca^{2+}$ transients were detected using template matching. For the aggregate peri-stimulus time histograms

(PSTHs), we calculated per individual frame the number of complex spikes detected and made a PSTH color coding the number of simultaneously detected complex spikes. Based on the total number of complex spikes and dendrites per recording, we calculated the expected number of simultaneous complex spikes per individual frame based upon a Poisson distribution. The actual number of simultaneous complex spikes was compared to this calculated distribution and a *p* value was derived for each number based upon the Poisson distribution.

## Characterization of sensory responses

For each PC recording, we constructed PSTHs of complex spikes and simple spikes separately using a bin size of 10 ms for display purposes. For further quantitative analyses of the PSTHs, we used a bin size of 1 ms and convolved them with a 21 ms wide Gaussian kernel. Complex spike responses were characterized by their peak amplitude, defined as the maximum of the convolved PSTH and expressed in percentage of trials in which a complex spike occurred within a 1 ms bin. Latencies were taken as the time between stimulus onset and the time of the response peak, as determined from the convolved PSTH. For some analyses, we discriminated between the sensory response period (0-60 ms after stimulus onset) and inter-trial interval (500 to 200 ms before stimulus onset). We considered a PC responsive for sensory stimulation if the peak or trough in the PSTH in the 60 ms after the stimulus onset exceeded the threshold of 3 s.d. above or below the average of the pre-stimulus interval (1 ms bins convolved with a 21 ms Gaussian kernel, pre-stimulus interval 200 ms before stimulus onset). Long-term stability of electrophysiological recordings was verified by heat maps of time-shifted PSTHs. The time-shifted PSTH was processed by calculating the simple spike PSTH for 20 air-puffs per row, which were shifted by 5 air-puffs between neighboring rows. The simple spike rates per row are calculated at 1 ms resolution and convolved with a 21 ms Gaussian kernel and color-coded relative to baseline firing rate (-1000 to -200 ms relative to air-puff time).

## Cluster analysis

A principal component analysis showed that the heterogeneity among the sensory complex spike responses was driven almost exclusively by one parameter, the maximum amplitude peak of the convolved complex spike PSTH. We performed a univariate Gaussian mixture model using only that variable. The Bayesian information criterion (BIC) indicated that the model with two components with unequal variances yielded the best approximation of the data. Then we applied the function Mclust(data) in R (R Foundation, Vienna, Austria) which use the expectation-maximization algorithm in order to assert the main parameters of the resulting models (probability, mean and variance of each population).

## Spike-whisker movement correlation matrix

Trial-by-trial correlation between instantaneous simple spike firing rate and whisker position was performed as described before (Ten Brinke et al., 2015). In short: spike density functions

were computed for all trials by convolving spike occurrences across 1 ms bins with an 8 ms Gaussian kernel. Both spike and whisker data were aligned to the 200 ms baseline. For cell groups, data was standardized for each cell for each correlation, and then pooled. The spike-whisker Pearson correlation coefficient R was calculated in bin of 10 ms, resulting in a 40x40 R-value matrix showing correlations for -100 to 300 ms around the air-puff presentation.



## Statistical analysis

Group sizes of the blindly acquired data sets were not defined a priori as the effect size and variation were not known beforehand. A post hoc power calculation based upon the results of the potentiation of the PC responses to whisker pad stimulation of the "weak complex spike responders" indicated a minimum group size of 12 PCs ($\alpha$ = 5%, $\beta$ = 20%, $\Delta$ = 9.65%, s.d. = 10.59%, paired *t* test). This number was obtained for the "weak complex spike responders" in WT (*n* = 35), *Pcp2-Ppp3r1* (*n* = 21) and *Pcp2-Gria3* PCs (*n* = 13), as well as for the relatively rare "strong complex spike responders" in WT mice (*n* = 20). This was further substantiated by other independent analyses, including ANOVA and linear regression, as described in the Results section. Variations in success rate, especially considering recordings of longer duration in combination with video tracking, explain why some groups are larger than others. Data was excluded only in case of a signal to noise ratio that was insufficient to warrant reliable analysis. For data visualization and statistical analysis, we counted the number of PCs as the number of replicates for the spike-based analyses and the number of mice for the behavior-based analyses. We tested whether the observed increase in coherence after sensory stimulation (Figure 3 – figure supplement 2D-G) was more than expected from the increased firing rate induced by the stimulation. The expected coherence based on the firing rate was calculated from 1000 bootstrapped traces from the inhomogeneous Poisson spike trains made for each neuron. The resultant distribution was compared to the measured distribution using a two-sample Kolmogorov-Smirnov test. Stacked line plots were generated by cumulating the values of all subjects per time point. Thus, the first line (darkest color) represents the first subject, the second line the sum of the first two, the third line the first three, etcetera. The data are divided by the number of subjects, so that the last line (brightest color) represents, next to the increase from the one but last value, also the population average. Sample size and measures for mean and variation are specified throughout the text and figure legends. For normally distributed data (as evaluated using the Kolmogorov-Smirnov test) parametric tests were used. Comparisons were always made with 2-sided tests when applicable. Unpaired *t* test were always made with Welch correction for possible differences in s.d.

## Data and software availability

The data for the box plots is available as Source Data Files. Custom written Matlab code to complement the whisker tracking analysis by the BIOTACT Whisker Tracking Tool was used as described previously (Rahmati et al., 2014) and is available via GitHub (Spanke and Negrello, 2018).

## REFERENCES


Ahl, A. S. 1986. The role of vibrissae in behavior: a status review. *Vet Res Commun*, 10, 245-68, 10.1007/BF02213989.

Albus, J. S. 1971. Theory of cerebellar function. *Math Biosci*, 10, 25-61, 10.1016/0025-5564(71)90051-4.

Anjum, F. & Brecht, M. 2012. Tactile experience shapes prey-capture behavior in Etruscan shrews. *Front Behav Neurosci*, 6, 28, 10.3389/fnbeh.2012.00028.

Apps, R. & Hawkes, R. 2009. Cerebellar cortical organization: a one-map hypothesis. *Nat Rev Neurosci*, 10, 670-81, 10.1038/nrn2698.

Arkley, K., Tiktak, G. P., Breakell, V., Prescott, T. J. & Grant, R. A. 2017. Whisker touch guides canopy exploration in a nocturnal, arboreal rodent, the Hazel dormouse (*Muscardinus avellanarius*). *J Comp Physiol A Neuroethol Sens Neural Behav Physiol*, 203, 133-142, 10.1007/s00359-017-1146-z.

Badura, A., Schonewille, M., Voges, K., Galliano, E., Renier, N., Gao, Z., Witter, L., Hoebeek, F. E., Chedotal, A. & De Zeeuw, C. I. 2013. Climbing fiber input shapes reciprocity of Purkinje cell firing. *Neuron*, 78, 700-13, 10.1016/j.neuron.2013.03.018.

Barski, J. J., Dethleffsen, K. & Meyer, M. 2000. Cre recombinase expression in cerebellar Purkinje cells. *Genesis*, 28, 93-8, 10.1002/1526-968X(200011/12)28:3/4<93::AID-GENE10>3.0.CO;2-W.

Bellavance, M. A., Takatoh, J., Lu, J., Demers, M., Kleinfeld, D., Wang, F. & Deschênes, M. 2017. Parallel inhibitory and excitatory trigemino-facial feedback circuitry for reflexive vibrissa movement. *Neuron*, 95, 673-82, 10.1016/j.neuron.2017.06.045.

Berg, R. W. & Kleinfeld, D. 2003. Rhythmic whisking by rat: retraction as well as protraction of the vibrissae is under active muscular control. *J Neurophysiol*, 89, 104-17, 10.1152/jn.00600.2002.

Boele, H. J., Peter, S., Ten Brinke, M. M., Verdonschot, L., IJpelaar, A. C. H. G., Rizopoulos, D., Gao, Z., Koekkoek, S. K. E. & De Zeeuw, C. I. 2018. Impact of parallel fiber to Purkinje cell long-term depression is unmasked in absence of inhibitory input. *Sci Adv*, 4, eaas9426, 10.1126/sciadv.aas9426

Bosman, L. W. J., Houweling, A. R., Owens, C. B., Tanke, N., Shevchouk, O. T., Rahmati, N., Teunissen, W. H. T., Ju, C., Gong, W., Koekkoek, S. K. E. & De Zeeuw, C. I. 2011. Anatomical pathways involved in generating and sensing rhythmic whisker movements. *Front Integr Neurosci*, 5, 53, 10.3389/fnint.2011.00053.

Bosman, L. W. J., Koekkoek, S. K. E., Shapiro, J., Rijken, B. F. M., Zandstra, F., van der Ende, B., Owens, C. B., Potters, J. W., de Gruijl, J. R., Ruigrok, T. J. H. & De Zeeuw, C. I. 2010. Encoding of whisker input by cerebellar Purkinje cells. *J Physiol*, 588, 3757-83, doi:10.1113/jphysiol.2010.195180.

Brecht, M. 2007. Barrel cortex and whisker-mediated behaviors. *Curr Opin Neurobiol*, 17, 408-16, 10.1016/j.conb.2007.07.008.

Brown, I. E. & Bower, J. M. 2001. Congruence of mossy fiber and climbing fiber tactile projections in the lateral hemispheres of the rat cerebellum. *J Comp Neurol*, 429, 59-70, 10.1002/1096-9861(20000101)429:1<59::AID-CNE5>3.0.CO;2-3 [pii].

Brown, S. T. & Raman, I. M. 2018. Sensorimotor integration and amplification of reflexive whisking by well-timed spiking in the cerebellar corticonuclear circuit. *Neuron*, 10.1016/j.neuron.2018.06.028.

Chaumont, J., Guyon, N., Valera, A. M., Dugué, G. P., Popa, D., Marcaggi, P., Gautheron, V., Reibel-Foisset, S., Dieudonné, S., Stephan, A., Barrot, M., Cassel, J. C., Dupont, J. L., Doussau, F., Poulain, B., Selimi, F., Léna, C. & Isope, P. 2013. Clusters of cerebellar Purkinje cells control their afferent climbing fiber discharge. *Proc Natl Acad Sci U S A*, 110, 16223-8, 10.1073/pnas.1302310110.

Chen, S., Augustine, G. J. & Chadderton, P. 2016. The cerebellum linearly encodes whisker position during voluntary movement. *Elife*, 5, e10509, 10.7554/eLife.10509.

Chu, C. P., Bing, Y. H. & Qiu, D. L. 2011. Sensory stimulus evokes inhibition rather than excitation in cerebellar Purkinje cells *in vivo* in mice. *Neurosci Lett*, 487, 182-6, 10.1016/j.neulet.2010.10.018.

Coesmans, M., Weber, J. T., De Zeeuw, C. I. & Hansel, C. 2004. Bidirectional parallel fiber plasticity in the cerebellum under climbing fiber control. *Neuron*, 44, 691-700, 10.1016/j.neuron.2004.10.031.

D'Angelo, E., Mapelli, L., Casellato, C., Garrido, J. A., Luque, N., Monaco, J., Prestori, F., Pedrocchi, A. & Ros, E. 2016. Distributed circuit plasticity: new clues for the cerebellar mechanisms of learning. *Cerebellum*, 15, 139-51, 10.1007/s12311-015-0711-7.

D'Angelo, E., Nieus, T., Maffei, A., Armano, S., Rossi, P., Taglietti, V., Fontana, A. & Naldi, G. 2001. Theta-frequency bursting and resonance in cerebellar granule cells: experimental evidence and modeling of a slow k+-dependent mechanism. *J Neurosci*, 21, 759-70, 10.1523/JNEUROSCI.21-03-00759.2001.

De Gruijl, J. R., Hoogland, T. M. & De Zeeuw, C. I. 2014. Behavioral correlates of complex spike synchrony in cerebellar microzones. *J Neurosci*, 34, 8937-44, 10.1523/JNEUROSCI.5064-13.2014.

De Zeeuw, C. I., Hoebeek, F. E., Bosman, L. W. J., Schonewille, M., Witter, L. & Koekkoek, S. K. 2011. Spatiotemporal firing patterns in the cerebellum. *Nat Rev Neurosci*, 12, 327-44, doi:10.1038/nrn3011.

De Zeeuw, C. I., Lang, E. J., Sugihara, I., Ruigrok, T. J., Eisenman, L. M., Mugnaini, E. & Llinás, R. 1996. Morphological correlates of bilateral synchrony in the rat cerebellar cortex. *J Neurosci*, 16, 3412-26, 10.1523/JNEUROSCI.16-10-03412.1996.

De Zeeuw, C. I. & Ten Brinke, M. M. 2015. Motor learning and the cerebellum. *Cold Spring Harb Perspect Biol*, 7, a021683, 10.1101/cshperspect.a021683.

De Zeeuw, C. I., Wylie, D. R., Stahl, J. S. & Simpson, J. I. 1995. Phase relations of Purkinje cells in the rabbit flocculus during compensatory eye movements. *J Neurophysiol*, 74, 2051-64, 10.1152/jn.1995.74.5.2051.

Dehnhardt, G., Mauck, B., Hanke, W. & Bleckmann, H. 2001. Hydrodynamic trail-following in harbor seals (*Phoca vitulina*). *Science*, 293, 102-4, 10.1126/science.1060514.

Dere, E., Huston, J. P. & De Souza Silva, M. A. 2007. The pharmacology, neuroanatomy and neurogenetics of one-trial object recognition in rodents. *Neurosci Biobehav Rev*, 31, 673-704, 10.1016/j.neubiorev.2007.01.005.

Deschênes, M., Takatoh, J., Kurnikova, A., Moore, J. D., Demers, M., Elbaz, M., Furuta, T., Wang, F. & Kleinfeld, D. 2016. Inhibition, not excitation, drives rhythmic whisking. *Neuron*, 90, 374-87, 10.1016/j.neuron.2016.03.007.

Ferezou, I., Haiss, F., Gentet, L. J., Aronoff, R., Weber, B. & Petersen, C. C. H. 2007. Spatiotemporal dynamics of cortical sensorimotor integration in behaving mice. *Neuron*, 56, 907-23., 10.1016/j.neuron.2007.10.007.

Gao, Z., Van Beugen, B. J. & De Zeeuw, C. I. 2012. Distributed synergistic plasticity and cerebellar learning. *Nat Rev Neurosci*, 13, 619-35, 10.1038/nrn3312.

Gogan, P. 1970. The startle and orienting reactions in man. A study of their characteristics and habituation. *Brain Res*, 18, 117-35, 10.1016/0006-8993(70)90460-9.

Gutierrez-Castellanos, N., Da Silva-Matos, C. M., Zhou, K., Canto, C. B., Renner, M. C., Koene, L. M. C., Ozyildirim, O., Sprengel, R., Kessels, H. W. & De Zeeuw, C. I. 2017. Motor learning requires Purkinje cell synaptic potentiation through activation of AMPA-receptor subunit *Gria3*. *Neuron*, 93, 409-424, 10.1016/j.neuron.2016.11.046.

Haidarliu, S., Kleinfeld, D., Deschênes, M. & Ahissar, E. 2015. The musculature that drives active touch by vibrissae and nose in mice. *Anat Rec (Hoboken)*, 298, 1347-58, 10.1002/ar.23102.

Halverson, H. E., Khilkevich, A. & Mauk, M. D. 2015. Relating cerebellar Purkinje cell activity to the timing and amplitude of conditioned eyelid responses. *J Neurosci*, 35, 7813-32, 10.1523/JNEUROSCI.3663-14.2015.

Hansel, C., Linden, D. J. & D'Angelo, E. 2001. Beyond parallel fiber LTD: the diversity of synaptic and non-synaptic plasticity in the cerebellum. *Nat Neurosci*, 4, 467-75, 10.1038/87419.

Heiney, S. A., Wohl, M. P., Chettih, S. N., Ruffolo, L. I. & Medina, J. F. 2014. Cerebellar-dependent expression of motor learning during eyeblink conditioning in head-fixed mice. *J Neurosci*, 34, 14845-53, 10.1523/JNEUROSCI.2820-14.2014.

Herfst, L. J. & Brecht, M. 2008. Whisker movements evoked by stimulation of single motor neurons in the facial nucleus of the rat. *J Neurophysiol*, 99, 2821-32, 01014.2007 [pii]10.1152/jn.01014.2007.

Herzfeld, D. J., Kojima, Y., Soetedjo, R. & Shadmehr, R. 2015. Encoding of action by the Purkinje cells of the cerebellum. *Nature*, 526, 439-42, 10.1038/nature15693.

Herzfeld, D. J., Kojima, Y., Soetedjo, R. & Shadmehr, R. 2018. Encoding of error and learning to correct that error by the Purkinje cells of the cerebellum. *Nat Neurosci*, 21, 736-743, 10.1038/s41593-018-0136-y.

Hoogland, T. M., De Gruijl, J. R., Witter, L., Canto, C. B. & De Zeeuw, C. I. 2015. Role of synchronous activation of cerebellar Purkinje cell ensembles in multi-joint movement control. *Curr Biol*, 25, 1157-65, 10.1016/j.cub.2015.03.009.

Ito, M. 2001. Cerebellar long-term depression: characterization, signal transduction, and functional roles. *Physiol Rev*, 81, 1143-95., 10.1152/physrev.2001.81.3.1143.

Ito, M. 2003. Long-term depression. *Annu Rev Neurosci*, 12, 85-102, 10.1146/annurev.ne.12.030189.000505.

Jirenhed, D. A., Bengtsson, F. & Hesslow, G. 2007. Acquisition, extinction, and reacquisition of a cerebellar cortical memory trace. *J Neurosci*, 27, 2493-502, 10.1523/JNEUROSCI.4202-06.2007.

Ju, C., Bosman, L. W. J., Hoogland, T. M., Velauthapillai, A., Murugesan, P., Warnaar, P., Negrello, M. & De Zeeuw, C. I. 2018. Neurons of the inferior olive respond to broad classes of sensory input while subject to homeostatic control. *bioRxiv*, 379149, 10.1101/379149.

Kitazawa, S., Kimura, T. & Yin, P. B. 1998. Cerebellar complex spikes encode both destinations and errors in arm movements. *Nature*, 392, 494-7, 10.1038/33141.

Kleinfeld, D., Berg, R. W. & O'Connor, S. M. 1999. Anatomical loops and their electrical dynamics in relation to whisking by rat. *Somatosens Mot Res*, 16, 69-88,

Koekkoek, S. K. E., Hulscher, H. C., Dortland, B. R., Hensbroek, R. A., Elgersma, Y., Ruigrok, T. J. H. & De Zeeuw, C. I. 2003. Cerebellar LTD and learning-dependent timing of conditioned eyelid responses. *Science*, 301, 1736-9, 10.1126/science.1088383.

Konnerth, A., Dreessen, J. & Augustine, G. J. 1992. Brief dendritic calcium signals initiate long-lasting synaptic depression in cerebellar Purkinje cells. *Proc Natl Acad Sci U S A*, 89, 7051-5., 10.1073/pnas.89.15.7051.

Kubo, R., Aiba, A. & Hashimoto, K. 2018. The anatomical pathway from the mesodiencephalic junction to the inferior olive relays perioral sensory signals to the cerebellum in the mouse. *J Physiol*, 10.1113/JP275836.

Lev-Ram, V., Mehta, S. B., Kleinfeld, D. & Tsien, R. Y. 2003. Reversing cerebellar long-term depression. *Proc Natl Acad Sci U S A*, 100, 15989-93, 10.1073/pnas.2636935100.

Lev-Ram, V., Wong, S. T., Storm, D. R. & Tsien, R. Y. 2002. A new form of cerebellar long-term potentiation is postsynaptic and depends on nitric oxide but not cAMP. *Proc Natl Acad Sci U S A*, 99, 8389-93., 10.1073/pnas.122206399.

Lisberger, S. G. 1998. Physiologic basis for motor learning in the vestibulo-ocular reflex. *Otolaryngol Head Neck Surg*, 119, 43-8, 10.1016/S0194-5998(98)70172-X.

Lisberger, S. G. & Miles, F. A. 1980. Role of primate medial vestibular nucleus in long-term adaptive plasticity of vestibuloocular reflex. *J Neurophysiol*, 43, 1725-45, 10.1152/jn.1980.43.6.1725.

Loewenstein, Y., Mahon, S., Chadderton, P., Kitamura, K., Sompolinsky, H., Yarom, Y. & Häusser, M. 2005. Bistability of cerebellar Purkinje cells modulated by sensory stimulation. *Nat Neurosci*, 8, 202-11, 10.1038/nn1393.

Ly, R., Bouvier, G., Schonewille, M., Arabo, A., Rondi-Reig, L., Léna, C., Casado, M., De Zeeuw, C. I. & Feltz, A. 2013. T-type channel blockade impairs long-term potentiation at the parallel fiber-Purkinje cell synapse and cerebellar learning. *Proc Natl Acad Sci U S A*, 110, 20302-7, 10.1073/pnas.1311686110.

McElvain, L. E., Bagnall, M. W., Sakatos, A. & du Lac, S. 2010. Bidirectional plasticity gated by hyperpolarization controls the gain of postsynaptic firing responses at central vestibular nerve synapses. *Neuron*, 68, 763-75, 10.1016/j.neuron.2010.09.025.

McElvain, L. E., Friedman, B., Karten, H. J., Svoboda, K., Wang, F., Deschênes, M. & Kleinfeld, D. 2018. Circuits in the rodent brainstem that control whisking in concert with other orofacial motor actions. *Neuroscience*, 368, 152-170, 10.1016/j.neuroscience.2017.08.034.

Medina, J. F. & Lisberger, S. G. 2008. Links from complex spikes to local plasticity and motor learning in the cerebellum of awake-behaving monkeys. *Nat Neurosci*, 11, 1185-92, 10.1038/nn.2197.

Moore J. D., Deschênes, M., Furuta, T., Huber, D., Smear, M. C., Demers, M. & Kleinfeld, D. 2013. Hierarchy of orofacial rhythms revealed through whisking and breathing. *Nature* 497, 205-10, 10.1038/nature12076.

Moreno-Paublete, R., Canlon, B. & Cederroth, C. R. 2017. Differential neural responses underlying the inhibition of the startle response by pre-pulses or gaps in mice. *Front Cell Neurosci*, 11, 19, 10.3389/fncel.2017.00019.

Mukamel, E. A., Nimmerjahn, A. & Schnitzer, M. J. 2009. Automated analysis of cellular signals from large-scale calcium imaging data. *Neuron*, 63, 747-60, 10.1016/j.neuron.2009.08.009.

Narain, D., Remington, E. D., De Zeeuw, C. I. & Jazayeri, M. 2018. A cerebellar mechanism for learning prior distributions of time intervals. *Nat Commun*, 9, 469, 10.1038/s41467-017-02516-x.

Nguyen, Q. T. & Kleinfeld, D. 2005. Positive feedback in a brainstem tactile sensorimotor loop. *Neuron*, 45, 447-57, 10.1016/j.neuron.2004.12.042.

Ohtsuki, G., Piochon, C. & Hansel, C. 2009. Climbing fiber signaling and cerebellar gain control. *Front Cell Neurosci*, 3, 4, 10.3389/neuro.03.004.2009.

Ozden, I., Dombeck, D. A., Hoogland, T. M., Tank, D. W. & Wang, S. S. 2012. Widespread state-dependent shifts in cerebellar activity in locomoting mice. *PLoS One*, 7, e42650, 10.1371/journal.pone.0042650.

Ozden, I., Lee, H. M., Sullivan, M. R. & Wang, S. S. H. 2008. Identification and clustering of event patterns from in vivo multiphoton optical recordings of neuronal ensembles. *J Neurophysiol*, 100, 495-503, 01310.2007 [pii] 10.1152/jn.01310.2007.

Ozden, I., Sullivan, M. R., Lee, H. M. & Wang, S. S. H. 2009. Reliable coding emerges from coactivation of climbing fibers in microbands of cerebellar Purkinje neurons. *J Neurosci*, 29, 10463-73, 10.1523/JNEUROSCI.0967-09.2009.

Perkon, I., Kosir, A., Itskov, P. M., Tasic, J. & Diamond, M. E. 2011. Unsupervised quantification of whisking and head movement in freely moving rodents. *J Neurophysiol*, 105, 1950-62, 10.1152/jn.00764.2010.

Peter, S., Ten Brinke, M. M., Stedehouder, J., Reinelt, C. M., Wu, B., Zhou, H., Zhou, K., Boele, H. J., Kushner, S. A., Lee, M. G., Schmeisser, M. J., Boeckers, T. M., Schonewille, M., Hoebeek, F. E. & De Zeeuw, C. I. 2016. Dysfunctional cerebellar Purkinje cells contribute to autism-like behaviour in *Shank2*-deficient mice. *Nat Commun*, 7, 12627, 10.1038/ncomms12627.

Prescott, T. J., Diamond, M. E. & Wing, A. M. 2011. Active touch sensing. *Philos Trans R Soc Lond B Biol Sci*, 366, 2989-95, 10.1098/rstb.2011.0167.

Proville, R. D., Spolidoro, M., Guyon, N., Dugué, G. P., Selimi, F., Isope, P., Popa, D. & Léna, C. 2014. Cerebellum involvement in cortical sensorimotor circuits for the control of voluntary movements. *Nat Neurosci*, 17, 1233-9, 10.1038/nn.3773.

Rahmati, N., Owens, C. B., Bosman, L. W. J., Spanke, J. K., Lindeman, S., Gong, W., Potters, J. W., Romano, V., Voges, K., Moscato, L., Koekkoek, S. K. E., Negrello, M. & De Zeeuw, C. I. 2014. Cerebellar potentiation and learning a whisker-based object localization task with a time response window. *J Neurosci*, 34, 1949-62, 10.1523/JNEUROSCI.2966-13.2014.

Ramakrishnan, K. B., Voges, K., De Propris, L., De Zeeuw, C. I. & D'Angelo, E. 2016. Tactile stimulation evokes long-lasting potentiation of Purkinje cell discharge *in vivo*. *Front Cell Neurosci*, 10, 36, 10.3389/fncel.2016.00036.

Ruigrok, T. J. H., Teune, T. M., van der Burg, J. & Sabel-Goedknegt, H. 1995. A retrograde double-labeling technique for light microscopy. A combination of axonal transport of cholera toxin B-subunit and a gold-lectin conjugate. *J Neurosci Methods*, 61, 127-38, 10.1016/0165-0270(94)00034-E.

Sanchis-Segura, C., Borchardt, T., Vengeliene, V., Zghoul, T., Bachteler, D., Gass, P., Sprengel, R. & Spanagel, R. 2006. Involvement of the AMPA receptor GluR-C subunit in alcohol-seeking behavior and relapse. *J Neurosci*, 26, 1231-8, 10.1523/JNEUROSCI.4237-05.2006.

Schonewille, M., Belmeguenai, A., Koekkoek, S. K., Houtman, S. H., Boele, H. J., van Beugen, B. J., Gao, Z., Badura, A., Ohtsuki, G., Amerika, W. E., Hosy, E., Hoebeek, F. E., Elgersma, Y., Hansel, C. & De Zeeuw, C. I. 2010. Purkinje cell-specific knockout of the protein phosphatase *Ppp3r1* impairs potentiation and cerebellar motor learning. *Neuron*, 67, 618-28, 10.1016/j.neuron.2010.07.009.

Schonewille, M., Gao, Z., Boele, H. J., Vinueza-Veloz, M. F., Amerika, W. E., Simek, A. A. M., De Jeu, M. T., Steinberg, J. P., Takamiya, K., Hoebeek, F. E., Linden, D. J., Huganir, R. L. & De Zeeuw, C. I. 2011. Reevaluating the role of LTD in cerebellar motor learning. *Neuron*, 70, 43-50, 10.1016/j.neuron.2011.02.044 [doi].

Schultz, S. R., Kitamura, K., Post-Uiterweer, A., Krupic, J. & Häusser, M. 2009. Spatial pattern coding of sensory information by climbing fiber-evoked calcium signals in networks of neighboring cerebellar Purkinje cells. *J Neurosci*, 29, 8005-15, 10.1523/jneurosci.4919-08.2009.

Shin, S. L., Hoebeek, F. E., Schonewille, M., De Zeeuw, C. I., Aertsen, A. & De Schutter, E. 2007. Regular patterns in cerebellar Purkinje cell simple spike trains. *PLoS One*, 2, e485, 10.1371/journal.pone.0000485.

Simony, E., Bagdasarian, K., Herfst, L., Brecht, M., Ahissar, E. & Golomb, D. 2010. Temporal and spatial characteristics of vibrissa responses to motor commands. *J Neurosci*, 30, 8935-52, 10.1523/JNEUROSCI.0172-10.2010.

Spanke, J. K., & Negrello, M. 2018. BWTT_PP. GitHub. https://github.com/MRIO/BWTT_PP.

Staudacher, E. M., Gebhardt, M. & Dürr, V. 2005. Antennal movements and mechanoreception: Neurobiology of active tactile sensors. *Adv Insect Physiol*, 32, 49-205, 10.1016/S0065-2806(05)32002-9.

Suvrathan, A., Payne, H. L. & Raymond, J. L. 2016. Timing Rules for Synaptic Plasticity Matched to Behavioral Function. *Neuron*, 92, 959-967, 10.1016/j.neuron.2016.10.022.

Swerdlow, N. R., Caine, S. B., Braff, D. L. & Geyer, M. A. 1992. The neural substrates of sensorimotor gating of the startle reflex: a review of recent findings and their implications. *J Psychopharmacol*, 6, 176-90, 10.1177/026988119200600210.

Ten Brinke, M. M., Boele, H. J., Spanke, J. K., Potters, J. W., Kornysheva, K., Wulff, P., IJpelaar, A. C. H. G., Koekkoek, S. K. E. & De Zeeuw, C. I. 2015. Evolving models of Pavlovian conditioning: cerebellar cortical dynamics in awake behaving mice. *Cell Rep*, 13, 1977-88, 10.1016/j.celrep.2015.10.057.

Teune, T. M., van der Burg, J., van der Moer, J., Voogd, J. & Ruigrok, T. J. 2000. Topography of cerebellar nuclear projections to the brain stem in the rat. *Prog Brain Res*, 124, 141-72, 10.1016/S0079-6123(00)24014-4.

Thier, P., Dicke, P. W., Haas, R., Thielert, C. D. & Catz, N. 2002. The role of the oculomotor vermis in the control of saccadic eye movements. *Ann N Y Acad Sci*, 978, 50-62, 10.1111/j.1749-6632.2002.tb07555.x.

Tsutsumi, S., Yamazaki, M., Miyazaki, T., Watanabe, M., Sakimura, K., Kano, M. & Kitamura, K. 2015. Structure-function relationships between aldolase C/zebrin II expression and complex spike synchrony in the cerebellum. *J Neurosci*, 35, 843-52, 10.1523/JNEUROSCI.2170-14.2015.

van Beugen, B. J., Gao, Z., Boele, H. J., Hoebeek, F. & De Zeeuw, C. I. 2013. High frequency burst firing of granule cells ensures transmission at the parallel fiber to purkinje cell synapse at the cost of temporal coding. *Front Neural Circuits*, 7, 95, 10.3389/fncir.2013.00095.

Vincent, S. B. 1913. The tactile hair of the white rat. *J Comp Neurol*, 23, 1-36, 10.1002/cne.900230101.

Voges, K., Wu, B., Post, L., Schonewille, M. & De Zeeuw, C. I. 2017. Mechanisms underlying vestibulocerebellar motor learning in mice depend on movement direction. *J Physiol*, 595, 5301-5326, 10.1113/JP274346.

Voigts, J., Herman, D. H. & Celikel, T. 2015. Tactile object localization by anticipatory whisker motion. *J Neurophysiol*, 113, 620-32, 10.1152/jn.00241.2014.

Voogd, J. & Glickstein, M. 1998. The anatomy of the cerebellum. *Trends Neurosci*, 21, 370-5, 10.1016/S0166-2236(98)01318-6.

Welker, W. I. 1964. Analysis of sniffing of the albino rat. *Behaviour*, 22, 223-244, 10.1163/156853964X00030.

Welsh, J. P., Lang, E. J., Suglhara, I. & Llinas, R. 1995. Dynamic organization of motor control within the olivocerebellar system. *Nature*, 374, 453-7, 10.1038/374453a0.

Witter, L., Canto, C. B., Hoogland, T. M., de Gruijl, J. R. & De Zeeuw, C. I. 2013. Strength and timing of motor responses mediated by rebound firing in the cerebellar nuclei after Purkinje cell activation. *Front Neural Circuits*, 7, 133, 10.3389/fncir.2013.00133.

Woolsey, T. A., Welker, C. & Schwartz, R. H. 1975. Comparative anatomical studies of the SmI face cortex with special reference to the occurrence of “barrels” in layer IV. *J Comp Neurol*, 164, 79-94, 10.1002/cne.901640107.

Yang, Y. & Lisberger, S. G. 2014. Purkinje-cell plasticity and cerebellar motor learning are graded by complex-spike duration. *Nature*, 510, 529-32, 10.1038/nature13282.

Yang, Y. & Lisberger, S. G. 2017. Modulation of complex-spike duration and probability during cerebellar motor learning in visually guided smooth-pursuit eye movements of monkeys. *eNeuro*, 4, 10.1523/ENEURO.0115-17.2017.

Zeng, H., Chattarji, S., Barbarosie, M., Rondi-Reig, L., Philpot, B. D., Miyakawa, T., Bear, M. F. & Tonegawa, S. 2001. Forebrain-specific calcineurin knockout selectively impairs bidirectional synaptic plasticity and working/episodic-like memory. *Cell*, 107, 617-29, 10.1016/S0092-8674(01)00585-2.

Zerari-Mailly, F., Pinganaud, G., Dauvergne, C., Buisseret, P. & Buisseret-Delmas, C. 2001. Trigemino-reticulo-facial and trigemino-reticulo-hypoglossal pathways in the rat. *J Comp Neurol*, 429, 80-93,

Zhang, W. & Linden, D. J. 2006. Long-term depression at the mossy fiber-deep cerebellar nucleus synapse. *J Neurosci*, 26, 6935-44, 10.1523/JNEUROSCI.0784-06.2006.

Zhou, H., Lin, Z., Voges, K., Ju, C., Gao, Z., Bosman, L. W. J., Ruigrok, T. J. H., Hoebeek, F. E., De Zeeuw, C. I. & Schonewille, M. 2014. Cerebellar modules operate at different frequencies. *eLIFE*, 3, e02536, 10.7554/eLife.02536.

## SUPPLEMENTARY MATERIAL

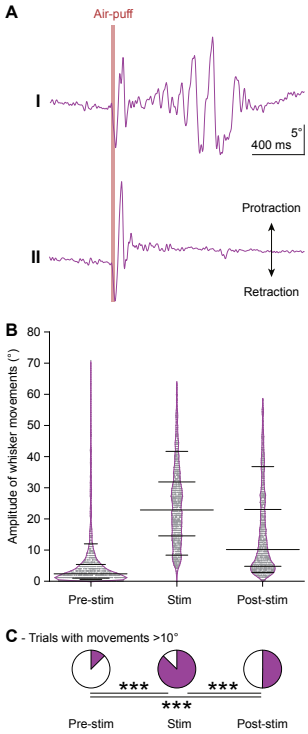


**Figure 1 – figure supplement 1.** Whisker movements are largely restricted to the period after the air-puff
**A.** During a prolonged period of 0.5 Hz whisker pad stimulation, in roughly half the trials the stereotypic whisker movement – retraction followed by a large active forward sweep – is followed by a prolonged period of more variable whisker movements. The traces show here the whisker movement (averaged over all trackable whiskers) during the two trials marked "I" and "II" in Figure 1D. **B.** Violin plots showing the amplitudes (difference between maximal retraction and maximal protraction in three 200 ms interval (relative to the start of the air-puff: -200 – 0 ms (Pre-stim), 0 – 200 ms (Stim) and 200 – 400 ms (Post-stim))) of individual trials of 16 mice (with approximately 100 trials per mouse). Horizontal lines represent 10$^{th}$, 25$^{th}$, 50$^{th}$, 75$^{th}$ and 90$^{th}$ percentiles. **C.** Fractions of trials with movements exceeding 10°. Asterisks indicate significantly different fractions of trials with movement. *** $p < 0.001$ ($\chi^2 = 1470.24$; 3x2 $\chi^2$ test).

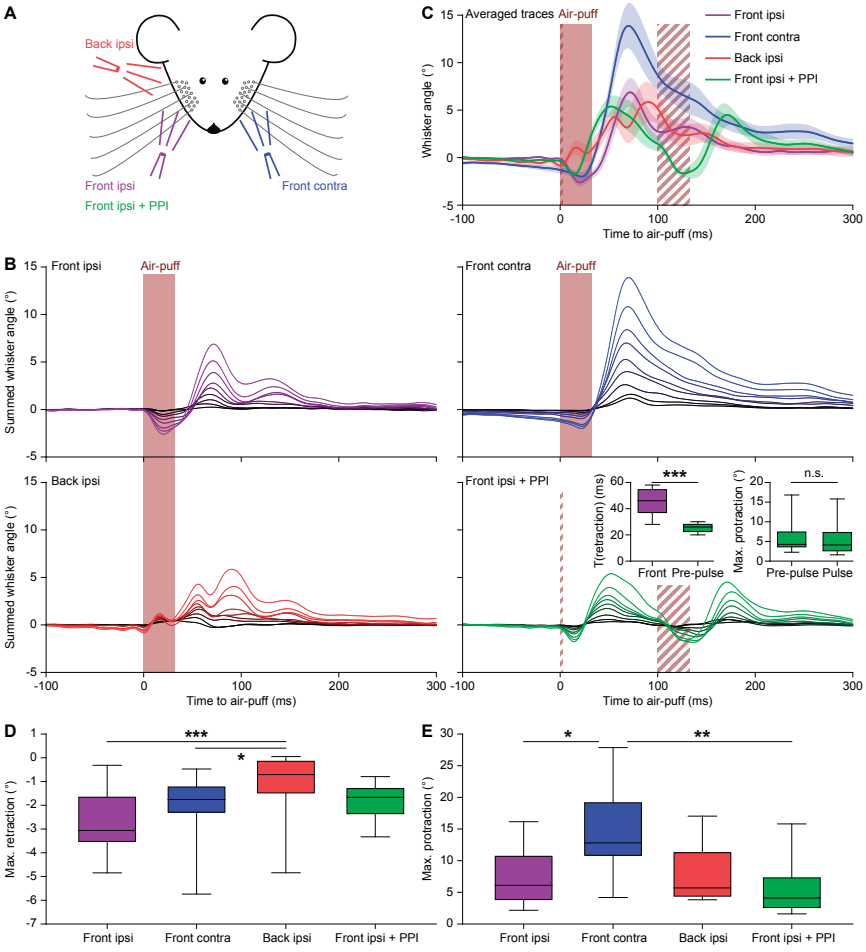


**Figure 1 – figure supplement 2.** Air-puffs induce reflexive whisker movements

**A.** Schematic drawing of the experimental layout. Air-puffs lasting 30 ms were delivered from three different locations. In addition, some air-puffs delivered ipsilaterally from the front were preceded by a brief air-puff (2 ms) 100 ms before the 30 ms air-puff to test for pre-pulse inhibition (PPI). The four stimulus conditions were applied in a random order. **B.** For each of the 9 mice tested, we calculated the average whisker response (always on the side with the two puffers) and represented these as summed line plots. The stacked line plots are scaled such that the brightest line (on top) depicts the average of all mice. The insets show the duration of the retraction (until the whiskers reached the baseline position again) comparing the 2 ms and the 30 ms pulses (left) and the maximal protraction amplitudes upon the pre-pulse compared to the pulse (right). The retraction upon the short pre-pulse was less intense, but the consecutive protractions were of similar amplitude, indicating the absence of pre-pulse inhibition ($p$ = 0.0078 and $p$ = 0.4961, respectively; Wilcoxon matched-pairs tests; significance level = 0.025 after Bonferroni correction for multiple comparisons). **C.** Overlay of averaged ipsilateral whisker responses with shaded areas indicating ± SEM. The three ipsilateral conditions resulted in similar amounts of protraction. Note that the puff from the back did not cause a retraction preceding the protraction and that the pre-pulse did not affect the size of the protraction following the second air-puff. The brief pre-pulse induced a shorter retraction, but this had no effect on the protraction. Air-puffs to the contralateral whisker pad caused stronger protractions than the ipsilateral stimuli. **D.** The maximum retraction was largest when the air-puffer was in front of the ipsilateral whiskers. The shorter pre-pulse did cause a briefer retraction (see inset in **B**), but the amplitude was not significantly different from the retraction caused by the longer pulse ($p$ = 0.268; Dunn's pairwise post-hoc test after Friedman's two-way ANOVA; see Table S1). Puffing from the contralateral whiskers or the ipsilateral whiskers from the back caused the least retraction, indicating that the initial retraction is largely passive and caused by the

air flow of the stimulator. **E.** The maximum protraction reached was similar for all conditions, except in case the contralateral whiskers were stimulated, which led to a stronger protraction on the ipsilateral side. n.s. $p > 0.05$; * $p < 0.05$; *** $p < 0.001$; *** $p < 0.001$. See also Source Data file.

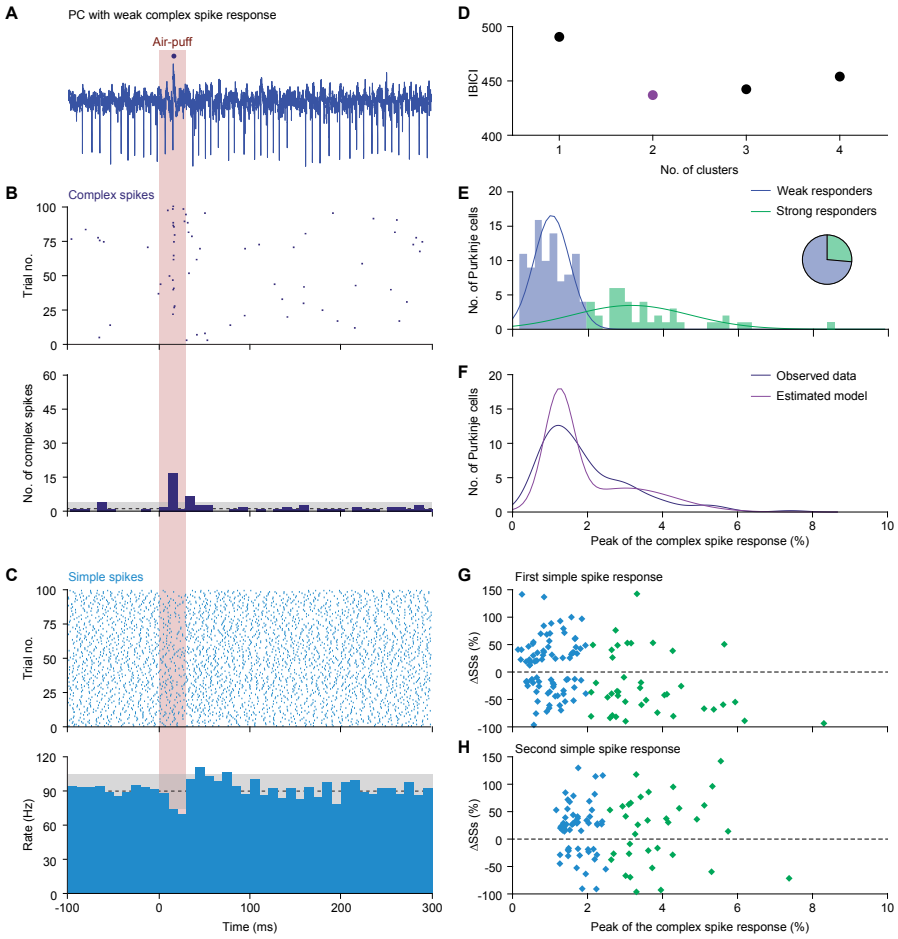


**Figure 2 – figure supplement 1.** Diversity in Purkinje cell responses

**A.** Single trial of a PC showing a relatively weak complex spike response to air-puff stimulation of the ipsilateral whisker pad. The dark blue dot indicates a complex spike. **B.** Raster plot and peri-stimulus time histogram (PSTH) of the complex spikes of the same neuron as in **A**. Note that although the initial response is relatively weak, being present only in about 15% of the trials, this is still much more than could be expected based on the frequency during the inter-trial intervals. The dashed line indicates the average complex spike rate in between trials with the grey area representing ± 3 s.d.. **C.** The same for the simple spike response. This PC has a bimodal simple spike response, first a decrease and then an increase in simple spike activity. **D.** Based upon the complex spike response probability, defined as the peak of the complex spike response in the convolved PSTH, clustering the PCs into two clusters yielded the smallest Bayesian information criterion (BIC) value. **E.** The majority (66%) of the PCs could be classified as “weak responders” and the minority (34%) as “strong responders” (see pie diagram). This classification was obtained using a univariate Gaussian mixture model (blue and green lines, representing the two clusters). **F.** Comparison of the distribution of the observed complex spike responses and that expected by our model. **G.** The strength of the complex spike response and the first peak or trough (cf. panel **C**) in the simple spike (SS) response were not significantly correlated. Only the PCs with a very strong complex response tended to have a decrease in the simple spike response. **H.** The same applied for the second extremum of the simple spike response. For this later phase the complex spike and the simple spike responses were even less correlated.

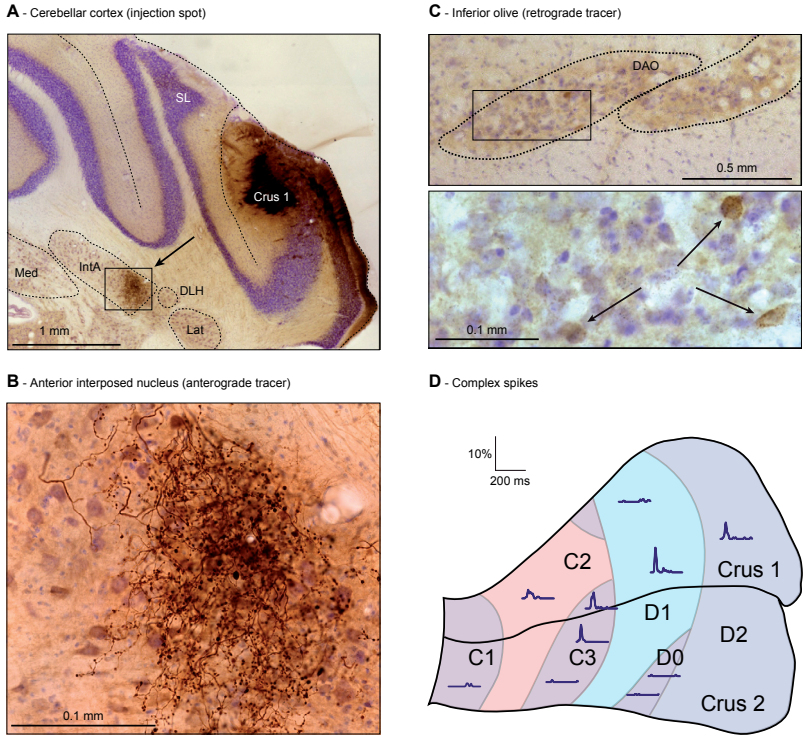


**Figure 2 – figure supplement 2.** Anatomy of the whisker region in the cerebellar hemispheres

**A.** PC locations could be retrieved by neural tracer injection (BDA 3000) after completion of the recording. In this example, tracer was found in the anterior interposed nucleus (IntA) (see arrow, area enlarged in **B**). SL = simple lobule; Med = medial nucleus; Lat = lateral nucleus; DLH = dorsolateral hump. Anterograde staining was observed in the cerebellar nuclei (**B**) and retrograde staining in the inferior olive (**C**) after a survival period of around 1 week. The rectangle in the top micrograph of **C** indicates the area enlarged in the lower micrograph. **D.** A map is shown of the approximated locations of the recorded PCs. The names of the cerebellar zones are indicated. The response kinetics of complex spikes are shown as convolved peri-stimulus time histograms. In these traces, the left-most point represents the onset of the air-puff. Note that strong complex spike responses were observed in C3, D1 and D2 zones. DAO = dorsal accessory olive; PO = principal olive.

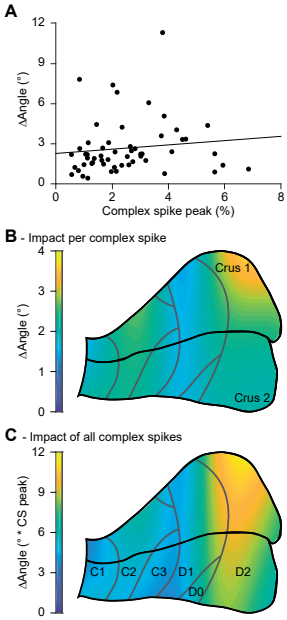


**Figure 3 – figure supplement 1.** Correlation between complex spike firing and whisker protraction is especially strong in the D2 zone

**A.** There was no obvious correlation between the strength of the complex spike response of any given PC and the difference in touch-induced whisker protraction in trials with and without a complex spike. **B.** Indeed, and with the exception of the lateral most portion of crus 1, the predictive value of the occurrence of a complex spike was quite evenly distributed over crus 1 and crus 2. Together with the findings of **A**, this implies that the extent of stronger protraction in trials with a complex spike does not depend on the response characteristics of a PC. In other words, the predictive value of a complex spike is similar whether it originates from a weak or from a strong responder. However, as the PCs in the lateral zones display more complex spikes, their overall impact on whisker protraction is larger (**C**). Thus, complex firing in the D2 zone had the strongest predictive value for increased touch-induced whisker protraction.

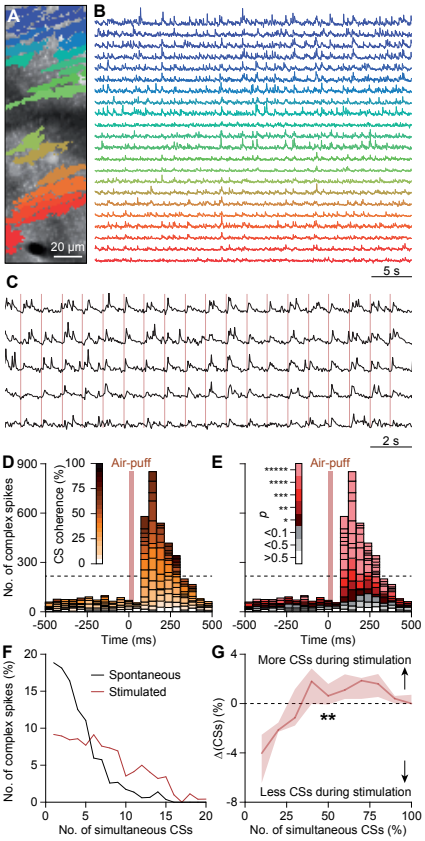


**Figure 3 – figure supplement 2.** Coherent complex spike firing is specifically enhanced by whisker pad stimulation

**A.** Field of view of a piece of crus 1 recorded using two-photon $Ca^{2+}$ imaging in an awake mouse. The colored areas indicate 22 regions of interest, corresponding to PC dendrites. The accompanying fluorescent traces show $Ca^{2+}$ transients, which are most likely complex spikes (**B**; cf. Schultz et al., 2009). In the absence of tactile stimulation coherent activity of groups of PCs is rare. **C.** Following air-puff stimulation of the whisker pad (brown vertical lines), complex spike coherence occurs often as illustrated by five responsive PCs recorded simultaneously. **D.** Aggregate peri-stimulus time histogram of all PCs in the field of view shown in panel **A**. The colors represent the coherence of PC firing, defined as the fraction of PCs active during each frame of 40 ms. Complex spike coherence is relatively rare during inter-trial intervals, but strongly enhanced following air-puff stimulation. **E.** The same peri-stimulus histogram as in **D**, but with colors indicating the chance of occurrence of the level of coherence found based upon Poisson distribution of all complex spikes in this recording, emphasizing that coherence occurred more than expected, mainly during the sensory response. Indeed, during 1 Hz air-puff stimulation, complex spikes were observed to be produced by large ensembles. In the absence of tactile stimulation, ensemble sizes tended to be smaller (**F**). The data presented in panels **D-F** come from the field of view shown in panel **A**. **G.** There was a shift from complex spikes fired by a single or a few Purkinje cells towards complex spikes fired by larger ensembles when introducing air-puff stimulation. Presented are the median and the inter-quartile range of the differences between the two histograms as illustrated for an example experiment in panel **F** ($n$ = 10). The increase in coherence directly after stimulation was highly significant ($p$ = 0.001; Fr = 28.878; df = 9; Friedman's two-way ANOVA). * $p < 0.05$; ** $p < 0.01$, *** $p < 0.001$, **** $p < 0.0001$, ***** $p < 0.00001$.

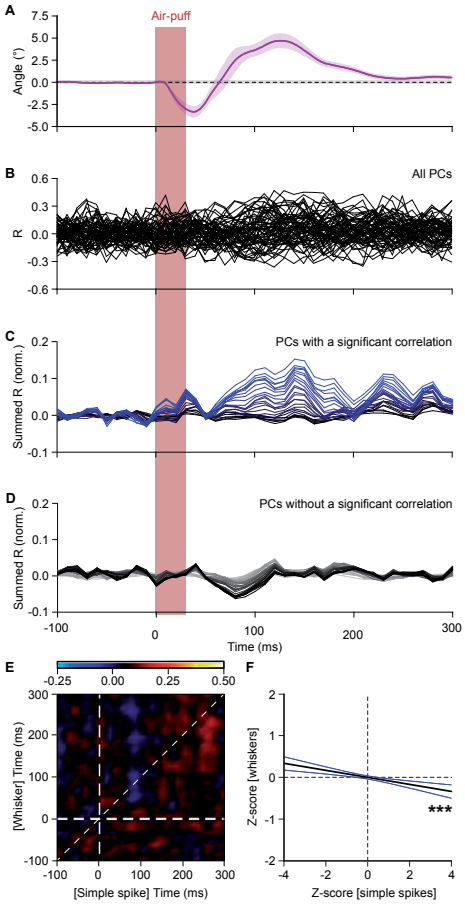


**Figure 4 – figure supplement 1.** Simple spike firing is predominantly associated with protraction

**A.** The average whisker response to air-puff stimulation (for reference, copied from Figure 4D). **B.** Overlaid plots of the correlation between whisker angle and instantaneous simple spike frequency based on a trial-by-trial analysis of all 56 PCs measured in this way (see Figure 6). The correlation values are based upon the zero-lag correlation (thus along the "45° line" in Figure 4C, D). **C.** Stacked line plot of the 25 PCs with a significant correlation between whisker angle and simple spike firing. The cells are ordered based upon their correlation value and scaled so that the brightest line corresponds to the average. **D.** As in **C**, but now of the 31 PCs that did not show a significant correlation between their simple spike firing and the whisker position. Although the correlation is not significant when regarded per cell, overall there is a negative correlation between simple spike firing and whisker position. The darkest line corresponds to the average. **E.** Correlation matrix showing the correlation between whisker protraction (on the y axis) and instantaneous simple spike frequency (on the x-axis) of the 31 PCs that did not have a significant correlation between these two parameters. The heatmap represent the average R value for each bin ($n$ = 31 PCs). The lookup table shows the color coding for the R values. **F.** Despite the lack of correlation at the single-cell level, at the population level these PCs correlated weakly but significantly in a negative manner (R = -0.067; $p < 0.001$; Pearson correlation), implying that they correlated more with retraction than with protraction. The black line indicates the linear regression line and the blue lines the 95% confidence interval. *** $p < 0.001$

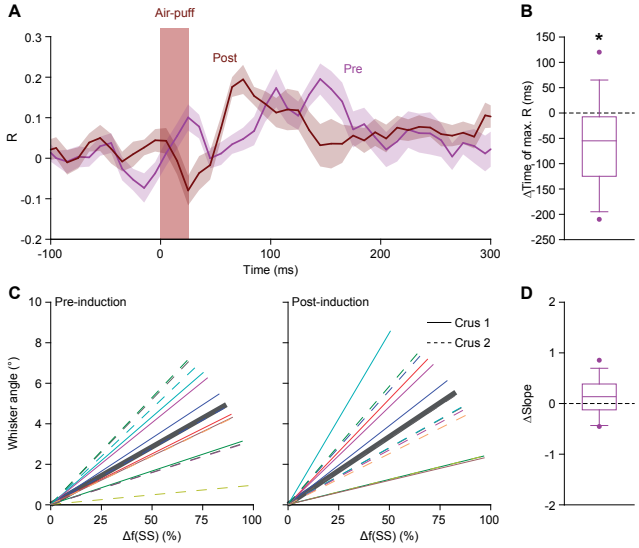


**Figure 5 – figure supplement 1.** Simple spike response anticipates after 4 Hz air-puff stimulation

**A.** Averaged zero-lag correlation (across the 45° line in Fig. 5F) of the instantaneous simple spike rate and whisker position before (magenta) and after (brown) 4 Hz air-puff stimulation, highlighting the faster achievement of the moment of maximal correlation after induction. This shift (again, along the 45° line) is further quantified and illustrated with a box plot (**B**). * $p < 0.05$. **C**. The slopes of the correlations between instantaneous simple spike firing rate and the angle of the whisker are shown before and after 4 Hz air-puff stimulation for the 14 individual PCs that showed significant correlation. Despite the cells with the highest R correlation values were located in the lateral Crus 2, no clear difference was observed between the slope of the correlation of the PCs of Crus 1 (solid lines) and PCs of Crus 2 (dashed lines). **D**. No slopes change was observed after 4 Hz air-puff stimulation. This indicates that the plasticity induction did not change the amount of movement that corresponded to a certain number of spikes. See also Source Data file.

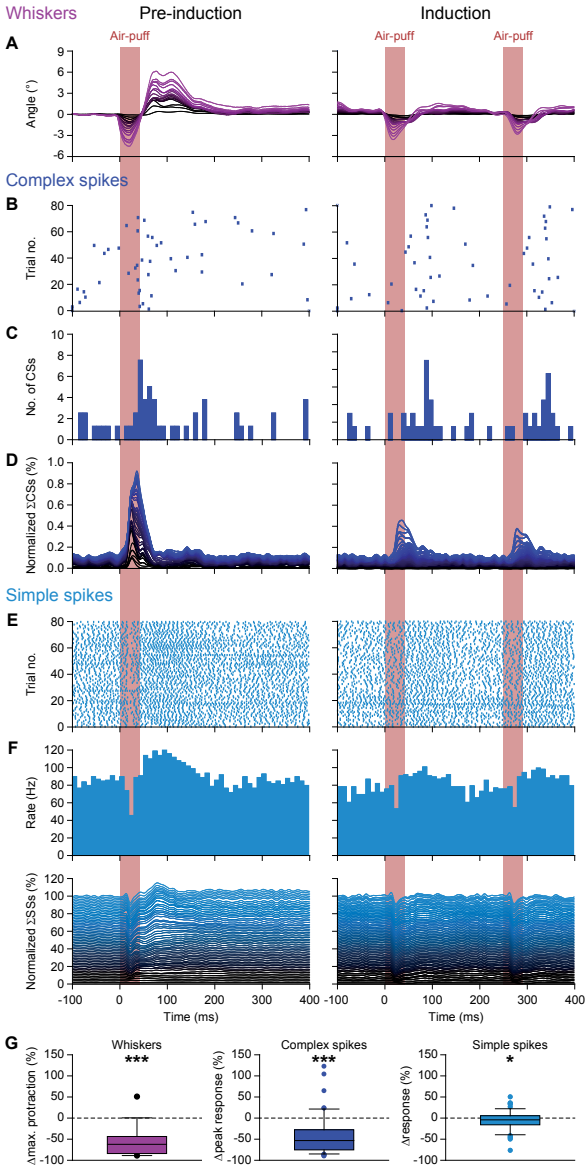


**Figure 5 - figure supplement 2.** Purkinje cell responses during 4 Hz air-puff stimulation

**A.** Normalized stacked line plots showing the whisker movement in 16 mice during the pre-induction block (100 trials; left) and during the induction block (80 trials; right). The retraction caused by the air flow is largely intact, but the subsequent touch-induced whisker protraction is largely reduced during 4 Hz stimulation as compared to 0.5 Hz stimulation during the pre-induction block. **B.** Raster plots of the complex spike responses to whisker pad air-puff stimulation during the first 80 trials of a pre-induction block and during the 80 trials of the induction block with the accompanying peri-stimulus time histograms (**C**). **D.** Normalized stacked line plots show that the rate of complex spike responses is reduced upon a higher stimulation frequency ($n$ = 55). **E-F.** The same plots depicted for the simple spike response. **G.** Box plots showing the decreased whisker, complex spike peak response and simple spike modulation during the first 200 ms after puff onset. * $p < 0.05$; *** $p < 0.001$ (Wilcoxon matched-pairs test). See also Source Data File.

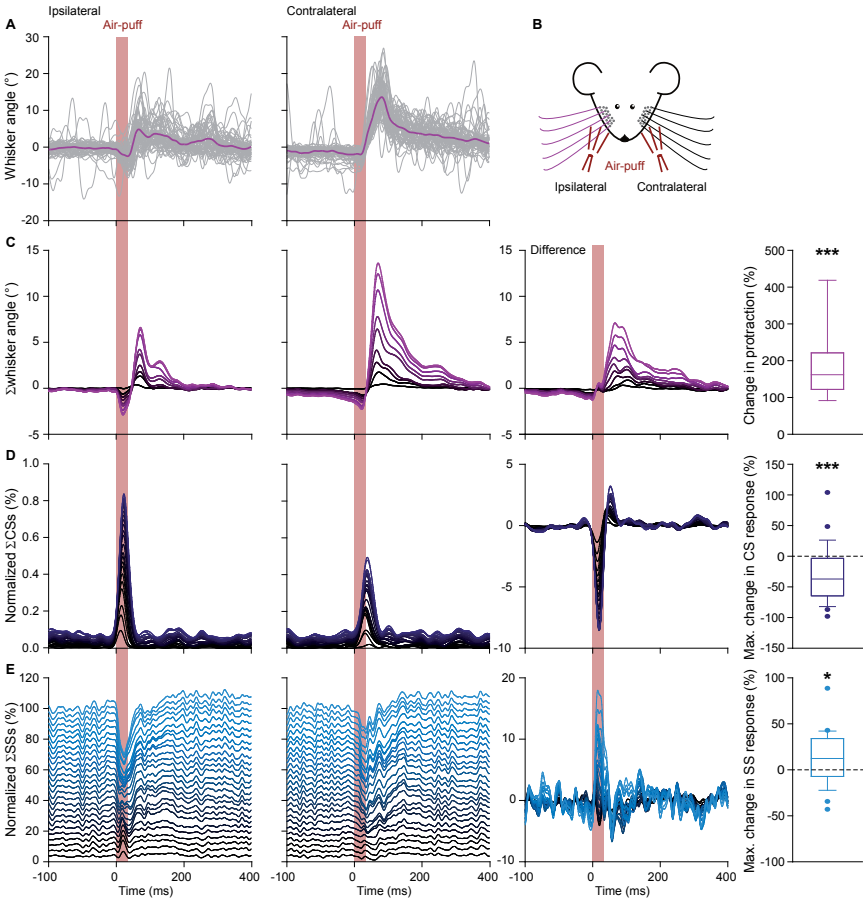


**Figure 5 – figure supplement 3.** Contralateral whisker pad stimulation induces stronger whisker protraction and stronger simple spike responses

**A.** Whisker traces of a representative mouse following air-puff stimulation of the ipsilateral (left panel) and contralateral (right panel) whisker pad (see scheme in **B**). Despite a similar strength of stimulation, the protraction of the whiskers was larger upon contralateral stimulation (cf. Figure 1 – figure supplement 2). **C.** Stacked line plots of the averaged whisker traces of 9 mice with the difference between the contralateral and ipsilateral stimulation depicted in the third column. **D.** Complex spike responses, on the other hand, were more prominent upon ipsilateral stimulation. **E.** The observation that increased simple spike firing correlates to enhanced whisker protraction (cf. Figure 4) was confirmed under these experimental conditions. * $p < 0.05$; *** $p < 0.001$. See also Data Source File.

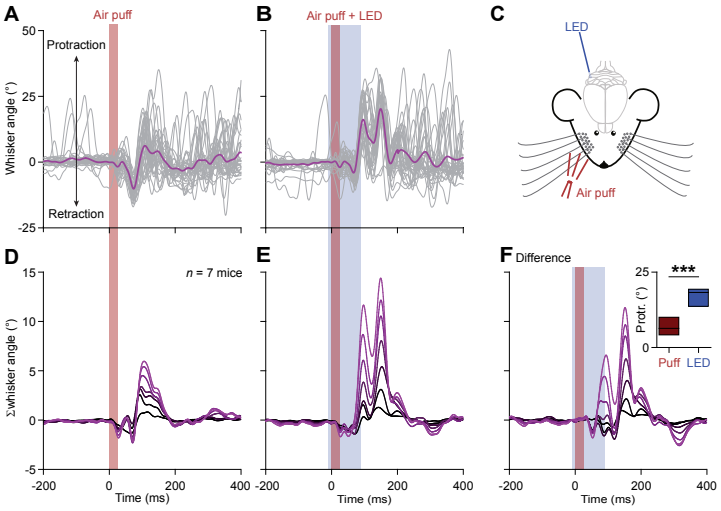


**Figure 5 – figure supplement 4.** Optogenetic stimulation of Purkinje cells increases whisker protraction following air-puff stimulation

**A.** Air-puff stimulation of the whisker pad induces reflexive touch-induced whisker protraction. **B.** This protraction is enhanced when the sensory stimulus is paired with optogenetic stimulation of PCs. These two panels show whisker traces from a *Pcp2-Ai27* mouse that expresses ChR2 specifically in its PCs. An optic fiber with a diameter of 400 µm was placed on the surface of the cerebellum centrally at the fissure between crus 1 and crus 2 (**C**). Optogenetic stimulation of these mice results in increased simple spike firing. Stacked line plots of the whisker traces of 7 mice tested in this way following air-puff stimulation alone (**D**) and in combination with PC stimulation (**E**). **F.** The increased PC activity correlated with stronger protraction as evidenced by the differential traces. The inset shows a comparison of the maximal protraction (Protr.) under the two stimulus conditions; *** $p < 0.001$ (paired $t$ test). See also Source Data File.

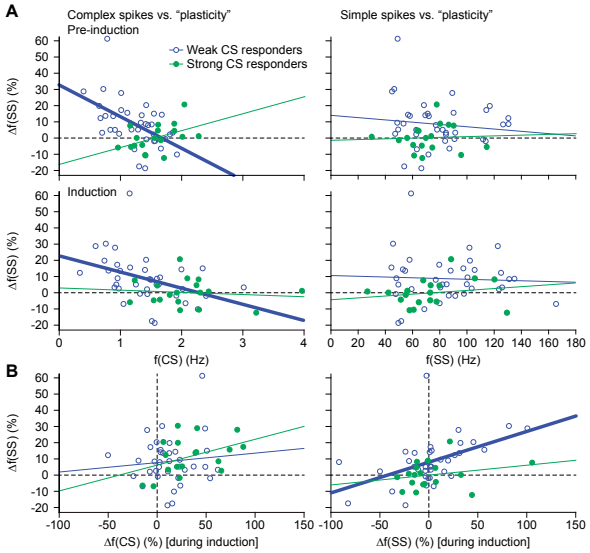


**Figure 6 – figure supplement 1.** Complex spike rates are negatively correlated with sensory-induced potentiation

**A.** Scatter plots with linear regression lines between complex spike (CS) (left) and simple spike (SS) frequency (right) during the pre-induction (top) and the induction (bottom) period with the percentage of change in simple spike response between post- and pre-induction. The complex spike firing rate was negatively correlated with the change in simple spike responses in those PCs that had weak complex spike responses (see Figure 2 - figure supplement 1) – both during the pre-induction and during the induction interval. However, no such significant correlation was found in the strong complex spike responders. The simple spike rate did not have a significant correlation with simple spike responses. **B.** In contrast to the absolute firing rate, the difference in complex spike firing during the pre-induction versus the induction block did not show a clear correlation with changes in simple spike responsivity (left). Increased simple spike firing during the induction block, however, correlated well with increased sensory simple spike responses during the post-induction block. Thick lines indicate significant linear correlations ($p < 0.002$).

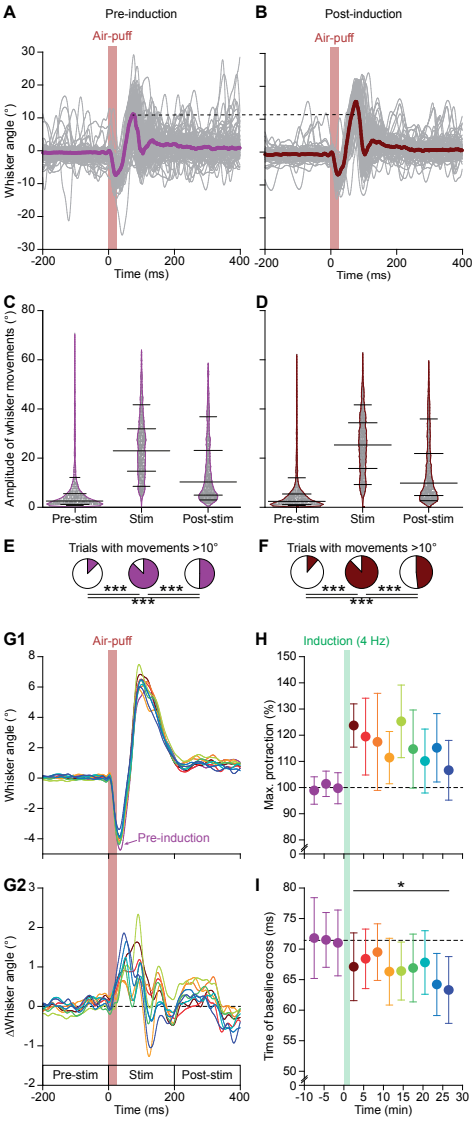


**Figure 6 – figure supplement 2.** 4 Hz air-puff stimulation enhances reflexive whisker protraction for at least 30 minutes

**A.** The variability in whisker movements is illustrated by superimposing the average whisker angle during the 100 trials before 4 Hz air-puff stimulation. The thick line indicates the median. **B.** The first 100 trials after induction of the same experiment as in **A**, showing a clear increase in whisker protraction. Violin plots showing the amplitudes (differences between maximal retraction and maximal protraction in the indicated 200 ms intervals; see **G2**) of individual trials before (**C**) and after (**D**) induction. Obviously, the most prominent whisker movements were observed in the period between 0 and 200 ms after whisker pad air-puff stimulation, as compared to the 200 ms intervals before and after this period ($n$ = 16 mice). Horizontal lines denote the 10$^{th}$, 25$^{th}$, 50$^{th}$, 75$^{th}$ and 90$^{th}$ percentiles. Fractions of trials with movements exceeding 10° before (**E**) and after (**F**) induction. Especially the active protraction during the first 200 ms after the stimulus is clearly enhanced. Note that the panels **A**, **C** and **E** are the same as in Figure 1 – figure supplement 1 and are displayed here to illustrate the impact of 4 Hz stimulation on whisker movements. **G1.** Averaged whisker traces (ordered per 100 trials) of seven mice where video data were available for the whole recording, showing less retraction and more protraction after induction. For clarity, only the average of the last 100 trials pre-induction is plotted. Color codes as in panel **H**. **G2.** Differential traces show that whiskers remain further protracted, but that over time this became faster. **H.** 4 Hz air-puff stimulation caused increased whisker protraction during the whole recording (30 min). The switch from retraction to protraction (calculated as the time at which the whisker were back at the resting position after the initial retraction) remained faster throughout the recording (**I**). * $p < 0.05$; *** $p < 0.001$.

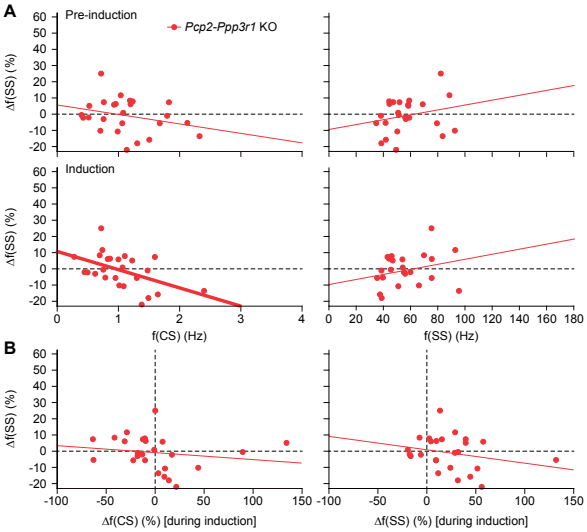


**Figure 7 – figure supplement 1.** Also in *Pcp2-Ppp3r1* KO mice, complex spike rates are negatively correlated with sensory-induced potentiation

**A.** Scatter plots with linear regression lines between complex spike (CS) (left) and simple spike (SS) frequency (right) during the pre-induction (top) and the induction (bottom) period with the percentage of change in simple spike response between post- and pre-induction in *Pcp2-Ppp3r1* KO mice (see Figure 6 – figure supplement 1 for the results of the WT littermates). The complex spike firing rate was negatively correlated with the change in simple spike responses, in particular during the induction interval. The simple spike rate did not have a significant correlation with simple spike responses. **B.** In contrast to the absolute firing rate, the difference in complex spike firing during the pre-induction versus the induction block did not show a clear correlation with changes in simple spike responsivity (left). In this mutant, a correlation between CS firing (during induction) and changes in simple sensitivity was still observed, possibly reflected the fact that parallel fiber LTD is still intact in these mice. Thick lines indicate significant linear correlations ($p < 0.002$).

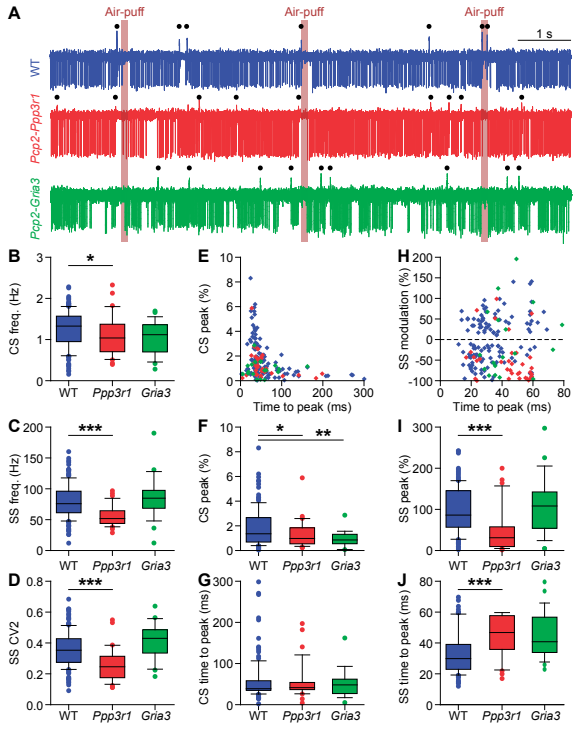


**Figure 8 – figure supplement 1.** Purkinje cell responses to whisker pad stimulation in *Pcp2-Ppp3r1* and *Pcp2-Gria3* mice

**A.** Example recordings of Purkinje cell activity in a wild-type (WT) (top), a *Pcp2-Ppp3r1* deficient (middle) and a *Pcp2-Gria3* deficient mouse (bottom). The timing of air-puffs to the whisker pad is indicated with light brown lines and that of the complex spikes with black dots above the traces. Compared to their WT littermates, *Pcp2-Ppp3r1* mice had a mildly reduced complex spike rate (**B**), as well as fewer simple spikes (**C**) that on top were fired more regularly (lower CV2; **D**). In contrast, the *Pcp2-Gria3* mice showed firing patterns that were more similar to their WT littermates. For clarity, the two WT groups are pooled for visualization, but statistics were performed between mutants and their respective control littermates. **E.** Complex spike responses to air-puff stimulation were quite similar in the three groups, although the mutants tended to have lower peak responses (**F**) with normal timing (**G**). **H.** Simple spike responses to air-puff stimulation were similar between WT and *Pcp2-Gria3* mice, but *Pcp2-Ppp3r1* mice showed more inhibition upon stimulation (**I**) with a longer latency (J). * $p < 0.05$; ** $p < 0.01$; *** $p < 0.001$. See also Table S3 and Source Data File.

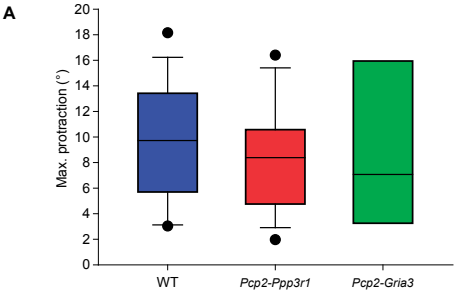


**Figure 8 – figure supplement 2.** Before induction, touch-induced whisker protraction is not affected by *Pcp2-Ppp3r1* and *Pcp2-Gria3* mutations

The maximal touch-induced whisker protraction is similar between wild-type (n = 16), *Pcp2-Ppp3r1* (n = 13) and *Pcp2-Gria3* (n = 6) mutant mice, indicating that the amplitude of the reflex itself is not affected by any of the mutations involved. $p = 0.860$, F = 0.152, ANOVA. See also Source Data file.

**Table S1.** Overview of statistical tests on whisker movements – belonging to Figure 1 – figure supplement 2

| Stimulus condition | Maximal retraction | ***p* < 0.001**; Fr = 18.200; df = 3; *n* = 9 mice Friedman's two-way ANOVA | | |
|---|---|---|---|---|
| | | Front contra | Back ipsi | Front ipsi + PPI |
| Front ipsi | -3.06° (1.19°) | *p* = 0.865 | ***p* < 0.001** | *p* = 0.268 |
| Front contra | -1.76° (0.73°) | | ***p* = 0.037** | *p* = 1.000 |
| Back ipsi | -0.71° (1.00°) | | | *p* = 0.171 |
| Front ipsi + PPI | -1.67° (0.84°) | | | |
| | Maximal protraction | ***p* = 0.003**; Fr = 13.933; df = 3; *n* = 9 mice Friedman's two-way ANOVA | | |
| Front ipsi | 6.10° (5.88°) | ***p* = 0.021** | *p* = 1.000 | *p* = 1.000 |
| Front contra | 12.80° (4.95°) | | *p* = 0.268 | ***p* = 0.003** |
| Back ipsi | 5.69° (4.29°) | | | *p* = 0.865 |
| Front ipsi + PPI | 4.24° (2.04°) | | | |

Summary of statisical analysis belonging to Figure 1 – figure supplement 2. Data are represented as medians (inter-quartile range). Bold values indicate *p* values considered to be statistically significant. contra = contralateral; df = degrees of freedom; ipsi = ipsilateral; PPI = paired-pulse inhibition.

**Table S2.** Overview of statistical tests – belonging to Figure 5.

| Whiskers | Maximal protraction | | |
|---|---|---|---|
| Pre-induction | 9.72° (6.51°) | ***p* < 0.001** | Wilcoxon matched-pairs test |
| Post-induction | 11.39° (9.10°) | *n* = 16 mice | |
| Complex spikes | Maximal response | | |
| Pre-induction | 1.27% (1.89%) | *p* = 0.163 | Wilcoxon matched-pairs test |
| Post-induction | 1.23% (1.22%) | *n* = 55 PCs | |
| Simple spikes | Spike rate (norm.) | | |
| Pre-induction | 98.50% (27.3%) | ***p* = 0.003** | Wilcoxon matched-pairs test |
| Post-induction | 102.84% (23.70%) | *n* = 55 PCs | |

Summary of statisical analysis belonging to Figure 5. Data are represented as medians (inter-quartile range). Bold values indicate *p* values considered to be statistically significant.

**Table S3.** Overview of statistical tests – belonging to Figure 8 – figure supplement 1.

| Basic firing properties (panels B-D) | | | |
|---|---|---|---|
| Complex spike frequency | | ***p* = 0.014**; df = 2; Kruskal-Wallis test | |
| WT[1] | 1.33 Hz (0.61 Hz) | | *n* = 147 PCs |
| L7-PP2B | 1.04 Hz (0.59 Hz) | ***p* = 0.010**[2] | *n* = 37 PCs |
| L7-GluA3 | 1.12 Hz (0.59 Hz) | *p* = 0.780[2] | *n* = 25 PCs |
| Simple spike frequency | | ***p* < 0.001**; df = 2; Kruskal-Wallis test | |
| WT[1] | 75.86 Hz (33.59 Hz) | | *n* = 147 PCs |
| L7-PP2B | 51.72 Hz (15.67 Hz) | ***p* < 0.001**[2] | *n* = 37 PCs |
| L7-GluA3 | 84.78 Hz (25.60 Hz) | *p* = 0.289[2] | *n* = 25 PCs |
| Simple spike CV2 | | ***p* < 0.001**; df = 2; Kruskal-Wallis test | |
| WT[1] | 0.35 (0.15) | | *n* = 147 PCs |
| L7-PP2B | 0.25 (0.13) | ***p* < 0.001**[2] | *n* = 37 PCs |
| L7-GluA3 | 0.43 (0.14) | *p* = 0.252[2] | *n* = 25 PCs |
| Complex spike response properties (panels E-G) | | | |
| Amplitude (% of spikes / 1 ms bin) | | ***p* = 0.034**; df = 2; Kruskal-Wallis test | |
| WT[1] | 1.34% (1.97%) | | *n* = 129 PCs |
| L7-PP2B | 0.96% (1.26%) | ***p* = 0.019**[2] | *n* = 34 PCs |
| L7-GluA3 | 0.85% (1.08%) | ***p* = 0.007**[2] | *n* = 19 PCs |
| Latency to peak | | *p* = 0.733; df = 2; Kruskal-Wallis test | |
| WT[1] | 39 (23) ms | – | *n* = 129 PCs |
| L7-PP2B | 42 (16) ms | – | *n* = 34 PCs |
| L7-GluA3 | 53 (13) ms | – | *n* = 19 PCs |
| Simple spike response properties (panels H-J) | | | |
| Amplitude (% of baseline) | | ***p* < 0.001**; df = 2; Kruskal-Wallis test | |
| WT[1] | 89.47% (89.22%) | | *n* = 137 PCs |
| L7-PP2B | 31.00% (47.19%) | ***p* < 0.001**[2] | *n* = 35 PCs |
| L7-GluA3 | 108.22% (73.47%) | *p* = 0.074[2] | *n* = 25 PCs |
| Latency to peak | | ***p* < 0.001**; df = 2; Kruskal-Wallis test | |
| WT[1] | 31 (17) ms | | *n* = 137 PCs |
| L7-PP2B | 47 (21) ms | ***p* < 0.001**[2] | *n* = 35 PCs |
| L7-GluA3 | 41 (20) ms | *p* = 0.275[2] | *n* = 25 PCs |

Summary of statisical analysis belonging to Figure 8 – figure supplement 1. Data are represented as medians (inter-quartile range). Bold values indicate *p* values considered to be statistically significant. df = degrees of freedom; PC = Purkinje cell; PPI = paired-pulse inhibition.

[1]For ease of comparison, WT PCs are grouped (including L7-PP2B WT and L7-GluA3 WT PCs).

[2]Compared to littermate controls.

# 4

# Quasiperiodic rhythms of the inferior olive

Mario Negrello[1,3,4], Pascal Warnaar[1,3], Vincenzo Romano[1], Cullen B. Owens[1], Sander Lindeman[1], Elisabetta Iavarone[1], Jochen K. Spanke[1], Laurens W.J. Bosman[1,4] and Chris I. De Zeeuw[1,2,4]

[1] Department of Neuroscience, Erasmus MC, Rotterdam, the Netherlands
[2] Netherlands Institute for Neuroscience, Royal Academy of Arts and Sciences, Amsterdam, the Netherlands
[3] These authors contributed equally
[4] Correspondence to: M. Negrello, Department of Neuroscience, Erasmus MC, PO Box 2040, 3000 CA Rotterdam, the Netherlands, m.negrello@erasmusmc.nl, L.W.J. Bosman, Department of Neuroscience, Erasmus MC, PO Box 2040, 3000 CA Rotterdam, the Netherlands, l.bosman@erasmusmc.nl, or C.I. De Zeeuw, Department of Neuroscience, Erasmus MC, PO Box 2040, 3000 CA Rotterdam, the Netherlands, c.dezeeuw@erasmusmc.nl

## ABSTRACT

Inferior olivary activity causes both short-term and long-term changes in cerebellar output underlying motor performance and motor learning. Many of its neurons engage in coherent subthreshold oscillations and are extensively coupled via gap junctions. Studies in reduced preparations suggest that these properties promote rhythmic, synchronized output. However, the interaction of these properties with torrential synaptic inputs in awake behaving animals is not well understood. Here we combine electrophysiological recordings in awake mice with a realistic tissue-scale computational model of the inferior olive to study the relative impact of intrinsic and extrinsic mechanisms governing its activity. Our data and model suggest that if subthreshold oscillations are present in the awake state, the period of these oscillations will be transient and variable. Accordingly, by using different temporal patterns of sensory stimulation, we found that complex spike rhythmicity was readily evoked but limited to short intervals of no more than a few hundred milliseconds and that the periodicity of this rhythmic activity was not fixed but dynamically related to the synaptic input to the inferior olive as well as to motor output. In contrast, in the long-term, the average olivary spiking activity was not affected by the strength and duration of the sensory stimulation, while the level of gap junctional coupling determined the stiffness of the rhythmic activity in the olivary network during its dynamic response to sensory modulation. Thus, interactions between intrinsic properties and extrinsic inputs can explain the variations of spiking activity of olivary neurons, providing a temporal framework for the creation of both the short-term and long-term changes in cerebellar output.

## AUTHOR SUMMARY

Activity of the inferior olive, transmitted via climbing fibers to the cerebellum, regulates initiation and amplitude of movements, signals unexpected sensory feedback, and directs cerebellar learning. It is characterized by widespread subthreshold oscillations and synchronization promoted by strong electrotonic coupling. In brain slices, subthreshold oscillations gate which inputs can be transmitted by inferior olivary neurons and which will not - dependent on the phase of the oscillation. We tested whether the subthreshold oscillations had a measurable impact on temporal patterning of climbing fiber activity in intact, awake mice. We did so by recording neural activity of the postsynaptic Purkinje cells, in which complex spike firing faithfully represents climbing fiber activity. For short intervals (<300 ms) many Purkinje cells showed spontaneously rhythmic complex spike activity. However, our experiments designed to evoke conditional responses indicated that complex spikes are not predominantly predicated on stimulus history. Our realistic network model of the inferior olive explains the experimental observations via continuous phase modulations of the subthreshold oscillations under the influence of synaptic fluctuations. We conclude that complex spike activity emerges from a quasiperiodic rhythm that is stabilized by electrotonic coupling between its dendrites, yet dynamically influenced by the status of their synaptic inputs.

## INTRODUCTION

A multitude of behavioral studies leave little doubt that the olivo-cerebellar system organizes appropriate timing in motor behavior (1-3), perceptual function (4-6) and motor learning (7-10). Furthermore, the role of the inferior olive in motor function is evinced in (permanent and transient) clinical manifestations, such as tremors, resulting from olivary lesions and deficits (11-16). Although the consequences of olivary dysfunctions are rather clear, the network dynamics producing functional behavior are controversial. At the core of the controversy is the question whether inferior olive cells are oscillating during the awake state and whether these oscillations affect the timing of the inferior olivary output (17-19). The inferior olive is the sole source of the climbing fibers, the activity of which dictates complex spike firing by cerebellar Purkinje cells (for review, see (20)). Climbing fiber activity is essential for motor coordination, as it contributes to both initiation and learning of movements (8, 10, 21-26), and it may also be involved in sensory processing and regulating more cognitive tasks (27-30). Understanding the systemic consequences of inferior olivary spiking is therefore of great importance.

The dendritic spines of inferior olivary neurons are grouped in glomeruli, in which they are coupled by numerous gap junctions (10, 31-33), which broadcast the activity state of olivary neurons. Due to their specific set of conductances (34-40), the neurons of the inferior olive can produce subthreshold oscillations (STOs) (41-43). The occurrence of STOs does not require gap junctions per se (44), but the gap junctions appear to affect the amplitude of STOs and engage larger networks in synchronous oscillation (10, 16, 42). Both experimental and theoretical studies have demonstrated that STOs may mediate phase-dependent gating where the phase of the STO helps to determine whether excitatory input can or cannot evoke a spike (45, 46). Indeed, whole cell recordings of olivary neurons in the anesthetized preparation indicate that their STOs can contribute to the firing rhythm (42, 43) and extracellular recordings of Purkinje cells in the cerebellar cortex under anesthesia often show periods of complex spike firing around the typical olivary rhythm of 10 Hz (17, 47-49). However, several attempts to capture clues to these putative oscillations in the absence of anesthesia have, so far, returned empty handed (19, 50).

It has been shown that in the anesthetized state both the amplitude and phase of the STOs can be altered by synaptic inputs (10). Inhibitory inputs to the inferior olive originate in the cerebellar nuclei and have broadly distributed terminals onto compact sets of olivary cells (51-53). Excitatory terminals predominantly originate in the spinal cord and lower brainstem, mainly carrying sensory information, and in the nuclei of the meso-diencephalic junction in the higher brainstem, carrying higher-order input from the cerebral cortex (Fig. 1A) (15, 54, 55). In addition, the inferior olive receives modulating, depolarizing, level-setting inputs from areas like the raphe nuclei (55). Unlike most other brain regions, the inferior olive is virtually devoid of interneurons (56, 57). Thus, the long-range projections to the inferior olive in conjunction with presumed STOs and gap junctions jointly determine the activity pattern of the complex

spikes in Purkinje cells. How these factors contribute to functional dynamics of the olive in awake mammals remains to be elucidated.

Here, we combine recordings in awake mice – in the presence and absence of gap junctions – with network simulations using a novel inferior olivary model to study the functional relevance of STOs in terms of resonant spikes. We are led to propose a view of inferior olivary function that is more consistent with the interplay between STOs, gap junctions and inputs to the inferior olive. Rather than acting as a strictly periodic metronome, the inferior olive appears more adequately described as a quasiperiodic ratchet, where cycles with variable short-lasting periods erase long-term phase dependencies.



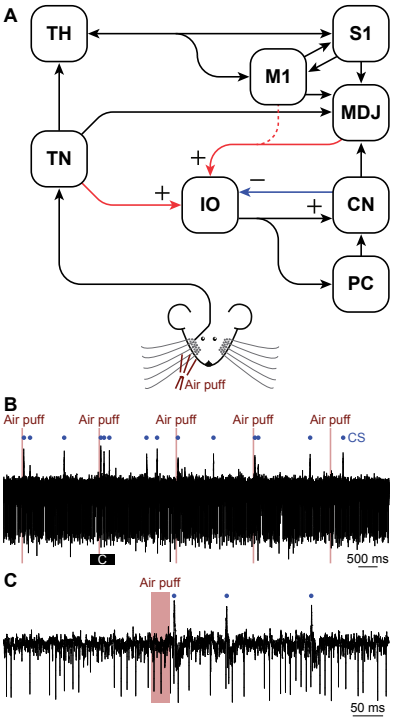


**Figure 1.** Circuit involved in the production and modulation of complex spikes.
**(A)** Simplified scheme of the inputs to the inferior olive (IO). Sensory input reaches the IO directly from the brainstem and spinal cord. In our study, we used facial whisker input that is relayed via the sensory trigeminal nuclei (TN). This input is considered the "sensory input" in our modeling studies. The IO also receives continuous inputs from other brain regions, which we modeled as the "contextual input". The contextual input consists of excitatory input from the cerebral cortex (e.g., the motor (M1) and somatosensory cortex (S1)), either directly or relayed via the nuclei of the meso-diencephalic junction (MDJ), as well as of inhibitory input from the cerebellar nuclei (CN). The output of the IO is directed via its climbing fibers to the Purkinje cells (PCs) in the cerebellar cortex and via its climbing fiber collaterals to the CN. Sensory input also affects the contextual input indirectly, via the strong pathway from the TN via the thalamus (TH) to the cerebral cortex. **(B)** Representative trace of Purkinje cell activity showing simple spikes (as downward deflections) occurring at a high frequency and occasionally complex spikes (CS; marked with a blue dot). A part of the trace is enlarged in **(C)**. All recordings were made in awake mice.

# RESULTS

## Stimulation promotes oscillatory patterns in profiles of complex spikes over short periods

To study the conditions for, and consequences of, rhythmic activity of the inferior olive, we made single-unit recordings of cerebellar Purkinje cells in lobules crus 1 and crus 2 (*n* = 52 cells in 16

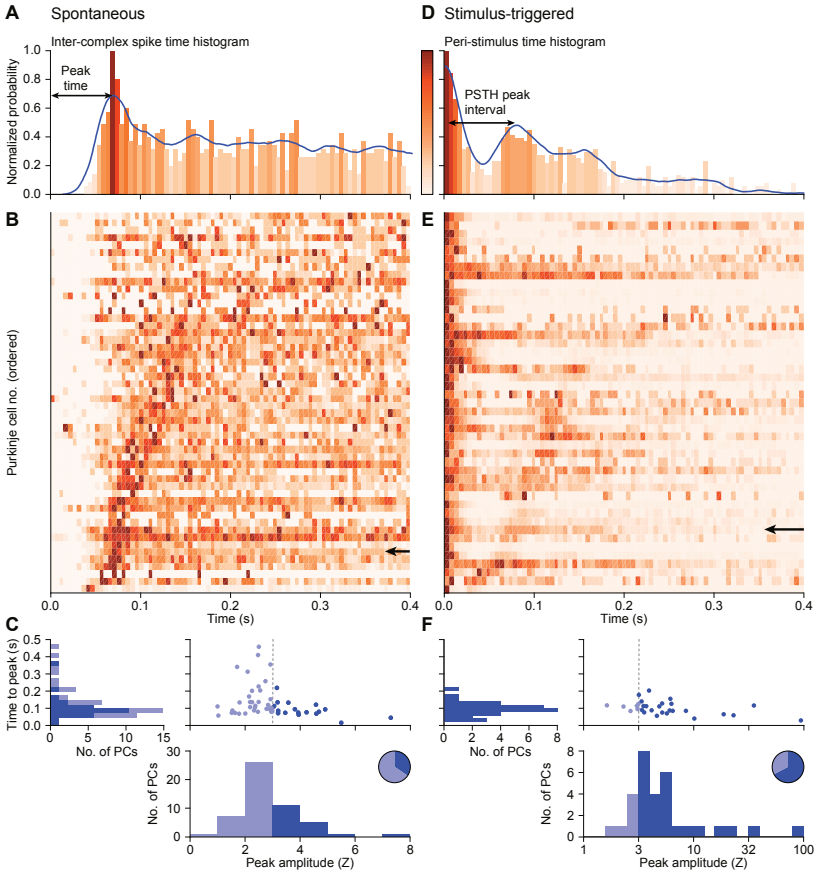


**Figure 2.** Oscillatory dynamics in complex spike firing *in vivo*.

(**A**) Representative inter-complex spike-interval (ICSI) histogram of spontaneous firing of a representative Purkinje cell, together with the convolved probability density function (in blue). The shades of the bins represent the normalized oscillation strength. Note that the peak at 0 ms is removed to improve visibility. (**B**) Heat map showing the normalized oscillation strengths of 52 Purkinje cells, which were ordered by the time to the first side peak. The arrow in **B** indicates the cell illustrated in **A**. (**C**) The peak times of the ICSI distributions during spontaneous firing, as observed in **B**, against the Z-scores of these peaks. A Z-score <3 was taken as sign for the absence of rhythmicity (light blue fillings). The pie diagram shows the fraction of Purkinje cells with rhythmic complex spike firing (Z-score > 3; dark blue fillings). (**D**)-(**F**) The corresponding plots for the 46 (out of the 52) cells that showed a significant complex spike response following whisker air puff stimulation. Complex spike rhythmicity is displayed using peri-stimulus time histograms (PSTHs) aligned on the peak of the first response and ordered based on the latency to the second peak.

awake mice) in the presence and absence of short-duration (30 ms) whisker air puff stimulation (Fig. 1B-C). In the absence of sensory stimulation, the complex spikes of 35% of the Purkinje cells (18 out of 52) showed rhythmic activity (Fig. 2A-C; S1 Fig.) with a median frequency of 8.5 Hz (inter-quartile range (IQR): 4.7-11.9 Hz). Upon sensory stimulation, 46 out of the 52 cells (88%) showed statistically significant complex spike responses. Of these, 31 (67%) had sensory-induced rhythmicity (Fig. 2D-F), which was a significantly larger proportion than during spontaneous behavior ($p$ = 0.002; Fisher's exact test). The median frequency of the oscillatory activity following stimulation was 9.1 Hz (IQR: 7.9-13.3 Hz). Hence, the preferred frequencies in the presence and absence of sensory stimulation were similar ($p$ = 0.22; Wilcoxon rank sum test) (Fig. 2C, F and 3). The duration of the enhanced rhythmicity following stimulation was relatively short in that it lasted no more than 250 ms. With our stringent Z-score criterion (>3), only a single neuron showed 3 consecutive significant peaks in the peri-stimulus time histogram (PSTH). The minimum inter-complex spike interval (ICSI) across cells was around 50 ms, putatively representing the refractory period. We conclude that complex spikes also display rhythmicity in awake behaving mice, and that sensory stimulation can amplify these resonances in periods of a few hundred milliseconds, even though stimulation is not required for the occurrence of rhythmicity per se.



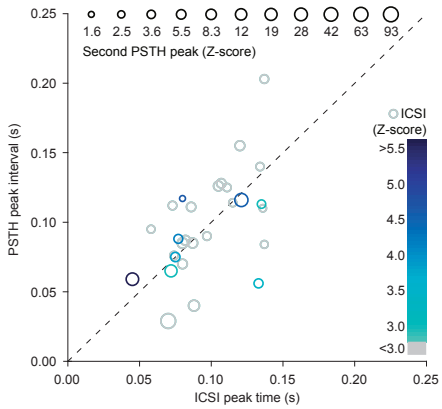


**Figure 3.** Similarity between spontaneous and sensory-induced rhythmicity.
For each of the 30 oscillating Purkinje cells that were recorded in both the presence and absence of sensory stimulation, we compared the timing of the maximum of the first side peak in the inter-complex spike interval (ICSI) histogram in the absence of sensory stimulation (x-axis) with the timing of the difference between the maxima of the first and second peak in the peri-stimulus time histogram (PSTH; y-axis) following sensory stimulation. Color and size of data points indicate amplitude (in Z-score) of the ICSI peak and of the interval between first and second response peaks of the PSTH, respectively. Grey circles indicate the data-points falling in the low Z-score (<3) group during spontaneous firing. Note that colored circles are preferably located around the identity line.

## Rhythmic patterns of complex spikes following stimulation are transient

The pattern of rhythmic complex spike responses that was apparent for a couple of hundred milliseconds after a particular air puff stimulus repeated itself in a stable manner across the

1,000 trials (applied at 0.25 Hz) during which we recorded (Fig. 4A-B). For example, the level of rhythmicity of the first 100 trials was not significantly different from that during the last 100 trials (comparing spike counts in first PSTH peak, $p = 0.824$; $\chi^2$ test, or latency to first spike, $p = 0.727$, $t$ test). This strongly indicates that there is – in a substantial fraction of the Purkinje cells – persistent oscillatory gating of the probability for complex spikes after a sensory stimulus resulting in time intervals ("windows of opportunity") during which complex spikes preferentially occur (Fig. 4B-E). These windows of opportunity become even more apparent when sorting the

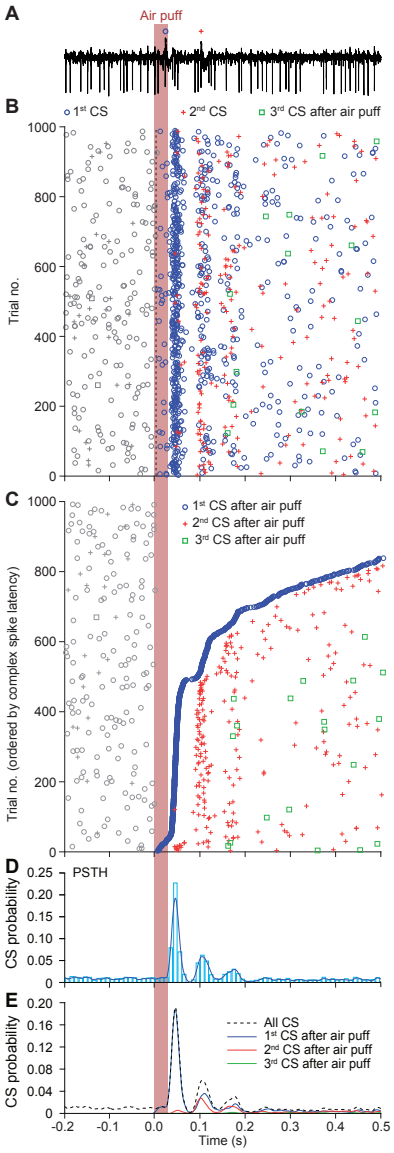


**Figure 4.** Stability of rhythmic complex spike activity in a Purkinje cell of an awake mouse

(**A**) Rhythmic complex spike (CS) responses to whisker pad air puff stimulation in a representative Purkinje cell recorded in crus 1. Representative trial from an extracellular recording with a stimulation frequency of 0.5 Hz. In this and subsequent panels, CSs are marked with symbols representing their order of occurrence following the stimulus within each trial. (**B**) Rhythmic behavior of CSs becomes apparent in a raster plot. Note that the rhythmicity is relatively stable over the 1,000 trials. (**C**) Same as in **B** but with trials sorted by the latency to first CS. This reveals that the occurrence of CSs is largely organized in temporal windows of opportunity. Some CSs appear in later response peaks without prior firing in earlier windows of opportunity. As the CS response may appear in the early and/or in the late window, this is suggestive of a readout from an underlying oscillatory process. This phase dependence would not appear if it would be solely due to a reset followed by transient oscillation evoked exclusively in the spiking cell. If CS firing during the later peaks was predicated on an earlier phase-aligned CS, then later CS responses would have no reason to align with the second or the third peaks of the PSTH (in **D** and **E**). (**D**) PSTH of CS firing. The bin-width is 10 ms and the blue line shows the convolved histogram with a 5 ms kernel. (**E**) The same PSTH as in **D**, but now the probabilities of the first, second and third CS after the stimulus shown separately, highlighting the occurrence of windows of opportunity for stimulus triggered CSs.

trials on the basis of response latency: the first complex spikes with a long latency following the stimulus align with the second spikes of the short latency responses. Similarly, there are trials during which complex spikes appear only at the third cycle (Fig. 4C, seen as a steeper rise around trial no. 650). The occurrence of spikes during later cycles, not predicated on prior spikes, argues against refractory periods or rebound spiking as the sole explanations for such rhythmic firing (58) and highlight the putative existence of network-wide coherent oscillations.

## Behavioral correlates of complex spikes patterns following stimulation



Since sensory stimulation of the whiskers can trigger a reflexive whisker protraction (59-61) and complex spike firing is known to correlate with the amplitude of this protraction (61), we examined the relation between periodic complex spike firing and whisker protraction. To this end, we further analyzed an existing dataset of simultaneously recorded Purkinje cells and whisker movements during 0.5 Hz air puff stimulation of the ipsilateral whisker pad. In line with our previous findings (61), trials during which a single complex spike occurred within 100 ms of whisker pad stimulation had on average a slightly, but significantly stronger protraction (from 6.1 ± 5.4° to 6.8 ± 5.3° (medians ± IQR), $n$ = 35 Purkinje cells, $p$ = 0.033, Wilcoxon-matched pairs test after Benjamini-Hochberg correction; Fig. S2A-C). Our new analysis revealed that also the occurrence of a second complex spike was correlated with a stronger whisker protraction. This could be observed as a second period of increased protraction during trials with two complex spikes. When compared to the increase in trials with a single complex spike, this second protraction was highly significant ($p < 0.001$, Wilcoxon-matched pairs test after Benjamini-Hochberg correction; Fig. S2D). The second complex spike was unlikely a mere reflection of stronger protraction following the first complex spike, as there was no difference in whisker protraction between the trials that had a complex spike during the first, but not the second 100 ms after stimulus onset, and the trials with the opposite pattern (a complex spike during the second, but not the first 100 ms; $p$ = 0.980, Wilcoxon-matched pairs test after Benjamini-Hochberg correction). The rhythmic firing pattern of complex spikes was thus reflected in the behavioral output of mice.

## STOs can explain windows of opportunity

The existence of windows of opportunity for complex spike activity is compatible with the assumption of an underlying STO, and cannot solely be explained by rebound activity without invoking circuit-wide extrinsic mechanisms. To test the implications of assuming olivary STOs, we proceeded to reproduce a detailed network with a tissue-scale computer model of the inferior olive neuropil. The model is constituted by 200 biophysically plausible model cells (40, 46, 62) embedded in a topographically arranged 3D-grid (Fig. 5A-C). It has the scale of a sheet of olivary neurons of about 10% of the murine principal olivary nucleus (cf. (63)). The model was designed to test hypotheses about the interaction between intrinsic parameters of olivary neurons, such as STOs and gap junctional coupling, and extrinsic parameters including synaptic inputs during the generation of complex spike patterns.

Each neuron in the model is composed of a somatic, an axonal and a dendritic compartment, each endowed with a particular set of conductances, including a somatic low threshold $Ca^{2+}$ channel ($Ca_v3.1$; T-type), a dendritic high threshold $Ca^{2+}$ channel ($Ca_v2.1$; P/Q-type) and a dendritic $Ca^{2+}$-activated $K^+$ channel, chiefly regulating STO amplitudes, while a somatic HCN channel partially determines the STO period (Fig. 5B; see also Methods). The dendrites of each neuron are connected to the dendrites of, on average, eight nearby neighbors (within a radius of three nodes in the grid, representing a patch of about 400 µm x 400 µm of the murine inferior olive), simulating anisotropic and local gap junctional coupling (Fig. 5C). As the inferior olive

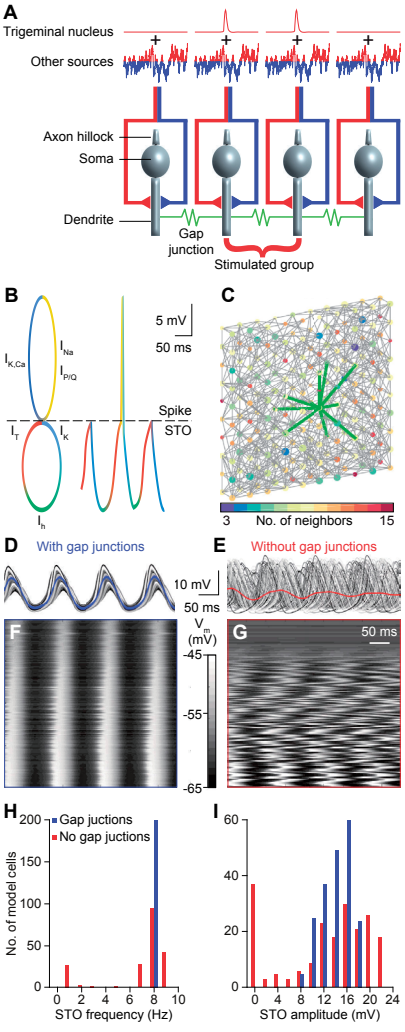


**Figure 5.** A tissue-scale network model of the inferior olive.

**(A)** To study the relative impact of the different components of the inferior olive we employed a biologically realistic network consisting of 200 model neurons embedded in a 3D grid of 10 x 10 x 2. The model neurons received input from two sources: a phasic input dubbed "sensory input" and a continuous fluctuating current, emulating a "contextual input". The "sensory input" reaches a subset of neurons synchronously and is modeled as an activation of glutamate receptor channels with a peak amplitude of 5 pA/cm². The "sensory input" is complemented with a continuous input that is a mixture of excitatory and inhibitory synapses representing signals from different sources (see Fig. 1A). The "contextual input" is modeled as an Ornstein-Uhlenbeck noise process delivered to all neurons in the model network, with a 20 ms decay, representing temporally correlated input. The model neurons are interconnected by gap junctions. **(B)** The model neurons display subthreshold membrane oscillations (STOs), represented by the lower circle, and spiking, represented by the upper circle. The colors indicate which current dominates which part of the activity pattern. An $I_h$ current (green), a hyperpolarization-activated cation current, underlies a rise in membrane potential; the $I_T$ current (red), mediated by low threshold T-type $Ca^{2+}$ channels ($Ca_v3.1$), further drives up the membrane potential and from here either the subthreshold oscillation continues (lower circle) or a spike is generated (upper circle), mediated through $I_{Na}$ and $I_K$ currents (yellow and blue, respectively); both after a spike or a subthreshold peak, influx of $Ca^{2+}$ through the P/Q-type type $Ca^{2+}$ channels ($Ca_v2.1$) leads to a hyperpolarization due to $Ca^{2+}$-dependent $K^+$ channels (blue); this hyperpolarization in turn will activate the $I_h$ current resuming the oscillation cycle. A resulting trace of the STO punctuated with one spike is diagrammatically displayed on the right. For a full description of currents, consult methods. **(C)** 3D connectivity scheme of the 200 neurons in the network model. Links indicate gap junctional interconnections; the color of each neuron in the model represents the number of neurons to which that cell is connected. The thick green lines indicate first order neighbors of the center cell. **(D-E)** Membrane potential of cells in the absence of input, for networks with and without gap junctional coupling. **(F-G)** Cell activity sorted by amplitude, indicating that coupling the neurons of the network brings non-oscillating cells into the synchronous oscillation. **(H-I)** Distribution of STO frequency and amplitude for coupled and uncoupled model networks.

itself, our model has boundaries which have impact on local connectivity characteristics, such as the clustering coefficient, though these did not have significant impact on the average firing rate between edge and center cells ($p$ = 0.812, comparing edge and center cells, Kolmogorov-Smirnov test; S3 Fig.). The coupling coefficient between model cells varied between 0 and 10%, as reported for experimental data (45, 64, 65).

Sensory input was implemented as excitatory synaptic input, simulating the whisker signals originating from the sensory trigeminal nuclei that were synchronously delivered to a subset of model neurons. Additionally, a "contextual input" was implemented as a combination of inhibitory feedback from the cerebellar nuclei and a level setting modulating input (Fig. 1A and 5A). This contextual input is modeled after an Ohrstein-Uhlenbeck process, essentially a random exploration with a decay parameter that imposes a well-defined mean yet with controllable temporal correlations (see Methods). The amplitude of the contextual input drives the firing rate of the model neurons, which we set around 1 Hz (S4 Fig.), corresponding to what has been observed *in vivo* (28, 43, 66). Thus, our model network recapitulates at least part of the neural behavior observed *in vivo* due to biophysically plausible settings of intrinsic conductances, gap junctional coupling and synaptic inputs.



## Characteristics of STO dependent spiking in the network model

Whether a model neuron at rest displays STOs or not is largely determined by its channel conductances. Activation of somatic T-type $Ca^{2+}$ channels can trigger dendritic $Ca^{2+}$-dependent $K^+$ channels that can induce $I_h$, which in turn can again activate T-type $Ca^{2+}$ channels, and so forth. This cyclic pattern can cause STOs that could occasionally produce spikes (Fig. 5B). In our model, the conductance parameters were randomized (within limits, see Methods) so as to obtain an approximate 1:3 ratio of oscillating to non-oscillating cells (S5 Fig.) guided by proportions observed *in vivo* (43). Sensitivity analysis with smaller ratios (down to 1:5) did not qualitatively alter the results (data and analyses scripts are available online in https://osf.io/6x5uy/).

In the absence of contextual input, model neurons were relatively silent, but when triggered by sensory input, as occurred in our behavioral data (Figs. 2 and 4), STOs synchronized by gap junctions would occur for two or three cycles (Fig. 6A-B). Our network model confirms that gap junctional coupling can broaden the distribution of STO frequencies and that even non-oscillating cells may, when coupled, collectively act as oscillators (S6 Fig.) (67). Adding contextual input to the model network can lead to more spontaneous spiking in between two sensory stimuli. Compared to the situation in the absence of contextual input, the STOs are much less prominent and the post-spike reverberation is even shorter (Fig. 6C). Accordingly, despite the significant levels of correlation in the contextual input (10%), the periods between oscillations are more variable due to the interaction of the noisy current and the phase response properties of the network. In addition, in the presence of contextual input our model could readily reproduce the appearance of preferred time windows for spiking upon sensory stimulation as observed *in vivo* (Fig. 6D-F, cf. Fig. 4). This was particularly true for the model

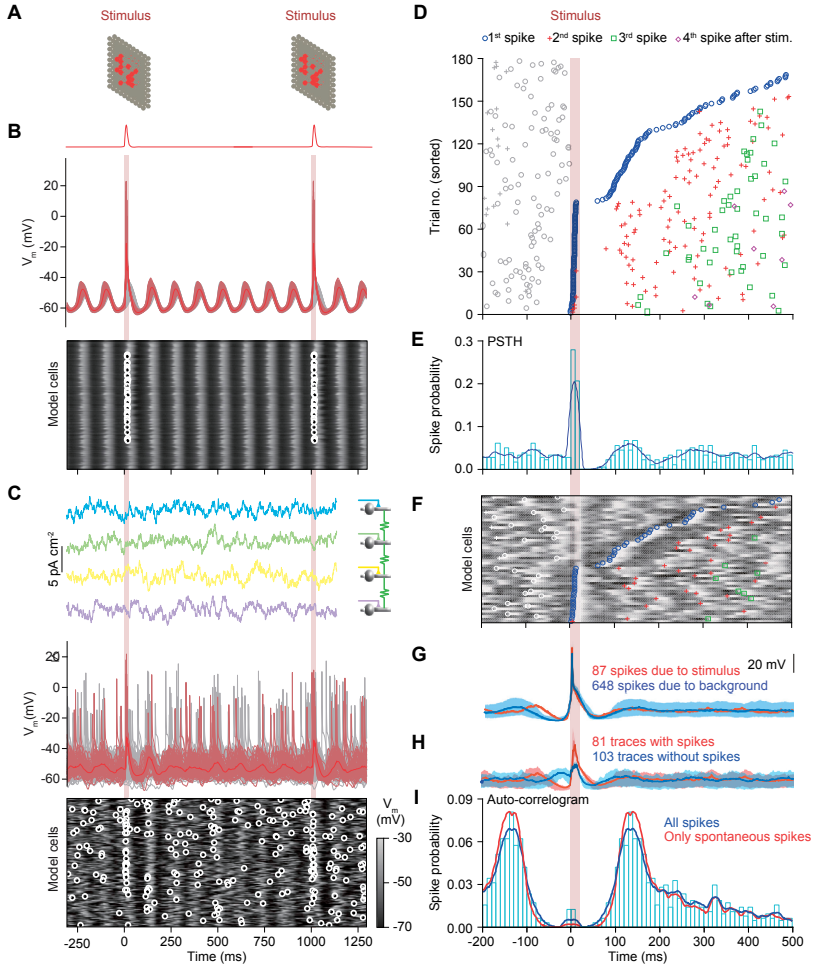


**Figure 6.** Synaptic input strongly affects the oscillatory behavior in a network model of the inferior olive.
(**A**) A phasic and synchronous input mimicking sensory input (see Fig. 5A) was delivered to a subset of cells (indicated in red) of the model network. (**B**) Membrane potentials of all 200 cells in the network model in the absence of contextual input. Red trace (top) displays membrane potential average of cells receiving sensory input (see masks in **A**). Below are the membrane potentials of the model cells as a heat map. Each row exhibits the membrane potential of one model cell with the small circles indicating spikes. In the absence of contextual input, model neurons displayed long lived, synchronous and regular transient subthreshold oscillations. Note that the fact that the two stimuli fall in similar phases is coincidental. (**C**) Patterns of spiking responses changed dramatically in the presence of contextual input. Whereas in the absence of contextual input model neurons showed synchronous subthreshold oscillations and were silent except upon receiving sensory input, in the presence of contextual input the subthreshold oscillations are irregular and not strictly synchronous, while spikes occur throughout the simulation (~1 Hz average network firing). Note that despite the largely uncorrelated (90%) contextual input, model cells did not fire homogenously as in **B**, though loose clusters of synchronously firing cells did emerge. (**D**) Rhythmic responses to stimulation are reproduced by the inferior olivary network model. A representative cell of the model network with responses to sensory input reproduces rhythmic features of the PSTH and an auto-correlogram as found in vivo (see Fig. 4). Raster plot of olivary spiking triggered by 182 stimuli, ordered by latency to the first spike following the stimulus. As seen in the in vivo data, the first spike after the stimulus can fall in one of multiple windows of opportunity. For this simulation, we included the contextual input. (**E**) Peri-stimulus time histogram showing the response peaks upon sensory input. (**F**) Raster plot like in **C**, but with overlaying membrane potentials. For clarity only the first 50 stimuli are displayed. Spike symbols follow conventions as in **D**. Trials with low latency were preceded by a dip in the preceding membrane potential, a phenomenon that can also be

cells that directly received sensory inputs (Fig. 6G-H). Moreover, the observed rhythmicity in model cells as observed in their STO activity was in tune with that of the auto-correlogram (Fig. 6D-I) in that the timing of the STOs and that of the spiking were closely correlated (cf. Fig. 5B). It should be noted though that model cells adjacent to cells directly receiving sensory input showed only a minor effect of stimulation. Thus, even though the gap junction currents in the model were chosen as the ceiling physiological value for the coupling coefficient (≤10%) (45, 67), these currents alone were not enough to trigger spikes in neighboring cells.

Both directly stimulated model cells and those receiving only contextual input exhibited phase preferences, seen in the spike-triggered membrane potential average as well as in the spike-triggered average of the input currents (Fig. 6G-I). Spike-triggered averages of membrane potentials for any cell showed depolarization followed by hyperpolarization. In contrast, trials in which no spike was generated showed a depolarization just before the occurrence of the input. Similarly, the average of the input showed a long-lived phase preference, not only for a hyperpolarization before the spike, but also a preference for a depolarization in the previous peak of the STO, more than 100 ms earlier. These results are in line *in vitro* experiments under dynamic clamp and noisy input (68, 69). Likewise, the model indicates that for short durations STOs can induce clear phase dependencies for spiking, which fades under the variation of period durations dependent on the trial-specific contextual input (as seen in our data).



## Phase-dependent gating in the network model

Depolarizing sensory input delivered onto a subset of the model cells can reset the STO phase in oscillatory cells and create resonant transients in others (Fig. 7A-B; see also S7 Fig. on the appearance of rebound firing). If a second stimulus is delivered during this short-lasting transient, the response probability is increased. As in most cells with resonant short-lasting dynamics, inputs delivered during different phases can cause phase advances or delays. Hyperpolarization advanced the phase between $0 - \pi$ and delayed the phase between $\pi - 2\pi$, whereas depolarization had roughly the opposite effect, in addition to phase advancements with spikes in later cycles between $\pi - 2\pi$ (Fig. 7C-E). Thus, there is a mutual influence of synaptic inputs and STOs on periodicity. While STOs can lead to phase-dependent gating, synaptic input can either modulate or reset the phase of the STOs, generating variable periods that range between 40-160 ms for the chosen amplitude of the contextual input (Fig. 8; S6 Fig.).

observed in **D** and **H**. (**G**) Average membrane potential of this neuron aligned by spikes that were either due to sensory input (87 spikes; red) or produced spontaneously (648 spikes; blue). The light shaded backgrounds represent the 10% and 90% percentile ranges of membrane potential. Dips in membrane potentials preceding the spikes reveal that for both groups a prior inhibition increased the probability of spiking. Importantly, except for a refractory period, we did not observe a clear oscillation pattern following either spike type, due to variability imposed by the contextual input. (**H**) shows the difference in spike triggered membrane potential averages for stimulus triggered and "spontaneous" spikes. (**I**) Auto-correlograms comparing rhythmicity of spikes produced during stimulation with spikes due to background (spontaneous) activity. Periodic stimuli delivered to the network **reduced** rhythmic responses at the peak. The extreme short-latency responses (in the center of the auto-correlogram) are due to the spikelets detected in the model traces that can also be seen in **D**.

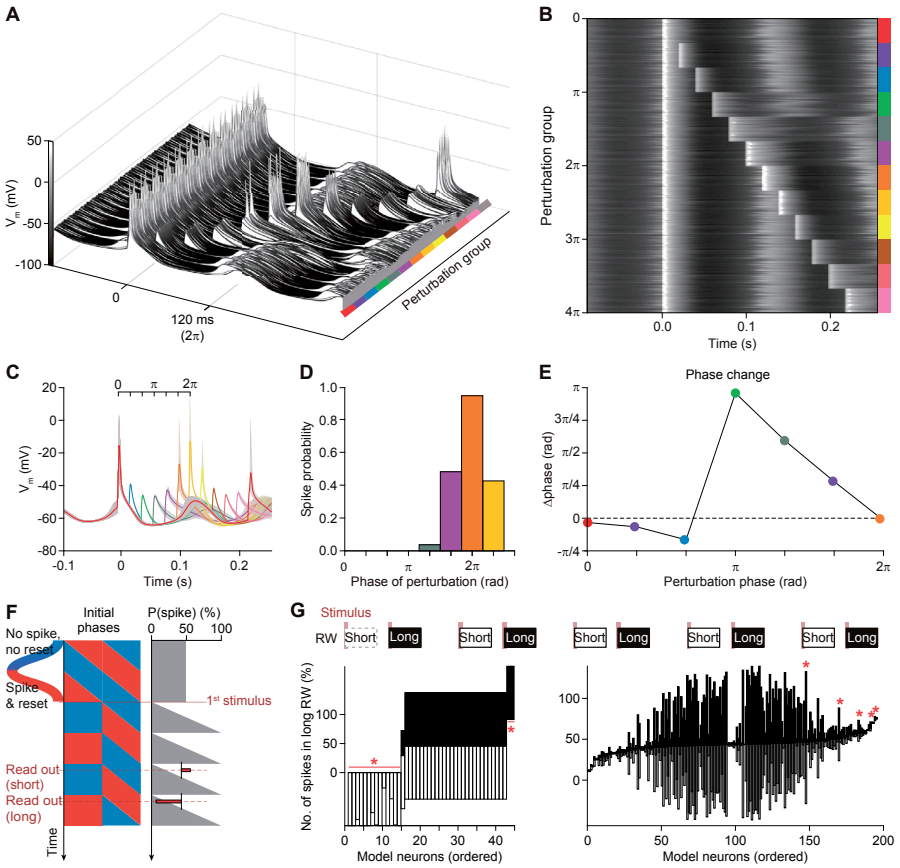


**Figure 7.** Synaptic input determines the phase-dependent gating properties of the inferior olive network model.

**(A)** Phase-dependent spiking was prominent in our network model of the inferior olive in the absence of contextual input. We repeatedly stimulated the same 54 model cells with synchronous sensory input (cf. Fig. 5A). The other 146 neurons of the network model were present, but not directly stimulated. Phase-dependent gating was studied using tandem stimulation with varying inter-stimulus intervals. The membrane potential of each of these 54 model neurons is plotted in **A** as a waterfall plot and in **B** as a heat map. The simulations are grouped by the interval between the two stimuli, starting with a single stimulation (red), and continuing with two stimuli with small to large intervals. In 13 equal steps two whole cycles of the subthreshold oscillation were covered. **(C)** Average and inter-quartile range (shaded area) of membrane potentials of neurons in the network that were only perturbed once at 0 ms (red) or twice (other colors). The phase of the subthreshold oscillations of the "synchronized" cells in the network was used to compute the data displayed in **D** and **E**. Note that the average membrane potential at the perturbation at 0 ms only went up to -15 mV and not up to the average spike peak of approximately 10 mV, because in the population only a fraction of neurons spiked. **(D)** Spike probability plot as measured for the second perturbation at the different phases of the membrane oscillation. Spike probability was computed as the number of neurons firing divided over the total number of neurons getting input. The first perturbation given at the peak of the oscillation is demarked as the start of the oscillation cycle. Perturbations at both a half and one-and-a half cycle (π and 3π, respectively) did not trigger spikes, whereas perturbations at either one or two full oscillation cycles (2π and 4π, respectively) did (see also **A** and **B**). The repetition of the 'sinusoidal' probability curve shows that gating is not (only) due to a refractory period, but follows the hyperpolarized phase of the oscillation (not shown). **(E)** Phase response curve showing that perturbations early in the oscillation phase did not have a large impact on the timing of the spike, but halfway the oscillation the perturbations advanced the ongoing phase considerably, with impact declining linearly to the end of the full cycle. **(F)** Gallop stimuli provide indirect evidence for an underlying oscillatory process. This idealized diagram illustrates the impact of a resetting stimulus on the future spiking probabilities. Here we assume that resetting spikes occur only during the rising phases of the STO (red)

## Gallop stimuli provide indirect evidence for STOs

The only means of settling the question about the prevalence of STOs in awake and behaving mice would be intracellular recordings of inferior olivary neurons, which remains a daunting experimental challenge. We therefore looked for a non-invasive method that could read out, from indirect and infrequent complex spikes, the presence or absence of STOs. We have developed one such paradigm inspired by auditory studies (70, 71) using a rhythmic gallop stimulus that we first applied to the network model (Fig. 7F). In the gallop paradigm, stimuli are applied in quick succession with alternating intervals, comparable to the putative period of the underlying oscillation. Enough stimuli should be applied such that after multiple presentations the stimuli sample a uniform distribution of phases. In the context of auditory stimuli, the standard gallop experiment involves different tones and is used to test perceptual separation of auditory streams. Such rhythmic stimuli can help indicate resonances or physical limitations of the system, and distinguish across possible models for this separation (such as in neural resonance theory (71)). One possible mechanism of auditory stream separation is an underlying oscillatory process which resets in certain phases and is less responsive in others. According to the *in vitro* inferior olive literature (41-43) this behavior is to be expected, and hence, such a stimulus can help distinguish underlying processes.



If spikes are modulated by an oscillatory process, the presence of spikes on a short interval should be able to predict, in the next interval, the absence or presence of spikes. Indeed, if the underlying process producing spikes has oscillatory components and a relatively stable period, the probability of spikes in each interval is systematically different, which would appear as asymmetric ratios of response in the different intervals (Fig. 7F). This can be inspected as the length of the empty and filled vertical bars representing ratio of probabilities of spiking for long or short stimulation intervals (Fig. 7G). Thus, if the period of the STO rhythm would be regular and cause phase-dependent gating, complex spike responses following each stimulus interval are expected to show preferences for the short or long window of stimulation; these preferences were indeed observed (Fig. 7G, left). However, this clear phase dependency only appears in the noiseless model scenario. After adding a moderate amount of contextual input, this dependency washes off, rendering the responses in the two windows more symmetric (Fig. 7G, right), with only a few cells (5/200) displaying significant ratio differences (tested against bootstrap with shuffled spikes).

and not during the falling phases (blue). One can query for the impact on spiking probability for any given initial phase at any time after the first stimulus. Different intervals lead to biased response ratios. **(G)** In order to test the impact of the presumed phase of the inferior olivary neurons, we applied a "gallop" stimulation pattern, alternating short (250 ms) and long (400 ms) intervals (top row). "Sensory input" (vertical red shaded bars) were delivered and spikes were counted in response windows (RW) 0-180 ms post-stimulus. Response probabilities were compared between response windows (RW) in short (empty bars) and long intervals (filled bars). Many cells in the model prefer either the short or the long window (for spiking cells, see left lower panel). However, in the presence of contextual noise, this preference largely washes off, seen as approximately symmetric responses in each of the intervals. Asterisks indicate that a tiny fraction of cells still displayed significant preference for particular intervals, which could be attributed to the low number of spikes fired by these cells.

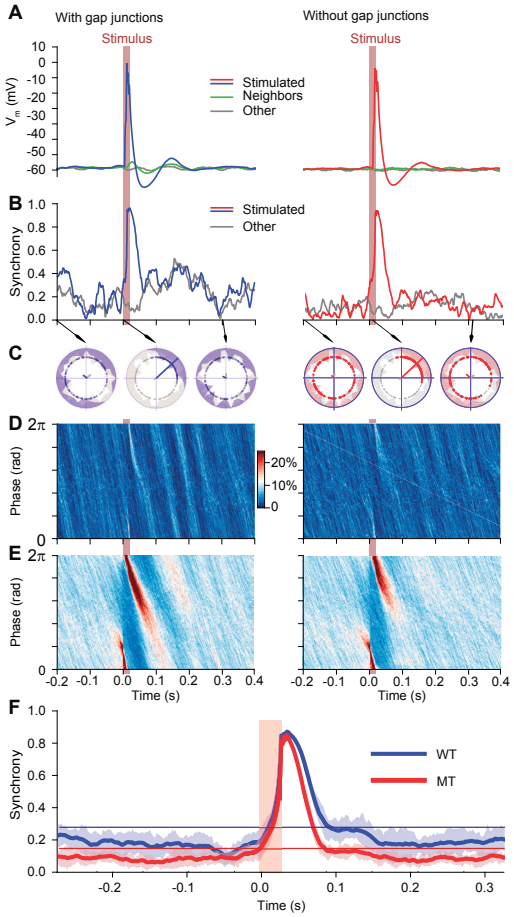


**Figure 8.** Gap junctions reinforce synchronous behavior after sensory stimulation. Impact of periodic stimulation on network phase in the presence of contextual stimuli for networks with (left column) and without gap junctions (right column). Brown bars indicate stimulation time. **(A)** Stimulus triggered membrane potential for all cells in the network (n = 100 stimuli). Stimulation causes a peak in the membrane potential of the directly stimulated cells (red line; cf. mask in Fig. 5A). The effect of the current spreading through gap junctions is visible in the cells immediately neighboring the stimulated cells (green line), whereas it is absent in the network model without gap junctions. **(B)** Increase of synchrony in the network due to a single stimulus. Synchrony is displayed as phase concentration over time (the Kuramoto parameter) for cells under the stimulation mask (colored) and other cells (gray). Stimulation generated a similar synchrony peak in both networks, but the transient synchrony after the peak is considerably higher and longer lived in the network with gap junctions. **(C)** Polar plots indicating network phase distribution for snapshots (arrows) for stimulated (colored distribution) and non-stimulated cells (gray distribution). Phase alignment of subthreshold oscillations of the inferior olivary network model was reduced in the absence of gap junctions. The lines in the middle of the plots indicate average phases for either the stimulated cells (in color) or all cells (gray). **(D)** Phase distribution of cells over time. Color code represents the proportion of neurons occupying a certain phase at a given time (phase bin size 2π/100, time bin is 1 ms). Dark/light bands indicate that the phase alignment propagates to most cells in the network and subsists for longer durations for the WT network. Nevertheless, contextual input overruled the phase alignment within a few hundred milliseconds (~300 ms in this case). In the absence of gap junctions, the impact of the stimulus is restricted to stimulated cells, so that the coherence induced by stimulus on the network was much smaller. **(E)** Same as in **D** but displaying averaged phase distributions for 100 stimuli. The stimulus hardly evoked an effect after 200 ms, and it did not induce any entrainment, which would have been visible as vertical bands before the stimulus. The effect of the stimulus is not stereotypical, due to dependency on network state driven by contextual input (see also Fig. 9). **(F)** Average network synchrony triggered on the stimulus. The horizontal lines in the bottom plot are the 95% inclusion boundaries taken from the 5 s of spontaneous network behavior to contextual input (no periodic "sensory" pulses). The model network with gap junctions displayed after the early stimulus response curve an elevated synchrony plateau, which ended after about 200 ms, whereas the model without gap junctions hardly showed any secondary plateau. There was no preceding synchrony, indicating complete absence of entrainment to the periodic stimulus.

## Model exhibits network activity that is synchronous and oscillating, but quasiperiodic

In line with the experimental *in vivo* data (e.g., Fig. 2 and 4), the olivary spike rhythmicity in the network model was steadily present over longer periods, and for a wide range of contextual input parameters (S5 Fig.). In addition, it also comprised, as in the experimental data, variations in frequency and amplitude during shorter epochs (Fig. 8 and S6). Analysis of the network parameters indicates that these latter variations in oscillatory behavior can be readily understood by their sensitivity to both the amplitude (parameter 'sigma') and kinetics (parameter 'tau', temporal decay) of the contextual input. Indeed, because of the underlying Ornstein-Uhlenbeck process, the generation of contextual input converges to a specified mean and standard deviation, but in short intervals the statistics including the average network STO frequency can drift considerably (Fig. 6C and 8). Since relatively small differences in oscillation parameters such as frequency can accumulate, they can swiftly overrule longer-term dependencies created by periodically resetting stimuli, as an analysis of phase distributions shows (Fig. 9). Thus, based upon the similar outcomes of the network model and *in vivo* experiments, we are led to propose that (1) the STOs in the inferior olive may well contribute to the continuous generation of short-lasting patterns of complex spikes in awake behaving animals, and that (2) the synaptic input to the inferior olive may modify the main parameters of these STOs. Note that in the absence of input, periodic rhythmic behavior should be the default behavior of oscillating cells. Thus, in all likelihood, even if the inferior olive oscillates endemically, sustained but variable input should induce highly contextual spike responses to variable periods and render the olivary responses quasiperiodic, rather than regularly periodic as observed in reduced preparations.

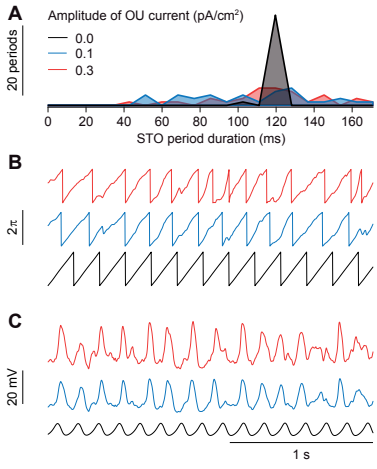


**Figure 9.** Significant variability of oscillatory periods induced by contextual input on oscillation period of a single model cell.

**(A)** Distribution of inter-peak intervals for a single model cell under 5 s of contextual stimulus (OU current) of different amplitudes. To gauge period variability without introducing refractory periods, input levels were chosen for non-spiking subthreshold dynamics only. The unperturbed model cell (in black) produces regular periods, while weak levels of contextual input are sufficient to create substantial variability (red and blue). **(B)** Example traces of membrane potential and **(C)** phase for the single cell under perturbations, for the same random seed. Note that under contextual input there was substantial variation in periods, but similar STO periodicity despite different levels of input.

## Galloping stimuli show little to no conditional spiking in the experimental data

In line with *in vivo* whole cell recordings made under anesthesia (10, 43) our awake data support the possibility that the moment of spiking may be related to the phase of olivary STOs, especially during the period of several hundred ms following stimulation (Figs. 2 and 4). As discussed above, a gallop stimulus would expose such an oscillatory process underlying the response probabilities. Four idealized scenarios about the expected results can be constructed, as follows: first, one can start with a complete absence of STOs, which would result in a response probability unrelated to stimulus intervals; second, it could be that there were STOs, but no phase-dependent firing (to be expected if the STO amplitude is small), which would also lead to complex spike firing irrespective of stimulus intervals; third, there could be STOs, but each stimulus would evoke a phase-reset, which again, would not lead to interval dependencies; and fourth, there could be STOs in combination with phase-dependent gating, which would result in a clear dependency of complex spike firing on the previous interval length (Fig. 7G, left panel). It should be noted that the large majority of studies on inferior olivary physiology, especially in reduced preparations, found evidence for the fourth situation (STOs + phase-dependent gating) (41, 43, 67).

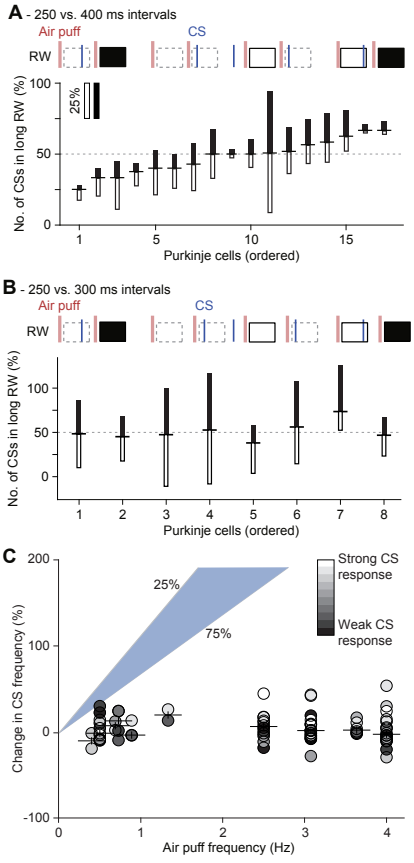


**Figure 10.** No phase-dependent spiking probabilities observed *in vivo*

**(A)** In order to test the impact of the presumed phase of the inferior olivary neurons *in vivo*, we applied a "gallop" stimulation pattern, alternating short (250 ms) and long (400 ms) intervals. Air puffs were delivered to the whisker pad. Complex spikes were counted in response windows (RWs) 20-200 ms post-stimulus and cells were sorted as a function of the ratio between the numbers of complex spikes in short and long intervals (indicated as horizontal dash between filled and empty bars). In this analysis, we included only the RWs that followed an RW with at least one complex spike; i.e. the RWs indicated by a dashed border were ignored. For each Purkinje cell the relative response probabilities for the long and short intervals are illustrated as the length of the filled and open bars, respectively. None of the Purkinje cells showed a significant difference in the response probability between the two intervals (all $p > 0.05$ on Fisher's exact test). **(B)** The same for the alternation of 250 and 300 ms intervals, showing even less response bias than in **A**. **(C)** If sensory stimulation triggers complex spikes, one would expect that a higher frequency of stimulation would lead to a higher frequency of complex spikes. However, such a relation was absent. For this analysis, we included only sensory-responsive Purkinje cells of which the complex spike response exceeded a bootstrap-derived 99% probability threshold. The gray scaling of the symbols indicates the response probability. Purkinje cells displaying a higher complex spike response rate had a slightly increased firing rate upon higher stimulus frequencies, but this was far from the expected increase (based upon a linear relationship; the shaded area indicates the 25-75% range).

To study whether phase-dependent gating in conjunction with an underlying oscillatory process could shape complex spike response timing *in vivo* we applied both a 250 vs. 400 ms and a 250 vs. 300 ms gallop stimulation using air puffs to the whiskers. Using only trials with a CS in the previous trial to calculate the ratio of responses ('conditional firing') a slight bias could be observed in the 250 vs. 400 ms paradigm (Fig. 10A) and to a lesser extent in the 250 vs. 300 ms (Fig. 10B). Analysis including all trials ('non-conditional') is included in S8 Fig. and shows no significant bias for any of the cells tested. Hence, our *in vivo* data are in line with the results from the network model subjected to synaptic noise, and show that the timing of complex spike responses to sensory stimulation is biased but not strongly determined by STOs.



## High-frequency stimulation does not evoke resonant complex spike firing

Our experimental data provided evidence for phase-dependent complex spike firing during brief intervals, but gallop stimulation did not expose a strong impact of STOs on complex spike response probabilities. Therefore, we sought an alternative approach to study the impact – if any – of STOs on complex spike firing *in vivo*. We reasoned that, if a sensory stimulus triggers a complex spike response with a certain probability, higher stimulation frequency should result in a proportional increase in complex spike firing. In particular, stimulus frequencies that would be in phase with the underlying STO would be expected to show signs of resonance and result in disproportionally increased complex spike firing. However, over periods of tens of seconds the complex spike frequency was resilient to varying the stimulus frequency between 1 and 4 Hz (linear regression = −0.02; $R^2 = 0.1$) (Fig. 10C) and did not show signs of resonance with any of the stimulus frequencies, as there were no frequencies at which the complex spike firing was substantially increased. Only a very high rate of sensory stimulation (10 Hz), commensurable with the average duration of windows of opportunity, could induce a mild increase in complex spike firing frequency, albeit at the cost of a highly reduced response probability (average increase: 71 ± 64% corresponding to an average increase from 1.12 Hz to 1.92 Hz; $n = 5$; $p < 0.05$; paired *t* test). This examination indicates that the average complex spike frequency is robust and stiff to modulation over longer time periods, imposing a hard limit on the frequency with which complex spikes can respond to sensory stimuli, confirming recent reports on complex spike homeostasis (72).

## STOs may contribute to complex spike firing during shorter periods

As stimulus triggered resonances were not observed at any of the stimulation frequencies, we turned to a more sensitive measure for the detection of oscillatory components in complex spike firing. We developed a statistical model that extrapolated from frequencies inferred through inter-complex spike intervals and stimulus triggered histograms (Fig. 11A-B). We reasoned that phase-dependent gating would imply that the interval between the last complex spike before and the first one after sensory stimulation aligns to the preferred frequency. In contrast, if sensory stimulation would typically evoke a phase reset, as suggested by our network model

(Fig. 7), no such relation would be found. The method was applied only to Purkinje cells with highly rhythmic complex spike firing. For each of those, we calculated their preferred frequency in the absence (Fig. 11C) or presence of sensory stimulation (Fig. 11D). We used that frequency to construct statistical models representing idealized extremes of phase-dependent (oscillatory) and -independent (uniform) responses. For the oscillatory component we employed an oscillatory gating model, where the timing of the first complex spike after stimulus onset would be in-phase with the ongoing oscillation. This model was contrasted to a linear response model in which sensory stimulus could evoke a complex spike independent of the moment of the last complex spike before that stimulus, apart from a refractory period. For each Purkinje cell, we compared the distribution of the intervals between the last complex spike before and the first complex spike after stimulus onset with the predicted distributions based on the linear model, the oscillatory model and nine intermediate models, mixing linear and oscillatory components with different relative weights (Fig. 11A-E). For the two extreme models as well as for the nine

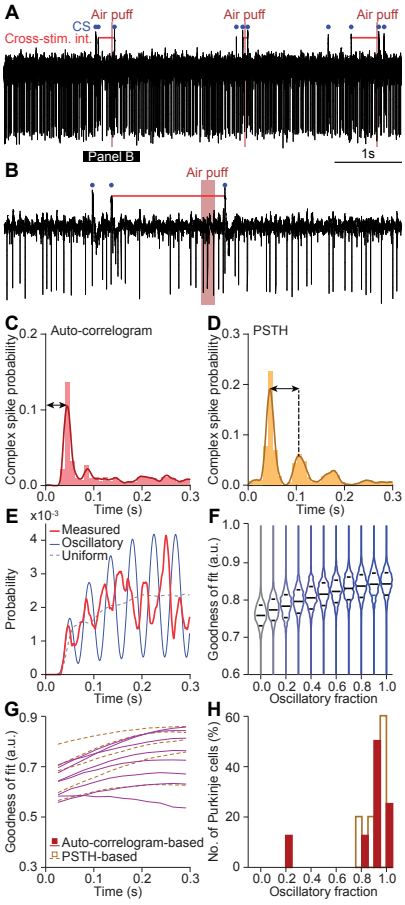


**Figure 11.** Complex spike responses to stimuli in most Purkinje cells are not conditioned on recent history.
We quantified the impact of presumed subthreshold oscillations on the occurrence and timing of complex spikes by assuming a preferred firing frequency for each individual Purkinje cell according to peri-stimulus time histogram and auto-correlograms. This approach is illustrated by a representative Purkinje cell **(A-E)**. A representative trace is shown in **A** and enlarged in **B**, showing the cross-stimulus interval (horizontal red line). (**C-D**) For each Purkinje cell, the preferred frequency was derived from the auto-correlogram **(C)** and the peri-stimulus time histogram (PSTH; **D**; cf. Fig. 2). (**E**) Intervals between the last complex spike before and the first complex spike after stimulus for each trial yielded a model of the preferred response windows (red line). The observed probability density function was compared with a probability density function based on a uniform complex spike distribution (dotted line), an oscillatory complex spike distribution (blue line), and 9 intermediate mixed models (see Methods). (**F**) The distributions of the goodness-of-fit for each of the 11 models showed a clear bias towards the uniform model, casting doubt on the impact of subthreshold oscillations on sensory-induced complex spike firing. The middle line indicates the average of all runs, while the upper and lower lines indicate 75 and 25% quartiles, respectively. (**G**) Distributions of the goodness-of-fit of all Purkinje cells that showed clear rhythmicity (see Methods). **(H)** Histograms of the best mix model shown in **G** indicate that the impact of the subthreshold oscillations on sensory complex spike responses is present, though small.

intermediate models we calculated a goodness-of-fit per Purkinje cell. Overall, when using these relatively long periods (300 ms), the linear model was superior to the oscillatory model, although a contribution of the oscillatory model could often improve the goodness-of-fit (Fig. 11F-H). Despite the apparent failure of the oscillatory model to fit the data, the data did show an oscillatory profile for many of the cells (Fig. 11E). This lends support to our observations that short-lived, but reliable, oscillations are apparent in complex spike timing, although they have little impact on the timing or probability of sensory triggered CS responses.



## Gap junctions facilitate frequency modulation of rhythmic complex spike firing

Apart from the STOs, extensive gap junctional coupling between dendrites is a second defining feature of the cyto-architecture of the inferior olive (31, 33, 73). Absence of these gap junctions leads to relatively mild, but present deficits in reflex-like behavior and learning thereof (10, 74). We analyzed the inter-complex spike interval times in Purkinje cells of mutant mice that lack

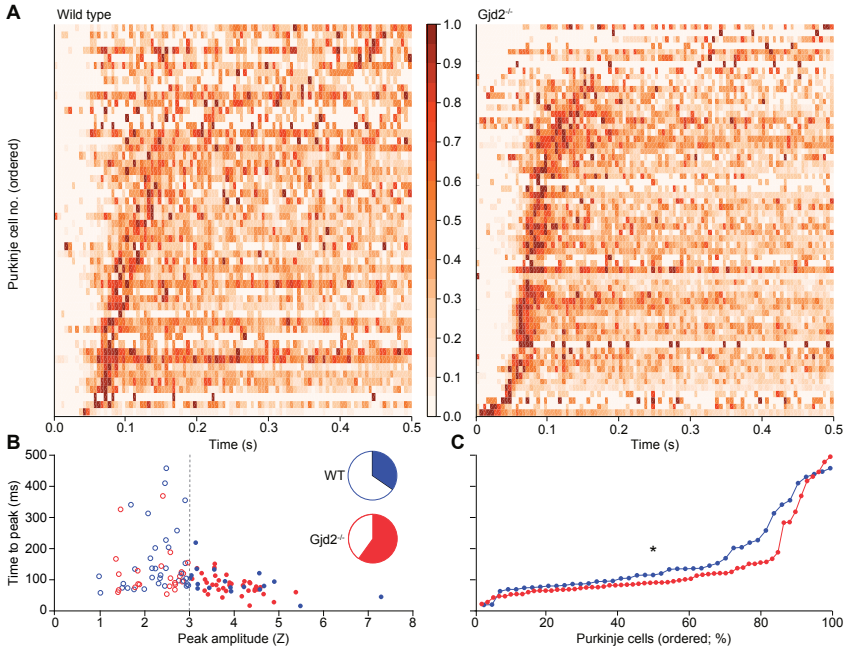


**Figure 12.** Oscillatory dynamics in spontaneous firing *in vivo* in the presence and absence of gap junctions. (**A**) Color-coded inter-complex spike-interval (ICSI) histogram of spontaneous firing of 60 Gjd2$^{-/-}$ and 52 wild-type Purkinje cells, normalized to the bin with the highest complex spike count per Purkinje cell. (**B**) The Gdj2$^{-/-}$ Purkinje cell distribution shows higher Z-scores than the wild-type population, indicating a stronger rhythmicity during spontaneous firing in the absence of gap junctions (p = 0.003; Kolmogorov-Smirnov test). A Z-score >3 was taken as sign for the presence of rhythmicity – which occurred more often in the Gjd2 KO than in the WT Purkinje cells (colored fraction in the pie diagrams; p = 0.005; Fisher's exact test). In the absence of gap junctions, rhythmic firing was more stereotypical, as illustrated by less variation in the time to peak (**C**); p = 0.0431; U = 1030.0; Mann-Whitney test). Note that the left panel of **A** is a copy of Fig. 2B and presented here to facilitate comparison.

the Gjd2 (Cx36) protein and are hence unable to form functional gap junctions in their inferior olive (69). In line with the predictions made by our network model (Fig. 5H and S6), the absence of gap junctions did not quench rhythmic complex spike firing during spontaneous activity (Fig. 12A). In fact, the fraction of Purkinje cells showing significant rhythmicity in the Gjd2 KO mice was larger than that in the wild-type littermates (Gjd2 KO: 38 out of 65 Purkinje cells (58%) vs. WT: 15 out of 46 Purkinje cells (33%); $p = 0.0118$; Fisher's exact test), with their average rhythmicity being significantly stronger ($p = 0.003$; Kolmogorov-Smirnov test), measured by Z-scores

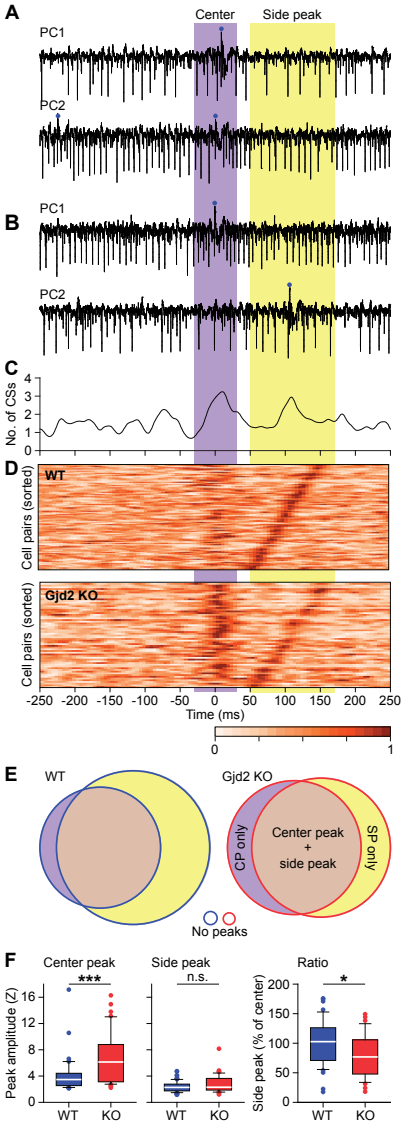


**Figure 13.** Coherence of complex spike firing of Purkinje cells over time

(**A**) Two Purkinje cells recorded simultaneously in a wild type (WT) mouse during spontaneous activity, showing an epoch with near-synchronous complex spike firing with both spikes in the center-time interval. (**B**) Another epoch of the same cell pair, but now the second Purkinje cell fired a complex spike at the next cycle, leading to a double-peaked cross-correlogram for this cell pair, seen in **C**. (**D**) Heat map representations of cross-correlograms between simultaneously recorded Purkinje cells in WT and Gjd2 KO mice. Only pairs with a significant center or side peak are plotted. The cross-correlation of each pair is normalized to the bin with maximal correlation. The latency of the strongest side peak was used to order the cell pairs (including cells where center peaks were significant, but side peaks were not). Correlation direction was selected so that the strongest side peaks were always positioned on the right side. Note that while the center peak is stronger in Gjd2 KO, the side peak is more prominent in WT pairs. This side peak can be regarded as a "network echo". (**E**) Venn diagrams showing the relative occurrence of center and side peaks in the presence and absence of gap junctions. (**F**) In the absence of gap junctions, the center peak, but not the side peak, was stronger (left and middle panel). Likewise, the normalized ratio of the side peak vs that of the center peak was lower in the Gjd2 KO mice (right panel). * and *** indicate $p < 0.05$ and $p < 0.001$, respectively (*t* test).

of side peaks (Fig. 12B). Indeed, the variation in oscillatory frequencies across Purkinje cells of the mutants was significantly less than that in their wild-type littermates in that the latency to peak times per Purkinje cell were less variable ($p$ = 0.0431; Mann-Whitney test; Fig. 12C). This latter finding is at first sight contradictory to our findings in the network model, where we show that gap junctions promote more uniform firing rates through increased synchrony between neurons (Fig. 5H). These simulations were run in the absence of synaptic input, though. Addition of contextual input also creates more variability in the wild type cells (S6B Fig.). As the lack of gap junctions increases cell excitability (10, 69), it is likely that synaptic input has a larger impact in the absence of gap junctions, leaving less room for inter-cell heterogeneity. Overall, removal of gap junctions affected the temporal and spatial dynamics by increasing the stereotypical rhythmicity of complex spike firing.



## Temporal relations of complex spikes of different Purkinje cells

We made paired recordings of Purkinje cells in awake mice to study the temporal relations of their complex spikes during spontaneous activity. The cell pairs were recorded with two electrodes randomly placed in a grid of 8 x 4, with 300 µm between electrode centers. For each pair of simultaneously recorded Purkinje cells, we made a cross correlogram. The median number of complex spikes in the reference cell used for these cross-correlograms was 827 (range: 74-2174). Cell pairs showed coherent activity in that they could show a central peak and/or a side peak in their cross-correlogram (Fig. 13A-C). The side peaks could appear at different latencies, similar to the range observed in auto-correlograms of single Purkinje cells (cf. Fig. 2B). Moreover, Purkinje cell pairs that did not produce signs of synchronous spiking in the center peak could still produce an "echo" in the side peak after 50-150 ms. Counter-intuitively, cross-correlograms of Purkinje cell pairs of the wild type mice showed less often a significant center peak than those of Gjd2 KOs (WT: 51 out of 96 pairs (53%; $N$ = 4 mice); Gjd2 KO: 44 out of 61 pairs (72%; $N$ = 7 mice); $p$ = 0.0305; Fisher's exact test). In line with the more stereotypic firing observed in single cells in the absence of gap junctions (Fig. 12), the strength of the center peak was on average enhanced in the mutants ($Z$-scores of significant center peaks (median ± IQR): WT: 3.47 ± 1.82; Gjd2 KO: 5.75 ± 5.58; $p$ = 0.0002; Mann-Whitney test) (Fig. 13D-F). Instead, the side peak of Gjd2 KO Purkinje cell pairs was not stronger than that of WTs ($Z$-scores of significant side peaks (median ± IQR): WT: 3.01 ± 0.89; Gjd2 KO: 3.04 ± 1.52; $p$ = 0.194; Mann-Whitney test), leading to a lower ratio between center and side peak (mean ± SEM: WT: 90.70 ± 5.17%; Gjd2 KO: 72.86 ± 6.52%; $p$ = 0.036; $t$ = 2.143; df = 67; $t$ test) (Fig. 13E-F). Interestingly, the occurrence of side peaks in Purkinje cell pairs was unidirectional in approximately half the cell pairs (WT: 47 out of 82 pairs with at least one side peak (57%); Gjd2 KO: 25 out of 47 pairs (53%); $p$ = 0.714; Fisher's exact test), which means that one of the neurons of a pair was leading the other, but not *vice versa*. As this was consistent in the Gjd2 KO as well as the WT Purkinje cells, these data could reflect traveling waves across the inferior olive, which, however, must have extrinsic sources (44, 75). Thus, the paired recordings are compatible with the findings

highlighted above in that the presence of coupling can affect the coherence of STOs for short periods up to a few hundred milliseconds, while leaving the window for later correlated events open.

## DISCUSSION

Given the major impact of complex spikes on Purkinje cell processing and motor behavior (10, 11, 25, 76, 77), resolving the mechanisms underlying their timing is critical to understand the role of the olivo-cerebellar system in motor coordination and learning (20, 22, 24, 78). Synchronized subthreshold oscillations (STOs) of olivary neurons have been suggested to contribute to the formation of temporal patterning of complex spike firing, but most of the evidence for STOs has been obtained in decerebrate or anesthetized animals *in vivo* or, even more indirectly, *in vitro* (10, 41-43, 45, 47, 79, but see 80). Our experiments and model were designed to inquire the existence of an *in vivo* STO, and on its ability to display phase-dependent responses in the awake brain. We evaluated rhythmic complex spike firing in behaving animals responding to peripheral stimuli and investigated their match with simulations of a tissue-scale model of the inferior olivary network. The model and data would be consistent with STOs whose period can be readily adjusted upon synaptic fluctuations from other brain regions, an effect that is consistent with the known response properties of the inferior olive (46, 67).

### Complex spike patterns are explained by cell physiology and network-wide properties

During spontaneous activity, Purkinje cells generally fire a complex spike roughly once a second, but this frequency can be increased to about 10 Hz by systemically applying drugs, like harmaline, which directly affect conductances mediating STOs in the inferior olive (41, 81). Since these drugs also induce tremorgenic movements beating at similar frequencies, it has been proposed that the inferior olive may serve as a temporal framework for motor coordination (11, 82). This oscillatory firing behavior of the olivary neurons may mirror limb resonant properties and act as an inverse controller, for example by dampening the dynamics of the muscles involved (83).

In line with previous recordings (22-24, 28, 61, 72, 76, 78, 84), the current data indicate that only a small fraction of Purkinje neurons respond to sensory stimulation with a complex spike response probability larger than 50%. This probability falls substantially with increasing frequency of stimulation, as the overall spike frequency only marginally increases to high frequency stimulation. Even after applying different temporal patterns of sensory stimulation for longer epochs, we observed no substantial deviation from the stereotypic 1 Hz firing rate. Moreover, it should be noted that even if the frequency of underlying oscillations has bearing on the pattern of responses of the gallop stimuli, conditional dependencies should be expected

for most STO frequencies, unless the ratio of the interval of gallop and the STO period has no remainder. Given the seemingly consistent frequencies predicted by PSTH's and autocorrelograms of single cells (Figs. 2 and 3, but also seen in cross correlograms, as in Fig. 13), we chose gallop intervals with periods commensurate with a representative frequency of 8 Hz, each of which should sample different phases in the oscillation. If at all present, we should have observed conditional dependencies on at least a few cells.

In our study, complex spikes remain as unpredictable as ever. Thus, regulatory mechanisms keep the complex spike rate relatively stable over longer time periods (72). No resonance is exhibited, irrespective of an enduring powerful sensory stimulus in a variety of frequencies. Save few exceptions, the presence of a complex spike in an interval is compensated by the absence in another. Thus, it looks as if the complex spikes rearrange themselves in time in order to keep close to its proverbial 1 Hz frequency. It remains to be shown to what extent the mechanisms involved are intrinsic (cell-dependent) and/or extrinsic (network-dependent). A possible candidate for setting the overall level of excitability through intrinsic mechanisms is given by $Ca^{2+}$-activated $Cl^-$ channels, which are prominently expressed in olivary neurons along with $Ca^{2+}$-dependent BK and SK $K^+$ channels (85, 86). In addition, the olivo-cerebellar module itself could partly impose this regulation (86-88). Indeed, the long-term dynamics within the closed olivo-cortico-nuclear loop may well exert homeostatic control, given that increases in complex spikes lead to enhanced inhibition of the inferior olive via the cerebellar nuclei (20). The impact of such a network mechanism may even be more prominent when changes in synchrony are taken into account (89). We propose that a closed-loop experiment conducted while imaging from a wide field, producing stimulation as a function of the degree of complex spike synchrony, could tease out conditional complex spike probabilities. Increasing our capability of predicting complex spikes is instrumental to elucidate the control of inferior olivary firing.



## Inferior olivary STOs

The existence of temporal windows of opportunity for complex spike responses following sensory stimulation highlighted a potential impact of STOs on conditional complex spike gating (10, 41, 43, 90). Indeed, autocorrelogram peaks correlated well with interspike intervals following stimulation, arguing for an underlying rhythm. Complex spikes could appear in a particular window even when they were not preceded by a complex spike in a previous window during a single trial, arguing against a prominent role of refractory periods in creating rhythmic complex spike responses. Comparing actual firing patterns with statistical models mixing linear or oscillatory interval distributions indicated a potential impact of oscillations. The mild impact of the oscillatory component on explaining the data may in part depend on the assumption that cells have a well-defined frequency. In other words, a variable rebound time could offset the phase response by a couple of milliseconds, reducing the contribution of the oscillatory model, though phase preferences due to prior spikes may still occur (i.e., Fig. 11E). Our biophysical model suggests that fluctuating inputs, such as those mediating inhibition from the cerebellar

nuclei or those relaying depolarizing modulation from the raphe nuclei (91, 92), may induce variations in the oscillation period on a cycle-by-cycle basis (Figs. 8 and 9). As these contextual inputs are absent or suppressed in decerebrate or anesthetized preparations, as well as *in vitro*, they may also explain why many earlier studies systematically encountered cells with well-defined STO frequencies (10, 41, 43, 45, 47, 79, 93, 94). In the network model, in which we mimicked the contextual input as an Ornstein-Uhlenbeck process with local variations but no long-term drifts of the mean (95), the results agree well with the experimental observations in terms of synchronous firing, phase shifts, cross-correlogram peaks and side peaks, as well as overall firing frequency. Indeed, the absence of resonant responses over longer time windows and the inconsistency of individual olivary cells to fire on every trial or cycle indicate that the STOs are not regularly periodic, but rather quasiperiodic, while still being synchronous.

## Can rebound firing explain rhythmic complex spike responses?

Even though several lines of evidence suggest a role for STOs (see above), we did not observe an unequivocal, significant conditional dependence of complex spikes in the gallop paradigm, as expected by a noiseless model. How can a system with rhythmic responses at least partially fail to be phase modulated by such periodic stimuli? An attractive alternative explanation for rhythmicity might be the occurrence of high-threshold $Ca_v2.1$ P/Q-type $Ca^{2+}$ channel-dependent rebound spikes (S7 Fig.) (12, 62). If impulse-like input to the olive can evoke a spike, and if this spike produces a rebound spike some tens of milliseconds later, this could explain the alignment between the PSTHs and cross-correlograms. However, this argument cannot explain stimulus triggered spikes at the second or third window of opportunity, without an earlier spike as observed in Fig. 4. As the occurrence of the rebound spike is predicated on a prior spike, a spike in the second or third window without a prior spike cannot be explained by the rebound spiking phenomenon, at least not within the same cell. In other words, the spikes happening exclusively in the second (or third) window of opportunity cannot be the result of a previous spike in the same cell, unless there is a shared rhythm in the network. It is also conceivable that strong hyperpolarization that is synchronized with the complex spike rhythm could promote reverberating firing, but this is an extrinsic mechanism, discussed below. As they stand, our findings do not support the idea that the post-spike hyperpolarization is a prerequisite for the complex spike pattern observed. Multiple windows of opportunity could, according to our model, be enhanced by transient oscillations induced by resets relayed by gap junctions to the local olivary circuit.

## The role of gap junctions in complex spike timing

Apart from the almost complete absence of interneurons, the presence of STOs and the exclusive projection to the cerebellum, the abundance of dendro-dendritic gap junctions is another defining feature of the inferior olive. The absence of these gap junctions does not lead to gross motor deficits, but prevents proper acquisition and execution of more challenging tasks (10,

16, 74), which is in line with the relatively minor impact found on complex spike activity in Gjd2 KO mice. At first sight, the effects of deleting gap junctions seem counterintuitive. Synchronous and rhythmic patterns are exacerbated, rather than diminished by the loss of gap junctions. However, the side peak of the auto-correlogram is significantly squashed, indicating that the gap junctions have a role in the increased coherence of the upcoming oscillation. Gap junctions do not only facilitate synchronization of coupled neurons, they also lower their excitability by increasing the membrane resistance (69). Together, this results in less direct coupling, observed as reduced synchrony of direct neighbors (16, 96), and increased responsiveness to synaptic input. This leads to more long-range coherence and as a consequence gap junction networks may act as a "noise filter", promoting short-range quorum-voting on phase (a term coined by Winfree (97)). This effect is visible in our model as spikes are most likely to occur when excitation follows inhibition (Fig. 6H). This is in line with the finding that complex spikes of nearby Purkinje cells have a preference to fire together (72, 98, 99). This concept also agrees with the possibility that coupled olivary neurons may control movements by dampening the dynamics of the muscles involved at an appropriate level (83, 100), as both the resonances and movement oscillations increase shortly after sensory stimulation in Gjd2 KO mice (16).



## Reverberating loops

Network resonances are a pervasive feature of brain circuits and they can be induced by subthreshold oscillations of particular cell types (101, 102). In addition to the autochthonous dynamics of the inferior olive, reverberating loops through the circuit could help explain some features of complex spike firing, including the occurrence of complex spike doublets and side peaks in cross-correlograms. Such phenomena could be explained by "network echoes", where complex spikes in one cycle would induce complex spikes in the next cycle (87, 103, 104). The most obvious candidate loop to produce is that via the cerebellum and the nuclei of the meso-diencephalic junction (55, 105). The output of the inferior olive is mainly directed via exceptionally strong synapses to the Purkinje cells (106). These Purkinje cells in turn inhibit neurons of the cerebellar nuclei that can show rebound firing after a period of inhibition (88, 107). This rebound activity can excite the inferior olive again via a disynaptic connection via the nuclei of the meso-diencephalic junction. While an isolated complex spike is unlikely to evoke such a rebound activity, a larger group of Purkinje cells could be successful in doing so (20, 107, 108). The travel time for this loop (around 50-100 ms) has been indirectly assessed in the awake preparation (8, 10, 26), and corresponds to the latency of the rebound firing in the cerebellar nuclei under anesthesia (87, 88, 107, 109). This implies that the travel times for the entire loop would be in the same order as found for the preferred frequencies of complex spike firing. Other, more elaborate loops involving for instance the forebrain may also exist (110) and could play an additional role in shaping complex spike patterns.

A putative impact of reverberating loops on rebound activity could be a network phenomenon, as the impact of an isolated complex spike may not be sufficient to trigger this loop. This

is in line with the reduced "echo" in the cross-correlograms of the Gjd2 KO mice and enhanced doublets following lesions of the nucleo-olivary tract as occurs in olivary hypertrophy (111). Taken together, rebound spiking, STOs and reverberating loops all seem to promote in a cooperative manner complex spike rhythmicity at a time scale of about 200 ms. Through modeling, we found that not only the state of the inferior olivary oscillations determines which inputs are transmitted, but that these inputs also determine the state of the network. Thus, inputs from both the cerebellum and the cerebrum determine the probability of complex spike responses on a cycle-by-cycle basis providing a quasiperiodic framework to align synchronous groups. This sharply contrasts with a view in which the inferior olive is a clock with regular periodicity. A circuit-wide understanding of cerebellar resonances on the basis of such a mechanism could open a novel pathway to explore the cerebellar gating by other brain regions.

The combination of delayed gap junctions and delayed inhibition, as found in the olivocerebellar loop (104, 112), can affect oscillatory behavior (113). The interplay between STOs and delayed inhibition is therefore also relevant for other neural circuitries, for instance for creating filter settings for the perception of sounds with specific oscillatory properties (114-116) or orchestrating rhythmic movements as shown in the present study (see also 117).

### A ratchet rather than a metronome

Well-coordinated movement sequences are not timed rigidly; they must be enacted flexibly and contextually. In order to catch a ball, or a prey, or to perform any other appropriately timed movement, it is essential to fine-tune the duration and onsets of multiple coordinated output systems. An inferior olive that responds contextually to time varying input by advancing and delaying cycles does not act as a rigid clock or metronome, but more contextually, as a ratchet-pole system, with the frequency of 'clicks' of the ratchet reflecting the recent history of applied torque. The properties we have encountered in this study are consistent with a 'ratchet-like' dynamics for the inferior olive, which integrates time-varying stimulus in a phase-dependent manner. According to this view, the inferior olive responds to all inputs (sensory and otherwise), by producing phase changes that are informative about the recent history of input, and dictate the appearance of coherent complex spike waves arriving at the cerebellar cortex.

## METHODS

### Ethics Statement

All experimental procedures were approved *a priori* by an independent animal ethical committee (DEC-Consult, Soest, The Netherlands) as required under Dutch law.

## Animals

Experiments were performed on 16 adult (9 males and 7 females of 25 ± 14 weeks old) homozygous Gjd2$^{tm1Kwi}$ (Gjd2 KO, formerly known as Cx36 KO mice (10)) mice which were compared to 15 wild-type littermates (8 males and 7 females of 26 ± 13 weeks old; means ± sd). The generation of these mice has been described previously (118). The data described in S2 Fig. originated from previously published recordings in 35 wild-type mice (61). All mice had a C57BL6/J background. The mice received a magnetic pedestal that was attached to the skull above bregma using Optibond adhesive (Kerr Corporation, Orange, CA) and a craniotomy of the occipital bone above lobules crus 1 and crus 2. The surgery was performed under isoflurane anesthesia (2-4% V/V in $O_2$). Post-surgical pain was treated with 5 mg/kg carprofen ("Rimadyl", Pfizer, New York, NY) and 1 μg lidocaine (Braun, Meisingen, Germany). Mice were habituated during 2 daily sessions of 30-60 min.



## Electrophysiology

Extracellular recordings of Purkinje cells were made in the cerebellar lobules crus 1 and 2 of awake mice as described previously (28). Briefly, an 8 x 4 matrix of quartz-platinum electrodes (2-4 MΩ; Thomas Recording, Giessen, Germany) was used to make recordings that were amplified and digitized at 24 kHz using an RZ2 BioAmp processor (Tucker-Davis Technologies, Alachua, FL). The signals were analyzed offline with SpikeTrain (Neurasmus, Rotterdam, The Netherlands) using a digital band-pass filter (30-6,000 Hz). Complex spikes were recognized based on their waveform consisting of an initial spike followed by one or more spikelets. A recording was accepted as that of a single Purkinje cell when a discernible pause of at least 8 ms in simple spike firing followed the complex spikes and when the complex spikes were of similar shape and amplitude throughout the recording.

Sensory stimulation was applied as air puffs of 20 psi and 25 ms duration directed at the whisker pad ipsilateral to the side of recording. The stimuli were given in trains of 100 or 360 pulses either at regular or alternating intervals. During a recording, trains with different stimulus intervals were played in a random sequence.

## Whisker movement tracking

Whisker videos were made from above using a bright LED panel as backlight (λ = 640 nm) at a frame rate of 1,000 Hz (480 x 500 pixels using an A504k camera from Basler Vision Technologies, Ahrensburg, Germany). The whiskers were not trimmed or cut. Whisker movements were tracked offline as described previously (119) using a method based on the BIOTACT Whisker Tracking Tool (120). We used the average angle of all trackable large facial whiskers for further quantification of whisker behavior.

## Complex spike pattern analysis

Of each Purkinje cell we computed the probability density function (PDF) of both its complex spike autocorrelogram and its distribution of intervals between consecutive complex spikes (inter-complex spike intervals (ICSIs)). PDFs were calculated with an Epanechnikov kernel (with finite support) with a width of 10 ms. In order to exclude stimulus-induced alterations in complex spike firing, complex spikes detected between 20 and 200 ms after a stimulus were omitted from this phase of the analysis. PDFs were calculated from 0 up till 500 ms. The peak in the ICSI PDF was considered as the "preferred ICSI interval" and its strength was expressed as the Z-score by dividing the peak value by the standard deviation of the PDF. To understand the impact of Purkinje cell with little or no preference for specific ICSI intervals on the analysis, we chose to look both at the Purkinje cells with high and low Z-scores. Thus, we grouped Purkinje cells into high and low level Z-scores, using a threshold of 3.

Air-puff stimulations frequently triggered double complex spike response peaks, suggestive of an underlying inferior olivary oscillation. For further analysis of the conditional responses, an estimate of the putative inferior olivary frequency was derived from the interval between these two response peaks. First, it was established for each Purkinje cell whether two peaks were present in the PSTH. To this end, we set a threshold for each of these two peaks. For the first peak, this was calculated by reshuffling the ICSIs over the recording followed by calculating a stimulus-triggered pseudo-PSTH, repeating this procedure 10,000 times and selecting the 99% upper-bound. We considered the first response peak to be significant if it crossed the upper-bound uninterruptedly for at least 10 ms. Since the second response peak typically is much smaller than the first one, we calculated a new threshold for the second peak by excluding the time-window for the first response peak. This window was set from the time of the stimulus until where the response probability drops to the average response frequency, the response frequency as expected if stimuli do not trigger complex spikes, following the significant 'first' responsive peak. In 5 out of 98 Purkinje cells, the PDF of the response rate between clear peaks remained above the average response rate, in which case we used the time point where the amplitude drop in the PDF was more than twice the difference between upper bound and average response probability. The rest of the bootstrap method was identical to that for the first response peak. Only peaks up to 0.5 s after the stimulus were included in the population analysis.

## Prediction of response probability based on inferred olivary oscillation frequency

In order to test whether the phase of the inferior olivary oscillations affected the complex spike response probability, we compared the complex spike intervals over an air-puff for each stimulus that triggered a complex spike. To this end, we analyzed the recordings of 25 Purkinje cells (10 WT and 15 Gjd2 KO) that were measured previously in crus 1 and crus 2 of awake, adult mice. We included only Purkinje cells that displayed clear oscillatory complex spike firing

indicated by the display of a secondary complex spike response peak, as evaluated according to the bootstrap method described above, and/or significant peaks in the ICSI histogram. Only stable recordings covering at least 500 stimuli at frequencies below 1 Hz were considered for this analysis.

For each recording we compared two idealized statistical models of the observed ICSI distributions: an oscillatory model showing phase-dependent spiking and stable olivary oscillation frequencies and a uniform model lacking phase-dependencies. For the oscillatory model, we created complex spike probability functions for the pre-stimulus interval (-300 to 0 ms) based on the oscillatory period established either for the ICSI distribution or from the interval between the two complex spike response peaks. We fitted a sine wave with the observed frequency, having its peak at the moment of the first complex spike in the stimulus response window (20-200 ms after the air puff) and derived spike probability levels during the pre-stimulus interval from these fits, with the trough representing zero probability. Frequency and amplitude of every cycle were kept constant for the whole recording. In the uniform model, we calculated the pre-stimulus spiking probability with a uniform distribution based on the complex spike frequency of each Purkinje cell. We did include a refractory period, being the shortest ICSI observed for each recording, to reflect the inability of consecutive complex spikes to occur with a very short time interval. Refractory periods were comparable between mutants and wild types; 49 ± 15 ms for Gjd2 KO cells and 50 ± 20 ms for WT cells. Subsequently, we constructed compound fits consisting of linear summations of the two models. One extreme was the oscillatory model and the other the uniform model and we considered nine intermediate combinations (e.g., 0.3 x the oscillatory model + 0.7 x the uniform model). Every compound fit was run for 10,000 times. The goodness of fit was computed as the absolute differences of every single run of the model with the actual ICSI distribution.



## Data availability

Summarized data and analyses scripts are available online at https://osf.io/6x5uy/. README files are provided at the same repository.

## Biophysically plausible IO model

The model networks used here are comprised of a topographical grid of 200 coupled cells, in a 10x10x2 lattice arrangement, which may resemble an area of about 400 µm x 400 µm of the inferior olive, for instance, the rostral portion of the dorsal lamella of the principle olive of the mouse. It is available online at https://github.com/MRIO/OliveTree, branch 'Warnaar'. For instructions on how to run the model and reproduce analysis, check README_Warnaar.txt'.

## Single cell model

Each cell within these networks was modelled according to the single cell model described in (46), which is an elaboration of a previous model (62) with an added axon and modified

fast sodium channel. Equations are provided in the appendix of that publication at (https://doi.org/10.1371/journal.pcbi.1002814.s002), and can be checked in the MATLAB functions *IOcell* and *createDefaultNeurons* in the codebase. The model includes three compartments (soma, dendrite, axon hillock) with 12 conductances. In addition to the ionic mechanisms, the dendrite of the model cell has a $Ca^{2+}$ concentration state variable, which is related to the intrusion through the $Ca_v2.1$ channels. The main ionic conductances responsible for the oscillation are the somatic T-type $Ca^{2+}$ and the $Ca^{2+}$-activated $K^+$ (SK) channels present in the dendritic compartment. The crucial parameters governing the emergence of subthreshold oscillations are randomized, reflecting the experimental facts that about one third of the cells oscillate endemically (*in vivo*) with intrinsic variations in oscillatory frequencies (43). The behavior of the STO of the model cells in our network as a function of their parameters, for models with and without gap junctions, are included in S5 and S6 Fig. Cell parameters are found in supplementary table 1.

## Gap junction connectivity

Connectivity is created with the function 'createW.m' in the MATLAB codebase. Briefly, cells within a specified radius of each other were connected according to a probability function such as to ensure the specified mean degree in the network ($n = 8$), chosen to resemble the observed connectivity distributions reported in the literature. The connectivity parameters (distance and average connection probability) were chosen to match experimental values (radius ≤ 120 μm) and average connection probability (~8 neighbors). The procedure to obtain connectivity is as follows. First, pairwise distances between all cells are calculated. Then, a binary adjacency matrix is created by thresholding those distances within a specified radius. Thereafter, we assign a random number between 0 and 1 to each link from a uniform distribution. Finally, this matrix is made binary by comparing each entry with a probability so that the average number of connections approximates a given mean connectivity. This binary adjacency matrix is then multiplied by the mean gap junction conductance parameter. Finally, gap junction conductance values are then randomized by a uniform jittering of the conductance by 10% of their original value.

## Gap junctions

The conductance of gap junctions was normalized with a saturating factor by difference of potential between the neighboring cells, according to (62) based on findings from (121) with the following function:

FORMULA 1: $$\bar{g}_c(\Delta V) = g_c\,(0.8\, e^{(-\Delta V^2/100)} + 0.2)$$

Where $\Delta V$ is the voltage difference between the connected cells, $g_c$ is the nominal coupling and $\bar{g}_c$ is the effective coupling.

## Network inputs

Two inputs are given to the model, one emulating the sensory input from whisker pad stimulation and the other representing a stimulus-independent background reflecting diverse excitatory and inhibitory inputs to the inferior olive. The latter consisted of a continuous stochastic process with known mean and standard deviation with a relaxation parameter following the Ornstein-Uhlenbeck process (95), succinctly described underneath.

Only one subset of cells in the center of the network (40% of the cells in a mask spanning a radius of 3 cells from the center of the network) representing efferent arborization, receives the "sensory input", with "sensory" currents being delivered to the soma of modelled cells ($g_{AMPA}$ = 0.15 mS/cm²). "Sensory input" was modeled according to O'Donnel et al. (122). The mask is represented in Fig. 5A.



The cells of the inferior olivary network most likely share input sources due to overlapping arborizations of efferent projections (123). To represent both shared and independent input, we have modeled the current source in each cell as having an independent process and a shared process, with a mix parameter (alpha) of 10% input correlation shared by all the cells in the network. This level of correlation leads to a coherent background oscillation in the cells of the network, which is exacerbated in the presence of gap junctions (S5 Fig.).

## Ornstein-Uhlenbeck noise process

Ornstein-Uhlenbeck (OU) is a noise process that ensures that the mean current delivered is well behaved and that the integral of delivered current over time converges to a constant value (95). The OU current is a good approximation for synaptic inputs originating in a large number of uncorrelated sources, where synaptic events are generated randomly and each event decays with a given rate (τ). We use a recursive implementation according to the following recursive formula:

FORMULA 2: $$\eta_i(t+1) = \eta_i(n,t) \times \exp(-\delta/\tau) + (1/\tau)(\mu - \eta_i(t)) + \sigma \times \sqrt{\delta} \times \xi_i$$

Where $\eta_i(t)$ is the noise amplitude of neuron i at time $t$. The noise process is parameterized by $\tau$, $\sigma$, $\mu$ where $\tau$ represents the synaptic decay time constant, $\delta$ is the integration step time for our forward Euler integrator, $\sigma$ is the standard deviation of the noise process and $\mu$ is its mean. The random draw from a Gaussian distribution at every time step is represented by $\xi_i$.

Neurons in the inferior olive receive broad arborizations, leading to input correlations across nearby neurons. In our model this is represented via a mixture of an independent process for each neuron $n_{independent}$ and a shared process, $n_{all}$, common to all the neurons in the network, parameterized by a mixing parameter $\alpha$, called 'noise correlation':

FORMULA 3: $$n_i(t) = \alpha \times n_{independent} + (1 - \alpha) \times n_{all}(t)$$

Simulation results throughout the article come from simulations with noise use an $\alpha$ where neurons share 10% of their noise input. Reported results are qualitatively robust to changes in this value (Fig. S5).

## Network parameter spaces

To examine the dependence of network dynamics on the characteristics of the incoming input, we computed the 200 neuron network sweeping a grid of the main input parameters ($\tau$, $\sigma$, $\mu$, $\alpha$) of the Ornstein-Uhlenbeck noise process. The network response in terms of STO frequency, population firing rates, proportion of firing neurons was analyzed with respect to a grid of input parameters. For comparability of statistics and reproducibility of results, all results displayed in this article were obtained from a single random seed. We have tested the network with multiple seeds and the results are qualitatively indistinguishable.

The parameters of the Ornstein-Uhlenbeck process were tuned such that the network emulating the wildtype network (with gap junctions, WT) produced an average frequency of 1 Hz and more than 95% of the model cells fire at least once every 5 seconds (the parameter space for the network responses including STO, population firing rate and proportion of cells that fire within 3s is found in S5B Fig.). The parameters to achieve these criteria are dependent on the total leak through the gap junctions. There are multiple methods to compensate the absent leak in the gapless network. In the present case, the network without gap junctions has been tuned to produce the same firing frequency as the network with gaps by increasing the membrane leak currents from 0.010 to 0.013 mS/cm$^2$. This results in a similar excitability but slightly lower STO frequency in the “mutant”. The average firing rate behavior of the network shows a linear relationship with the standard deviation of the OU process (S4 Fig.). For the present network with balanced connectivity and a single gap conductance of 0.04 mS/cm$^2$, the Ornstein-Uhlenbeck parameters are ($\tau$, $\sigma$, $\mu$, $\alpha$) $\mu$ = −0.6 pA/cm$^2$, $\sigma$ = 0.6 pA/cm$^2$ and $\tau$ = 20 ms. $\tau$ is a decay parameter that represents the synaptic decay times expected for olivary inputs, in this case chosen to emulate dendritic GABA according to Devor and Yarom (124).

## Synchrony and frequency estimation

Both synchrony and instantaneous frequency were estimated on the basis of a novel phase transformation of the membrane potential, which is more robust than the standard Hilbert transform, and can produce a linear phase response to the non-linear shape of the subthreshold oscillations (125). This transformation improves the estimation of the momentary phase and compensates for the fact that ionic mechanisms induce different rates of membrane potential change at different phases of the oscillation. This phases analysis was conducted with the DAMOCO toolbox (126). From the instantaneous phase, the instantaneous frequency is simply the inverse of the first order finite difference of phase. Synchrony across cells is estimated with the Kuramoto order parameter ($K$):

FORMULA 4: $K(t) = \left|\frac{1}{N}\sum e^{i(\Psi(t) - \phi_n(t))}\right|$

Where $\phi_n$ is the phase of each neuron, N is the number of neurons and $\Psi$ is the phase average of all oscillators.

### Post-Spike phase responses

To estimate a phase response curve of the stimulated neurons, first a "sensory stimulus" is delivered at a phase known to produce an action potential (and resetting). The location of the first peak after stimulation is recorded. Subsequently, eight more simulations receive another stimulus, with same parameters as the resetting stimulus, but at different phases (at incremental intervals of $2\pi/8$). The effect of that stimulation (delay or advance) on the next peak is recorded as a phase delta. Results are plotted in Fig. 7 (A-E).



## ACKNOWLEDGEMENTS

The authors wish to thank Ilja IJpelaar and Mandy Rutteman for technical support, Sungho Hong, Marcel De Jeu, Jornt De Gruijl, Tycho Hoogland, Marcel van der Heijden, Michiel Ten Brinke, Marylka Uusisaari, Yosef Yarom, Ben Torben-Nielsen and Rodolfo Llinás for memorable discussions.

## REFERENCES


1. Roth MJ, Synofzik M, Lindner A. The cerebellum optimizes perceptual predictions about external sensory events. Curr Biol. 2013;23(10):930-5.
2. Grube M, Cooper FE, Chinnery PF, Griffiths TD. Dissociation of duration-based and beat-based auditory timing in cerebellar degeneration. Proc Natl Acad Sci U S A. 2010;107(25):11597-601.
3. Ashe J, Bushara K. The olivo-cerebellar system as a neural clock. Advances in Experimental Medicine and Biology. 2014;829:155-65.
4. Braitenberg V. Is the cerebellar cortex a biological clock in the millisecond range? Prog Brain Res. 1967;25:334-46.
5. Keele SW, Ivry R. Does the cerebellum provide a common computation for diverse tasks? A timing hypothesis. Ann N Y Acad Sci. 1990;608:179-207.
6. Ivry RB, Spencer RM, Zelaznik HN, Diedrichsen J. The cerebellum and event timing. Ann N Y Acad Sci. 2002;978:302-17.
7. Herzfeld DJ, Kojima Y, Soetedjo R, Shadmehr R. Encoding of error and learning to correct that error by the Purkinje cells of the cerebellum. Nat Neurosci. 2018;21(5):736-43.
8. Ten Brinke MM, Boele HJ, Spanke JK, Potters JW, Kornysheva K, Wulff P, et al. Evolving models of Pavlovian conditioning: cerebellar cortical dynamics in awake behaving mice. Cell Rep. 2015;13(9):1977-88.
9. Ohmae S, Medina JF. Climbing fibers encode a temporal-difference prediction error during cerebellar learning in mice. Nat Neurosci. 2015;18(12):1798-803.
10. Van Der Giessen RS, Koekkoek SK, van Dorp S, De Gruijl JR, Cupido A, Khosrovani S, et al. Role of olivary electrical coupling in cerebellar motor learning. Neuron. 2008;58(4):599-612.
11. Llinás R, Walton K, Hillman DE, Sotelo C. Inferior olive: its role in motor learing. Science. 1975;190(4220):1230-1.
12. Choi S, Yu E, Kim D, Urbano FJ, Makarenko V, Shin HS, et al. Subthreshold membrane potential oscillations in inferior olive neurons are dynamically regulated by P/Q- and T-type calcium channels: a study in mutant mice. J Physiol. 2010;588(Pt 16):3031-43.
13. Horn KM, Deep A, Gibson AR. Progressive limb ataxia following inferior olive lesions. J Physiol. 2013;591(22):5475-89.
14. Koeppen AH. The pathogenesis of spinocerebellar ataxia. Cerebellum. 2005;4(1):62-73.
15. De Gruijl JR, Bosman LWJ, De Zeeuw CI, De Jeu MTG. Inferior olive: All ins and outs. In: Manto M, Schmahmann JD, Rossi F, Gruol DL, Koibuchi N, editors. Handbook of the Cerebellum and Cerebellar Disorders. 3. Dordrecht: Springer Netherlands; 2013. p. 1013-58.
16. De Gruijl JR, Hoogland TM, De Zeeuw CI. Behavioral correlates of complex spike synchrony in cerebellar microzones. J Neurosci. 2014;34(27):8937-44.
17. Blenkinsop TA, Lang EJ. Block of inferior olive gap junctional coupling decreases Purkinje cell complex spike synchrony and rhythmicity. J Neurosci. 2006;26(6):1739-48.
18. Friedman-Hill S, Maldonado PE, Gray CM. Dynamics of striate cortical activity in the alert macaque: I. Incidence and stimulus-dependence of gamma-band neuronal oscillations. Cereb Cortex. 2000;10(11):1105-16.

19. Keating JG, Thach WT. Nonclock behavior of inferior olive neurons: interspike interval of Purkinje cell complex spike discharge in the awake behaving monkey is random. J Neurophysiol. 1995;73(4):1329-40.

20. De Zeeuw CI, Hoebeek FE, Bosman LWJ, Schonewille M, Witter L, Koekkoek SK. Spatiotemporal firing patterns in the cerebellum. Nat Rev Neurosci. 2011;12(6):327-44.

21. Wang JJ, Kim JH, Ebner TJ. Climbing fiber afferent modulation during a visually guided, multi-joint arm movement in the monkey. Brain Res. 1987;410(2):323-9.

22. Kitazawa S, Kimura T, Yin PB. Cerebellar complex spikes encode both destinations and errors in arm movements. Nature. 1998;392(6675):494-7.

23. Yang Y, Lisberger SG. Purkinje-cell plasticity and cerebellar motor learning are graded by complex-spike duration. Nature. 2014;510(7506):529-32.

24. Ito M. Long-term depression. Annu Rev Neurosci. 2003;12:85-102.

25. Welsh JP, Lang EJ, Suglhara I, Llinas R. Dynamic organization of motor control within the olivocerebellar system. Nature. 1995;374(6521):453-7.

26. Ten Brinke MM, Heiney S, Wang X, Proietti-Onori M, Boele HJ, Bakermans J, et al. Dynamic modulation of activity in cerebellar nuclei neurons during pavlovian eyeblink conditioning in mice. Elife. 2017;6.

27. Watson TC, Jones MW, Apps R. Electrophysiological mapping of novel prefrontal - cerebellar pathways. Front Integr Neurosci. 2009;3:18.

28. Bosman LWJ, Koekkoek SKE, Shapiro J, Rijken BFM, Zandstra F, van der Ende B, et al. Encoding of whisker input by cerebellar Purkinje cells. J Physiol. 2010;588(19):3757-83.

29. Gautier H, Remmers JE, Bartlett Jr D. Control of the duration of expiration. Respiration physiology. 1973;18(2):205-21.

30. Heffley W, Song EY, Xu Z, Taylor BN, Hughes MA, McKinney A, et al. Coordinated cerebellar climbing fiber activity signals learned sensorimotor predictions. Nat Neurosci. 2018;21(10):1431-41.

31. Sotelo C, Llinás R, Baker R. Structural study of inferior olivary nucleus of the cat: morphological correlates of electrotonic coupling. J Neurophysiol. 1974;37(3):541-59.

32. Ruigrok TJH, de Zeeuw CI, van der Burg J, Voogd J. Intracellular labeling of neurons in the medial accessory olive of the cat: I. Physiology and light microscopy. J Comp Neurol. 1990;300(4):462-77.

33. De Zeeuw CI, Hertzberg EL, Mugnaini E. The dendritic lamellar body: a new neuronal organelle putatively associated with dendrodendritic gap junctions. J Neurosci. 1995;15(2):1587-604.

34. Llinás R, Yarom Y. Electrophysiology of mammalian inferior olivary neurones *in vitro*. Different types of voltage-dependent ionic conductances. J Physiol. 1981;315:549-67.

35. Yarom Y, Llinás R. Long-term modifiability of anomalous and delayed rectification in guinea pig inferior olivary neurons. J Neurosci. 1987;7(4):1166-77.

36. Gutnick MJ, Yarom Y. Low threshold calcium spikes, intrinsic neuronal oscillation and rhythm generation in the CNS. J Neurosci Methods. 1989;28(1-2):93-9.

37. Yarom Y. Rhythmogenesis in a hybrid system--interconnecting an olivary neuron to an analog network of coupled oscillators. Neuroscience. 1991;44(2):263-75.

38. Kirkman E. Respiration: control of ventilation. Anaesth Intensive Care Med. 2018;18(12):630-3.

39. Lampl I, Yarom Y. Subthreshold oscillations and resonant behavior: two manifestations of the same mechanism. Neuroscience. 1997;78(2):325-41.

40. Manor Y, Rinzel J, Segev I, Yarom Y. Low-amplitude oscillations in the inferior olive: a model based on electrical coupling of neurons with heterogeneous channel densities. J Neurophysiol. 1997;77(5):2736-52.

41. Llinás R, Yarom Y. Oscillatory properties of guinea-pig inferior olivary neurones and their pharmacological modulation: an in vitro study. J Physiol. 1986;376:163-82.

42. Bazzigaluppi P, De Gruijl JR, van der Giessen RS, Khosrovani S, De Zeeuw CI, de Jeu MTG. Olivary subthreshold oscillations and burst activity revisited. Front Neural Circuits. 2012;6:91.

43. Khosrovani S, Van Der Giessen RS, De Zeeuw CI, De Jeu MTG. *In vivo* mouse inferior olive neurons exhibit heterogeneous subthreshold oscillations and spiking patterns. Proc Natl Acad Sci U S A. 2007;104(40):15911-6.

44. Leznik E, Llinás R. Role of gap junctions in synchronized neuronal oscillations in the inferior olive. J Neurophysiol. 2005;94(4):2447-56.

45. Mathy A, Clark BA, Häusser M. Synaptically induced long-term modulation of electrical coupling in the inferior olive. Neuron. 2014;81(6):1290-6.

46. De Gruijl JR, Bazzigaluppi P, de Jeu MTG, De Zeeuw CI. Climbing fiber burst size and olivary subthreshold oscillations in a network setting. PLoS Comput Biol. 2012;8(12):e1002814.

47. Wylie DR, De Zeeuw CI, Simpson JI. Temporal relations of the complex spike activity of Purkinje cell pairs in the vestibulocerebellum of rabbits. J Neurosci. 1995;15(4):2875-87.

48. Bell CC, Kawasaki T. Relations among climbing fiber responses of nearby Purkinje Cells. J Neurophysiol. 1972;35(2):155-69.

49. Lang EJ, Sugihara I, Welsh JP, Llinás R. Patterns of spontaneous purkinje cell complex spike activity in the awake rat. J Neurosci. 1999;19(7):2728-39.

50. Hakimian S, Norris SA, Greger B, Keating JG, Anderson CH, Thach WT. Time and frequency characteristics of Purkinje cell complex spikes in the awake monkey performing a non-periodic task. J Neurophysiol. 2008.

51. De Zeeuw CI, Holstege JC, Calkoen F, Ruigrok TJH, Voogd J. A new combination of WGA-HRP anterograde tracing and GABA immunocytochemistry applied to afferents of the cat inferior olive at the ultrastructural level. Brain Res. 1988;447(2):369-75.

52. De Zeeuw CI, Holstege JC, Ruigrok TJ, Voogd J. Ultrastructural study of the GABAergic, cerebellar, and mesodiencephalic innervation of the cat medial accessory olive: anterograde tracing combined with immunocytochemistry. J Comp Neurol. 1989;284(1):12-35.

53. Vrieler N, Loyola S, Yarden-Rabinowitz Y, Hoogendorp J, Medvedev N, Hoogland TM, et al. Variability and directionality of inferior olive neuron dendrites revealed by detailed 3D characterization of an extensive morphological library. Brain Struct Funct. In press.

54. Kubo R, Aiba A, Hashimoto K. The anatomical pathway from the mesodiencephalic junction to the inferior olive relays perioral sensory signals to the cerebellum in the mouse. J Physiol. 2018.

55. De Zeeuw CI, Simpson JI, Hoogenraad CC, Galjart N, Koekkoek SKE, Ruigrok TJH. Microcircuitry and function of the inferior olive. Trends Neurosci. 1998;21(9):391-400.

56. Nelson BJ, Mugnaini E. The rat inferior olive as seen with immunostaining for glutamate decarboxylase. Anat Embryol (Berl). 1988;179(2):109-27.

57. Walberg F, Ottersen OP. Demonstration of GABA immunoreactive cells in the inferior olive of baboons (*Papio papio* and *Papio anubis*). Neurosci Lett. 1989;101(2):149-55.

58. Bloedel JR, Ebner TJ. Rhythmic discharge of climbing fibre afferents in response to natural peripheral stimuli in the cat. J Physiol. 1984;352:129-46.

59. Bellavance MA, Takatoh J, Lu J, Demers M, Kleinfeld D, Wang F, et al. Parallel inhibitory and excitatory trigemino-facial feedback circuitry for reflexive vibrissa movement. Neuron. 2017;95(3):673-82.

60. Apps R, Hawkes R, Aoki S, Bengtsson F, Brown AM, Chen G, et al. Cerebellar modules and their role as operational cerebellar processing units. Cerebellum. 2018;17(5):654-82.

61. Romano V, De Propris L, Bosman LWJ, Warnaar P, ten Brinke MM, Lindeman S, et al. Potentiation of cerebellar Purkinje cells facilitates whisker reflex adaptation through increased simple spike activity. eLife. 2018;7:e38852.

62. Schweighofer N, Doya K, Kawato M. Electrophysiological properties of inferior olive neurons: A compartmental model. J Neurophysiol. 1999;82(2):804-17.

63. Yu Y, Fu Y, Watson C. The inferior olive of the C57BL/6J mouse: a chemoarchitectonic study. Anat Rec (Hoboken). 2014;297(2):289-300.

64. Lefler Y, Yarom Y, Uusisaari MY. Cerebellar inhibitory input to the inferior olive decreases electrical coupling and blocks subthreshold oscillations. Neuron. 2014;81(6):1389-400.

65. Turecek J, Yuen GS, Han VZ, Zeng XH, Beyer KU, Welsh JP. NMDA receptor activation strengthens weak electrical coupling in mammalian brain. Neuron. 2014;81(6):1375-88.

66. Zhou H, Lin Z, Voges K, Ju C, Gao Z, Bosman LWJ, et al. Cerebellar modules operate at different frequencies. eLife. 2014;3:e02536.

67. Lefler Y, Torben-Nielsen B, Yarom Y. Oscillatory activity, phase differences, and phase resetting in the inferior olivary nucleus. Front Syst Neurosci. 2013;7:22.

68. Manor Y, Yarom Y, Chorev E, Devor A. To beat or not to beat: a decision taken at the network level. J Physiol Paris. 2000;94(5-6):375-90.

69. De Zeeuw CI, Chorev E, Devor A, Manor Y, Van Der Giessen RS, De Jeu MT, et al. Deformation of network connectivity in the inferior olive of connexin 36-deficient mice is compensated by morphological and electrophysiological changes at the single neuron level. J Neurosci. 2003;23(11):4700-11.

70. Rogers WL, Bregman AS. An experimental evaluation of three theories of auditory stream segregation. Percept Psychophys. 1993;53(2):179-89.

71. Tal I, Large EW, Rabinovitch E, Wei Y, Schroeder CE, Poeppel D, et al. Neural entrainment to the beat: the “missing-pulse” phenomenon. J Neurosci. 2017;37(26):6331-41.

72. Ju C, Bosman LWJ, Hoogland TM, Velauthapillai A, Murugesan P, Warnaar P, et al. Neurons of the inferior olive respond to broad classes of sensory input while subject to homeostatic control. J Physiol. 2019.

73. Llinás R, Baker R, Sotelo C. Electrotonic coupling between neurons in cat inferior olive. J Neurophysiol. 1974;37(3):560-71.

74. Placantonakis DG, Bukovsky AA, Zeng XH, Kiem HP, Welsh JP. Fundamental role of inferior olive connexin 36 in muscle coherence during tremor. Proc Natl Acad Sci U S A. 2004;101(18):7164-9.

75. Latorre R, Aguirre C, Rabinovich MI, Varona P. Transient dynamics and rhythm coordination of inferior olive spatio-temporal patterns. Front Neural Circuits. 2013;7:138.

76. Coesmans M, Weber JT, De Zeeuw CI, Hansel C. Bidirectional parallel fiber plasticity in the cerebellum under climbing fiber control. Neuron. 2004;44(4):691-700.

77. Badura A, Schonewille M, Voges K, Galliano E, Renier N, Gao Z, et al. Climbing fiber input shapes reciprocity of Purkinje cell firing. Neuron. 2013;78(4):700-13.

78. Simpson JI, Wylie DR, De Zeeuw CI. On climbing fiber signals and their consequence(s). Behav Brain Sci. 1996;19(2):384-98.

79. Mathy A, Ho SSN, Davie JT, Duguid IC, Clark BA, Häusser M. Encoding of oscillations by axonal bursts in inferior olive neurons. Neuron. 2009;62(3):388-99.

80. Ebner TJ, Bloedel JR. Climbing fiber action on the responsiveness of Purkinje cells to parallel fiber inputs. Brain Res. 1984;309(1):182-6.

81. Llinás R, Volkind RA. The olivo-cerebellar system: functional properties as revealed by harmaline-induced tremor. Exp Brain Res. 1973;18(1):69-87.

82. Llinás RR. Inferior olive oscillation as the temporal basis for motricity and oscillatory reset as the basis for motor error correction. Neuroscience. 2009;162(3):797-804.

83. Alvarez-Icaza R, Boahen K. Inferior olive mirrors joint dynamics to implement an inverse controller. Biol Cybern. 2012;106(8-9):429-39.

84. Armstrong DM, Edgley SA, Lidierth M. Complex spikes in Purkinje cells of the paravermal part of the anterior lobe of the cat cerebellum during locomotion. J Physiol. 1988;400:405-14.

85. Zhang Y, Zhang Z, Xiao S, Tien J, Le S, Le T, et al. Inferior olivary TMEM16B mediates cerebellar motor learning. Neuron. 2017;95(5):1103-11 e4.

86. Chen X, Kovalchuk Y, Adelsberger H, Henning HA, Sausbier M, Wietzorrek G, et al. Disruption of the olivo-cerebellar circuit by Purkinje neuron-specific ablation of BK channels. Proc Natl Acad Sci U S A. 2010;107(27):12323-8.

87. Chaumont J, Guyon N, Valera AM, Dugué GP, Popa D, Marcaggi P, et al. Clusters of cerebellar Purkinje cells control their afferent climbing fiber discharge. Proc Natl Acad Sci U S A. 2013;110(40):16223-8.

88. Witter L, Canto CB, Hoogland TM, de Gruijl JR, De Zeeuw CI. Strength and timing of motor responses mediated by rebound firing in the cerebellar nuclei after Purkinje cell activation. Front Neural Circuits. 2013;7:133.

89. Tang T, Blenkinsop TA, Lang EJ. Complex spike synchrony dependent modulation of rat deep cerebellar nuclear activity. Elife. 2019;8.

90. Bal T, McCormick DA. Synchronized oscillations in the inferior olive are controlled by the hyperpolarization-activated cation current I(h). J Neurophysiol. 1997;77(6):3145-56.

91. Best AR, Regehr WG. Inhibitory regulation of electrically coupled neurons in the inferior olive is mediated by asynchronous release of GABA. Neuron. 2009;62(4):555-65.

92. Wiklund L, Björklund A, Sjölund B. The indolaminergic innervation of the inferior olive. 1. Convergence with the direct spinal afferents in the areas projecting to the cerebellar anterior lobe. Brain Res. 1977;131(1):1-21.

93. Kazantsev VB, Nekorkin VI, Makarenko VI, Llinás R. Self-referential phase reset based on inferior olive oscillator dynamics. Proc Natl Acad Sci U S A. 2004;101(52):18183-8.

94. Leznik E, Makarenko V, Llinás R. Electrotonically mediated oscillatory patterns in neuronal ensembles: An *in vitro* voltage-dependent dye-imaging study in the inferior olive. J Neurosci. 2002;22(7):2804-15.

95. Uhlenbeck GE, Ornstein LS. On the theory of Brownian motion. Phys Rev. 1930;36(5):823-41.

96. Marshall SP, van der Giessen RS, de Zeeuw CI, Lang EJ. Altered olivocerebellar activity patterns in the connexin36 knockout mouse. Cerebellum. 2007;6(4):287-99.

97. Winfree AT. The geometry of biological time. 1 ed: Springer Science; 1980.

98. Ozden I, Sullivan MR, Lee HM, Wang SSH. Reliable coding emerges from coactivation of climbing fibers in microbands of cerebellar Purkinje neurons. J Neurosci. 2009;29(34):10463-73.

99. Schultz SR, Kitamura K, Post-Uiterweer A, Krupic J, Häusser M. Spatial pattern coding of sensory information by climbing fiber-evoked calcium signals in networks of neighboring cerebellar Purkinje cells. J Neurosci. 2009;29(25):8005-15.

100. White JJ, Sillitoe RV. Genetic silencing of olivocerebellar synapses causes dystonia-like behaviour in mice. Nat Commun. 2017;8:14912.

101. Ros H, Sachdev RNS, Yu Y, Sestan N, McCormick DA. Neocortical networks entrain neuronal circuits in cerebellar cortex. J Neurosci. 2009;29(33):10309-20.

102. de Solages C, Szapiro G, Brunel N, Hakim V, Isope P, Buisseret P, et al. High-frequency organization and synchrony of activity in the purkinje cell layer of the cerebellum. Neuron. 2008;58(5):775-88.

103. Kistler WM, van Hemmen JL, De Zeeuw CI. Time window control: a model for cerebellar function based on synchronization, reverberation, and time slicing. Prog Brain Res. 2000;124:275-97.

104. Kistler WM, van Hemmen JL. Delayed reverberation through time windows as a key to cerebellar function. Biol Cybern. 1999;81(5-6):373-80.

105. Ruigrok TJH, Voogd J. Cerebellar influence on olivary excitability in the cat. Eur J Neurosci. 1995;7(4):679-93.

106. Szentágothai J, Rajkovits K. Über den Ursprung der Kletterfasern des Kleinhirns. Z Anat Entwicklungsgesch. 1959;121(2):130-41.

107. Hoebeek FE, Witter L, Ruigrok TJH, De Zeeuw CI. Differential olivo-cerebellar cortical control of rebound activity in the cerebellar nuclei. Proc Natl Acad Sci U S A. 2010;107(18):8410-5.

108. Dykstra S, Engbers JDT, Bartoletti TM, Turner RW. Determinants of rebound burst responses in rat cerebellar nuclear neurons to physiological stimuli. J Physiol. 2016;594(4):985-1003.

109. Bengtsson F, Ekerot CF, Jörntell H. *In vivo* analysis of inhibitory synaptic inputs and rebounds in deep cerebellar nuclear neurons. PLoS One. 2011;6(4):e18822.

110. Rowland NC, Jaeger D. Responses to tactile stimulation in deep cerebellar nucleus neurons result from recurrent activation in multiple pathways. J Neurophysiol. 2008;99(2):704-17.

111. De Zeeuw CI, Ruigrok TJH, Schalekamp MPA, Boesten AJ, Voogd J. Ultrastructural study of the cat hypertrophic inferior olive following anterograde tracing, immunocytochemistry, and intracellular labeling. Eur J Morphol. 1990;28(2-4):240-55.

112. Kistler WM, De Zeeuw CI. Time windows and reverberating loops: a reverse-engineering approach to cerebellar function. Cerebellum. 2003;2(1):44-54.

113. Guo D, Wang Q, Perc M. Complex synchronous behavior in interneuronal networks with delayed inhibitory and fast electrical synapses. Physical Review E. 2012;85(6 Pt 1):061905.

114. Rau F, Clemens J, Naumov V, Hennig RM, Schreiber S. Firing-rate resonances in the peripheral auditory system of the cricket, Gryllus bimaculatus. J Comp Physiol A Neuroethol Sens Neural Behav Physiol. 2015;201(11):1075-90.

115. Bürck M, van Hemmen JL. Neuronal identification of signal periodicity by balanced inhibition. Biol Cybern. 2009;100(4):261-70.

116. Patel M, Joshi B. Decoding synchronized oscillations within the brain: phase-delayed inhibition provides a robust mechanism for creating a sharp synchrony filter. Journal of Theoretical Biology. 2013;334:13-25.

117. Szücs A, Huerta R, Rabinovich MI, Selverston AI. Robust microcircuit synchronization by inhibitory connections. Neuron. 2009;61(3):439-53.

118. Güldenagel M, Ammermüller J, Feigenspan A, Teubner B, Degen J, Söhl G, et al. Visual transmission deficits in mice with targeted disruption of the gap junction gene connexin36. J Neurosci. 2001;21(16):6036-44.

119. Rahmati N, Owens CB, Bosman LWJ, Spanke JK, Lindeman S, Gong W, et al. Cerebellar potentiation and learning a whisker-based object localization task with a time response window. J Neurosci. 2014;34(5):1949-62.

120. Perkon I, Kosir A, Itskov PM, Tasic J, Diamond ME. Unsupervised quantification of whisking and head movement in freely moving rodents. J Neurophysiol. 2011;105(4):1950-62.

121. Moreno AP, Rook MB, Fishman GI, Spray DC. Gap junction channels: distinct voltage-sensitive and -insensitive conductance states. Biophys J. 1994;67(1):113-9.

122. O'Donnell C, Nolan MF, van Rossum MCW. Dendritic spine dynamics regulate the long-term stability of synaptic plasticity. J Neurosci. 2011;31(45):16142-56.

123. Scheibel ME, Scheibel AB. The inferior olive; a Golgi study. J Comp Neurol. 1955;102(1):77-131.

124. Devor A, Yarom Y. Electrotonic coupling in the inferior olivary nucleus revealed by simultaneous double patch recordings. J Neurophysiol. 2002;87(6):3048-58.

125. Kralemann B, Frühwirth M, Pikovsky A, Rosenblum M, Kenner T, Schaefer J, et al. *In vivo* cardiac phase response curve elucidates human respiratory heart rate variability. Nat Commun. 2013;4:2418.

126. Kralemann B, Cimponeriu L, Rosenblum M, Pikovsky A, Mrowka R. Phase dynamics of coupled oscillators reconstructed from data. Physical Review E. 2008;77(6 Pt 2):066205.

## SUPPLEMENTARY FIGURE CAPTIONS

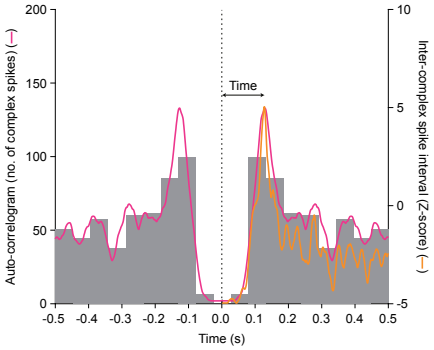


**Figure S1.** Comparison of autocorrelogram with inter-complex spike interval histogram
The autocorrelogram of the same Purkinje cell as shown in Fig. 2A (10 ms bins) convolved with a 5 ms kernel (red curve) compared to the convolved inter-complex spike interval (ICSI) histogram (orange curve). The auto-correlogram includes also intervals between non-consecutive complex spikes. Consequently, on a short time scale, both auto-correlogram and ICSI histogram are identical, but they diverge at longer time scales.

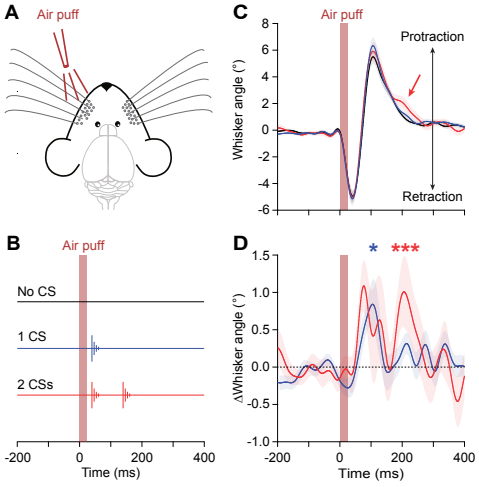


**Figure S2.** Complex spikes correlate with whisker protraction
**(A)** Mice received air puff stimulation of their whisker pad. **(B)** Purkinje cell recordings during sensory stimulation revealed that most trials had either no, one or two complex spikes during the 200 ms after stimulus onset. We separated the trials according to this classification. Note that for the trials with a single complex spike, we considered the trials with a complex spike during the first 100 ms, but not during between 100 and 200 ms. **(C)** Averaged whisker traces (based on $n$ = 35 Purkinje cells) show a reflexive whisker movement triggered by the air puff, consisting of an initial backward movement (largely caused directly by the air flow) followed by an active protraction. Trials in which a complex spike was detected only during the first 100 ms after the stimulus (blue line) had on average a slightly larger protraction than the trials without a complex spike (black line). The trials with two complex spikes also had a stronger protraction than the trials without a complex spike, but showed in addition a more protracted position later on during the trial (red arrow and red line). **(D)** Averaged subtracted traces showing the differences between trials with, respectively, a single complex spike (blue line) and two complex spikes (red line) and the trials without a complex spike. The occurrence of recurrent complex spike firing was thus reflected in the behavior of the mice. Shaded areas indicate the SEM. * $p < 0.05$; *** $p < 0.001$; Wilcoxon match-pairs test after Benjamini-Hochberg correction for multiple comparisons.

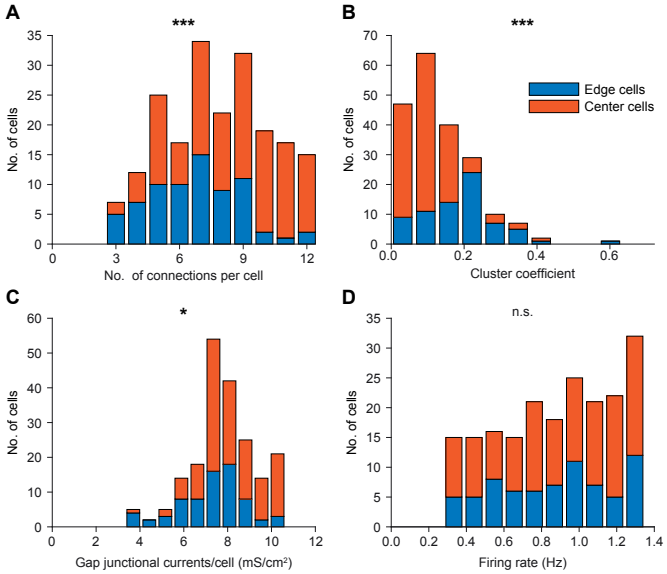


**Figure S3.** Behavior of cells on the edges of the model

The inferior olivary model has, as the inferior olive itself, boundaries. The impact of boundaries in connectivity of cells in the *in vivo* data (and by extension on the current leak through gap junctions) is, however, not known. The algorithm that generates connectivity enforces mean connectivity across cells, which increases the degree of clustering along the edges, but has at most a mild impact on the current leak through gap junctions. It is likely that the extra clustering degree along the edges may lead to a mild increase of coherence in STOs between neighbors, though this should not affect the overall conclusion – that the phase-dependency of the STO under the presence of noise is at most short-lived. The data are represented as stacked bar plots. All data were tested using Kolmogorov-Smirnov tests.

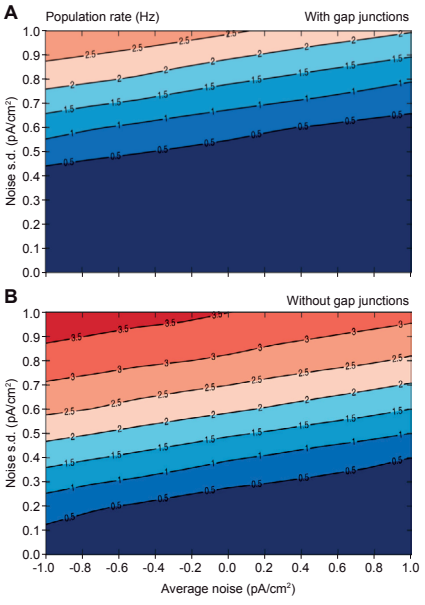


**Figure S4.** Contour plot indicating the average firing rate of networks as a function of the mean and standard deviation of the OU input

**(A)** Baseline input was chosen such that the cells of the model networks would produce approximately 1 Hz of spontaneous firing rate. The absence of gap junctional coupling in "mutant" model networks **(B)** leads to increased firing rate, which was compensated for by increasing the leak current of the membrane by 0.003 mS/cm².

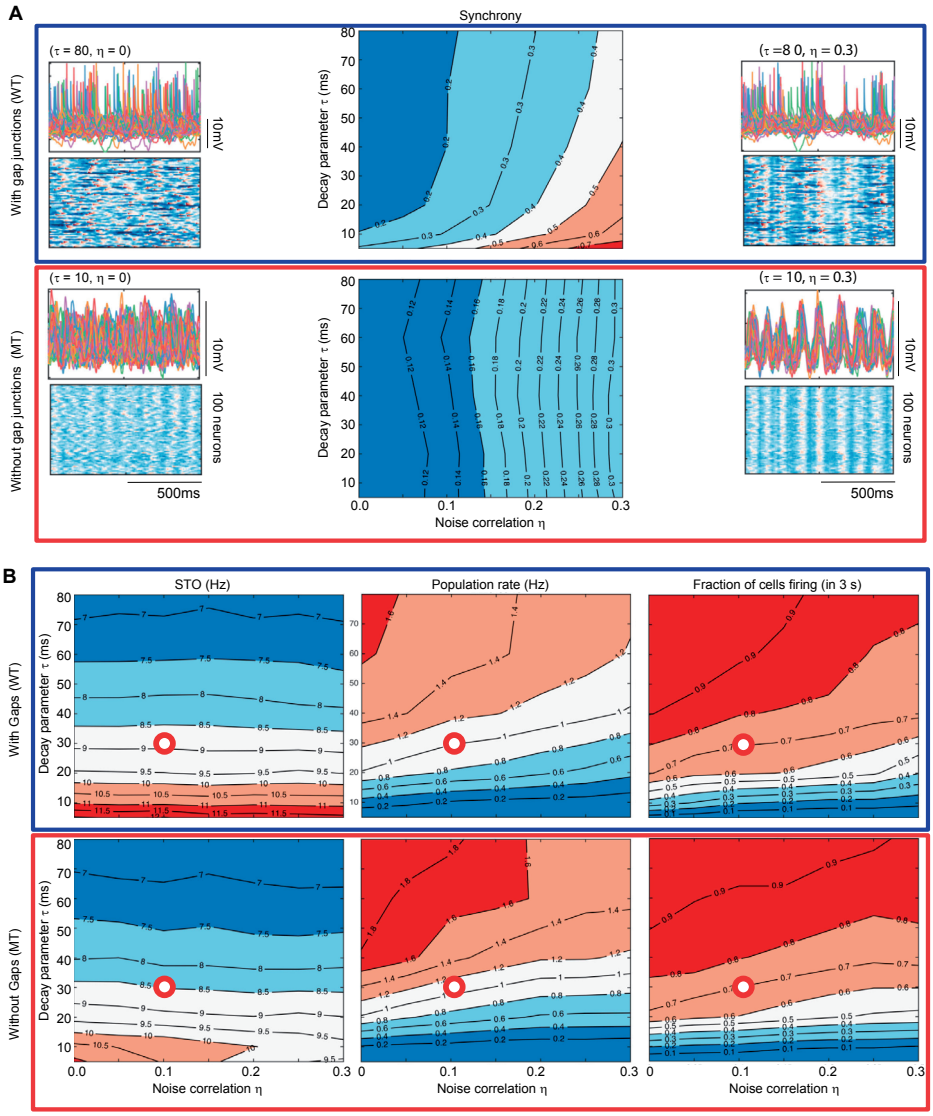


**Figure S5.** Behavior of model networks of identical composition as a function of the decay parameter of the Ornstein-Uhlenbeck process (τ) and the noise correlation (η)

Model networks have been computed using a systematic exploration of the parameter space using 56 instances of the network model. The contour plots indicate isolines for synchrony **(A)**, frequency of subthreshold oscillations (STOs), population firing rate and proportion of active cells **(B)**. The results presented in the main text come from a model network with parameters chosen such as to display STOs with mean of 9 Hz, a population rate of about 1 Hz and with more than 70% of cells firing in three seconds (95% of cells fire within 10 s of simulation time). The position of this network in the contour plots is indicated with a red circle. In **A**, the thumbnails exemplify behaviors of extreme instances of the model network both as membrane potentials traces (top) and as heatmaps of the membrane potential (bottom). Arrows indicate parameter space coordinates of these examples. The decay of the Ornstein-Uhlenbeck process (τ) mostly impacts the firing rate of the model networks, while noise correlation (η) has a direct effect on synchrony. **(B)** Gap junctions amplify the input correlation given to the neurons, while having a minor effect on other aspects of the network dynamics.

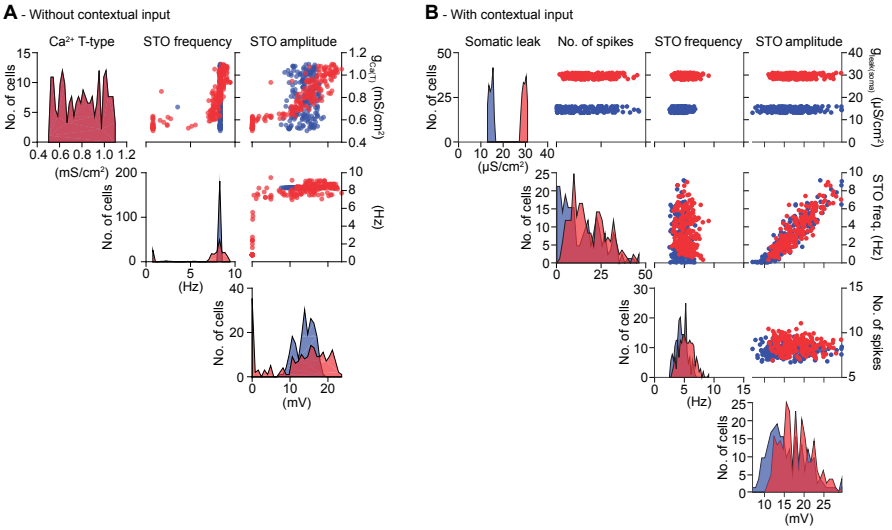


**Figure S6.** Physiological properties of the individual model cells as a function of $Ca^{2+}$ T-type conductance in the absence of contextual input in the presence and absence of gap junctional coupling

**(A)** The $Ca^{2+}$ T-type conductance is varied in the range of 0.5 to 1.1 mS/cm², resulting in a range of oscillatory properties of the individual model cells. The left axis in the panels of the main diagonal display cell counts for the histograms. The right axis besides the rightmost panel displays the indicated continuous variable. The set of non-oscillating (zero amplitude, zero frequency) cells constituted about 25% of the model network in the absence of gap junctions (red), were engaged in the oscillation when gaps were added to these cells (blue). In the absence of contextual input the distribution of frequencies had peaks at zero and sharply synchronizes at approximately in the absence of Ornstein-Uhlenbeck input. **(B)** Comparison between the activity of networks with (WT) and without (MT) gap junctions under contextual input. MT cells have received compensation in the leak conductance of the cell. A slight increase of firing rate for the MT can be observed, and also a narrower distribution of frequencies, in comparison with the noiseless case.

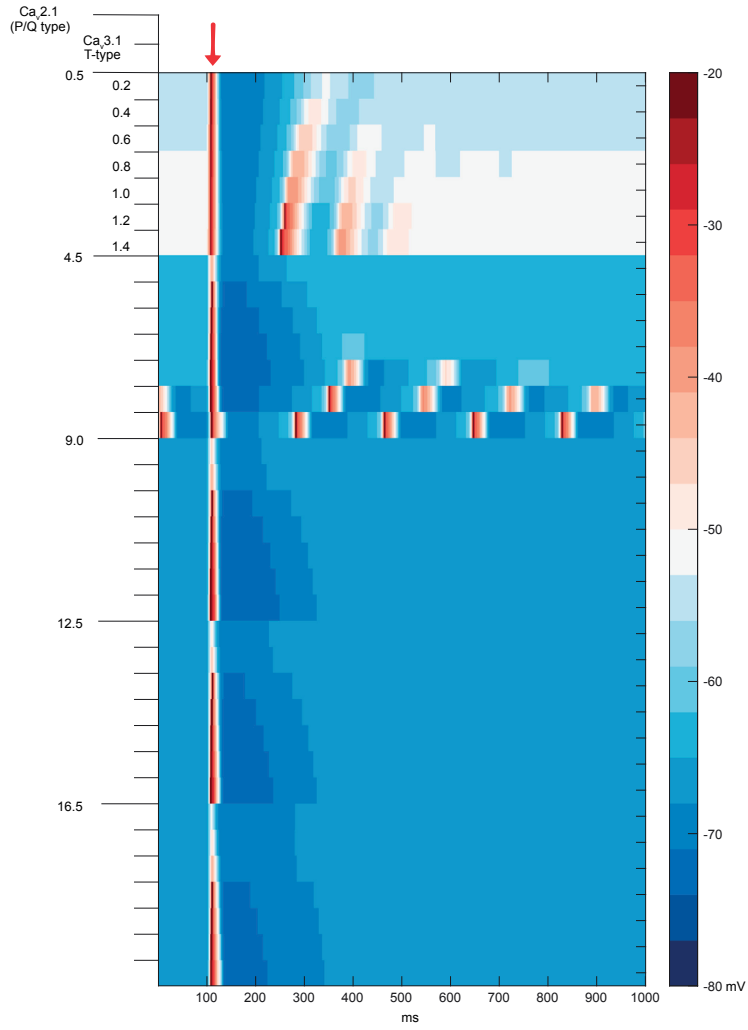


**Figure S7.** Rebound firing occurs only in a small region of parameter space

The post-spiking behavior of model neurons after a depolarization was examined for a grid of parameters, within known experimental values. A depolarizing current pulse triggers spikes at 100 ms. The rebound behavior is dependent on a complex interplay between a number of parameters, but most importantly, it exists in a rather narrow range of the parameter space between T- and P/Q-type $Ca^{2+}$ channels. For very low levels of Ca$_v$3.1 (T-type) expression, the model cell settles on an unphysiologically saturated depolarization after spiking. The cells in our model have Ca$_v$2.1 (P/Q-type) expression around 4.5 and Ca$_v$3.1 between 0.6 and 1.1.

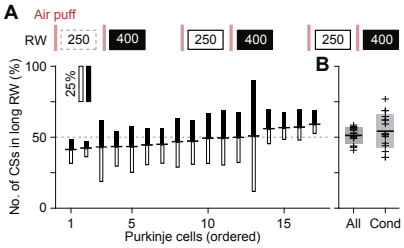


**Figure S8.** No phase-dependent spiking probabilities observed *in vivo*
**(A)** In order to test the impact of the presumed phase of the inferior olivary neurons in vivo, we applied a "gallop" stimulation pattern, alternating short (250 ms) and long (400 ms) intervals. Air puffs (vertical bars) were delivered to the whisker pad. Complex spikes were counted in response windows (RW) 20-200 ms post-stimulus and cells were sorted as a function of the ratio between the numbers of complex spikes in short and long intervals (indicated as horizontal dash between filled and empty bars). In this analysis, we included all RWs, irrespective of whether the preceding RW contained a complex spike or not (cf. Fig. 10). For each Purkinje cell the relative response probabilities for the long and short intervals are illustrated as the length of the filled and open bars, respectively. None of the Purkinje cells showed a significant difference in the response probability between the two intervals (all $p > 0.05$ on Fisher's exact test). **(B)** Comparison of the response biases between all trials ("All", **A**) and only those trials that followed an RW with at least one complex spike ("Cond", Fig. 10A). Shown are the 25 and 75 % quantiles and median per population.

# 5

# Functional convergence of autonomic and sensorimotor processing in the lateral cerebellum

Vincenzo Romano[1,3], Aoibhinn L. Reddington[1,3], Silvia Cazzanelli[1], Roberta Mazza[1], Yang Ma[1], Christos Strydis[1], Mario Negrello[1*], Laurens W.J. Bosman[1,4*] and Chris I. De Zeeuw[1,2]

[1] Department of Neuroscience, Erasmus MC, 3015 GE Rotterdam, The Netherlands
[2] Netherlands Institute for Neuroscience, Royal Academy of Arts and Sciences, 1105 BA Amsterdam, The Netherlands
[3] These authors contributed equally
[4] Lead contact
[*] Correspondence to: Mario Negrello (m.negrello@erasmusmc.nl) or Laurens Bosman (l.bosman@erasmusmc.nl)

The cerebellum is involved in control of voluntary and autonomic rhythmic behaviors, yet it is unclear to what extent it coordinates these in concerted action. Here, we studied Purkinje cell activity during unperturbed and perturbed respiration in cerebellar lobules simplex, crus 1 and 2. During unperturbed (eupneic) respiration complex spike and simple spike activity encoded respiratory activity, the timing of which corresponded with ongoing sensorimotor feedback. Instead, upon whisker stimulation mice concomitantly accelerated their simple spike activity, whisking behavior as well as inspiration in a phase-dependent manner. Moreover, the accelerating impact of whisker stimulation on respiration could be mimicked by optogenetic stimulation of Purkinje cells and prevented by cell-specific genetic modification of their AMPA receptors that hampered increases in simple spike firing. Thus, the impact of Purkinje cell activity on respiratory control is context- and phase-dependent, highlighting a coordinating role for the cerebellar hemispheres in aligning autonomic and sensorimotor behaviors.

**Key words:**
Cerebellum, respiration, whiskers, Purkinje cell, optogenetic stimulation, synchronous behavior, autonomic behaviors, orofacial behaviors, phase coupling, sensory perturbation, mouse

## INTRODUCTION

Rhythmic behaviors are part of everyday life of mammals. They can emerge from predominantly conscious activity such as locomotion, licking or whisking, but also from more subconscious behaviors like heart beat or respiration. Speed, amplitude and phase of rhythmic movements depend on the behavioral demands and context, and thereby they depend on each other (Cao et al., 2012; Kurnikova et al., 2017; Moore et al., 2013; Welker, 1964). Accordingly, many of the motor domains involved in rhythmic movements serve multiple functions and many of these functions can be coordinated in a concerted action. For example, inspiration is driven by the diaphragm and intercostal muscles, which are also involved in postural control (Hodges and Gandevia, 2000; Rimmer et al., 1995), and respiration and posture are synergistically controlled during processes like vocalization, swimming or parturition (Holstege, 2014; Jakovljevic and McConnell, 2009; Tomori and Widdicombe, 1969).



When different forms of sensorimotor behaviors have to be coordinated, the olivocerebellar system is often involved in optimal fine-tuning in time and space (Kitazawa et al., 1998; Owens et al., 2018; Vinueza Veloz et al., 2015). This presumably not only holds for non-rhythmic behaviors, but also for rhythmic behaviors like respiration (Cao et al., 2012; Critchley et al., 2015; Gozal et al., 1995; Isaev et al., 2002; McKay et al., 2003; Park et al., 2016; Parsons et al., 2001; Raux et al., 2013). Accordingly, rare, but dramatic, cases of sudden infant death syndrome (SIDS) have been attributed to acute respiratory arrest in relation to inferior olivary hypoplasia or delayed maturation of the cerebellar cortex (Cortez and Kinney, 1996; Cruz-Sánchez et al., 1997; Harper, 2000; Katsetos et al., 2014; Lavezzi et al., 2013), while cerebellar dysfunction has been observed in congenital central hypoventilation syndrome, which entails the inability to react to dyspnea (Harper et al., 2015; Harper et al., 2005; Kumar et al., 2008). Likewise, patients with a cerebellar tumor or hemorrhage frequently need mechanical ventilation, often showing a relatively slow recovery of respiration after neurosurgery (Arnone et al., 2017; Chen et al., 2005; Gewaltig and Diesmann, 2007; Lee et al., 2013; Tsitsopoulos et al., 2012). Moreover, most cerebellar ataxia patients have trouble to modulate their breathing during exercise (De Joanna et al., 2008; Deger et al., 1999; Ebert et al., 1995). Thus, there is ample evidence for a role of the olivocerebellar system in controlling respiration and adjusting it according to behavioral demands, pointing towards a role in synergistic integration of autonomic and voluntary behaviors.

At present, it is unclear to what extent different rhythmic behaviors can be controlled by the same cerebellar region and cells, and if so, how they might contribute to synergistic control of the different motor domains involved. Here, we studied the activity of Purkinje cells in the lateral cerebellum in relation to respiratory control, while interfering with their whisker system. We focused on lobule simplex in conjunction with lobules crus 1 and crus 2, because they are strongly related to rhythmic whisker movements and because their cells have been shown to respond to a variety of somatosensory inputs from the face, possibly integrating different sensorimotor behaviors (Bosman et al., 2010; Brown and Raman, 2018; Chen et al.,

2016; Ju et al., 2019; Romano et al., 2018; Shambes et al., 1978). We found that Purkinje cells in these lobules co-modulate their firing rate with multiple phases of the respiratory cycle during unperturbed breathing. When we briefly stimulated the whiskers, the mice advanced the phase of their simple spike activity and breathing behavior concomitantly. The Purkinje cells that responded to whisker stimulation and also contributed to acceleration of respiration were particularly prominent in medial crus 1. Moreover, the respiratory adjustment following whisker stimulation could be induced by transiently stimulating these Purkinje cells in the lateral cerebellum optogenetically, whereas it was significantly impaired following Purkinje cell-specific impairment of postsynaptic AMPA receptors. Together, our data implicate that the cerebellar hemispheres can control respiratory behavior and align its rhythm with that of other behaviors in a phase-dependent manner, highlighting their putative role in synergistic integration of different sensorimotor activities.

## RESULTS

### Unperturbed respiratory behavior

To find out to what extent Purkinje cells in the cerebellar hemispheres encode the three phases of unperturbed (eupneic) respiration, defined as a cycle of inspiration, post-inspiration and expiration (Anderson and Ramirez, 2017; Richter and Smith, 2014), we studied their activity patterns in awake head-restrained mice. During inspiration, contractions of the diaphragm and external intercostal muscles generate a volume expansion of the lungs, while during post-inspiration the inspiration muscles relax and laryngeal constriction muscles retard lung compression (Dutschmann and Paton, 2002). During active expiration, abdominal and internal intercostal muscles contract depending upon metabolic demand (Aliverti et al., 1997; Bianchi and Gestreau, 2009). The respiration phases of awake head-restrained mice were measured with a pressure sensor placed under the abdomen and analyzed upon phase transformation. Under these conditions, the mice had a median breathing frequency of 2.4 Hz (inter-quartile range (IQR): 1.0 Hz, $n$ = 13 mice), with a median CV of 0.51 (IQR: 0.35), indicating the fast nature as well as substantial level of variability of their breathing rhythm at rest (Fig. S1A-C).

### Purkinje cell complex spike activity peaks after inspiration

In the first set of experiments we recorded the activity of 43 Purkinje cells during unperturbed respiration. These cells had a median complex spike firing frequency of 1.37 Hz (IQR: 0.54 Hz) (Fig. S1D). The extent of complex spike firing rate modulation along the respiratory cycle was quantified per Purkinje cell by comparing the measured distributions of complex spikes with randomly shuffled ones. The random shuffling was performed 500 times, upon which the 99% confidence interval ($Z$ = 3) was calculated. Firing patterns exceeding this 99% confidence interval were considered indicative of a statistically significant modulation (Fig. 1A). Of the 43

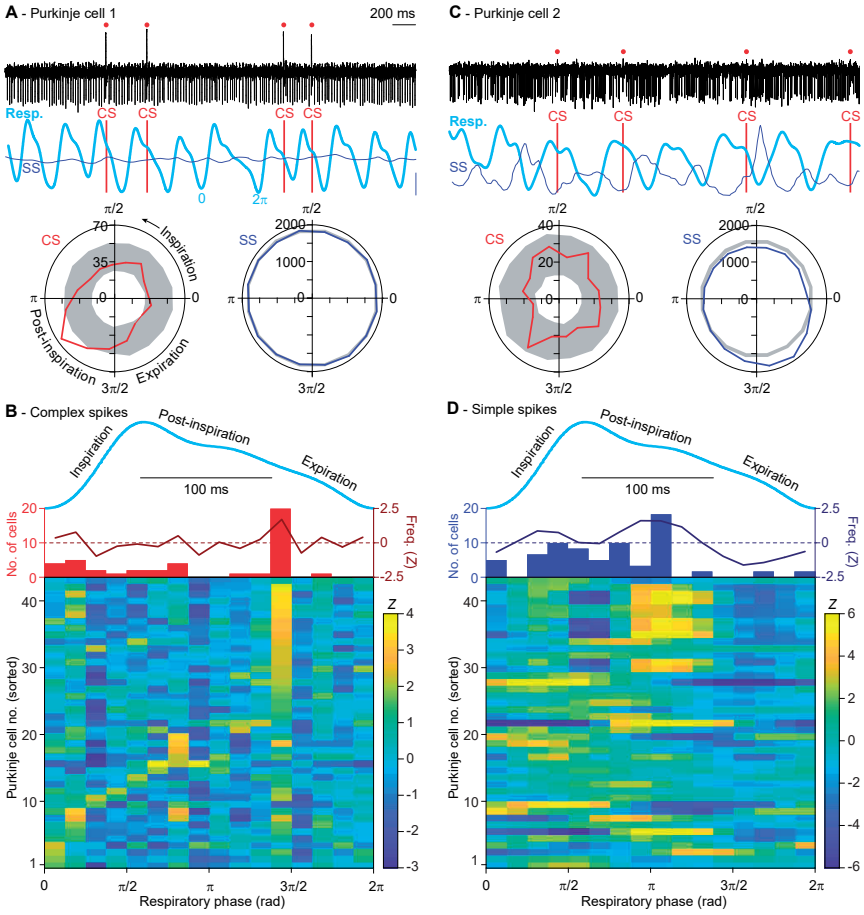


**Figure 1.** Purkinje cells in the lateral cerebellum encode eupneic breathing

**A** An example recording of a Purkinje cell showing complex spike (CS), but no simple spike (SS), modulation during unperturbed (eupneic) respiration in an awake mouse. The complex spikes are indicated by red dots and vertical lines. The instantaneous simple spike rate (thin blue line) is indicated in combination with the respiratory signal (thick cyan line). The blue scale bar on the right indicates 25 Hz of simple spike modulation. The raw signal indicates that the complex spikes preferably occurred around the transition from post-inspiration to expiration as confirmed by a polar plot summarizing the whole recording. The radial axes represent the number of spikes per bin. The gray areas indicate the 99% confidence interval after bootstrap. **B** Of the 43 Purkinje cells recorded during eupneic respiration, 19 displayed their maximal complex spike firing around 3π/2. This is illustrated as the average modulation in firing rate (red line, middle), the distribution of the phases of strongest modulations (histogram; middle) and a heat map illustrating the complex spike firing patterns of 43 Purkinje cells (bottom). This analysis was performed without pre-selection of Purkinje cells. For comparison, a randomly chosen respiratory cycle is indicated (cyan). Note that the respiratory trace is plotted based on time, while the heat map and histogram are based on the phase. **C** An example of another Purkinje cell, showing relatively weak complex spike modulation, but strong simple spike modulation during eupneic respiration. **D** The same analysis as in **B**, but for the simple spikes, revealing a preference for simple spike firing during post-inspiration (just before the complex spike peak) and a relatively low firing rate during expiration (following the complex spike peak). Note that the Purkinje cells of both heat maps are sorted by the phase of the maximal increase in complex spike firing. Consequently, the cell numbers of **B** and **D** refer to the same Purkinje cells. See also Fig. S1.

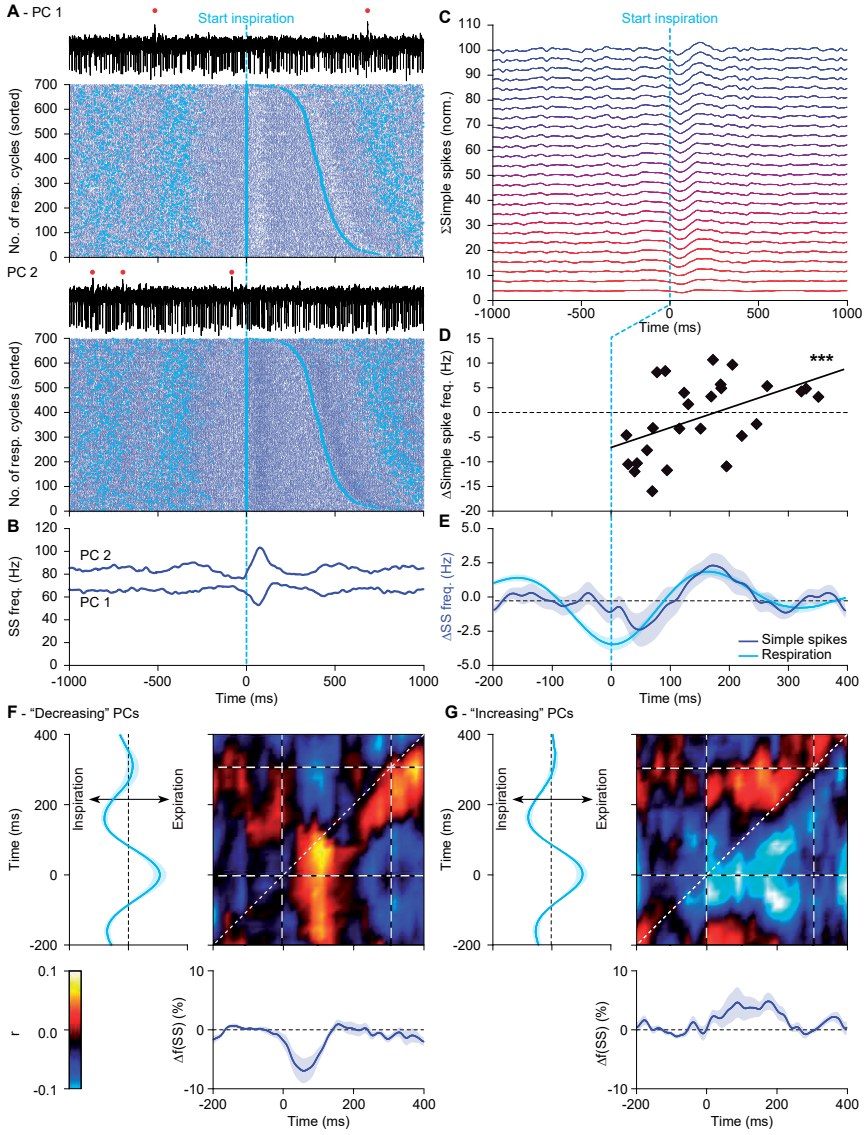


**Figure 2.** Eupneic respiration is associated with both increased and decreased simple spike firing

**A** During the respiratory cycle, simple spike (SS) modulation can either be predominantly decreasing or increasing as illustrated by two representative Purkinje cells (PCs) recorded simultaneously in the same animal. The raster plots are aligned on inspiration start and sorted according to the interval to the next inspiration. Large cyan dots indicate inspiration start and small blue dots the SSs. The redv dots on top of the traces indicate complex spikes. **B** Convolved peri-stimulus time histograms of the two PCs shown in **A**. **C** Stacked line plot of the instantaneous SS firing rates of all 26 PCs displaying a statistically significant SS modulation firing during unperturbed breathing. SS firing is displayed in percentage of baseline firing and normalized so that the upper line reflects the population average. The PCs are ordered from the strongest decrease (bottom, red line) to the strongest increase (top, blue line) in SS modulation. Each trace is aligned to inspiration. **D** Scatter plot of moments of maximal modulation per PC, showing a correlation between the time of maximum modulation and its amplitude (r = 0.54, $p < 0.001$, Spearman rank correlation). Note that on average, as well as at individual cell level, the suppression of SSs preceded the increase. **E** Overall, the SSs were found to follow rather than to lead the respiration. **F** Correlation matrix showing a posi-

Purkinje cells, 9 (21%) displayed a statistically significant complex spike modulation, but also many of the other Purkinje cells showed some degree of modulation (Fig. S1E). For this analysis the entire epoch of recording was used without selecting only cycles including a complex spike. At the level of Purkinje cells, the average complex spike firing rate did not correlate well with the maximal complex spike modulation depth (r = 0.13, $p$ = 0.396, $n$ = 43 Purkinje cells, Spearman rank correlation; Fig. S1F). Of all 43 Purkinje cells, 19 (44%) displayed maximum complex spike firing in the period just before 3π/2 (Fig. 1B), which is around the transition from post-inspiration to expiration, whereas the other Purkinje cells typically peaked at a given phase during inspiration or post-inspiration, but not during expiration.

## Purkinje cell simple spike modulation is roughly complementary to complex spike activity



The median simple spike rate of the 43 Purkinje cells was 64.5 (IQR: 34.9) Hz (Fig. S1D). The simple spike activity of the majority of these cells (i.e., 35 or 81%) showed a statistically significant modulation across different phases of respiration (Fig. 1C; Fig. S1E). Compared to the modulation of complex spike firing, the preferred phases of the peaks of the simple spike modulation were more closely associated with the inspiration and early post-inspiration periods (Fig. 1D). When we considered the absolute timing – rather than the phase – of the modulation of simple spike activity of single Purkinje cells relative to the start of inspiration, we found that the simple spike rate modulation of 26 Purkinje cells exceeded a Z criterion of higher than 2 ($p$ < 0.05). In most of these Purkinje cells, simple spike modulation was essentially bi-directional (Fig. S2A). However, in half of the cells the amplitude of the increase in simple spike modulation was stronger than the decrease, whereas in the other half it was opposite (Fig. 2A-C; Fig. S2A). The peaks of the decreased firing generally preceded those of the increased firing, yielding a population average of a short-latency decrease followed by an increase of simple spike activity (Fig. 2C-E). This order of events of simple spike decreases and increases was substantiated by a positive correlation between the amplitude of the strongest correlation and its time of occurrence (r = 0.49, $p$ = 0.012, $n$ = 26, Spearman rank correlation; Fig. 2D). The preference for decreased or increased firing did not depend on the baseline simple spike frequency (r = -0.14, $p$ = 0.498, Spearman rank correlation; Fig. S2B). The population average of simple spike activity approximated the actual respiratory behavior rather well with zero phase-lag, suggesting the relevance of a population encoding mechanism (Fig. 2E).

tive correlation between SS firing (blue trace (bottom) shows convolved peri-stimulus time histogram triggered on inspiration start) and respiration (cyan trace, left) based on trial-by-trial variance analysis in PCs that predominantly showed decreased SS firing rate linked to the respiratory cycle. Average of 13 PCs during unperturbed breathing. Note that the main simple spike activity follows the respiration (red area is below the 45° line). **G** Similar analysis of the 13 PCs that predominantly showed increased SS firing during the respiratory cycle, with mostly negative correlation. Thus, for both types of PCs, the correlation was opposite to their mode of modulation, indicating that the shallower the respiration, the stronger the SS modulation. Lines indicate averages and shaded areas SEM. See also Fig. S2.

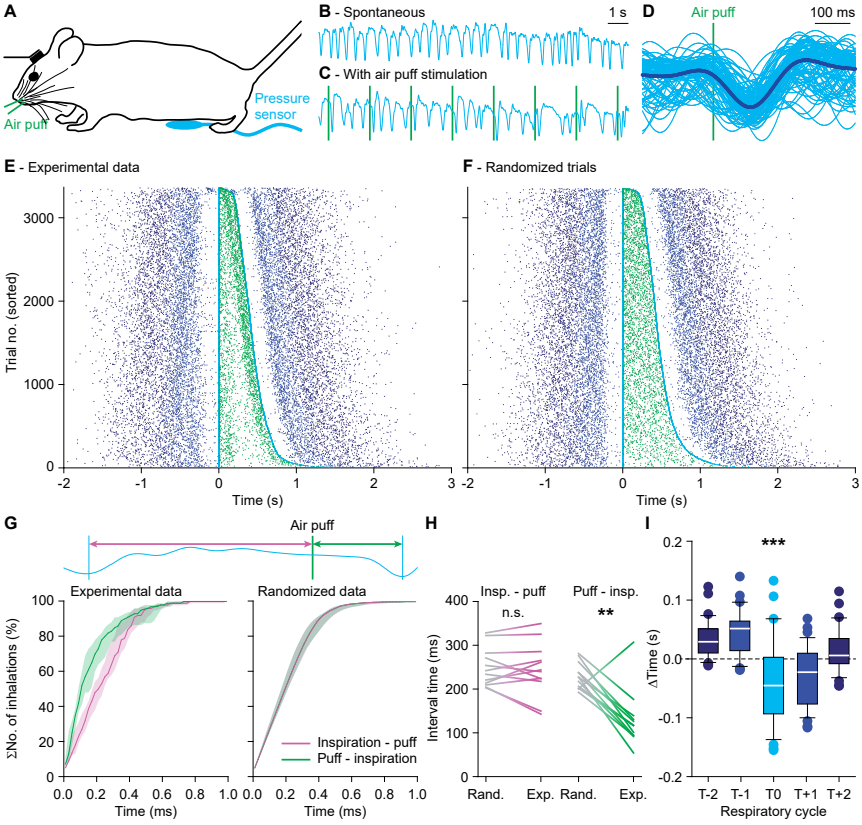


**Figure 3.** Whisker pad stimulation triggers inspiration

**A** Every 2 s, mice received an air puff to their whisker pad while their respiration was recorded using an abdominal pressure sensor. In comparison to the relatively regular breathing in the absence of air puff stimulation (**B**), the respiratory pattern appeared to be affected by sensory stimulation (**C**). Whisker pad stimulation (vertical lines) often triggered inspiration. **D** The raw respiratory signals around the air puff (90 trials of the same experiment as in **C** with the average (thick line) overlaid) demonstrate that whisker pad stimulation often triggers inspiration. **E** Raster plots showing respiratory cycles from 12 mice pooled together and sorted based upon the duration of the respiratory cycle during which the air puff (light green dots) was applied. The trials were aligned on the start of the last inspiration before the onset of the stimulus. Cyan dots indicate the start of the last inspiration before and the first inspiration after the air puff. The previous and subsequent respiratory cycles are indicated by increasingly darker shades of blue (see color code of **I**). In this plot, the air puffs are concentrated just after or just before the start of an inspiration. The latter reflect the triggering of the next inspiration by the air puff. This effect was not observed when the stimulation occurred just after the start of inspiration. **F** Upon random shuffling of the respiratory cycles, the air puffs are equally distributed over the respiratory cycle. **G** Cumulative distributions of 57 epochs (of approximately 100 trials each) originating from 12 mice demonstrate that the interval between the air puff and the start of the next inspiration was shortened relative to the interval between the start of the previous inspiration and the air puff (not visible in randomized data). Lines are medians and shaded areas indicate the interquartile ranges. **H** The anticipation of the start of the next inspiration was also obvious from the median intervals per mouse and comparing the interval between the start of the preceding inspiration and the air puff (left) to the interval between the air puff and the start of the next inspiration (right) in comparison between randomized (Rand.) and experimental (Exp.) data. The former interval did not differ between the randomized and the experimental data ($p = 0.937$), whereas the latter did (**$p = 0.01$, Wilcoxon signed rank tests). **I** Box plots of the duration of the respiratory cycles around the puff indicated that indeed the cycle during which the whisker pad stimulation was given were shorter. T0 is the cycle during which the air puff was given. See also Fig. S3 and Fig. S4.

We further explored whether trial-by-trial variations in simple spike firing correlated with variations in the respiratory signal. We designed a matrix of correlation in which, for each respiratory cycle, the respiratory signal was compared to the instantaneous simple spike rate aligned to the start of each inspiration. This analysis reveals the temporal relationships between both signals whereby a correlation along the 45° line indicates a synchronous event. Indeed, Purkinje cells with a preference for increased simple spike firing as well as those that predominantly show decreased simple spike firing displayed correlations between simple spikes and respiration. The strongest effects were found with the respiratory signal leading the simple spike firing (Fig. 2F-G). Thus, while simple spikes generally co-modulate with the phase of the respiratory signal with approximately a zero lag (Fig. 2E), the depth of their simple spike modulation reflected the depth of the respiration with a delay.



The complex spike and simple spike modulation of each Purkinje cell typically occurred during different phases of the respiratory cycle, although often not in exact anti-phase (Fig. S2C). The occurrence of increased simple spike firing around π correlated well with increased complex spike firing around 3π/2 ($r = 0.536$, $p < 0.001$, Spearman rank correlation; Fig. S2D). In turn, this latter peak in complex spike firing correlated with a subsequent decrease in simple spike firing during expiration ($r = -0.431$, $p = 0.004$, Spearman rank correlation; Fig. S2E). Thus, there were signs of reciprocity between complex spike and simple spike firing with a temporal shift of about 50-80 ms, which is reminiscent of studies of other cerebellar regions (Badura et al., 2013; Chaumont et al., 2013; Witter et al., 2013).

## Whisker stimulation increases the probability of a phase reset of inspiration

Given the intricate relationships between orofacial behaviors in general and the harmonization of respiratory and whisking behavior in rodents in particular (Kurnikova et al., 2017; Lu et al., 2013; Moore et al., 2013), we wondered how an air puff to the facial whiskers that triggers reflexive whisker protraction (Bellavance et al., 2017; Brown and Raman, 2018; Romano et al., 2018) would also affect the respiratory cycle. To evaluate this, we subjected 12 mice to periodic 0.5 Hz whisker stimulation while measuring their respiration (Fig. 3A-D). When delivered within 100 ms after the start of the previous inspiration, the air puff had little effect, but otherwise it accelerated the start of the next inspiration with a median latency of 91 (IQR: 106) ms (Fig. 3E; Fig. S3A). Thus, stimulation of the whiskers induced not only a response in whisker movements, but also a phase-dependent accelerating respiratory response, shortening the interval between the air puff and the start of the next inspiration (comparing experimental and randomized data: interval between start of inspiration and air puff: $Z = -0.078$, $p = 0.937$; interval between air puff and start of next inspiration: $Z = -2.589$, $p = 0.010$, $n = 12$ mice, Wilcoxon signed rank tests; Fig. 3F-H; Fig. S3A). Rather than entraining their respiratory rhythm to the (fixed) frequency of air puff stimulation, the mice adjusted the timing of inspiration of the respiratory cycle directly following sensory stimulation (Fig. 3I; Fig. S3B). Variations in the level of sensory-induced whisker protraction and depth of respiration were correlated; trial-by-trial variations revealed that

stronger whisker protractions preceded deeper levels of respiration, confirming the relationships between different orofacial behaviors in mice (Fig. S4).

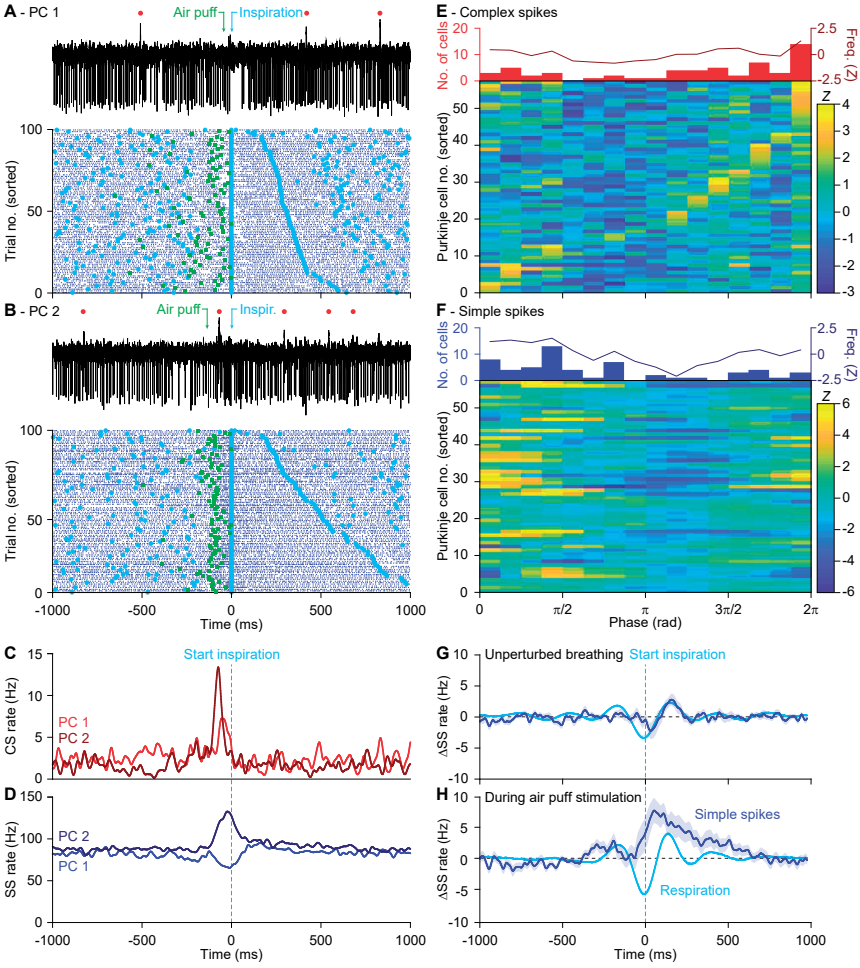


**Figure 4.** Purkinje cell activity anticipates respiratory responses

Representative Purkinje cell recordings showing either suppressed (**A**) or increased (**B**) simple spike firing upon whisker pad air puff stimulation. Above the trace, the complex spikes are indicated by red dots, the start of the air puff by a green arrow and the start of inspiration by a cyan arrow. Below the traces are raster plots of simple spike activity aligned on the start of the first inspiration after the air puff. In the raster plots, the air puffs are indicated by green squares. The trials are sorted based on the duration of the respiratory interval following the air puff. The starting moments of inspiration are indicated by cyan dots. Note that the complex spikes are not shown in the raster plots for reasons of clarity. Convolved histograms of the complex spikes (**C**) and simple spikes (**D**) of these two illustrated Purkinje cells aligned on the first inspiration onsets after stimulus. The complex spike (**E**) and simple spike (**F**) data of the entire population of 57 Purkinje cells measured in this way are indicated in heat maps. The Purkinje cells are sorted according to the moments of their maximal complex spike firing. In **G** is illustrated the same plot of Fig. 2E for comparison along with the homologous plots for the air puff induced anticipated inhalations (**H**). In both cases, a similarity can be observed between the profiles of the averaged respiratory signal and the averaged simple spike activity. In the latter case the simple spikes modulation anticipated the averaged respiration signal. See also Fig. S5 and Fig. S6.

## Purkinje cells sensitive for whisker stimulation jointly encode sensory stimulus and motor output

Given that Purkinje cells in the lateral cerebellum respond to whisker stimulation (Bosman et al., 2010; Brown and Raman, 2018; Romano et al., 2018) and modulate their firing rate along the respiratory cycle (Fig. 1), we examined whether Purkinje cells could mediate the stimulation-induced change in respiratory timing. To this end, we compared the spiking pattern of 57 Purkinje cells during periodic whisker stimulation (Fig. S5).

First, we examined the firing pattern during the whole period with 0.5 Hz whisker pad stimulation. As during unperturbed respiration, complex spike and simple spike firing were modulated in tune with the respiratory cycle, but the timing of both complex spikes and simple spikes was now different (Fig. 4A-F, Fig. S6A-B). The temporal relation between simple spike and complex spike firing, as found during unperturbed respiration (Fig. 1B,D; S2C-E), was disrupted and no longer significant during the whole period with 0.5 Hz whisker stimulation ($p > 0.05$ for simple spike firing in all bins compared to the bin with the strongest complex spike modulation; Pearson correlation tests with Benjamini-Hochberg correction for multiple comparisons) (Fig. 4E-F).



When we related simple spike modulation to the respiratory rhythm following whisker stimulation, we found that 20 out of the 32 (62%) Purkinje cells with a significant simple spike modulation predominantly increased their simple spike activity, whereas 12 (38%) predominantly decreased their simple spike firing. Compared to unperturbed respiration (Fig. 4G), the population increase of simple spike firing now peaked during earlier phases of the respiratory cycle, pointing towards an acceleration in their activity ($U = 922.5$, $p = 0.035$, Mann-Whitney test; Fig. 4H). Restricting the analysis to the cycle around the air puff, it became apparent that the population average of simple spike firing now preceded the change in respiratory behavior, suggesting that the air puff-triggered simple spike response could contribute to the observed acceleration of inspiration. We further examined this possibility by performing a trial-by-trial analysis of variation. During eupneic breathing the prevalence of correlation was below the 45° line for both suppressive and facilitating Purkinje cells, indicating that under these circumstances the simple spike modulation follows respiration and therefore cannot control it (Fig. 2F-G). However, during perturbed respiration, the modulation of simple spike firing preceded the ongoing respiration by a few tens of milliseconds (Fig. 5). Moreover, when we segregated the cells that showed simple spike modulation to whisker stimulation (Fig. 5C) from those that did not (Fig. 5D), we observed that the maximal correlations between respiration and simple spike firing were stronger in the whisker-related than in the non-whisker-related Purkinje cells (r = 0.30 (0.09) vs. 0.23 (0.10) (medians (IQR)); $U = 67$, $p = 0.013$, Mann-Whitney test). These data confirm that simple spike responses following whisker stimulation are endowed with the temporal features for accelerating respiratory responses, whereby the simple spike responses predict the strength of the inspiration.

To further substantiate the correlation between simple spikes, whisker movement and respiration at single cell level, we compared the maximal correlation between trial-by-trial variations in the instantaneous simple spike rate and whisker movements with that between the simple spike rate and respiration. We found that Purkinje cells whose fluctuations in the simple spike rate correlated well with whisker movement preferentially also showed a correlation between fluctuations in simple spike rate and inspiration (r = 0.44, $p$ = 0.010, Spearman rank correlation; Fig. S7A).

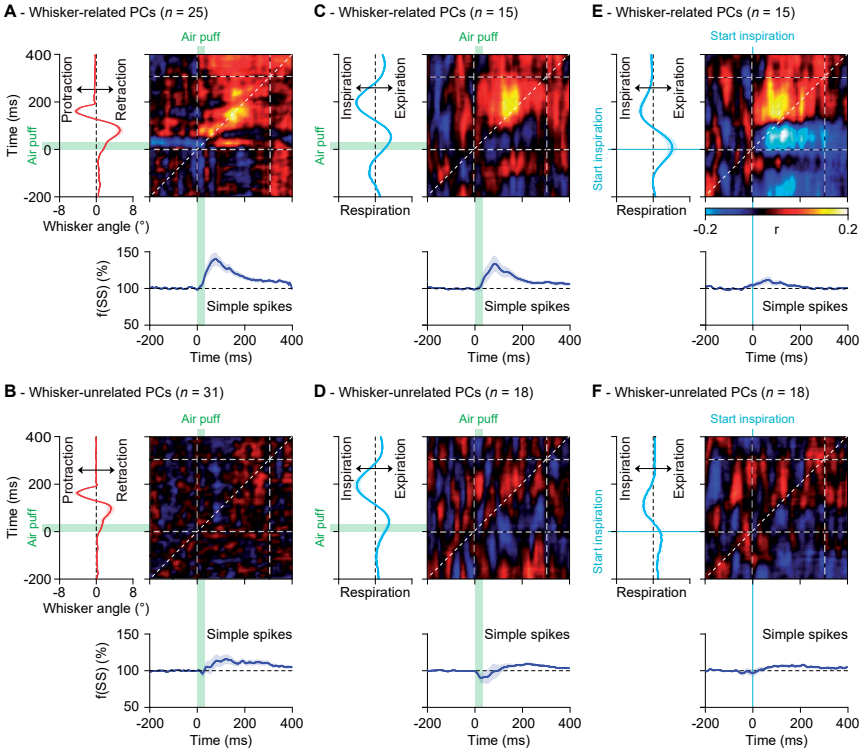


**Figure 5.** Modulation of simple spike firing precedes respiratory adaptation in whisker-related Purkinje cells
Correlation matrix between simple spike firing (blue trace at the bottom represents the averaged convolved peri-stimulus time histograms) and mean reflexive whisker protraction (red trace on the left) for Purkinje cells with (**A**, $n$ = 25) and without (**B**, $n$ = 31) significant correlation between simple spike firing and air puff-induced whisker movement (see Methods). For 15 out of the 25 whisker-related cells and 18 out of 31 whisker-unrelated cells the respiratory signal was simultaneously recorded and used for the respiration-spike matrix of correlation in **C** and **D**, respectively. The whisker-related Purkinje cells had a higher correlation between their instantaneous simple spike rate and respiration than the other Purkinje cells ($U$ = 67, $p$ = 0.013, Mann-Whitney test). The location of the maximal correlation above the 45° line indicates that in trials in which the Purkinje cells fired more simple spikes then, few tens of milliseconds later, the amplitude of the respiration was bigger and vice versa. In addition, the simple spike to whisker correlation (for the whisker-related cells) is stronger and earlier in time when the matrix of correlation is aligned to the puff-induced inhalation, rather than to the puff itself (**E**). Conversely, on average the whisker-unrelated cells did not show a clear correlation even when the signals were aligned to the air puff-induced inspiration (**F**). Shaded areas around the traces indicate SEM. See also Fig. S7.

During perturbed respiration, about half of the Purkinje cells showed their peak in complex spike activity during the last quarter of the respiratory cycle, corresponding to expiration (Fig. 4A-C, E), with the strongest peak in complex spike firing occurring around 40 ms after whisker pad stimulation (Fig. S6A-B), thus approximately 50 ms before the average start of the first inspiration after the stimulus (Fig. 4E). To test the possibility that the complex spikes can contribute to the acceleration of the next inspiration, we compared the timing of complex spike firing during individual trials relative to that of the start of the inspiration. However, we found no clear relation between them (Fig. S6A). Accordingly, when we compared trials with and without complex spikes, we could not find any obvious difference in the timing of the next or subsequent start of inspiration (Fig. S6C-E). Thus, we conclude that the complex spikes observed in the lateral cerebellum, although reacting to whisker stimulation, do not modulate the timing of respiratory responses to whisker pad stimulation in the short-term.



## Respiration related Purkinje cells are located in specific portions of the cerebellar cortex

Next, we mapped the location of the Purkinje cells recorded in this study. During unperturbed respiration, the strongest complex spike modulation was found laterally in crus 2 (Fig. 6A; left column). This complex spike hot spot extended rostrally into crus 1 during respiration perturbed by whisker stimulation (Fig. 6B). The Purkinje cells in crus 1 that were recruited during perturbed, but not during unperturbed respiration, were mainly those that responded with a complex spike response directly to the sensory stimulation (Fig. 6C). Of the 57 recorded Purkinje cells, 53 (93%) responded with a statistically significant complex spike response (Fig. S5D). The simple spike responses showed a distribution that was largely complementary to that of the complex spike responses (Fig. 6; right column). The Purkinje cells with a predominantly increased simple spike rate during an unperturbed respiratory cycle were largely found around the border between the vermis and the simple lobule and crus 1, with a few cells extremely lateral in crus 1 (Fig. 6A). The cells that showed decreased simple spike firing during unperturbed respiration were largely confined to a parasagittally oriented strip in the middle of crus 1 and crus 2. During perturbed respiration, this pattern was largely unaltered, although the lateral regions now also showed a decreased simple spike firing rate (Fig. 6B). Importantly, the Purkinje cells in medial crus 1 showed particularly strong correlations to both whisker inputs and respiration.

## Purkinje cell stimulation mimics the impact of whisker stimulation on respiratory timing

As our analyses revealed that during perturbed respiration increased simple spike firing preceded the accelerated inspiration, we wondered whether we could mimic the impact of whisker pad air puff stimulation on the timing of inspiration by transiently stimulating the Purkinje cells in the medial parts of lobule simplex as well as the crus 1 and crus 2 areas highlighted above. To

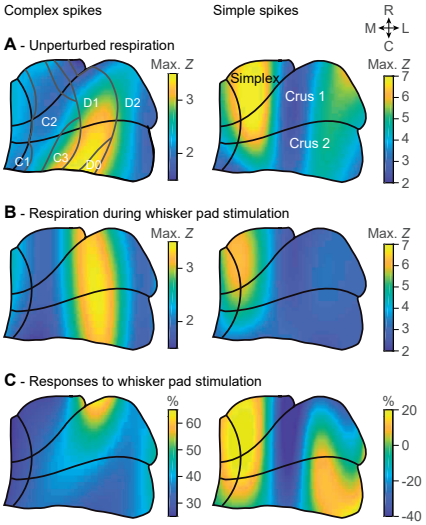


**Figure 6.** Respiration related Purkinje cells are located in specific portions of the cerebellar cortex
**A** Based upon the entry point of each electrode relative to a standardized map of the simplex, crus 1 and crus 2 lobules, a map was created indicating the spatial distribution of the maximal increase (in *Z* score) of complex spikes (left) and simple spikes (right) during the respiratory cycle in the absence of whisker pad stimulation. **B** The same during the presence of whisker pad stimulation. This analysis revealed an area with a relatively strong correlation between respiration and complex spike firing in the medio-lateral part of crus 2 extending rostrally in crus 1. Simple spikes correlated to respiration were mainly found medially in the simple lobule and crus 1. There were some differences in the spatial pattern of responses during unperturbed and perturbed respiration. These could be partially explained by the pattern of response probabilities (in percentage of baseline firing) to whisker pad air puff stimulation (**C**). In the left panel of **A**, the tentative locations of the cerebellar modules are indicated. C = caudal, L = lateral, M = medial, R = rostral.

this end, we made use of transgenic mice that expressed channelrhodopsin (ChR2) specifically in their Purkinje cells (*Pcp2-Ai27* mice) (Romano et al., 2018; Witter et al., 2013). In line with previous whole cell recordings *in vivo* (Witter et al., 2013), a brief pulse of blue light triggered a strong increase in simple spike firing (Fig. 7A-B). We randomly intermingled trials with and without optogenetic stimulation, the latter trials we considered as “sham controls”. Since the stimulation was periodic, the mouse could predict the arrival of the stimulus, thus the sham controls could be useful to exclude synchronization between stimuli and respiration. Purkinje cell optogenetic stimulation significantly accelerated the occurrence of the next respiratory cycle (Fig. 7C-D). The inspiration started 189 ms (median value, IQR: 243 ms) after the onset of optogenetic stimulation compared to 224 ms (IQR: 212 ms) during the sham control condition. Consequently, inspiration was accelerated due to optogenetic Purkinje cell stimulation ($Z = -2.760$, $p = 0.006$), but not in the sham control experiments ($Z = -0.105$, $p = 0.917$, $n = 13$ mice, Wilcoxon signed ranks tests; Fig. 7D). Supporting the idea that Purkinje cells in the same region of the cerebellar hemispheres can affect respiration as well as whisker movements, we found that the same optogenetic stimulus triggered inspiration as well as whisker protraction (Fig. S7B).

To investigate whether the increased simple spike firing during optogenetic stimulation induced the accelerated inspiration, or whether it was rather the rebound firing in the cerebellar nuclei following the optogenetic stimulation that did so, we compared optogenetic stimulation of 100 ms with that of 200 ms duration. Unlike whisker movements, that are facilitated by rebound firing in the cerebellar nuclei (Brown and Raman, 2018; Proville et al., 2014), we did not observe a 100 ms delay when comparing 200 ms and 100 ms stimulation (Fig. S8). To control for putative direct effects of light stimulation, not involving optogenetic stimulation of Purkinje cells, we repeated the experiments in Cre-negative mice that did not express the optogenetic

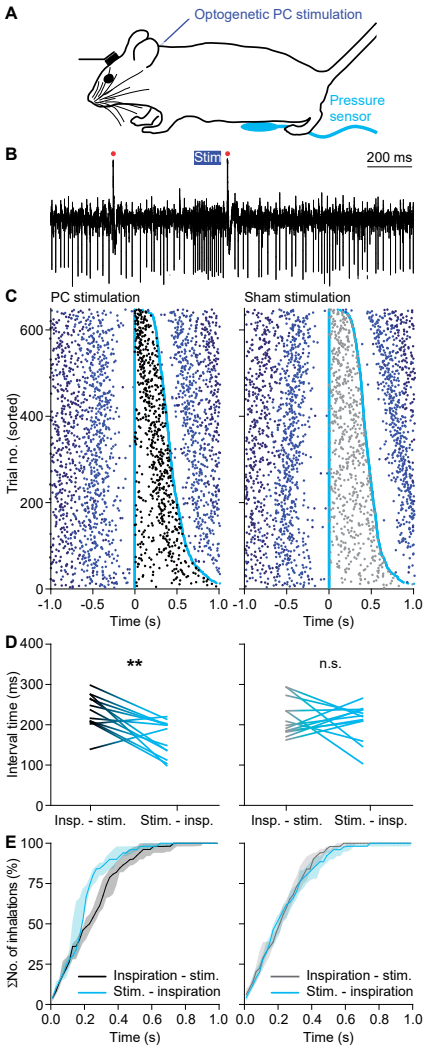


**Figure 7.** Optogenetic stimulation of Purkinje cells triggers accelerated inspiration

**A** The impact of optogenetic stimulation on respiratory timing was studied using transgenic mice expressing ChR2 exclusively in their Purkinje cells (PCs). **B** 100 ms blue light pulses caused brief increases in simple spike firing. Red dots indicate complex spikes. **C** Raster plots showing respiratory cycles from 13 mice pooled together and sorted based upon the duration of the respiratory cycle during which optogenetic Purkinje cell stimulus (black dots, left) or no stimulus (sham stimulation, grey dots, right) was applied. The trials were aligned on the start of the last inspiration before the onset of the stimulus. Cyan dots indicate the start of the last inspiration before and the first inspiration after the stimulus. The previous and subsequent respiratory cycles are indicated by increasingly darker shades of blue. Inspiration typically started around 200 ms after the onset of Purkinje cell stimulation. **D** Optogenetic Purkinje cell stimulation resulted in anticipation of the next inspiration, as the median interval between the stimulus and the start of the next inspiration was shorter than that between the start of the previous inspiration and the stimulus (** $p < 0.010$, Wilcoxon signed rank test). This effect was not present during trials without optogenetic stimulation (sham controls, right column). **E** Cumulative histograms of the intervals between the start of inspiration and the stimulus (grey) and between the start of the stimulus and the start of the next inspiration (cyan). Purkinje cell stimulation (left), but not sham stimulation (right), accelerates the start of the next inspiration. The cumulative histograms show the medians of the distributions per mouse (around 100 trials in 13 mice). The shaded areas indicate the interquartile ranges. See also Fig. S7 and Fig. S8.

protein. As expected, we could not identify any sign of a respiratory response to light stimulation alone in these mice ($Z = -0.734$, $p = 0.463$, $n = 5$ mice, Wilcoxon signed rank test; see Fig. S7C and Fig. S8B), suggesting that the results described above are indeed mediated by Purkinje cells. We conclude that optogenetic stimulation of the Purkinje cell activity in lobule simplex as well as crus 1 and crus 2 areas is sufficient to induce an acceleration in the occurrence of the next respiratory cycle.

## Modification of AMPA receptors at parallel fiber to Purkinje cell synapse cancels impact of whisker stimulation on respiratory timing

To find out whether functionally intact cerebellar Purkinje cells are necessary for the respiratory changes induced with whisker stimulation, we investigated this response in a mouse model that lacked the AMPA GluA3 subunit at their parallel fiber to Purkinje cell synapses (Gutierrez-Castellanos et al., 2017). This mutant (*Pcp2-Gria3*$^{-/-}$ mice) has been shown to be impaired in its simple spike modulation following whisker stimulation (Fig. 8A). The *Pcp2-Gria3*$^{-/-}$ mice showed a normal frequency of respiration during unperturbed respiration (2.7 (0.4) Hz versus 2.4 (1.0)

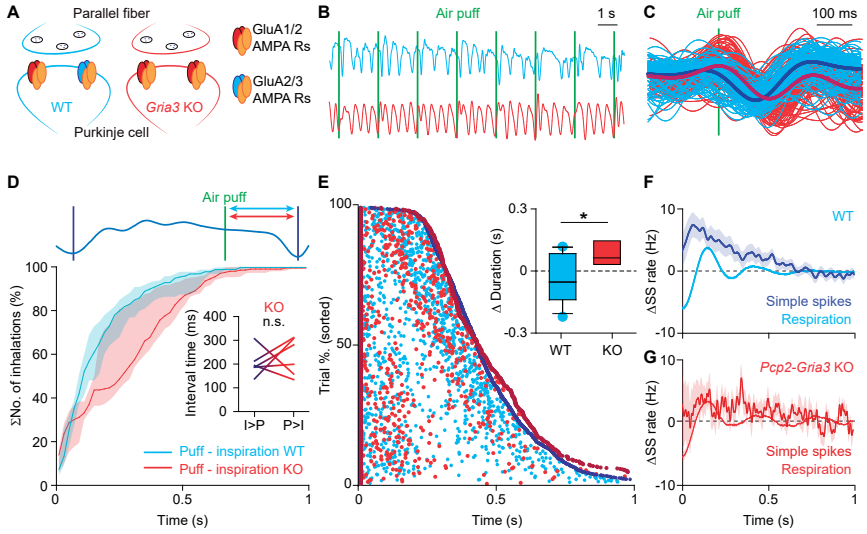


**Figure 8.** Impaired respiratory response in *Pcp2-Gria3* KO mice

**A** *Pcp2-Gria3* KO mice lack the gene for AMPA receptor GluA3 subunit specifically in Purkinje cells. Instead, they express more GluA1/GluA2-type AMPA receptors than wild type mice. **B** In *Pcp2-Gria3* KO mice, the whisker stimulation (vertical green lines) appeared to be less effective in triggering inspiration than in wild type mice. **C** The respiratory pattern of an exemplary *Pcp2-Gria3* KO mouse (red lines) around the air puff showing delayed inspiration when compared to a wild type mouse (the cyan lines are the same as in Fig. 3C-D). **D** While wild type mice accelerate the start of the next inspiration after whisker pad air puff stimulation (the blue line / area is a copy of the green line / area in Fig. 3G, left panel), *Pcp2-Gria3* KO mice (red line / area) do not. This is illustrated as cumulative distributions of the intervals between the stimulus and the start of the next inspiration, constructed of 100 trials per mouse ($n$ = 6 mice). The lines show the medians and the shaded areas the interquartile ranges. The inset shows that the averaged intervals between the start of the previous inspiration (I) and the air puff (P) were not systematically different from those between the air puff and the start of the next inspiration in *Pcp2-Gria3* KO mice ($p$ = 0.436, Wilcoxon signed rank test; inset), in contrast to in wild type mice (see Fig. 3H). **E** Raster plot showing the respiratory cycles perturbed by the air puffs sorted from the shortest (top) to the longest (bottom). The beginning and the end of each cycle are represented with dark blue dots for the wild type and dark red dots for the *Pcp2-Gria3* KO mice, while the relative time of the air puffs is depicted in cyan and red respectively. Looking at all the individual data points, both red and cyan dots are not randomly distributed and tend to accumulate before the subsequent inhalation. The delay to the start of the next inspiration is longer in *Pcp2-Gria3* KO mice than in wild type mice, in line with the results plotted in **D**. The impact of the puff on the overall duration of cycle containing the stimulus, relative to the duration of those that did not contain one, was different in wild type and *Pcp2-Gria3* KO mice ($p$ = 0.028, $F$ = 5.544, df = 1, two-way ANOVA, interaction puff*genotype; inset). **F** The simple spike activity of intact Purkinje cells increases during the air puff-triggered inspiration. This increase resembles, precedes and potentially affects the ongoing respiration. **G** Conversely, the simple spike activity of the *Pcp2-GriA3* KO mice modulates differently than in WT mice and does not resemble the respiration signal.

Hz for wild type mice, medians (IQR); $U$ = 37, $p$ = 0.898, Mann-Whitney test; Fig. 8B). However, the mutants were impaired in their ability to advance the respiratory response following whisker stimulation (difference in interval between start inspiration and air puff vs. interval between air puff and start of next inspiration: $Z$ = −0.734, $p$ = 0.436, $n$ = 6, *Pcp2-Gria3*$^{-/-}$ mice, Wilcoxon signed ranks test; Fig. 8C-E). Moreover, the timing of simple spike rate modulation of their Purkinje cells was significantly different from that in the wild types in that they did not precede respiration directly following whisker stimulation ($p$ = 0.040, *Pcp2-Gria3*$^{-/-}$ versus wild type, Wilcoxon Rank Sum test; Fig. 8F-G). In addition, the depth of the modulation was also different in that the mutant Purkinje cells showed less of an increase in their simple spike rate (WT: 12.0 (15.1)% vs. KO: -11.9 (33.5)%, medians (IQR), $U$ = 257, $p$ = 0.041, Mann-Whitney test). These data indicate that a cerebellar, cell-specific interference with a mechanism that has the potential to increase the simple spike firing rate results in a hampered ability to accelerate the respiratory response.



## DISCUSSION

Animals use periodic and oscillatory behaviors in a variety of functional movements and they display adaptation in the coordination of such behaviors as a function of systematic changes of the environment. For instance, during sniffing rodents coordinate the movements of their whiskers with those of the respiratory and olfactory system and this behavior can be adjusted to the discrimination task involved (Kurnikova et al., 2017; Welker, 1964). The way the brain organizes such control mechanisms is largely unknown. Here, we show that during eupneic respiration, Purkinje cells in the simplex, crus 1 and crus 2 lobules of the cerebellum fire in tune with specific phases of the respiratory rhythm. During unperturbed breathing, the activity of simple spikes and complex spikes can be described as an efference copy of the respiratory signal, modulated by specific phases of the respiratory rhythm. In contrast, stimulation of the whiskers with air puffs accelerated simple spike activity that in turn contributed to a faster onset of inspiration. Our data show that increases in simple spike activity in the lateral cerebellum are probably sufficient to drive and integrate different forms of rhythmic behavior, as optogenetically driven increases in simple spike activity both accelerated the respiratory cycle in a phase-dependent manner and induced whisker protraction. Moreover, cell-specific blockage of GluA3-containing AMPA receptor signaling in Purkinje cells impaired the ability of the mice to advance both their simple spike response and their respiratory response following air puff stimulation of the whiskers, highlighting the necessity of an intact cerebellum for synergistic phase control. These responses are consistent with the idea that efference copies of the respiratory signal are taken as predictions, which are then disrupted by the whisker stimulation, leading to a recalibration of the respiratory cycle.

Isolated rhythmic behaviors are often controlled as muscle synergies by local networks. For instance, coordination between the left and right hind-limb can still take place during locomotion even after the descending connections from the motor cortex and brainstem to the spinal cord are disrupted (Desrochers et al., 2019). Likewise, when cerebellar function is impaired, basic muscle activities of breathing and related orofacial behaviors can still take place (Bellavance et al., 2017; Chen et al., 2005; Gewaltig and Diesmann, 2007). Thus, local networks in spinal cord and brainstem are sufficient to generate basic antagonistic muscle activities that mediate rhythmic properties of locomotion and breathing, respectively (Bellavance et al., 2017; Kurnikova et al., 2017; Talpalar et al., 2013; Tresch et al., 1999). However, the integration of multiple rhythmic behaviors requires cerebellar coordination, exemplified by paradigms requiring front and hind limb movements, particularly in less stereotyped forms of locomotion and adaptation (Darmohray et al., 2019; Hoogland et al., 2015; Machado et al., 2015; Vinueza Veloz et al., 2015). Similarly, an intact cerebellum is required for adjusting the respiratory cycle during more complex tasks such as speech. We now provide evidence that changes in simple spike activity of Purkinje cells in the simplex, crus 1 and crus 2 areas, in which respiratory and whisking processing converge, contribute to re-adaptation of the respiratory timing signal following sensory perturbation of the facial whiskers. Natural or artificial activation of Purkinje cells sensitive for whisker stimulation can accelerate the occurrence of the next inspiration. The correlation between simple spike firing and respiration is particularly strong in the Purkinje cells whose simple spike firing co-modulate with whisker movement. In line with their instructive role following facial stimulation (Romano et al., 2018), optogenetic stimulation of Purkinje cells affects both respiration and whisker movements, providing synergistic control of two different forms of orofacial behavior.

This is one of the first studies indicating that simple spike activity of individual Purkinje cells can drive different forms of motor behavior, in this case the rhythmic behaviors represented by breathing and whisking. This finding elaborates on several behavioral studies demonstrating the role of the cerebellum in synergistic control of diverse motor domains. For example, the olivocerebellar system has been shown to be involved in the coordination between eye and hand movements (Kitazawa et al., 1998; Owens et al., 2018; Vinueza Veloz et al., 2015), between trunk and limb movements (Bakker et al., 2006; Caliandro et al., 2017), as well as between shoulder, arm and finger movements (Thach et al., 1993; Timmann et al., 2000). The current study amasses to that lot by demonstrating for the first time functional convergence of autonomic and sensorimotor behaviors on single Purkinje cells. Given their rich and diverse parallel fiber inputs mediating signals from different sensorimotor systems (De Zeeuw et al., 2011; Gao et al., 2012; Ito, 2000), we postulate that Purkinje cells in the cerebellar cortex mediate synergy and integration of different motor domains in both voluntary and autonomic systems.

The contribution of complex spikes to the acute changes in respiratory behavior remains to be elucidated. They have a relatively low frequency, considerably lower than that of the respira-

tory cycle. Given the strong convergence of Purkinje cells upon cerebellar nuclei neurons, it is likely that multiple Purkinje cells encode the phase of the respiratory cycle (see also Ju et al., 2019; Negrello et al., 2019). Nevertheless, comparing the acute respiratory responses during trials with and without complex spikes did not reveal any significant difference in behavior. We also could not find any differences in air puff-related inspiration comparing trials with and without complex spikes. This means that the phase related signal conveyed by the complex spike is robust to the sensory perturbation. The only prominent difference that occurred in the trials with unperturbed and perturbed breathing is that the interval between peak activity of the complex spikes and that of the simple spikes robustly changed in the trials with air puff stimulation, supporting a putative role in long-term plasticity (Coesmans et al., 2004; De Zeeuw and Ten Brinke, 2015; Gao et al., 2012; Suvrathan et al., 2016; Wang et al., 2000). Indeed, this possibility agrees with the fact that the complex spike frequency negatively correlates with the induction of long-term potentiation (LTP) at the parallel fiber to Purkinje cell synapse (Coesmans et al., 2004). It is also consistent with the observation that ablating this form of plasticity in the *Pcp2-Gria3*$^{-/-}$ mice corrupted the synergistic behavioral response following whisker stimulation. It will be interesting to investigate to what extent an induced shift in complex spike phase would have an impact on the relationship between different rhythms, including that of respiration.



It is likely that Purkinje cells in the cerebellar cortex influence the nuclei in the brainstem that control breathing and/or whisking. The cerebellar fastigial nucleus is known to modulate the respiratory cycle by sensing $CO_2$ in the blood (Martino et al., 2006; Martino et al., 2007; Xu and Frazier, 2000; Xu et al., 2001). The roles of other cerebellar nuclei, which do not seem to have correlates of pH sensors (Xu et al., 2001), are still controversial (Xu and Frazier, 2000). Possibly, the interposed nuclei play a role in control of the upper airways, as bilateral lesions of this region suppress coughing responses (Xu et al., 1997). The central pattern generator for respiration is located in the preBötzinger complex (Feldman et al., 2013; Moore et al., 2013; Ramirez et al., 2011; Smith et al., 1991). There is no direct connection from the cerebellar nuclei to the preBötzinger complex nor to the adjacent Bötzinger complex (Teune et al., 2000), which is consistent with our finding that the Purkinje cell-mediated impact of whisker stimulation changes the timing, not the frequency of respiration (Fig. 3I). Possibly, cerebellar nuclei project, downstream of the preBötzinger complex, to the region of the post-inspiratory complex at the border of the intermediate and gigantocellular reticular formation (Lu et al., 2013; Teune et al., 2000) and/or to the parabrachial complex, which projects to motor neurons of the diaphragm in the spinal cord (Dobbins and Feldman, 1994).

Thus, although the anatomical pathways via which the cerebellum could affect respiration are still matter of debate, individual Purkinje cells in the lateral cerebellum can synergistically coordinate multiple motor behaviours, such as respiration and whisking, by injecting accelerating signals into diverging downstream circuitries.

## ACKNOWLEDGEMENTS

The authors wish to thank Dr. Ruben van der Giessen for fruitful discussions, Dr. Davide Vidotto from Tilburg University for statistical consulting and Mandy Rutteman, Elize Haasdijk and Erica Goedknegt for technical support. Financial support was provided by the Netherlands Organization for Scientific Research (NWO-ALW; CIDZ), the Dutch Organization for Medical Sciences (ZonMW; CIDZ), Life Sciences (CIDZ), ERC-adv and ERC-POC (CIDZ), and Medical Neurodelta (CIDZ).

## AUTHOR CONTRIBUTIONS

Conceptualization: V.R., A.L.R., M.N., L.W.J.B. and C.I.D.Z.; Methodology: V.R., A.L.R., Y.M., C.S., M.N. and L.W.J.B.; Software: A.L.R., Y.M., C.S. and M.N.; Validation: V.R., A.L.R., M.N. and L.W.J.B.; Formal analysis: V.R., A.L.R., S.C. and R.M.; Investigation: V.R., A.L.R., R.M. and L.W.J.B.; Resources: M.N., L.W.J.B. and C.I.D.Z.; Data curation: V.R., M.N. and L.W.J.B.; Writing – original draft: V.R., A.L.R., S.C. and L.W.J.B.; Writing – review & editing: V.R., M.N., L.W.J.B. and C.I.D.Z.; Visualization: V.R., A.L.R., M.N. and L.W.J.B.; Supervision: V.R., C.S., M.N., L.W.J.B. and C.I.D.Z.; Project administration: V.R. and L.W.J.B.; Funding acquisition: C.S. and C.I.D.Z.

### Competing interests

The authors declare no competing interests.

# STAR METHODS

## Lead contact and materials availability

Further information and requests for resources and reagents should be directed to and will be fulfilled with the Lead Contact, Laurens Bosman (l.bosman@erasmusmc.nl). This study did not generate new unique reagents.

## Experimental model and subject details

### *Animals*

We used 18 WT adult mice with a C57BL/6J background (13 males and 5 females from Charles Rivers, Leiden, the Netherlands) for the electrophysiological recordings and compared their behavior to 13 *Tg*(*Pcp2-cre*)*2Mpin;Gt*(*ROSA*)*26Sor*$^{tm27.1(CAG-OP4*H134R/tdTomato)Hze}$ mice (Witter et al., 2013) expressing channelrhodopsin-2 (ChR2) for optogenetic stimulation of their Purkinje cells (6 males and 7 females from the same breeding colony as the WT mice, preferably using littermates). As controls for the optogenetic stimulation, we used five additional male Cre-negative *Gt*(*ROSA*)*26Sor*$^{tm27.1(CAG-OP4*H134R/tdTomato)Hz}$ mice. In addition, we used 6 *Tg*(*Pcp2-cre*)*2Mpin;Gria3*$^{tm2Rsp}$ KO mice (3 males and 3 females) (Gutierrez-Castellanos et al., 2017) mice, also on a C57BL/6J background. The mice had an age of 4-7 months. Mice were socially housed until surgery and single-housed afterwards with *ad libitum* access to food and water. The mice were kept at a 12/12 h light/dark cycle and had not been used for any other study before the start of the experiments described here. All mice were healthy and specific pathogen free (SPF). All experimental procedures were approved *a priori* by an independent animal ethical committee (DEC-Consult, Soest, The Netherlands) as required by Dutch law and conform the relevant institutional regulations of the Erasmus MC and Dutch legislation on animal experimentation. Permission was filed under the license numbers EMC3001, AVD101002015273 and AVD1010020197846.

## Method details

### *Surgeries*

All mice received a magnetic pedestal that was attached to the skull above bregma using Optibond adhesive (Kerr Corporation, Orange, CA) and a craniotomy that was made on top of crus 1 and crus 2. The surgical procedures were performed under isoflurane anesthesia (Pharmachemie, Haarlem, The Netherlands; 2-4% V/V in $O_2$). Post-surgical pain was treated with 5 mg/kg carprofen (“Rimadyl”, Pfizer, New York, NY), 1 µg lidocaine (AstraZeneca, Zoetermeer, The Netherlands), 50 µg/kg buprenorphine (“Temgesic”, Reckitt Benckiser Pharmaceuticals, Slough, United Kingdom) and 1 µg bupivacaine (Actavis, Parsippany-Troy Hills, NJ, USA). After three days of recovery, mice were habituated to the recording setup during at least 2 daily ses-

sions of approximately 45 min. In the recording setup they were head-fixed using the magnetic pedestal. Further body movements were prevented by using a customized restrainer and filling the empty space with paper tissues.

### *Whisker pad stimulation and behavioral recordings*

Sensory stimulation (0.5 Hz) was given to the center of the whisker pad of awake mice by means of air puffs given from approximately 5 mm at an angle of 30 degrees with the whisker pad. Each puff was around 2 bar and had a duration of 30 ms. Videos of the movements of the untrimmed large facial whiskers were made from above using a bright LED panel as back-light ($\lambda$ = 640 nm) at a frame rate of 1,000 Hz (480 x 500 pixels using an A504k camera from Basler Vision Technologies, Ahrensburg, Germany). Respiration was recorded using a PowerLab 4/30 analog-to-digital converter (AD Instruments, Oxford, United Kingdom) in combination with a pressure sensor that was placed at the abdomen of the mice.

### *Electrophysiology*

Electrophysiological recordings were performed in awake mice using quartz-coated platinum/tungsten electrodes (2-5 MΩ, outer diameter = 80 µm, Thomas Recording, Giessen, Germany). The latter electrodes were placed in an 8x4 matrix (Thomas Recording), with an inter-electrode distance of 305 µm. Prior to the recordings, the mice were lightly anesthetized with isoflurane to remove the dura, bring them in the setup and adjust all manipulators. Recordings started at least 60 min after termination of anesthesia and were made in lobules simplex, crus 1 and crus 2 ipsilateral to the side of the whisker pad stimulation at a minimal depth of 500 µm. The electrophysiological signal was digitized at 25 kHz, using a 1-6,000 Hz band-pass filter, 22x pre-amplified and stored using a RZ2 multi-channel workstation (Tucker-Davis Technologies, Alachua, FL).

### *Optogenetic stimulation*

LED photostimulation ($\lambda$ = 470 nm) driven by a Thorlabs LED driver (225 µW) was given through an optic fiber (400 µm in diameter, Thorlabs, Newton, NJ, USA). The optic fiber rested on the dura mater above the midline between crus 1, crus 2, approximately 1 mm lateral from the vermis, via the craniotomy. During experiments with optogenetic stimulation, trials without stimulation ("sham controls"), with 100 ms and with 200 ms optogenetic stimulation were randomly intermingled.

### *Experimental design*

During the experiments and formal analysis, the experimenters were blind to the genotype of the mice. All obtained data were included, provided the signal-to-noise ratio of the recordings allowed unbiased analysis. Regarding electrophysiological recordings, as an extra inclusion criterion we accepted only those recordings during which the amplitude and the width of the

spikes were constant over time for correlation with the respiratory signal. The recordings in which the amplitude or the width of more three consecutive simple spikes exceeded three standard deviations above or below their average were considered unstable and excluded. In this way, any change in spike rate due to the instability of the recordings was avoided. Only single-unit recordings of Purkinje cells with a minimum recording duration of 120 s were selected for further analysis.

## Quantification and statistical analysis

### *Phase transformation of respiratory recordings*



The signal from the abdominal pressure sensor was filtered with MATLAB's (MathWorks, Natick, MA, USA) Butterworth bandpass filter (cut-off frequencies 1 and 10 Hz, chosen to include respiratory frequencies visible on the Fourier transform of the raw signal). For the averages of the respiration signal around the stimulus, movement artefacts were removed by excluding trials in which the signal surpassed three times the standard deviation in a 200 ms window before the stimulus. The phase transform of the respiration signal was acquired with the co_hilbproto (which calculates a 'protophase' of a scalar time series using the Hilbert transform) and co_fbtrT (protophase to phase transformation) functions from MATLAB toolbox DAMOCO. As the default setting, the DAMOCO toolbox chooses as initial phase the maximum of the respiration signal, but for our analysis it was more beneficial to set zero phase at the moment when the mouse starts inspiration. Therefore, before the phase transform the respiration signal was multiplied by -1, so that no changes needed to be made to the functions of this toolbox.

### *Whisker movement tracking*

The whisker movements were tracked as described previously (Ma et al., 2017; Rahmati et al., 2014; Romano et al., 2018) using the BIOTACT Whisker Tracking Tool (Perkon et al., 2011) in combination with custom written code (https://github.com/elifesciences-publications/BWTT_PP).The whisker movements were described as the average angle of all trackable whiskers per frame.

### *Electrophysiological analysis*

Spikes were detected offline using SpikeTrain (Neurasmus, Rotterdam, The Netherlands). A recording was considered to originate from a single Purkinje cell when it contained both complex spikes (identified by the presence of stereotypic spikelets) and simple spikes, when the minimal inter-spike interval of simple spikes was 3 ms and when each complex spike was followed by a pause in simple spike firing of at least 8 ms.

### *Polar plots*

Polar plots were generated to describe the correlation between respiratory phase and Purkinje cell spiking activity. To this end, we attributed each spike to a phase (using 16 bins) of the respiration and we compared the recorded distribution with a bootstrap analysis based upon a re-sampling of the spike times after shuffling the inter-spike intervals. The bootstrap analysis was repeated 500 times after which the 99% confidence interval was established. The *Z* score of each bin was derived by dividing, for each bin, the dividing the difference between number of spikes of a Purkinje cell during that bin and the average number of spikes of all bins by the standard deviation of all bins. This analysis focuses on the relative timing of spikes. Respiratory cycles during which no complex spike was fired are not represented in the polar plots.

### *Trial-by-trial correlation analysis*

The inter-trial variations between the respiratory signal and the instantaneous simple spike firing rate (Figs. 2F-G and 5) or the average whisker angle (Figs. 5, S4) were calculated and represented according to a previously published method (Romano et al., 2018; Ten Brinke et al., 2015). Briefly, during each trial, the filtered respiration signal (see above) was compared to either the instantaneous simple spike rate or the relative whisker position without alignment to the baseline. The instantaneous simple spike rate was obtained by convolving spike occurrences across 1 ms bins with an 8 ms Gaussian kernel. The inter-trial variations were subsequently described by creating a matrix of Pearson correlation values for each 10 x 10 ms bin and visualized as heat maps. In Fig. 5, we separated between those Purkinje cells that had a significant correlation between their instantaneous simple spike rate and the whisker angle and those that had not. Significance was established by testing whether the correlation along the 45° line exceed the 99% confidence interval of a bootstrapped dataset in which the inter-spike times were randomly shuffled 500 times.

## Sorted raster plots

To visualize the relation between stimulation and respiration (Figs. 3E, 7C, 8E and S3B) or between complex spike firing and respiration (Fig. S6A), sorted raster plots were constructed. For each plot, a dataset composed of a balanced number of trials of all mice was generated and sorted based upon the duration of the respiratory cycle during which the stimulus was applied (Figs. 3E, 7C, 8E) or that of the respiratory cycle preceding the stimulus presentation (Fig. S3B). The trials presented in Fig. S6A were sorted based upon the interval from the air puff stimulus to the first complex spike following that moment. In Fig. S6A, some of the Purkinje cells were recorded simultaneously, leading to a larger number of trials than in the other plots that are based upon mice. The experimental data were compared to a random shuffling of the durations of the respiratory cycles within each experiment (Fig. 3F). During optogenetic stimulation, trials with and without stimulation were randomly intermingled and the trials without stimuli served as sham controls (Fig. 7C). The differences between experimental and control data

were substantiated by comparing the distribution of the intervals between the start of the last inspiration prior to stimulation and the moment of stimulation with the distribution of intervals between the stimulation and the start of the subsequent inspiration.

### *Anatomical maps*

To visualize the distribution of the spike-respiration correlation respiration throughout the lobules simplex, crus 1 and crus 2 we developed an anatomical map of the distribution of the *Z* scored values obtained by the polar plots (Fig. 6A-B). Since the electrophysiological recordings were performed using a grid of 8 x 4 electrodes (placed always on the same type of craniotomy), we could retrieve the approximate location of each cell and plot the corresponding maximum *Z* score on an 8 x 4 matrix. Linear interpolation was used to smooth the edges of adjacent patches and the Matlab function "imagesc" was eventually used to obtain the heating map that was overlapped to a schematic draw of the craniotomy. Similarly, also the air puff responses could be represented by plotting the values of maximum variation of firing rate of each cell (Fig. 6C).



### *Statistics and visualization*

Throughout the manuscript, mostly non-parametric statistics were used. An exception are the *Z* scores calculated per cell to evaluate the amplitude of the responses. Spike responses were considered statistically significant, if they exceeded a *Z* score of +/- 3. Whenever applicable, two-sided tests were used. Unless stated otherwise, data are summarized as medians with the interquartile ranges.

Box plots (e.g., see Fig. 3I) indicate the distribution of the data with the box indicating the interquartile-range around the median (horizontal line). The whiskers indicate the $10^{th}$ and $90^{th}$ percentiles. Data points outside the $10^{th}$-$90^{th}$ percentile range are indicated as separate dots. Violin plots (e.g., see Fig. S1D) indicate the distribution of all data points as dots. The contours indicate a convolved histogram of the data points (along the y axis, using a Gaussian kernel and reflected along the vertical axis) and the horizontal lines show the $10^{th}$, $25^{th}$, $50^{th}$, $75^{th}$ and $90^{th}$ percentiles.

CV2 was calculated as $2 \times |interval_{n+1} - interval_n| / (interval_{n+1} + interval_n)$.

## Data and code availability

All data are available from the Lead Contact upon request. The custom code complementing BWTT whisker tracking can be obtained via https://github.com/elifesciences-publications/BWTT_PP.

## Additional resources

n/a

## SUPPLEMENTARY MATERIAL

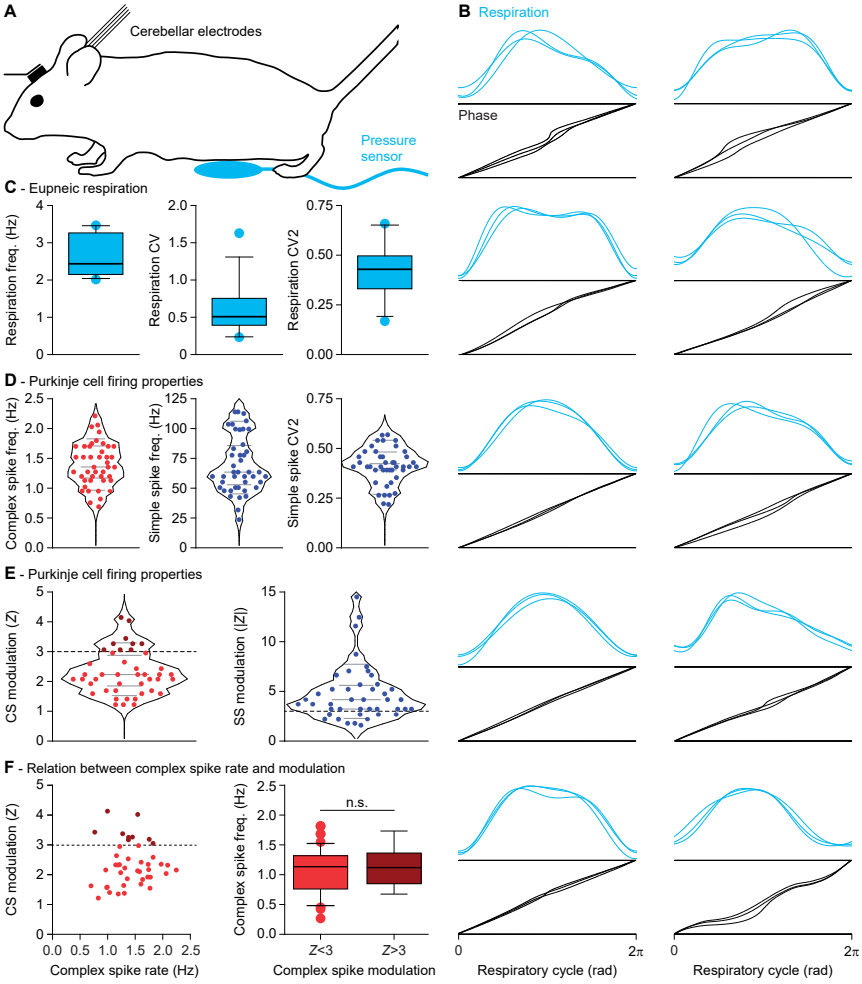


**Figure S1.** Purkinje cells in the lateral cerebellum encode eupneic breathing, Related to Fig. 1

**A** Single-unit recordings of Purkinje cells were made in the lobules simplex, crus 1 and 2 of awake, head-fixed mice during quiet, unperturbed (eupneic) respiration. **B** The pressure on the abdominal sensor was used as the raw respiratory signal (cyan). As the course and duration of each cycle could be quite variable, we used a phase transform (black) to obtain the instantaneous phase at each moment of the respiratory cycle. For ten mice, we show here three overlaid randomly selected cycles (during unperturbed breathing) with underneath it the three phase transforms. The three parts of the cycle, inspiration (starting at phase 0), post-inspiration and expiration can be seen in most traces. **C** Frequency, coefficient of variation (CV) and mean local coefficient of variation (CV2) of eupneic respiration in 13 mice. **D** The average complex spike (CS) and simple spike (SS) frequencies as well as the mean local coefficient of variation (CV2) of the simple spikes of 43 Purkinje cells recorded during eupneic respiration. **E** Violin plots indicating the distributions of the maximal (absolute) complex spike and simple spike modulation for each Purkinje cell during the respiratory cycle. The firing rate modulation is expressed as Z score related to the bootstrap analysis. Responses exceeding a $Z$ score of 3 ($p < 0.01$) were considered to be statistically significant, but it is clear that most Purkinje cells show at least some degree of modulation and any clear separation between modulating and non-modulating Purkinje cells would be subjective. Gray lines in the violin plots indicate 10$^{th}$, 25$^{th}$, 50$^{th}$, 75$^{th}$ and 90$^{th}$ percentiles. **F** There was no significant correlation between the complex spike rate and the depth of the complex spike modulation during the respiratory cycle (r = 0.133, $p$ = 0.396, Spearman rank correlation test; left). In line with this, the complex spike firing rates of Purkinje cells with weak ($Z$<3) or strong ($Z$>3) complex spike modulation were similar ($U$ = 148, $p$ = 0.895, Mann-Whitney test).

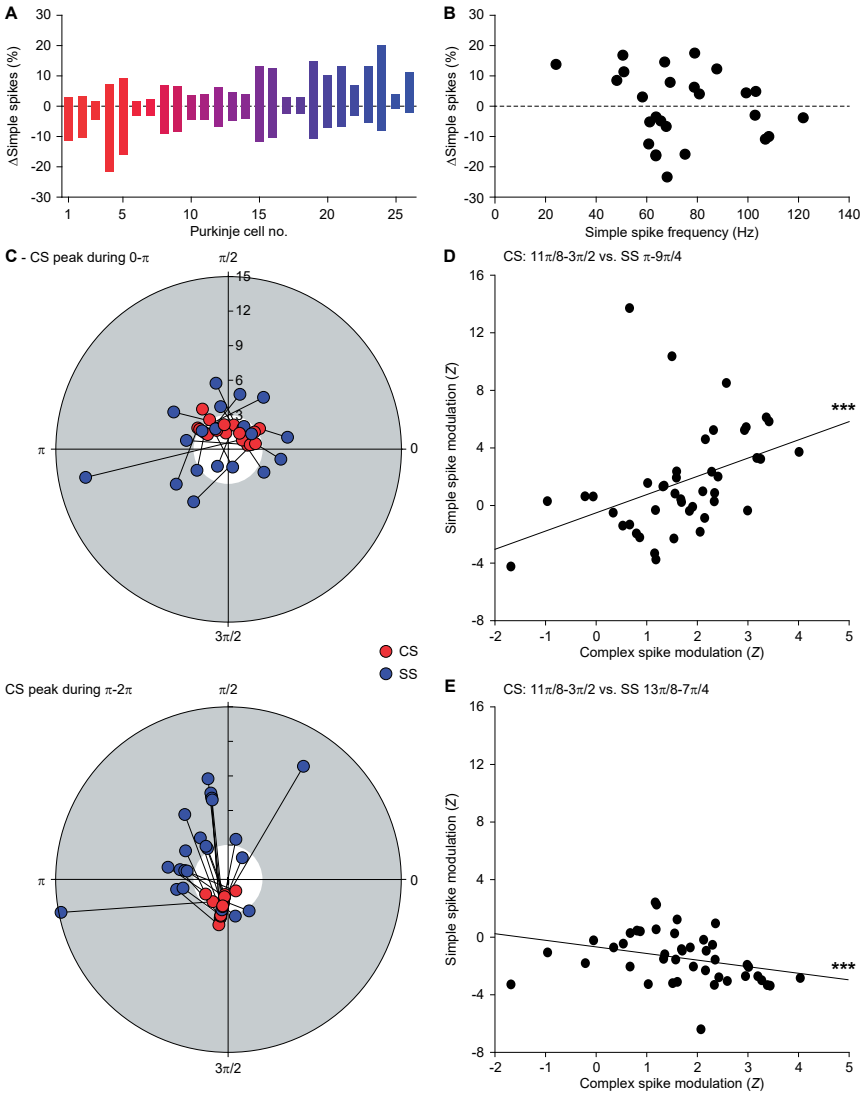


**Figure S2.** Complex spike and simple spike modulation occur during distinct phases of the respiratory cycle, Related to Fig. 2

**A** Maximal increase and decrease in simple spike firing in response to air puff stimulation per Purkinje cell. The cells are sorted based upon their bias towards decreased (left) of increased (right) simple spike firing. The Purkinje cells have the same color code as in Fig. 2C. **B** No correlation between average firing rate and maximal modulation in simple spikes (r = -0.14, $p$ = 0.487, Spearman rank correlation test). **C** Polar plot showing, for each Purkinje cell, the relation between the phase of maximal complex spike (red) and that of the strongest simple spike (blue) modulation during unperturbed respiration. The radial axis indicates the modulation strength (in absolute $Z$ score). The grey area indicates $|Z| > 3$. The neurons are separated based on the occurrence of the peak complex spike modulation during the first (top) or second half (bottom) of the respiratory cycle. **D** There was a positive correlation between the rate of simple spike firing around the transition between inspiration and post-inspiration (~π) and the occurrences of complex spikes during the transition from post-inspiration to expiration (~3 π/2) (r = 0.54, $p$ < 0.001, Spearman rank correlation). **E** Likewise, there was a negative correlation between complex spike firing around the transition from post-inspiration to expiration and the simple spike rate during expiration (~7π/4) (r = -0.43, $p$ = 0.004, Spearman rank correlation).

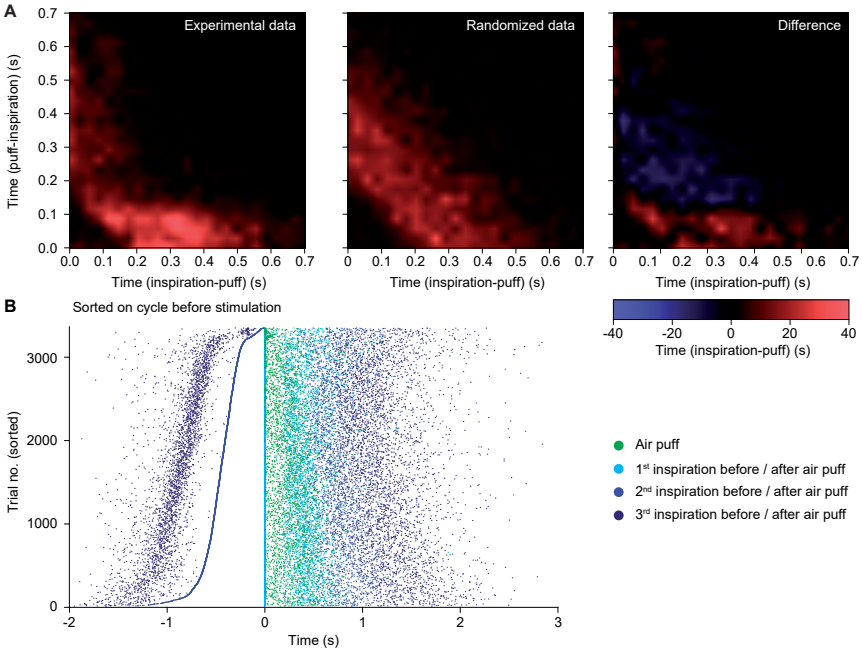


**Figure S3.** Whisker pad stimulation triggers inspiration, Related to Fig. 3

**A** Heat maps showing the distributions of the intervals between whisker pad stimulation and the start of the next inspiration (x axis) and the intervals between the start of the preceding inspiration and the whisker pad stimulation (y axis). The recorded data were compared to data were the times of the inspiration were randomly shuffled (cf. Fig. 3E-F). In the randomized data (middle), there is a clear symmetry between the time interval between the onset of inspiration and that of the stimulus ("inspiration - puff") and the time interval from stimulus onset to the start of the next inspiration ("puff - inspiration"). This symmetry is broken in the experimental data (left), showing a tendency to start the next inspiration within 100 ms of the stimulus (right). **B** Whisker pad air puff stimulation affected the timing of the subsequent inhalations, but the mice did not entrain their respiration on the fixed frequency of the air puff stimulation. This becomes clear from the raster plot showing the timing of the start of inspiration around the moment of air puff stimulation. The raster plot is constructed by combining trials from 12 mice, sorted on the duration of the cycle prior to the air puff stimulation.

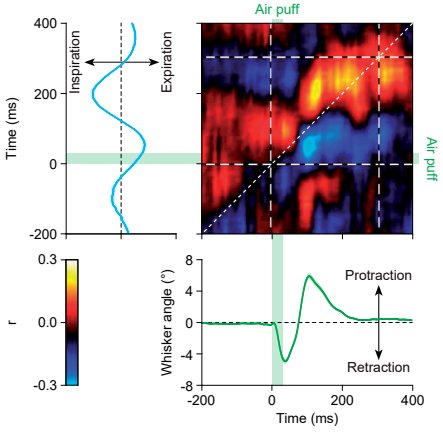


**Figure S4.** Accelerated inspiration follows reflexive whisker protraction, Related to Fig. 3

Air puff stimulation of the whisker pad induces a reflexive protraction of the facial whiskers that follows an initial, largely passive backwards movement (green trace, bottom). The same sensory stimulus also accelerates inspiration (cyan trace, left). Trial-by-trial variance analysis indicates that the execution of both behaviors is correlated: whisker protraction is linked with a delay to inspiration. The heat map and the traces are the averages of the 11 mice for which whisker data, of 100 trials per mouse, were available (shaded areas: SEM).

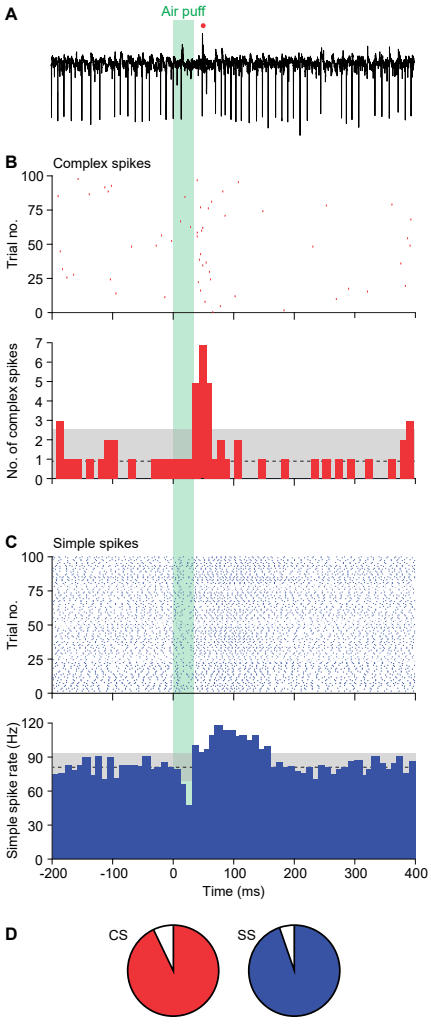


**Figure S5.** Purkinje cells respond to whisker pad air puff stimulation, Related to Fig. 4

**A** Extracellular recording of a representative Purkinje cell in crus 1 during air puff stimulation of the ipsilateral whisker pad. Of this same cell, raster plots and peri-stimulus time histograms of the complex spikes (**B**) and simple spikes (**C**) were made. Note the bidirectional modulation of the simple spikes. **D** Of the 57 recorded Purkinje cells, 53 (93%) responded with a statistically significant complex spike response to the whisker pad air puff. For the simple spikes, this number was 54 (95%).

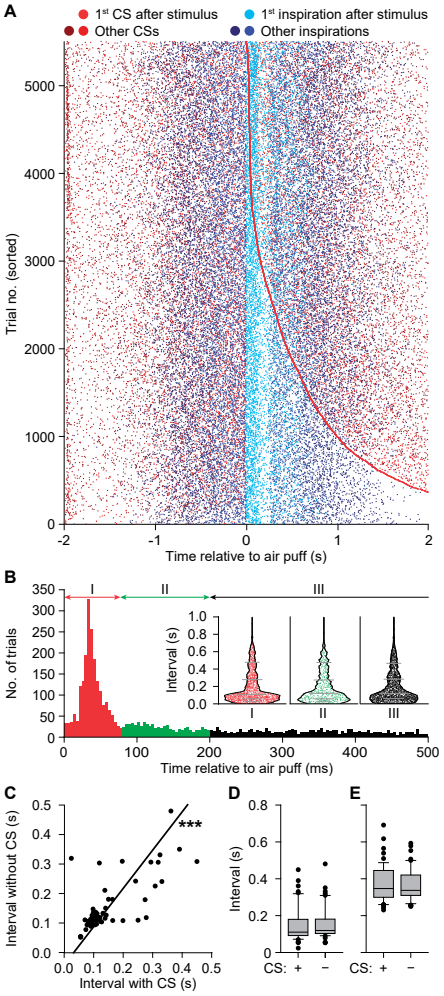


**Figure S6.** Complex spikes do not mediate the accelerated inspiration after whisker pad stimulation, Related to Fig. 4

**A** Air puff stimulation of the whisker pad triggers both complex spike firing (red dots) and accelerated inspiration (cyan dots). This raster plot shows the pooled trials of the 12 mice ordered on the interval between the start of the stimulus and the first complex spike afterwards. **B** Histogram of complex spikes during the first 500 ms after the air puff, composed of the data shown in **A**. The initial peak response occurs within 78 ms. Inset: Violin plots showing that the timing of the first inspiration after the air puff is not depending on the moment of complex spike firing. Left: trials with a complex spike between 0 and 78 ms after the air puff; middle: 78-200 ms; right: 200-500 ms. $p = 0.560$, KW = 1.158, Kruskal-Wallis test. **C** Scatter plot showing, for each Purkinje cell, the median interval between air puff and start of the next inspiration for trials with and without a complex spike within 78 ms of the air puff. The strong correlation demonstrates a lack of impact of complex spike firing on the start of the next inspiration (r = 0.693, $p < 0.001$, Spearman rank correlation). **D** Box plots of the intervals between the air puff and the start of the next inspiration in trials with and without a complex spike during the first 78 ms after the air puff ($p = 0.148$, Mann-Whitney test). **E** The same for the second respiratory interval after the air puff ($p = 0.302$, Mann-Whitney test).

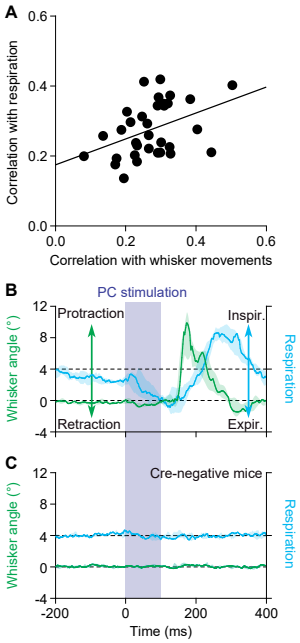


**Figure S7.** Purkinje cell stimulation alters both respiratory timing and whisker movements, Related to Fig. 5 and Fig. 7

**A** Based upon the trial-by-trial variations (see Fig. 5C-D), we calculated the maximal correlation between fluctuations in simple spike frequency and those in whisker position (x axis) and that between fluctuations in simple spike frequency and in inspiration (y axis). The maximal correlations were taken along the 45° line (see Fig. 5C-D). There appeared to be a positive correlation between these two correlations (r = 0.44, $p$ = 0.010, Spearman rank correlation), implying that the stronger Purkinje cell simple spike activity was correlated with whisker movement, the stronger the correlation of simple spikes from the same Purkinje with inspiration. Time course of whisker movements (green) and respiration (blue) recorded simultaneously upon optogenetic stimulation of Purkinje cells in mice expressing ChR2 exclusively in their Purkinje cells (**B**, $n$ = 13) and in Cre-negative mice that do not express the ChR2 protein (**C**, $n$ = 5).

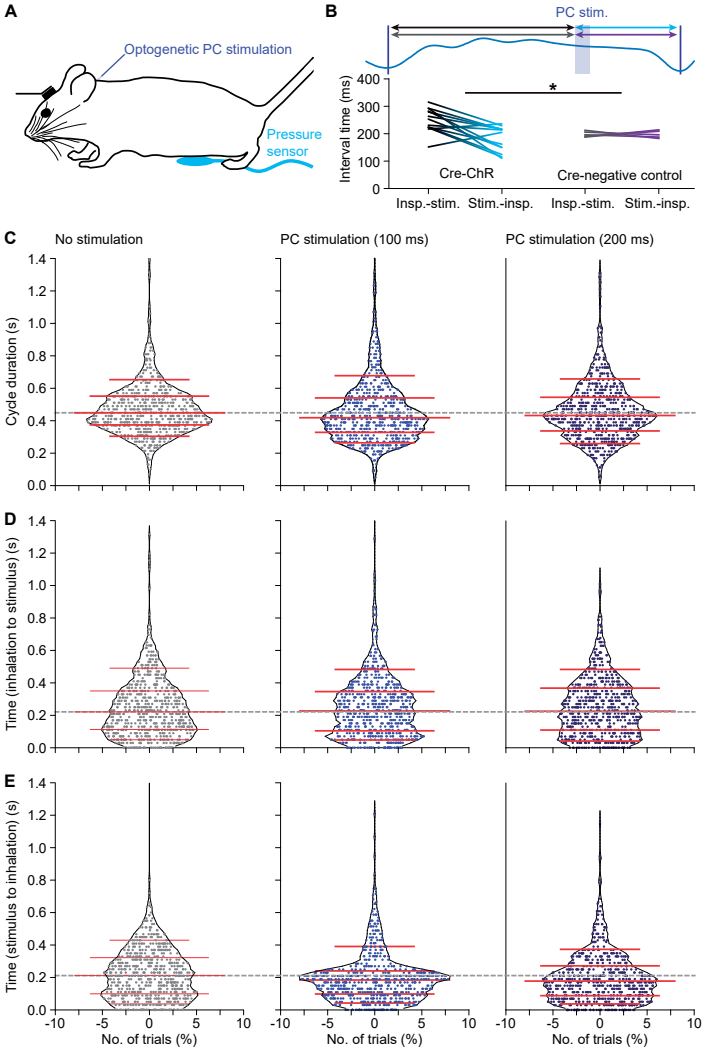


**Figure S8.** Purkinje cell stimulation affects respiratory timing, Related to Fig. 7

**A** The impact of optogenetic stimulation on respiratory timing was studied using transgenic mice expressing ChR2 exclusively in their Purkinje cells and control mice (Cre-negative mice not expressing ChR2 protein). **B** The impact of the light stimulation was different between the ChR2 and control mice ($p$ = 0.030, $F$ = 5.686, df = 1, two-way ANOVA, interaction optogenetic stimulation*genotype). Violin plots showing the duration of the respiratory cycle during which the stimulus was given (**C**), the interval between the start of inspiration to that of the stimulus (**D**) and the interval between the start of stimulation and that of the next inspiration (**E**). Left column: 100 ms stimulation, right column: 200 ms stimulation. The horizontal lines indicate the 10$^{th}$, 25$^{th}$, 50$^{th}$, 75$^{th}$ and 90$^{th}$ percentiles.

**KEY RESOURCES TABLE**

| REAGENT or RESOURCE | SOURCE | IDENTIFIER |
|---|---|---|
| Antibodies | | |
| n/a | | |
| Bacterial and Virus Strains | | |
| n/a | | |
| Biological Samples | | |
| n/a | | |
| Chemicals, Peptides, and Recombinant Proteins | | |
| Optibond adhesive | Kerr Corporation | 33381E |
| Isoflurane | Pharmachemie | 45.112.110 |
| Rimadyl | Pfizer | CAS 53716-49-7 |
| Lidocaine | Braun | RVG 07831 |
| Buprenorphine | Reckitt Benckiser Pharmaceuticals | RVG 08725 |
| Bupivacaine | Actavis | RVG 20949 |
| Critical Commercial Assays | | |
| n/a | | |
| Deposited Data | | |
| n/a | | |
| Experimental Models: Cell Lines | | |
| n/a | | |
| Experimental Models: Organisms/Strains | | |
| C57BL/6J mice | Charles River | IMSR_JAX:000664 |
| *Tg(Pcp2-cre)2Mpin;Gt(ROSA)26Sor*$^{tm27.1(CAG-OP4*H134R/tdTomato)Hze}$ | (Witter et al., 2013) | |
| *Tg(Pcp2-cre)2Mpin;Gria3*$^{tm2Rsp}$ | (Gutierrez-Castellanos et al., 2017) | |
| Oligonucleotides | | |
| n/a | | |
| Recombinant DNA | | |
| n/a | | |
| Software and Algorithms | | |
| MATLAB | MathWorks | |
| SpikeTrain | Neurasmus | |
| BIOTACT Whisker Tracking Tool | http://bwtt.sourceforge.net | |
| Custom whisker tracking code | https://github.com/MRIO/BWTT_PP | |
| Other | | |
| n/a | | |

## REFERENCES

Aliverti, A., Cala, S.J., Duranti, R., Ferrigno, G., Kenyon, C.M., Pedotti, A., Scano, G., Sliwinski, P., Macklem, P.T., and Yan, S. (1997). Human respiratory muscle actions and control during exercise. J Appl Physiol (1985) 83, 1256-1269.

Anderson, T.M., and Ramirez, J.M. (2017). Respiratory rhythm generation: triple oscillator hypothesis. F1000Res 6, 139.

Arnone, G.D., Esfahani, D.R., Wonais, M., Kumar, P., Scheer, J.K., Alaraj, A., Amin-Hanjani, S., Charbel, F.T., and Mehta, A.I. (2017). Surgery for cerebellar hemorrhage: a national surgical quality improvement program database analysis of patient outcomes and factors associated with 30-day mortality and prolonged ventilation. World Neurosurg 106, 543-550.

Badura, A., Schonewille, M., Voges, K., Galliano, E., Renier, N., Gao, Z., Witter, L., Hoebeek, F.E., Chedotal, A., and De Zeeuw, C.I. (2013). Climbing fiber input shapes reciprocity of Purkinje cell firing. Neuron 78, 700-713.

Bakker, M., Allum, J.H., Visser, J.E., Gruneberg, C., van de Warrenburg, B.P., Kremer, B.H., and Bloem, B.R. (2006). Postural responses to multidirectional stance perturbations in cerebellar ataxia. Experimental neurology 202, 21-35.

Bellavance, M.A., Takatoh, J., Lu, J., Demers, M., Kleinfeld, D., Wang, F., and Deschênes, M. (2017). Parallel inhibitory and excitatory trigemino-facial feedback circuitry for reflexive vibrissa movement. Neuron 95, 673-682.

Bianchi, A.L., and Gestreau, C. (2009). The brainstem respiratory network: an overview of a half century of research. Respir Physiol Neurobiol 168, 4-12.

Bosman, L.W.J., Koekkoek, S.K.E., Shapiro, J., Rijken, B.F.M., Zandstra, F., van der Ende, B., Owens, C.B., Potters, J.W., de Gruijl, J.R., Ruigrok, T.J.H., and De Zeeuw, C.I. (2010). Encoding of whisker input by cerebellar Purkinje cells. J Physiol 588, 3757-3783.

Brown, S.T., and Raman, I.M. (2018). Sensorimotor integration and amplification of reflexive whisking by well-timed spiking in the cerebellar corticonuclear circuit. Neuron 99, 564-575.

Caliandro, P., Iacovelli, C., Conte, C., Simbolotti, C., Rossini, P.M., Padua, L., Casali, C., Pierelli, F., Reale, G., and Serrao, M. (2017). Trunk-lower limb coordination pattern during gait in patients with ataxia. Gait & posture 57, 252-257.

Cao, Y., Maran, S.K., Dhamala, M., Jaeger, D., and Heck, D.H. (2012). Behavior-related pauses in simple-spike activity of mouse Purkinje cells are linked to spike rate modulation. J Neurosci 32, 8678-8685.

Chaumont, J., Guyon, N., Valera, A.M., Dugué, G.P., Popa, D., Marcaggi, P., Gautheron, V., Reibel-Foisset, S., Dieudonné, S., Stephan, A., et al. (2013). Clusters of cerebellar Purkinje cells control their afferent climbing fiber discharge. Proc Natl Acad Sci U S A 110, 16223-16228.

Chen, M.L., Witmans, M.B., Tablizo, M.A., Jubran, R.F., Turkel, S.B., Tavaré, C.J., and Keens, T.G. (2005). Disordered respiratory control in children with partial cerebellar resections. Pediatr Pulmonol 40, 88-91.

Chen, S., Augustine, G.J., and Chadderton, P. (2016). The cerebellum linearly encodes whisker position during voluntary movement. Elife 5, e10509.

Coesmans, M., Weber, J.T., De Zeeuw, C.I., and Hansel, C. (2004). Bidirectional parallel fiber plasticity in the cerebellum under climbing fiber control. Neuron 44, 691-700.

Cortez, S.C., and Kinney, H.C. (1996). Brainstem tegmental necrosis and olivary hypoplasia: a lethal entity associated with congenital apnea. J Neuropathol Exp Neurol 55, 841-849.

Critchley, H.D., Nicotra, A., Chiesa, P.A., Nagai, Y., Gray, M.A., Minati, L., and Bernardi, L. (2015). Slow breathing and hypoxic challenge: cardiorespiratory consequences and their central neural substrates. PLoS One 10, e0127082.

Cruz-Sánchez, F.F., Lucena, J., Ascaso, C., Tolosa, E., Quintò, L., and Rossi, M.L. (1997). Cerebellar cortex delayed maturation in sudden infant death syndrome. J Neuropathol Exp Neurol 56, 340-346.

Darmohray, D.M., Jacobs, J.R., Marques, H.G., and Carey, M.R. (2019). Spatial and temporal locomotor learning in mouse cerebellum. Neuron 102, 217-231 e214.

De Joanna, G., De Rosa, A., Salvatore, E., Castaldo, I., De Luca, N., Izzo, R., Manzo, V., Filla, A., and De Michele, G. (2008). Autonomic nervous system abnormalities in spinocerebellar ataxia type 2: a cardiovascular neurophysiologic study. J Neurol Sci 275, 60-63.

De Zeeuw, C.I., Hoebeek, F.E., Bosman, L.W.J., Schonewille, M., Witter, L., and Koekkoek, S.K. (2011). Spatiotemporal firing patterns in the cerebellum. Nat Rev Neurosci 12, 327-344.

De Zeeuw, C.I., and Ten Brinke, M.M. (2015). Motor learning and the cerebellum. Cold Spring Harb Perspect Biol 7, a021683.

Deger, K., Ziegler, W., and Wessel, K. (1999). Airflow tracking in patients with ataxic disorders. Clin Linguist & Phonet 13, 433-447.

Desrochers, E., Harnie, J., Doelman, A., Hurteau, M.F., and Frigon, A. (2019). Spinal control of muscle synergies for adult mammalian locomotion. J Physiol 597, 333-350.

Dobbins, E.G., and Feldman, J.L. (1994). Brainstem network controlling descending drive to phrenic motoneurons in rat. J Comp Neurol 347, 64-86.

Dutschmann, M., and Paton, J.F.R. (2002). Inhibitory synaptic mechanisms regulating upper airway patency. Respir Physiol Neurobiol 131, 57-63.

Ebert, D., Hefter, H., Dohle, C., and Freund, H.J. (1995). Ataxic breathing during alternating forearm movements of various frequencies in cerebellar patients. Neurosci Lett 193, 145-148.

Feldman, J.L., Del Negro, C.A., and Gray, P.A. (2013). Understanding the rhythm of breathing: so near, yet so far. Annual Review of Physiology 75, 423-452.

Gao, Z., Van Beugen, B.J., and De Zeeuw, C.I. (2012). Distributed synergistic plasticity and cerebellar learning. Nat Rev Neurosci 13, 619-635.

Gewaltig, M., and Diesmann, M. (2007). NEST (NEural Simulation Tool). Scholarpedia.

Gozal, D., Omidvar, O., Kirlew, K.A.T., Hathout, G.M., Hamilton, R., Lufkin, R.B., and Harper, R.M. (1995). Identification of human brain regions underlying responses to resistive inspiratory loading with functional magnetic resonance imaging. Proc Natl Acad Sci U S A 92, 6607-6611.

Gutierrez-Castellanos, N., Da Silva-Matos, C.M., Zhou, K., Canto, C.B., Renner, M.C., Koene, L.M.C., Ozyildirim, O., Sprengel, R., Kessels, H.W., and De Zeeuw, C.I. (2017). Motor learning requires Purkinje cell synaptic potentiation through activation of AMPA-receptor subunit GluA3. Neuron 93, 409-424.

Harper, R.M. (2000). Sudden infant death syndrome: a failure of compensatory cerebellar mechanisms? Pediatr Res 48, 140-142.

Harper, R.M., Kumar, R., Macey, P.M., Harper, R.K., and Ogren, J.A. (2015). Impaired neural structure and function contributing to autonomic symptoms in congenital central hypoventilation syndrome. Frontiers in neuroscience 9, 415.

Harper, R.M., Macey, P.M., Woo, M.A., Macey, K.E., Keens, T.G., Gozal, D., and Alger, J.R. (2005). Hypercapnic exposure in congenital central hypoventilation syndrome reveals CNS respiratory control mechanisms. J Neurophysiol 93, 1647-1658.

Hodges, P.W., and Gandevia, S.C. (2000). Changes in intra-abdominal pressure during postural and respiratory activation of the human diaphragm. J Appl Physiol (1985) 89, 967-976.

Holstege, G. (2014). The periaqueductal gray controls brainstem emotional motor systems including respiration. Progress in brain research 209, 379-405.

Hoogland, T.M., De Gruijl, J.R., Witter, L., Canto, C.B., and De Zeeuw, C.I. (2015). Role of synchronous activation of cerebellar Purkinje cell ensembles in multi-joint movement control. Curr Biol 25, 1157-1165.

Isaev, G., Murphy, K., Guz, A., and Adams, L. (2002). Areas of the brain concerned with ventilatory load compensation in awake man. J Physiol 539, 935-945.

Ito, M. (2000). Mechanisms of motor learning in the cerebellum. Brain Res 886, 237-245.

Jakovljevic, D.G., and McConnell, A.K. (2009). Influence of different breathing frequencies on the severity of inspiratory muscle fatigue induced by high-intensity front crawl swimming. J Strength Cond Res 23, 1169-1174.

Ju, C., Bosman, L.W.J., Hoogland, T.M., Velauthapillai, A., Murugesan, P., Warnaar, P., Negrello, M., and De Zeeuw, C.I. (2019). Neurons of the inferior olive respond to broad classes of sensory input while subject to homeostatic control. J Physiol 597, 2483-2514.

Katsetos, C.D., Anderson, C.E., Guzman, M.A., Pascasio, J.M., de Chadarévian, J.P., and Legido, A. (2014). Brainstem tegmental necrosis and olivary hypoplasia: raising awareness of a rare neuropathologic correlate of congenital apnea. Semin Pediatr Neurol 21, 177-183.

Kitazawa, S., Kimura, T., and Yin, P.B. (1998). Cerebellar complex spikes encode both destinations and errors in arm movements. Nature 392, 494-497.

Kumar, R., Macey, P.M., Woo, M.A., Alger, J.R., and Harper, R.M. (2008). Diffusion tensor imaging demonstrates brainstem and cerebellar abnormalities in congenital central hypoventilation syndrome. Pediatr Res 64, 275-280.

Kurnikova, A., Moore, J.D., Liao, S.M., Deschênes, M., and Kleinfeld, D. (2017). Coordination of orofacial motor actions into exploratory behavior by rat. Curr Biol 27, 688-696.

Lavezzi, A.M., Corna, M.F., Repetti, M.L., and Matturri, L. (2013). Cerebellar Purkinje cell vulnerability to prenatal nicotine exposure in sudden unexplained perinatal death. Folia Neuropathol 51, 290-301.

Lee, A., Chen, M.L., Abeshaus, S., Poliakov, A., and Ojemann, J.G. (2013). Posterior fossa tumors and their impact on sleep and ventilatory control: a clinical perspective. Respir Physiol Neurobiol 189, 261-271.

Lu, L., Cao, Y., Tokita, K., Heck, D.H., and Boughter, J.D., Jr. (2013). Medial cerebellar nuclear projections and activity patterns link cerebellar output to orofacial and respiratory behavior. Frontiers in neural circuits 7, 56.

Ma, Y., Geethakumari, P.R., Smaragdos, G., Lindeman, S., Romano, V., Negrello, M., Sourdis, I., Bosman, L.W.J., De Zeeuw, C.I., Al-Ars, Z., and Strydis, C. (2017). Towards real-time whisker tracking in rodents for studying sensorimotor disorders. In International Conference on Embedded Computer Systems: Architectures, Modeling, and Simulation (SAMOS), pp. 137-145.

Machado, A.S., Darmohray, D.M., Fayad, J., Marques, H.G., and Carey, M.R. (2015). A quantitative framework for whole-body coordination reveals specific deficits in freely walking ataxic mice. Elife 4.

Martino, P.F., Davis, S., Opansky, C., Krause, K., Bonis, J.M., Czerniak, S.G., Pan, L.G., Qian, B., and Forster, H.V. (2006). Lesions in the cerebellar fastigial nucleus have a small effect on the hyperpnea needed to meet the gas exchange requirements of submaximal exercise. J Appl Physiol (1985) 101, 1199-1206.

Martino, P.F., Davis, S., Opansky, C., Krause, K., Bonis, J.M., Pan, L.G., Qian, B., and Forster, H.V. (2007). The cerebellar fastigial nucleus contributes to $CO_2$-$H^+$ ventilatory sensitivity in awake goats. Respir Physiol Neurobiol 157, 242-251.

McKay, L.C., Evans, K.C., Frackowiak, R.S.J., and Corfield, D.R. (2003). Neural correlates of voluntary breathing in humans. J Appl Physiol (1985) 95, 1170-1178.

Moore, J.D., Deschênes, M., Furuta, T., Huber, D., Smear, M.C., Demers, M., and Kleinfeld, D. (2013). Hierarchy of orofacial rhythms revealed through whisking and breathing. Nature 497, 205-210.

Negrello, M., Warnaar, P., Romano, V., Owens, C.B., Lindeman, S., Iavarona, E., Spanke, J.K., Bosman, L.W.J., and De Zeeuw, C.I. (2019). Quasiperiodic rhythms of the inferior olive. PLoS Comput Biol 15, e1006475.

Owens, C.B., de Boer, C., Gennari, G., Broersen, R., Pel, J.J., Miller, B., Clapp, W., van der Werf, Y.D., and De Zeeuw, C.I. (2018). Early trajectory prediction in elite athletes. Cerebellum 17, 766-776.

Park, B., Palomares, J.A., Woo, M.A., Kang, D.W., Macey, P.M., Yan-Go, F.L., Harper, R.M., and Kumar, R. (2016). Disrupted functional brain network organization in patients with obstructive sleep apnea. Brain Behav 6, e00441.

Parsons, L.M., Egan, G., Liotti, M., Brannan, S., Denton, D., Shade, R., Robillard, R., Madden, L., Abplanalp, B., and Fox, P.T. (2001). Neuroimaging evidence implicating cerebellum in the experience of hypercapnia and hunger for air. Proc Natl Acad Sci U S A 98, 2041-2046.

Perkon, I., Kosir, A., Itskov, P.M., Tasic, J., and Diamond, M.E. (2011). Unsupervised quantification of whisking and head movement in freely moving rodents. J Neurophysiol 105, 1950-1962.

Proville, R.D., Spolidoro, M., Guyon, N., Dugué, G.P., Selimi, F., Isope, P., Popa, D., and Léna, C. (2014). Cerebellum involvement in cortical sensorimotor circuits for the control of voluntary movements. Nat Neurosci 17, 1233-1239.

Rahmati, N., Owens, C.B., Bosman, L.W.J., Spanke, J.K., Lindeman, S., Gong, W., Potters, J.W., Romano, V., Voges, K., Moscato, L., et al. (2014). Cerebellar potentiation and learning a whisker-based object localization task with a time response window. J Neurosci 34, 1949-1962.

Ramirez, J.M., Koch, H., Garcia, A.J., 3rd, Doi, A., and Zanella, S. (2011). The role of spiking and bursting pacemakers in the neuronal control of breathing. J Biol Phys 37, 241-261.

Raux, M., Tyvaert, L., Ferreira, M., Kindler, F., Bardinet, E., Karachi, C., Morelot-Panzini, C., Gotman, J., Pike, G.B., Koski, L., and Similowski, T. (2013). Functional magnetic resonance imaging suggests automatization of the cortical response to inspiratory threshold loading in humans. Respir Physiol Neurobiol 189, 571-580.

Richter, D.W., and Smith, J.C. (2014). Respiratory rhythm generation *in vivo*. Physiology (Bethesda) 29, 58-71.

Rimmer, K.P., Ford, G.T., and Whitelaw, W.A. (1995). Interaction between postural and respiratory control of human intercostal muscles. J Appl Physiol (1985) 79, 1556-1561.

Romano, V., De Propris, L., Bosman, L.W.J., Warnaar, P., ten Brinke, M.M., Lindeman, S., Ju, C., Velauthapillai, A., Spanke, J.K., Middendorp Guerra, E., et al. (2018). Potentiation of cerebellar Purkinje cells facilitates whisker reflex adaptation through increased simple spike activity. eLife 7, e38852.

Shambes, G.M., Gibson, J.M., and Welker, W. (1978). Fractured somatotopy in granule cell tactile areas of rat cerebellar hemispheres revealed by micromapping. Brain Behav Evol 15, 94-140.

Smith, J.C., Ellenberger, H.H., Ballanyi, K., Richter, D.W., and Feldman, J.L. (1991). Pre-Bötzinger complex: a brainstem region that may generate respiratory rhythm in mammals. Science 254, 726-729.

Suvrathan, A., Payne, H.L., and Raymond, J.L. (2016). Timing rules for synaptic plasticity matched to behavioral function. Neuron 92, 959-967.

Talpalar, A.E., Bouvier, J., Borgius, L., Fortin, G., Pierani, A., and Kiehn, O. (2013). Dual-mode operation of neuronal networks involved in left-right alternation. Nature 500, 85-88.

Ten Brinke, M.M., Boele, H.J., Spanke, J.K., Potters, J.W., Kornysheva, K., Wulff, P., IJpelaar, A.C.H.G., Koekkoek, S.K.E., and De Zeeuw, C.I. (2015). Evolving models of Pavlovian conditioning: cerebellar cortical dynamics in awake behaving mice. Cell Rep 13, 1977-1988.

Teune, T.M., van der Burg, J., van der Moer, J., Voogd, J., and Ruigrok, T.J. (2000). Topography of cerebellar nuclear projections to the brain stem in the rat. Progress in brain research 124, 141-172.

Thach, W.T., Perry, J.G., Kane, S.A., and Goodkin, H.P. (1993). Cerebellar nuclei: rapid alternating movement, motor somatotopy, and a mechanism for the control of muscle synergy. Revue Neurologique 149, 607-628.

Timmann, D., Watts, S., and Hore, J. (2000). Causes of left-right ball inaccuracy in overarm throws made by cerebellar patients. Exp Brain Res 130, 441-452.

Tomori, Z., and Widdicombe, J.G. (1969). Muscular, bronchomotor and cardiovascular reflexes elicited by mechanical stimulation of the respiratory tract. J Physiol 200, 25-49.

Tresch, M.C., Saltiel, P., and Bizzi, E. (1999). The construction of movement by the spinal cord. Nat Neurosci 2, 162-167.

Tsitsopoulos, P.P., Tobieson, L., Enblad, P., and Marklund, N. (2012). Prognostic factors and long-term outcome following surgical treatment of 76 patients with spontaneous cerebellar haematoma. Acta Neurochir (Wien) 154, 1189-1195.

Vinueza Veloz, M.F., Zhou, K., Bosman, L.W.J., Potters, J.W., Negrello, M., Seepers, R.M., Strydis, C., Koekkoek, S.K.E., and De Zeeuw, C.I. (2015). Cerebellar control of gait and interlimb coordination. Brain structure & function 220, 3513-3536.

Wang, S.S.H., Denk, W., and Häusser, M. (2000). Coincidence detection in single dendritic spines mediated by calcium release. Nat Neurosci 3, 1266-1273.

Welker, W.I. (1964). Analysis of sniffing of the albino rat. Behaviour 22, 223-244.

Witter, L., Canto, C.B., Hoogland, T.M., de Gruijl, J.R., and De Zeeuw, C.I. (2013). Strength and timing of motor responses mediated by rebound firing in the cerebellar nuclei after Purkinje cell activation. Frontiers in neural circuits 7, 133.

Xu, F., and Frazier, D.T. (2000). Modulation of respiratory motor output by cerebellar deep nuclei in the rat. J Appl Physiol (1985) 89, 996-1004.

Xu, F., Frazier, D.T., Zhang, Z., Baekey, D.M., and Shannon, R. (1997). Cerebellar modulation of cough motor pattern in cats. J Appl Physiol (1985) 83, 391-397.

Xu, F., Zhang, Z., and Frazier, D.T. (2001). Microinjection of acetazolamide into the fastigial nucleus augments respiratory output in the rat. J Appl Physiol (1985) 91, 2342-2350.

# 6

# Cerebellar Purkinje cells can differentially modulate coherence between sensory and motor cortex depending on region and behavior

Sander Lindeman[1,5], Lieke Kros[1,5], Sungho Hong[2], Jorge F. Mejias[3], Vincenzo Romano[1], Mario Negrello[1]*, Laurens W.J. Bosman[1]* and Chris I. De Zeeuw[1,4]

[1]Department of Neuroscience, Erasmus MC, 3015 GE Rotterdam, the Netherlands
[2]Computational Neuroscience Unit, Okinawa Institute of Science and Technology, 1919-1 Tancha, Okinawa 904-0495, Japan
[3]Swammerdam Institute for Life Science, University of Amsterdam, 1090 GE Amsterdam, the Netherlands
[4]Netherlands Institute for Neuroscience, Royal Academy of Arts and Sciences, 1105 BA Amsterdam, the Netherlands
[5]These authors contributed equally
*Correspondence to Laurens Bosman, Department of Neuroscience, Erasmus MC, PO Box 2040, 3000 CA Rotterdam, The Netherlands, Email: l.bosman@erasmusmc.nl;
or to Mario Negrello, Department of Neuroscience, Erasmus MC, PO Box 2040, 3000 CA Rotterdam, The Netherlands, Email: m.negrello@erasmusmc.nl

## ABSTRACT

Coherence among sensory and motor cortices is indicative of binding of critical functions in perception, motor planning, action and sleep. Evidence is emerging that the cerebellum can impose coherence between cortical areas, but how and when it does so is unclear. Here, we studied coherence between primary somatosensory (S1) and motor (M1) cortices during sensory stimulation of the whiskers in the presence and absence of optogenetic stimulation of cerebellar Purkinje cells in awake mice. Purkinje cell activation enhanced and reduced sensory-induced S1-M1 coherence in the theta and gamma bands, respectively. This impact only occurred when Purkinje cell stimulation was given simultaneously with sensory stimulation; a 20 ms delay was sufficient to alleviate its impact, suggesting the existence of a fast, cerebellar sensory pathway to S1 and M1. The suppression of gamma band coherence upon Purkinje cell stimulation was significantly stronger during trials with relatively large whisker movements, whereas the theta band changes did not show this correlation. In line with the anatomical distribution of the simple spike and complex spike responses to whisker stimulation, this suppression also occurred following focal stimulation of medial crus 2, but not of lateral crus 1. Granger causality analyses and computational modeling of the involved networks suggest that Purkinje cells control S1-M1 coherence most prominently via the ventrolateral thalamus and M1. Our results indicate that coherences between sensory and motor cortices in different frequency ranges can be dynamically modulated by cerebellar input, and that the modulation depends on the behavioral context and is site-specific.

### Keywords

Cerebellum, cerebral cortex, whisker system, laminar model, LFP

### Author Contributions

S.L., S.H., J.F.M., M.N., L.W.J.B. and C.I.D.Z. designed research; J.F.M. designed and executed computational model, S.L., L.K., V.R. and L.W.J.B. performed biological experiments; S.L., L.K., S.H., J.F.M., V.R., M.N., L.W.J.B. and C.I.D.Z. analyzed data; S.L., L.W.J.B. and C.I.D.Z. wrote the paper with contributions from all authors.

### Significance Statement

Coherent activity between sensory and motor areas is essential in sensorimotor integration. We show here that the cerebellum can differentially affect cortical theta and gamma band coherences evoked by whisker stimulation via a fast ascending and predictive pathway. In line with the functional heterogeneity of its modular organization, the impact of the cerebellum is region-specific and tuned to ongoing motor responses. These data highlight site-specific and context-dependent interactions between the cerebellum and the cerebral cortex that can come into play during a plethora of sensorimotor functions.

## INTRODUCTION

Coherent oscillations can bind different brain areas by affecting susceptibility of neurons to synaptic input and providing a timing mechanism for generating a common dynamical frame for cortical operations (1, 2). For example, coherence can create a temporal framework for concerted neural activity that facilitates integration of the activity of sensory and motor areas (3-5). Online integration is particularly relevant, when animals, including ourselves, explore their environment via active touch, requiring sensory input to be directly related to the momentary position and movement of eyes, fingertips, antennae, whiskers or other organs (6-8).

Coherence often occurs in specific frequency bands that can be associated with different functions. In the field of sensorimotor integration, skilled movements rely on intercortical coherence between sensory and motor areas that occur in the theta (4-8 Hz) range during force generation, while coherence at higher bands is engaged during the preparation thereof (9). Likewise, within the field of visual perception, coherence in the alpha (8-12 Hz) and gamma (30-100 Hz) bands have been found to contribute to feedback and feedforward processing, respectively (10, 11).



The appearance of coherence among different cortical regions implicates reciprocal connections between neurons distributed among different layers within the cerebral cortex (12-16) as well as inputs from subcortical structures like the thalamus (17-20) (Fig. 1A). Accordingly, one of the main inputs to the thalamus, i.e., the cerebellum, has a strong impact in organizing cortico-cortical coherence (21-23). Indeed, disruption of cerebellar function, whether inflicted pharmacologically in rats (22) or due to stroke in patients (21), affects cortico-cortical coherence.

Even though the impact of cerebellar activity on cortical coherence is well established (22, 24, 25), it remains to be elucidated to what extent and how the cerebellum can differentially influence different frequency bands, to what extent such potentially different impacts depend on the behavioral context, and whether these differential effects are mediated through different cerebellar modules (26-28). Here, we set out to address these questions by investigating the impact of Purkinje cell activity on coherence between the whisker areas of the primary somatosensory (wS1) and motor cortex (wM1) during stimulation of the whiskers in awake behaving mice. When we stimulated Purkinje cells optogenetically at different intervals with respect to air puff stimulation of the whiskers, we observed that these main output neurons differentially contribute to wS1-wM1 theta and gamma band coherences with opposite effects, depending on ongoing behavior and their precise site in the cerebellar hemispheres.

## RESULTS

### Purkinje cell stimulation modulates sensory responses in wS1 and wM1

Whisker stimulation triggers fast responses in wS1 and wM1 (29-31) as well as in the cerebellar cortex (28, 32, 33). Before studying the impact of cerebellar stimulation on the cortical coherence between wS1 and wM1, we first needed to determine to what extent the individual cortical responses within wS1 and wM1 depended on cerebellar activity.

Thereto, we compared local field potentials (LFPs) in wS1 during whisker stimulation in the absence or presence of optogenetic stimulation of Purkinje cells in the crus 1 and crus 2 area (Figs. 1B, S1). Air puffs applied to the whiskers evoked canonical LFP responses in wS1 in that they induced an initial fast decrease, first in layer IV and then also in the superficial and deep layers, followed by increased LFP signals (Figs. 1C, S2A, S3A). Decreases in LFP signal have been suggested to correspond with increased neuronal excitation (34), returned to baseline after roughly 200 ms.

Given the strong and direct trigemino-thalamo-cortical pathways (8, 35), a significant impact of Purkinje cell stimulation during whisker stimulation on the initial response in the input layer of wS1 would not be expected. Indeed, this was not the case ($p$ = 0.197, Fig. S4A; see Table S1 for details on statistical analysis). However, the spread of excitation to the deeper layers was enhanced by Purkinje cell stimulation ($p$ = 0.012, Fig. S4A). Likewise, Purkinje cell stimulation reduced the positive LFP peak in the deeper layers ($p$ = 0.024, Figs. 1E-F, S2A, S3A). Both effects were not observed when we postponed the Purkinje cell stimulation 20 ms relative to the whisker stimulation (Figs. 1G-H, S2A, S3A, S4A, Table S1). When we, as a control, stimulated the Purkinje cells in the absence of sensory stimulation, we observed that this induced a near-complete block of the output of cerebellar nucleus neurons, followed by rebound firing at the end of the 100 ms stimulus interval (Fig. S2B). Of note, the period of silencing led to a small, but observable increase in neural activity in wS1 (negative LFP) while the rebound firing in the cerebellar nuclei correlated with decreased neural activity in wS1 (positive LFP; Fig. 1D), suggesting that the connection between cerebellar nuclei and wS1 includes at least one inhibitory hub.

Similar to wS1, wM1 did not display a significant impact of Purkinje cell stimulation on the initial wave of neural excitation following sensory stimulation (Fig. S4B, Table S1). However, the subsequent positive peak in the LFP was reduced in the deeper layers ($p$ = 0.024, Figs. 1I-L, S2A, S3B). As for wS1, this effect was abolished by a 20 ms delay between whisker and Purkinje cell simulation (Fig. 1M-N). Thus, our data indicate a fast ascending pathway via the cerebellum disinhibiting sensory responses in the deeper layers of wS1 and slightly later also in wM1.

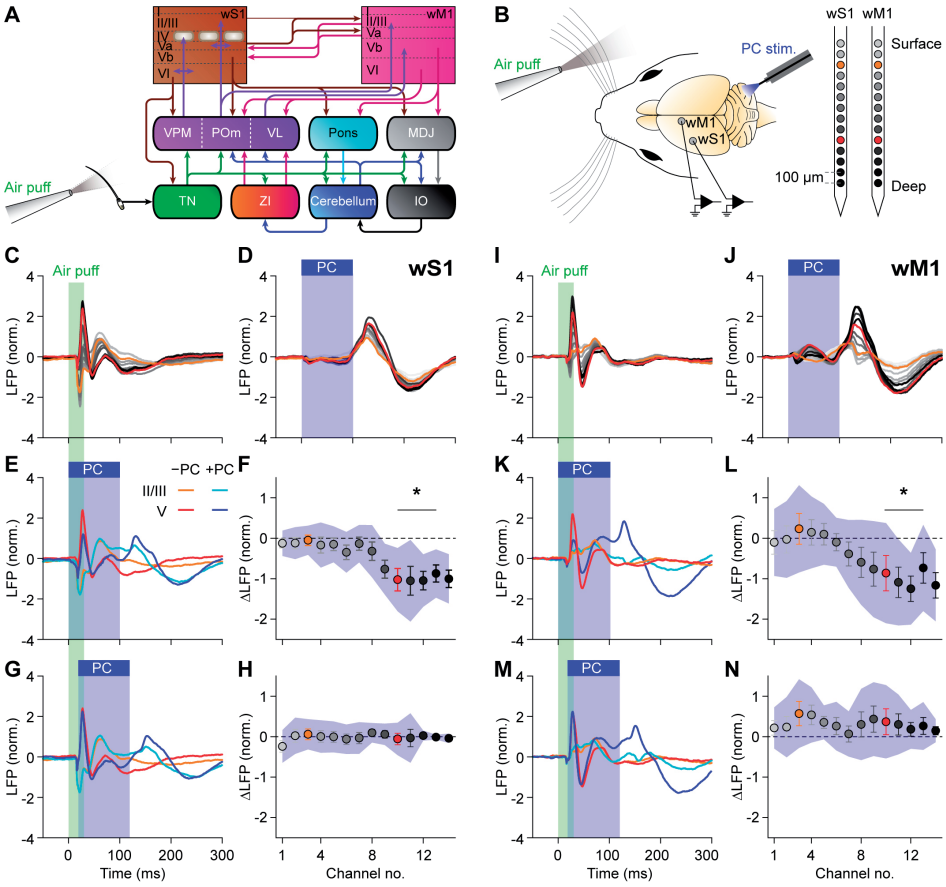


**Figure 1.** Purkinje cell stimulation disinhibits fast sensory responses in wS1 and wM1.

**A** Simplified scheme of anatomical pathways carrying whisker input to wS1, wM1 and the cerebellum, and the reciprocal cerebro-cerebral connections. IO = inferior olive; MDJ = nuclei of the mesodiencephalic junction; Pom = posterior medial nucleus; TN = trigeminal nuclei; VL = ventrolateral nucleus; VPM = ventroposterior medial nucleus; ZI = zona incerta. **B** Local field potentials (LFP) were recorded in wS1 and wM1 of awake mice using, for each area, 14 recording spots on linear silicon probes. Colors indicate their relative positions, with orange and red for the 3rd and 10th electrodes, representing the supra- and subgranular layers, respectively. Purkinje cells (PC) were stimulated optogenetically using an optic fiber with 400 µm diameter placed on the center of crus 1 (Fig. S1). **C** Whisker stimulation triggered fast responses in contralateral wS1, as illustrated by the averaged LFP traces (*n* = 100 trials per mouse, *N* = 8 mice). **D** Purkinje cell stimulation triggered delayed responses in wS1 after rebound firing in the cerebellar nuclei (Fig. S2B). **E** Comparison of the LFPs recorded during trials with whisker stimulation (orange / red) and with combined with sensory and Purkinje cell stimulation (cyan / blue). **F** During the early response period, especially the amplitude of the first positive LFP peak in the subgranular layers was affected, in addition to profound impact during later phases of sensory processing. Plotted are the averaged differences in amplitude of the first positive LFP peaks. Error bars indicate SEM and shaded area sd. **G-H** The impact of optogenetic Purkinje cell stimulation on the first positive LFP peak was largely abolished by introducing a 20 ms delay between the start of air puff sensory stimulation and the onset optogenetic Purkinje cell stimulation. **I-N** The same plots as **C-H**, but now for wM1, showing comparable impact of optogenetic Purkinje stimulation on the sensory-induced LFP signals.

## Cerebellar output differentially modulates S1-M1 coherence in theta and gamma bands

As we found cerebellar activity to be able to modulate early-phase sensory responses in both wS1 and wM1, we surmised that cerebellar activity could also affect sensory-related coherent activity between these areas. As there are particularly strong connections between the subgranular layers of wS1 and the supragranular layers of wM1 (5, 36) (Fig. 1A), we initially focused on the coherence between these layers. Air puff stimulation of the whiskers triggered a fast increase in S1-M1 coherence, particularly in the beta and lower gamma band range, and to a lesser extent in the theta range (Fig. 2). Instead, whereas sensory stimulation combined with simultaneous optogenetic Purkinje cell stimulation led to a further enhancement in the sensory-induced coherence at the theta band, the same combination prominently reduced the sensory-induced coherence at the gamma band (Fig. 2A,B,E). Both of these modifications could be alleviated by delaying the optogenetic stimulation with 20 ms relative to the onset of whisker stimulation (Fig. 2A,B,E). The fact that a 20 ms lag between sensory and Purkinje cell stimulation was sufficient to, at least in part, rescue the original amplitude of sensory-evoked signals corroborates the notion that under normal physiological circumstances cerebellar modulation of cerebral coherence is probably mediated by a fast pathway. Granger causality can measure how much of the wM1 signal in a certain frequency band is controlled by the wS1 and vice versa. Applying that analysis on the sensory-induced coherence revealed that, for the comparison of the deep layers of S1 and the superficial layers of M1, both areas were involved in generation of the coherence (Fig. 2C-D).

Examining the coherence between other cortical layers, which are probably less directly coupled (Fig. 1A), we observed that the cerebellar impact broadened, now also comprising beta and higher gamma bands (Fig. S5). Granger causality analysis revealed that the sensory-induced gamma band coherence is largely triggered by the superficial layers of wS1 and from there spreads to the deep layers of wS1 (Fig. S6A-B) and the deep layers of wM1 (Fig. S6C-D). Notably, there was more balance between the deep layers of wS1 and the superficial layers of wM1 (Figs. 2C-D and S6C-D), suggesting that sensory-induced coherence is a complex phenomenon involving reciprocal connections between wS1 and wM1. The Granger causality analysis of the Purkinje cell-induced theta band coherence did not systematically reveal a strict directionality, suggesting a reciprocal involvement of wS1 and wM1.

Thus, experimentally dampening the output of the cerebellar nuclei by enhancing Purkinje cell activity results in an array of changes in sensory-induced coherences between wS1 and wM1. Effects were detected in all layers, but the most specific and reproducible changes were revealed in the comparison between theta and gamma coherence across wS1 and wM1.

## Cerebellar impact on S1-M1 coherence depends on behavioral context

Air puff stimulation of the whiskers triggers reflexive protraction, the amplitude of which is correlated to cerebellar activity (28, 33). This suggests an interaction between cerebellar activ-

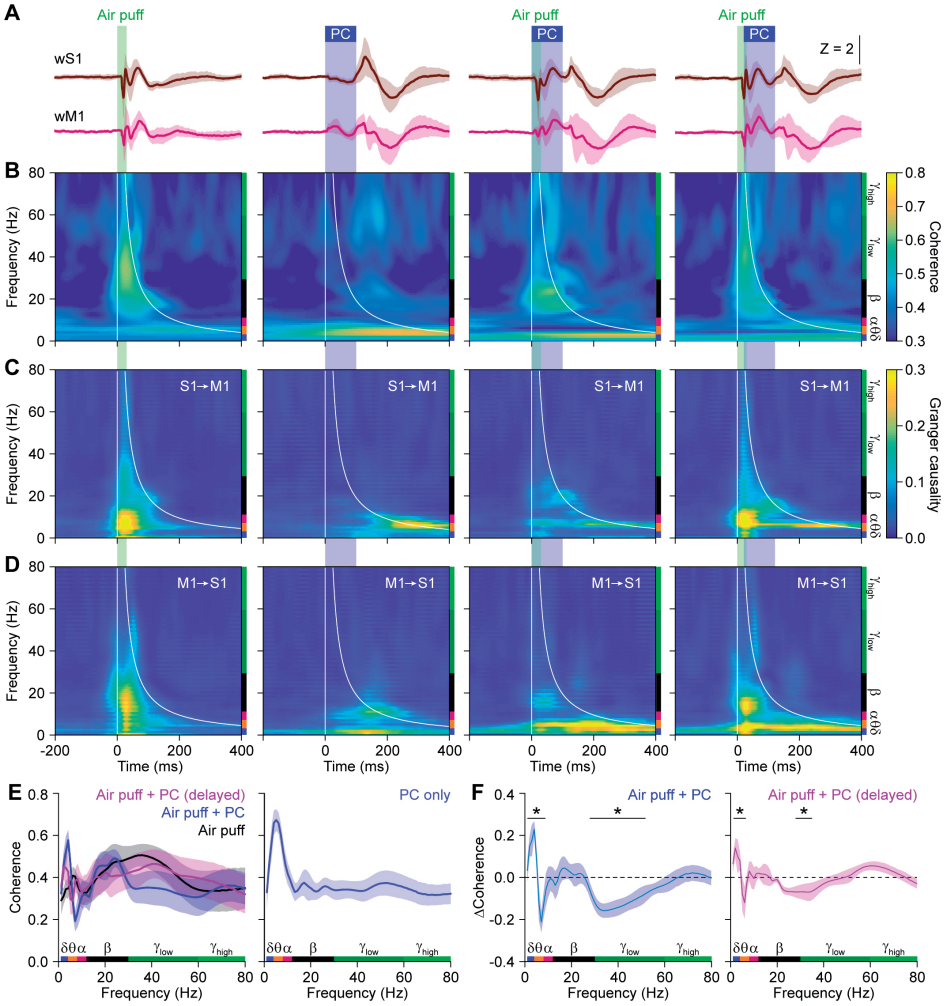


**Figure 2.** Reducing cerebellar output enhances and inhibits sensory-induced S1-M1 theta and gamma band coherence, respectively.

**A** Averaged LFP signals in subgranular wS1 and supragranular wM1 following either air puff stimulation of the contralateral facial whiskers, optogenetic Purkinje cell (PC) stimulation, or a combination of both. In the column on the right, there was a 20 ms delay between the onset of air puff and Purkinje cell stimulation. Purkinje cell stimulation was performed with an optic fiber with a 400 µm diameter placed on the center of crus 1. **B** Heat maps with the coherence strength for each frequency. Purkinje cell stimulation induced a delayed increase in the lower frequency range, mainly theta band. Sensory stimulation predominantly caused a rapid increase in the lower gamma band range. This increased coherence in the lower gamma band range could be suppressed by simultaneous optogenetic stimulation of Purkinje cells. This suppression was largely absent when the optogenetic stimuli were delayed by 20 ms, indicating the importance of fast cerebellar processing. **C** Heat maps showing Granger causality from wS1 to wM1. **D** Granger causality for wM1 to wS1. **E** Coherence after whisker stimulation (left) and for optogenetic Purkinje cell stimulation alone (right). **F** Simultaneous Purkinje cell stimulation enhanced and suppressed theta and gamma band coherence, respectively. These modulations were largely reduced by a 20 ms delay in the onset of Purkinje cell stimulation. The increased theta band activity may partly reflect a direct effect of Purkinje cell stimulation. Shaded areas indicate SEM. $N$ = 8 mice; * $p < 0.05$ ($\chi^2 > 3.84$; difference of coherence test, see Methods)

ity, whisker protraction and wS1-wM1 coherence. To sharpen this statement, we singled out, for each experiment, the 50% of the trials with the largest reflexive whisker protractions and compared these to the other 50% (Fig. 3A-B). During air puff stimulation, larger protractions were correlated to lower coherence levels than smaller protractions, which was opposite during combined whisker and Purkinje cell stimulation (Fig. 3C), alluding to a significantly stronger impact of cerebellar activity during larger movements (Fig. 3D-E). Again, this impact was absent when introducing a 20 ms delay between whisker and Purkinje cell stimulation (Fig. 3D). The cerebellum therefore seems to provide contextual input with a homeostatic effect, which was particularly clear in the beta and gamma bands, but absent in the theta band. Purkinje cell stimulation in the absence of whisker stimulation did not cause a whisker movement until the end of the stimulus, as described previously (25) (Fig. S7).

## Regional heterogeneity in cerebello-cerebral communication

The direction of Purkinje cell modulation upon whisker stimulation is related to the location within crus 1 and crus 2 receiving the stimulus (28). More specifically, whereas the increase in simple spike firing is most prominent in medial crus 2, that of the complex spikes, which may facilitate execution of touch-induced whisker protraction, is more robust in lateral crus 1 (28). Given this differential distribution in whisker-related Purkinje cell activity (Fig. 4A), we hypothesized that the changes in coherence described above depend on the specific area of optogenetic stimulation. To study the impact of spatial Purkinje cell stimulation on wS1 and wM1, we placed small optic fibers in a rectangular grid, targeting the medial and more lateral parts of crus 1 and crus 2. With these fibers we could reliably trigger a near-complete block of neuronal activity in the cerebellar nuclei and trigger whisker movements related to the rebound firing in these nuclei (Figs. S8 and S9). Yet, the illuminated volumes were small enough to reduce crosstalk between medial and lateral stimulus locations (Fig. S10). Consistent with the hypothesis described above, we found the most prominent differences in the impact of optogenetic stimulation during whisker stimulation between medial crus 2 and lateral crus 1 (Figs. 4B and S11). More specifically, comparison of the impact of Purkinje cell stimulation on the extent of sensory-induced coherence revealed that Purkinje cells in medial crus 2 and lateral crus 1 differed in their impact on gamma band coherence, but showed no significant difference on theta band coherence. Since these data on regional heterogeneity were based on differential Purkinje cell modulations during different forms of adaptive and reflexive whisking behavior (28), they are consistent with the prominent dependency of the gamma, but not theta, band coherence on behavioral context (Fig. 3).

## Dissecting the impact of neural pathways using a laminar model

We recapitulated the experimental findings by adapting a large-scale computational model of the laminar cortex and subcortical structures (16) to the anatomical pathways relevant for whisker and Purkinje cell stimulation (Fig. 5A). Increasing the intensity of Purkinje cell

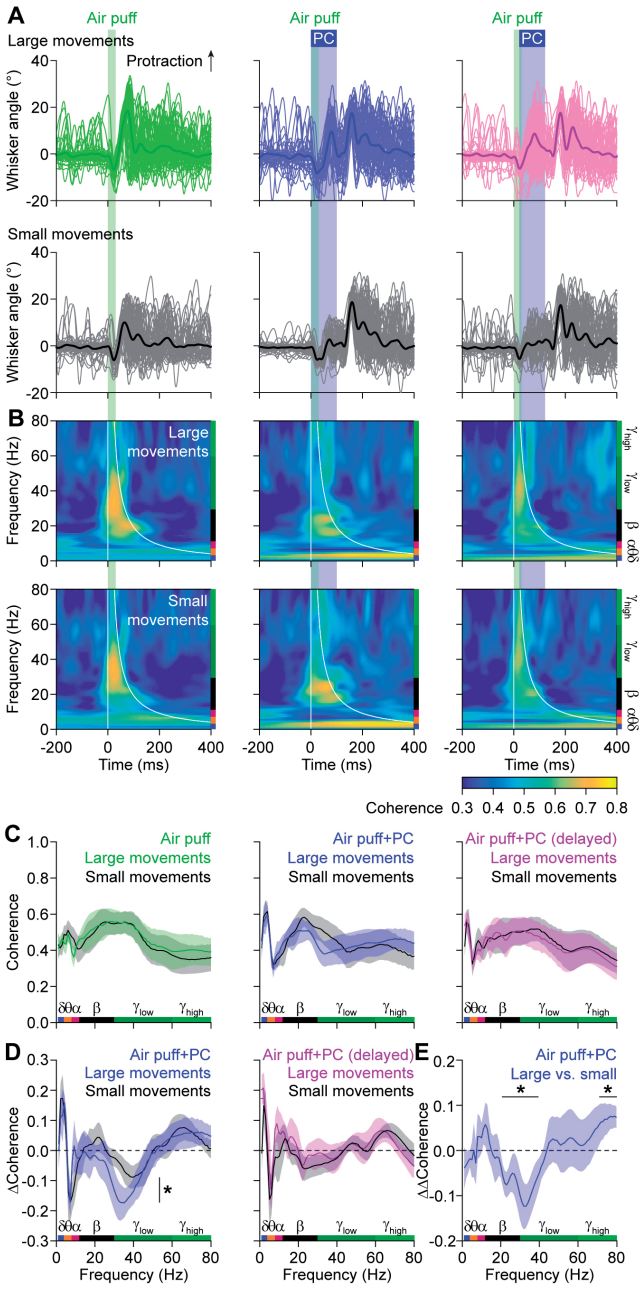


**Figure 3.** Cerebellar impact on wS1-wM1 coherence depends on behavior.

**A** Whisker stimulation triggers reflexive protraction. Trials were split between the 50% of the trials with the largest and the 50% with the smallest protractions. **B** The coherence between the subgranular layers of wS1 and the subgranular layers of wM1 were only mildly different between the trials with large (upper row) and small (bottom row) movements. **C** For each stimulus condition, the averaged coherence spectra are plotted, with colored traces representing the large whisker movements. Note that the difference in beta and lower gamma band activity are modulated in opposite fashion when adding optogenetic Purkinje cell stimulation to the air puff stimulation. **D** Accordingly, the impact of optogenetic Purkinje cell stimulation on sensory-induced wS1-wM1 coherence was stronger during trials with large whisker movements. This difference was statistically significant (DoC test, see **E**). This effect was abolished by a 20 ms delay between the start of whisker and Purkinje cell stimulation. **E** The difference in the impact of simultaneous Purkinje cell stimulation ("ΔΔCoherence") on sensory-induced beta and gamma band coherence was significantly larger during the trials with large movements than during those with small movements (DoC analysis). Lines in **C-E** indicate averages and the shades SEM. See also Fig. S7.

stimulation had differential effects on different regions, reflecting the contributions of excitatory and inhibitory connections between them (Fig. 5B). Stimulating the trigeminal nucleus, simulating whisker input, induced increased coherence in the theta and lower gamma range, the latter being inhibited by simultaneous Purkinje cell stimulation (Fig. 5C), mimicking the

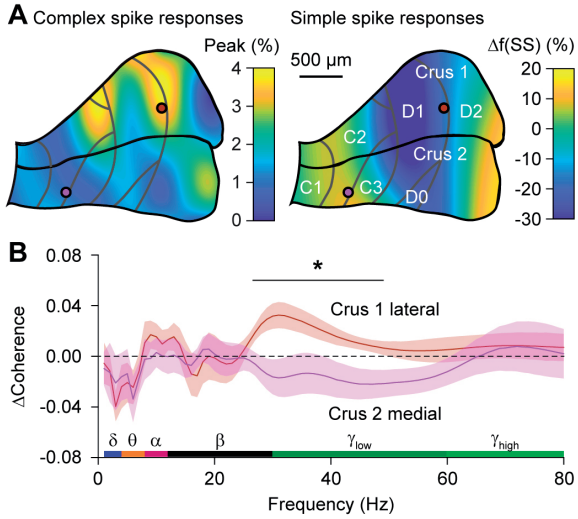


**Figure 4.** Regional heterogeneity in cerebello-cerebral communication.
**A** Air puff whisker pad stimulation results in bidirectional modulation of Purkinje cell simple spike firing. Heat map illustrates the distribution of the maximal modulation within 80 ms of stimulation, showing a difference between medial and lateral zones, modified with permission from (28). Note that whisker stimulation can either increase or decrease the simple spike rate. The grey lines indicate the tentative borders between the cerebellar zones. The two colored circles indicate the approximate positions of the 105 µm diameter optic fibers. **B** Compared to air puff stimulation in the absence of optogenetic stimulation, stimulation of Purkinje cells in the medial part of crus 2 and those in the lateral part of crus 1 had opposing effects specifically on sensory-induced gamma band coherence. See also Figs. S8-11.

experimental data (see Fig. 2). Granger causality analysis of the modeled data revealed that the sensory-induced gamma band coherence was approximately symmetrical between wS1 and wM1, while the theta band coherence caused by Purkinje cell activity was largely inflicted upon wS1 by wM1 (Fig. 5D). The balance between S1 and M1 in causing sensory-induced gamma band coherence proved to be particularly dependent on the reciprocal connectivity between the superficial layers of S1 and M1 (Fig. S12). Moreover, our model also fits with the results that Purkinje cell stimulation is responsible for the enhancement of theta coherence between cortical areas. Given the prominent similarity of the modeled and experimental datasets under various conditions, we next looked at the potential relevance of the different thalamic hubs that were not directly tested in the experiments. These modeling data suggest that the ventroposterior medial nucleus (VPM) and ventrolateral nucleus of the thalamus (VL) had a stronger impact than the medial posterior nucleus (Pom) in mediating the impact of cerebellar activation onto cortical coherence between wS1 and wM1 during sensory stimulation (Fig. S13), which is in line with the distribution of afferents from cerebellum and trigeminal nucleus to the thalamus (8).

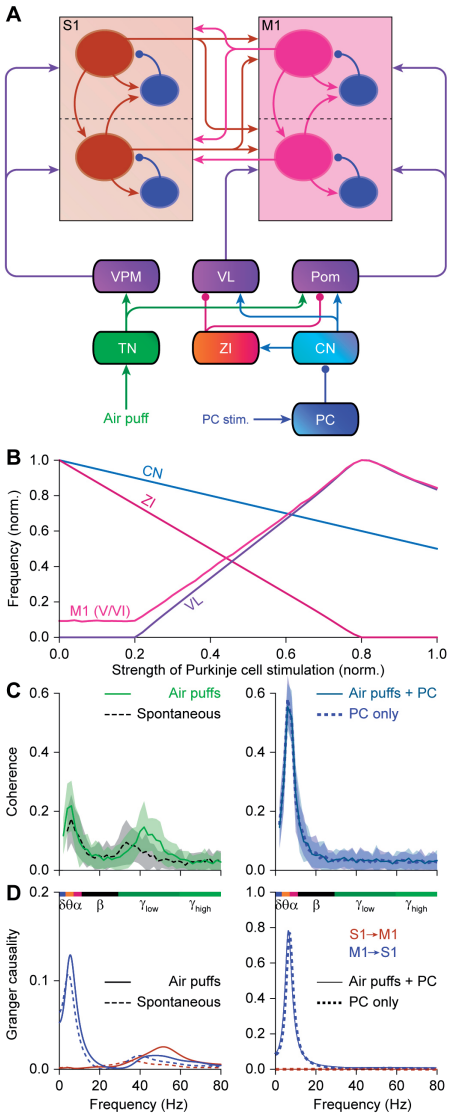


**Figure 5.** Laminar model.
**A** Schematic representation of the connections present in the computational model we used to study cortical coherence *in silico*. CN = cerebellar nuclei, PC = Purkinje cells, Pom = medial posterior nucleus of the thalamus, TN = sensory trigeminal nuclei, VL = ventrolateral nucleus of the thalamus, VPM = ventroposterior medial nucleus of the thalamus, ZI = zona incerta. **B** Impact of Purkinje cell stimulation on the firing rates of four different areas. **C** Coherence between S1 and M1 during stimulation of the trigeminal nuclei (simulating air puffs), the stimulation of Purkinje cells, and the combination of both stimuli. Trigeminal stimulation increased coherence in the gamma band, while Purkinje cell stimulation promoted theta band coherence. Adding Purkinje cell stimulation to trigeminal stimulation cancelled the increased gamma band coherence. Lines represent means and shaded areas sd. **D** Granger causality analysis revealing a largely bidirectional flow between S1 and M1 during gamma band coherence. Lower frequencies predominantly originated from M1. See also Figs. S12 and S13.

## DISCUSSION

Tactile inspection of the world requires acute motor control with fast integration of sensory feedback. This is how one adapts grasp force to keep a slipping cup, or how a tennis player adapts his stroke to side wind. To study fast sensorimotor integration in mammals, exploration by whisker touch has become a popular model system (6-8). In line with the behavioral relevance to mice, neural control of the facial whiskers is complex, involving synergistic control of cerebellum and neocortex (23). Here, we found for the first time that transient disruptions of

cerebellar output, induced by optogenetic stimulation of Purkinje cells, could disinhibit sensory LFP responses to whisker stimulation in wS1 and wM1 and differentially modulate sensory-induced wS1-wM1 theta and gamma band oscillations. The impact of Purkinje cell stimulation on the coherence in the gamma, but not theta, range depended on the acute behavior as well as the precise location in the cerebellar cortex.

The impact of Purkinje cell stimulation on the individual LFP responses in wS1 and wM1 can be readily explained by the anatomical pathways involved (8). Whisker sensory information is rapidly relayed to the granular layer of wS1 via lemniscal and extralemniscal pathways passing by the thalamic VPM nucleus (8, 35-40). Optogenetic silencing of cerebellar output did not affect the initial excitation in the wS1 granular layer, but it did promote the subsequent spread to the subgranular layers (Fig. S4). These effects may be due to the prominent projection of the cerebellar nuclei onto the zona incerta (8, 38). Indeed, the inhibitory activity of the zona incerta has been implicated in subcortical suppression of whisker sensory input during self-motion (8, 37, 39, 40), which highlights its role as an important intermediate between cerebellum and neocortex. The zona incerta sends GABAergic projections in particular to Pom, which receives direct inputs from the trigeminal nuclei and cerebellum, next to its inputs from wS1 (8, 40) and VL (41). Thus, during whisker motion, the cerebellum could, in conjunction with wM1 (39), activate the zona incerta that in turn suppresses thalamic activity. In wS1, Pom terminals can be found mainly in layers I and V (42), in line with our finding of cerebellar disinhibition of the subgranular layers. In wM1 too, Purkinje cell stimulation resulted in a disinhibition of the sensory response, which again is compatible with the projections from Pom. Moreover, in all cases, a brief delay between sensory and Purkinje cell stimulation reduced the cerebellar impact substantially, which follows our experimental finding that a fast input from the cerebellum appears to be essential for the normal responses in wS1 and wM1.

The impact of Purkinje cell stimulation on coherence between wS1 and wM1 showed that cerebellar output enhances and reduces sensory-induced coherence in the theta and gamma bands, respectively. However, the finding that only the impact in the gamma range depended on ongoing behavior and on the precise location of stimulation in the cerebellar cortex raises the possibility that the cerebellum exerts its functional effects in the cortex mainly through a more high-frequency mode of operation. Moreover, these findings also suggest that the cerebellum may better control motor behavior by temporarily downgrading the coherence with sensory relevant signals rather than enhancing them. These implications agree with the high-frequency mode of simple spike activity and modulation that take place during the preparation and execution of motor coordination (28, 33, 43, 44). Indeed, we found that the suppressive impact of Purkinje cell stimulation on gamma band oscillations was greater during larger movements and this impact could be specifically linked to the Purkinje cells in medial crus 2. Finally, our data

also align well with the differential frequencies of coherences that are implicated during the different stages of motor planning and execution (9, 22).

The impact of cerebellar activation on individual LFP signals in wS1 or wM1 as well as that on the coherence between these signals could be well replicated by our modeling work. We built our computational model on cerebellar modulation of cortical interactions by expanding our existing model on cortico-cortical and thalamo-cortical interactions (16, 20). The model, the connectivity of which is constrained by realistic anatomical routes, suggests that Purkinje cell activity triggers a disinhibitory effect via the zona incerta, which in turn mediates both the suppression of gamma coherence and the enhancement of theta coherence between S1 and M1. In agreement with the experimental data, the model revealed that sensory-induced gamma band coherence involved mainly signals originating from S1, but with a substantial contribution of M1. The impact of M1 on gamma band coherence depended on the extent of reciprocal connectivity of S1 and M1, rather than on thalamic activity (Figs. S12). Changing the connectivity of the Pom could alter the coherence at lower frequencies, with the stronger connectivity being more in line with the experimental data, but had little impact on the directionality of coherence (Fig. S13). Given the similarities between the modeling and experimental outcomes, even explaining counterintuitive findings, the current model may well provide detailed and valid predictions as to how the cerebellum may influence the different layers and areas of the cerebral cortex under a wider and richer variety of physiological behaviors.



## MATERIALS AND METHODS

**Animals.** Experiments were performed on heterozygous transgenic mice expressing the light-sensitive cation channel channelrhodopsin-2 under the Purkinje cell-specific *Pcp2* promoter (Tg(Pcp2-cre)2MPin;Gt(ROSA)26Sor$^{tm27.1(CAG-COP4*H134R/tdTomato)Hze}$) on a C57BL6/J background (45). We used 14 males and 12 females aged between 10 and 34 weeks. The mice were kept in a vivarium with controlled temperature and humidity and a 12/12 h light/dark cycle. The animals were group housed until surgery and single housed afterwards. A project license was obtained prior to the start of the experiments from the national authority (Centrale Commissie Dierproeven, The Hague, The Netherlands; license no. AVD101002015273) as required by Dutch law and all experiments were performed according to institutional, national and EU guidelines and legislation.

**Surgery.** The mice received a pedestal to allow head-fixation in the recording setup as well as one to three craniotomies to grant access to the brain. All surgical procedures were performed under anesthesia and the mice were given pain-killers before and after surgery. The animals were given three days of recovery after the surgery before they were habituated to the setup

on at least three consecutive days with increasing habituation times (from approx. 10 min the first session to approx. 2 h the last session). Further details can be found in the Supplementary Methods.

**Electrophysiology.** All recordings were made in awake, head restrained mice. Single unit activity of putative cerebellar nuclei neurons was measured using extracellular quartz-coated platinum-tungsten fiber electrodes (R = 2-5 MΩ; 80 µm outer diameter; Thomas Recording, Giessen, Germany) placed in a rectangular matrix (Thomas Recording) with an inter-electrode distance of 305 µm. LFP recordings were made in wS1 and wM1 using 16 channel, single shaft silicon probes with an inter-electrode distance of 100 µm (R = 1.5-2.5 MΩ, A1x16-5mm-100-177-A16, NeuroNexus Technologies, Ann Arbor, MI, USA). Each silicon probe was equipped with its own reference, placed in close proximity to the recording site. The two probes shared the same ground, which was placed either in the agar covering the recording sites or in the agar covering the cerebellar craniotomy. All electrodes were connected to a PZ5 NeuroDigitizer (Tucker-Davis Technologies). The signals were amplified, 1-6,000 Hz filtered, digitized at 24 kHz and stored using a RZ2 multi-channel workstation (Tucker-Davis Technologies). Recorded neurons were classified as putative cerebellar nuclei neurons if they were recorded at a depth of at least 1700 µm from the cerebellar surface and if the recording contained only a single type of action potentials typically showing both negative and positive parts, what differentiated them from Purkinje cell simple spikes. Spike times from single-unit recordings were retrieved off-line using Spiketrain (Neurasmus BV, Rotterdam, The Netherlands). Before any analysis was done on the LFP data, the raw traces were normalized using the z-score function in Matlab (MathWorks, Nattick, MA, USA). The current source density analysis was performed in custom written Matlab routines as detailed in the Supplementary Methods.

**Coherence analysis.** The phase coherence analysis was computed using the Fieldtrip toolbox as described in the Supplementary Methods. For this, LFP snippets of 5 second pre- and 5 second post-stimulus were used to calculate the coherence spectrum per trial. If necessary, 50 Hz line noise was removed. Next, the coherence in a 100 ms window after stimulus onset was averaged per frequency. The effect of Purkinje cell activation on the sensory triggered wS1-wM1 coherence was determined by subtracting the averaged air puff-induced coherence from the air puff with photostimulation evoked coherence. The Granger causality analysis was carried out by the Fieldtrip toolbox with the same preprocessing on the LFP data.

**Stimulation.** Optogenetic stimulation of the cerebellum occurred contralateral to the neocortical LFP recording sites using 470 nm LED drivers (M4703F, ThorLabs. Newton, NJ, USA) connected to a 4-channel LED driver (DC4104, ThorLabs) and optic fibers with diameters of 400 (Figs. 1-3) or 105 µm (Fig. 4) (ThorLabs). The 400 µm fibers were placed just above the dura of the cerebellum. The 105 µm fibers were adapted for insertion into the rectangular electrode

matrix by removing the cladding for ~15 cm and grinding the tip under microscope guidance. Unless stated otherwise, photostimulation was applied as 100 ms pulses with a power of 7.0 mW (400 µm fiber) or 0.2 mW (105 µm fiber). Sensory stimulations consisted of 30 ms air puffs at 1 bar directed at the mystacial macrovibrissae ipsilateral to cerebellar and contralateral to neocortical recording sites, using a MPPI-2 pressure injector (Applied Scientific Instrumentation, Eugene, OR, USA). The nozzle was positioned to minimize stimulation of the eye or ear. Stimuli were presented at 0.25 Hz in pseudorandom order.

**Whisker movement tracking.** Whisker movements in awake head-restrained mice were recorded with a high-speed video camera (frame rate 1,000 Hz; A504k camera, Basler, Ahrensburg, Germany), using a custom-made LED panel (λ = 640 nm) as back-light. All whiskers were kept intact. We tracked the whiskers as described previously (28, 46). For this study, the whisker position was defined as the average angle of all trackable whiskers. See the Supplementary Methods for more details.



**Computational model.** The computational model used is based on the one developed in (16), with (i) minimal variations in the cortical parameters based on the observed anatomical and physiological properties of wS1 and wM1 in mice and (ii) the addition of trigeminal nucleus, thalamic nuclei and cerebellar areas to the network.

**Neocortex.** Each cortical area is constituted by two cortical layers (or more generally, laminar modules) which describe the dynamics of superficial and deep layers, respectively. A laminar module contains one excitatory and one inhibitory population, and the dynamics of their respective firing rates $r_E(t)$ and $r_I(t)$ are described by the following equations:

$$\tau_E \frac{dr_E(t)}{dt} = -r_E t + F(I_E) + \sqrt{\tau_E}\,\sigma\,\xi(t)$$

$$\tau_I \frac{dr_I(t)}{dt} = -r_I t + F(I_I) + \sqrt{\tau_I}\,\sigma\,\xi(t)$$

Here, $\tau_E$, $\tau_I$ denote the time scales for the excitatory and inhibitory populations respectively, and $\xi_E(t)$, $\xi_I(t)$ are Gaussian white noise terms of zero mean and standard deviation $\sigma$. For superficial layers, we choose $\tau_E = 6$ ms, $\tau_I = 15$ ms and $\sigma = 0.3$, which leads to a noisy oscillatory dynamics in the gamma range, and for deep layers we choose $\tau_E = 48$ ms, $\tau_I = 120$ ms and $\sigma = 0.45$, which leads to noisy oscillations in the theta and low alpha range. Note that the relatively high values for the time constants in deep layers are thought to reflect other slow biophysical factors not explicitly included in the model, such as the dynamics of NMDA receptors.

The function $F(x) = x/(1 - \exp(-x))$ is the input-output transfer function of each population, which transforms the incoming input currents into their corresponding cell-averaged firing

rates. The argument of the transfer function is the incoming current for each population, which involves a background term, a local term and a long-range term. The background term is a default constant current only received by excitatory neurons in S1 and M1, and it is $I_{bg} = 4$ for superficial excitatory neurons and $I_{bg} = 1$ for deep excitatory neurons. The local term involves the input coming from neurons within the area, and it is given by

$$I^{E}_{local} = 1.5\, r_E - 3.25\, r_I + I^{E}_{interlaminar}$$

$$I^{I}_{local} = 3.5\, r_E - 2.5\, r_I + I^{I}_{interlaminar}$$

Here, the numbers denote the strengths of the synaptic projections considered. The interlaminar terms are contributions from a different layer than the one the population is in. The only interlaminar projections are from superficial excitatory to deep excitatory neurons, with synaptic strength 1, and from deep excitatory to superficial inhibitory neurons, with synaptic strength 0.75 (24).

Finally, the long-range term includes currents coming from other neocortical or subcortical areas. These currents follow the general form $J_{ab}r_b$, (with $J_{ab}$ being the synaptic strength from area 'b' to area 'a') and therefore we will specify only the synaptic coupling strengths to characterize them.

Following anatomical evidence (8), we consider excitatory projections from superficial S1 neurons to both superficial (strength 0.52) and deep (0.25) excitatory M1 neurons, and from deep S1 neurons to superficial (0.25) and deep (0.75) excitatory M1 neurons. In the opposite direction, we consider excitatory projections from superficial M1 neurons to both superficial (0.5) and deep (1) S1 excitatory neurons, and from deep M1 neurons to deep (1) S1 excitatory neurons.

The dynamics of the firing rate of the trigeminal nucleus (TN), the thalamic nuclei (VPM, VL and Pom) and cerebellar populations (PC, CN and ZI) are each described by equations of the type

$$\tau \frac{d\, r(t)}{dt} = -r(t) + f(I)$$

Here, $\tau = 10$ ms is the characteristic time constant and the transfer function is a threshold-linear function (i.e. $f(x) = Ax$, with $A$ being the gain of the population, for $x>0$, and $f(x) = 0$ otherwise). The gain parameter A takes the values 3, 10, 1, 1, 0.5, 5 and 0.2 for areas TN, PC, CN, ZI, VPM, VL and Pom, respectively. Air puffs are modeled as a constant input (max I=10) to TN, while optogenetic stimulation to PC is modeled as a constant input (I=1). Cerebellar areas CN and ZI receive inhibitory projections (both of strength 1) from PC and CN respectively. In addition, PC

and CN received excitatory background currents of 0.1 and 21 respectively, and ZI receives an inhibitory background current of 12 (which can be also interpreted as a high firing threshold). Thalamic nuclei VPM received an excitatory projection (strength 1) from TN, VL receives projections from CN (strength 1) and ZI (strength -3), and Pom receives projections from TN (1), CN (0.2) and ZI (-0.5). Projections from VPM reach superficial excitatory (strength 0.66), deep excitatory (0.13) and inhibitory (0.2) populations of S1. Regarding M1, it receives projections from Pom to all its excitatory (0.33) and inhibitory (0.5) populations, and deep excitatory M1 neurons also receive a projection (0.6) from VL. When projections from Pom to S1 are considered (see Fig. S13), they target both excitatory (0.2) and inhibitory (0.15) populations in S1.

To mimic the depth of the recording electrodes for wS1 and wM1 in experiments, we estimate the LFP signal in the model by a weighted average of the excitatory superficial and deep layers, with a superficial:deep ratio of 1:9 for wS1 (i.e. deep layers) and 4:6 for wM1 (as it targets more superficial layers but it would still pick up signals from apical dendrites' layer V neurons).



**Experimental design and statistical analysis.** We considered $p \leq 0.05$ as significant unless Benjamini-Hochberg correction for multiple comparisons was applied (see Table S1). Two-tailed testing was used for all statistical analyses. *N* indicates the number of mice; *n* indicates the number of stimuli/recordings. Further details are in the Supplementary Methods.

## ACKNOWLEDGMENTS

Financial support was provided by the Netherlands Organization for Scientific Research (NWO-ALW; CIDZ), the Dutch Organization for Medical Sciences (ZonMW; CIDZ), Life Sciences (CIDZ), ERC-adv and ERC-POC (CIDZ), as well as Crossover NWO-LSH INTENSE and Medical NeuroDelta. SH was supported by funding from the Okinawa Institute of Science and Technology Graduate University.

## REFERENCES


1. P. Fries, Rhythms for Cognition: Communication through Coherence. *Neuron* **88**, 220-235 (2015).
2. A. K. Engel, P. König, A. K. Kreiter, T. B. Schillen, W. Singer, Temporal coding in the visual cortex: new vistas on integration in the nervous system. *Trends Neurosci* **15**, 218-226 (1992).
3. S. L. Bressler, R. Coppola, R. Nakamura, Episodic multiregional cortical coherence at multiple frequencies during visual task performance. *Nature* **366**, 153-156 (1993).
4. T. Womelsdorf, P. Fries, Neuronal coherence during selective attentional processing and sensory-motor integration. *J Physiol Paris* **100**, 182-193 (2006).
5. K. F. Ahrens, D. Kleinfeld, Current flow in vibrissa motor cortex can phase-lock with exploratory rhythmic whisking in rat. *J Neurophysiol* **92**, 1700-1707 (2004).
6. T. J. Prescott, M. E. Diamond, A. M. Wing, Active touch sensing. *Philos Trans R Soc Lond B Biol Sci* **366**, 2989-2995 (2011).
7. M. J. Z. Hartmann, A night in the life of a rat: vibrissal mechanics and tactile exploration. *Annals of the New York Academy of Sciences* **1225**, 110-118 (2011).
8. L. W. J. Bosman *et al.*, Anatomical pathways involved in generating and sensing rhythmic whisker movements. *Front Integr Neurosci* **5**, 53 (2011).
9. F. I. Arce-McShane, C. F. Ross, K. Takahashi, B. J. Sessle, N. G. Hatsopoulos, Primary motor and sensory cortical areas communicate via spatiotemporally coordinated networks at multiple frequencies. *Proc Natl Acad Sci U S A* **113**, 5083-5088 (2016).
10. T. van Kerkoerle *et al.*, Alpha and gamma oscillations characterize feedback and feedforward processing in monkey visual cortex. *Proc Natl Acad Sci U S A* **111**, 14332-14341 (2014).
11. H. Shin, C. I. Moore, Persistent gamma spiking in SI nonsensory fast spiking cells predicts perceptual success. *Neuron* 10.1016/j.neuron.2019.06.014 (2019).
12. J. Veit, R. Hakim, M. P. Jadi, T. J. Sejnowski, H. Adesnik, Cortical gamma band synchronization through somatostatin interneurons. *Nat Neurosci* **20**, 951-959 (2017).
13. J. A. Cardin et al., Driving fast-spiking cells induces gamma rhythm and controls sensory responses. *Nature* **459**, 663-667 (2009).
14. G. Buzsáki, X. J. Wang, Mechanisms of gamma oscillations. *Annu Rev Neurosci* **35**, 203-225 (2012).
15. O. Jensen, E. Spaak, J. M. Zumer, "Human brain oscillations: From physiological mechanisms to analysis and cognition" in Magnetoencephalography: From Signals to Dynamic Cortical Networks, S. Supek, C. J. Aine, Eds. (Springer Berlin Heidelberg, Berlin, Heidelberg, 2014), 10.1007/978-3-642-33045-2_17, pp. 359-403.
16. J. F. Mejias, J. D. Murray, H. Kennedy, X. J. Wang, Feedforward and feedback frequency-dependent interactions in a large-scale laminar network of the primate cortex. *Sci Adv* **2**, e1601335 (2016).
17. Y. B. Saalmann, M. A. Pinsk, L. Wang, X. Li, S. Kastner, The pulvinar regulates information transmission between cortical areas based on attention demands. *Science* **337**, 753-756 (2012).
18. W. Song, J. T. Francis, Gating of tactile information through gamma band during passive arm movement in awake primates. *Frontiers in neural circuits* **9**, 64 (2015).
19. C. Pedroarena, R. Llinás, Dendritic calcium conductances generate high-frequency oscillation in thalamocortical neurons. *Proc Natl Acad Sci U S A* **94**, 724-728 (1997).

20. J. Jaramillo, J. F. Mejias, X. J. Wang, Engagement of pulvino-cortical feedforward and feedback pathways in cognitive computations. *Neuron* **101**, 321-336 e329 (2019).

21. F. Vecchio et al., Acute cerebellar stroke and middle cerebral artery stroke exert distinctive modifications on functional cortical connectivity: A comparative study via EEG graph theory. *Clinical Neurophysiology* **130**, 997-1007 (2019).

22. D. Popa et al., Functional role of the cerebellum in gamma-band synchronization of the sensory and motor cortices. *J Neurosci* **33**, 6552-6556 (2013).

23. S. M. O'Connor, R. W. Berg, D. Kleinfeld, Coherent electrical activity between vibrissa sensory areas of cerebellum and neocortex is enhanced during free whisking. *J Neurophysiol* **87**, 2137-2148 (2002).

24. L. Kros et al., Cerebellar output controls generalized spike-and-wave discharge occurrence. *Ann Neurol* **77**, 1027-1049 (2015).

25. R. D. Proville et al., Cerebellum involvement in cortical sensorimotor circuits for the control of voluntary movements. *Nat Neurosci* **17**, 1233-1239 (2014).

26. C. I. De Zeeuw et al., Spatiotemporal firing patterns in the cerebellum. *Nat Rev Neurosci* **12**, 327-344 (2011).

27. U. Proske, S. C. Gandevia, The kinaesthetic senses. *J Physiol* **587**, 4139-4146 (2009).

28. V. Romano et al., Potentiation of cerebellar Purkinje cells facilitates whisker reflex adaptation through increased simple spike activity. *eLife* **7**, e38852 (2018).

29. C. P. J. De Kock, R. M. Bruno, H. Spors, B. Sakmann, Layer and cell type specific suprathreshold stimulus representation in primary somatosensory cortex. *J Physiol* **581**, 139 (2007).

30. I. Ferezou et al., Spatiotemporal dynamics of cortical sensorimotor integration in behaving mice. *Neuron* **56**, 907-923. (2007).

31. D. Kleinfeld, R. N. S. Sachdev, L. M. Merchant, M. R. Jarvis, F. F. Ebner, Adaptive filtering of vibrissa input in motor cortex of rat. *Neuron* **34**, 1021-1034 (2002).

32. L. W. J. Bosman et al., Encoding of whisker input by cerebellar Purkinje cells. *J Physiol* **588**, 3757-3783 (2010).

33. S. T. Brown, I. M. Raman, Sensorimotor integration and amplification of reflexive whisking by well-timed spiking in the cerebellar corticonuclear circuit. *Neuron* **99**, 564-575 (2018).

34. K. H. Pettersen, E. Hagen, G. T. Einevoll, Estimation of population firing rates and current source densities from laminar electrode recordings. *J Comput Neurosci* **24**, 291-313 (2008).

35. C. Yu, D. Derdikman, S. Haidarliu, E. Ahissar, Parallel thalamic pathways for whisking and touch signals in the rat. *PLoS Biol* **4**, e124 (2006).

36. T. Mao et al., Long-range neuronal circuits underlying the interaction between sensory and motor cortex. *Neuron* **72**, 111-123 (2011).

37. T. Furuta, N. Urbain, T. Kaneko, M. Deschênes, Corticofugal control of vibrissa-sensitive neurons in the interpolaris nucleus of the trigeminal complex. *J Neurosci* **30**, 1832-1838 (2010).

38. T. M. Teune, J. van der Burg, J. van der Moer, J. Voogd, T. J. Ruigrok, Topography of cerebellar nuclear projections to the brain stem in the rat. *Progress in brain research* **124**, 141-172 (2000).

39. N. Urbain, M. Deschênes, A new thalamic pathway of vibrissal information modulated by the motor cortex. *J Neurosci* **27**, 12407-12412 (2007).

40. C. B. Schäfer, F. E. Hoebeek, Convergence of primary sensory cortex and cerebellar nuclei pathways in the whisker system. *Neuroscience* **368**, 229-239 (2018).

41. P. Barthó, T. F. Freund, L. Acsády, Selective GABAergic innervation of thalamic nuclei from zona incerta. *Eur J Neurosci* **16**, 999-1014 (2002).

42. W. Zhang, R. M. Bruno, High-order thalamic inputs to primary somatosensory cortex are stronger and longer lasting than cortical inputs. *Elife* **8**, e44158 (2019).

43. Z. Gao et al., A cortico-cerebellar loop for motor planning. *Nature* **563**, 113-116 (2018).

44. F. P. Chabrol, A. Blot, T. D. Mrsic-Flogel, Cerebellar contribution to preparatory activity in motor neocortex. *Neuron* **103**, 506-519 e504 (2019).

45. L. Witter, C. B. Canto, T. M. Hoogland, J. R. de Gruijl, C. I. De Zeeuw, Strength and timing of motor responses mediated by rebound firing in the cerebellar nuclei after Purkinje cell activation. *Frontiers in neural circuits* **7**, 133 (2013).

46. N. Rahmati et al., Cerebellar potentiation and learning a whisker-based object localization task with a time response window. *J Neurosci* **34**, 1949-1962 (2014).

## SUPPLEMENTARY METHODS

**Surgery.** All surgical procedures were performed under anesthesia (2-5% isoflurane in 1 l/min oxygen) in combination with treatment of surgical pain giving 5 mg/kg carprofen ("Rimadyl", Pfizer, New York, NY, USA), 1 µg bupivacaine (Actavis, Parsippany-Troy Hills, NJ, USA) and 50 µg/kg buprenorphine ("Temgesic", Indivior, Richmond, VA, USA). In addition, the mice received 1 µg lidocaine (Braun, Meisingen, Germany) subcutaneously at the surgical sites prior to the start of the surgery. The body temperature was maintained at 37 °C by a feed-back controlled heating pad.

For the placement of a pedestal, a part of the skin was removed and the skull was cleaned and treated with phosphoric acid to ensure all membranes were removed. Next, the exposed skull was treated with Optibond adhesive (Kerr Dental, Orange, CA, USA) and the mice received a magnetic pedestal that was placed on the skull between the eyes and secured with Charisma (Kerr Dental). Next, up to three craniotomies were performed allowing access to the whisker part of the left primary somatosensory (wS1, relative to bregma: 3.5 mm mediolateral and -1.5 mm anteroposterior) and motor cortex (wM1, relative to bregma: 1.5 mm mediolateral and 1.0 mm anteroposterior) and the right cerebellar hemisphere, each surrounded by a recording chamber made out of Charisma. The exposed dura was covered with tetracycline-containing ointment (Terra Cortril; Pfizer, New York, NY, USA) and the recording chambers were sealed with a silicon polymer (Kwik-Cast, WPI, Sarasota, FL, USA) and covered with bone wax (Ethicon, Somerville, NJ, USA). The animals were given three days of recovery after the surgery before they were habituated to the setup on at least three consecutive days with increasing habituation times (from approx. 10 min the first session to approx. 2 h the last session).

**Electrophysiology.** Local field potentials (LFP) were recorded in wS1 and wM1 using linear silicon probes. Each silicon probe was equipped with its own reference, placed in close proximity to the recording site. The two probes shared the same ground, which was placed either in the agar covering the recording sites or in the agar covering the cerebellar craniotomy. The platinum-tungsten electrodes as well as the silicon probes were connected to a PZ5 NeuroDigitizer (Tucker-Davis Technologies (TDT), Alachua, FL, USA). The signals were amplified, 1-6,000 Hz filtered, digitized at 24 kHz and stored using a RZ2 multi-channel workstation (TDT).

Before any analysis was done on the LFP data, the raw traces were normalized using the z-score function in MATLAB (MathWorks, Nattick, MA, USA). The current source density analysis was performed in custom written MATLAB routines using the Kernel Source Density Method as described in (1); see https://github.molgen.mpg.de/MPIBR-coattia/MatlabMain/tree/master/behaviorAnalysis/code/functions/kCSDv1.

In the cerebellum, recorded neurons were classified as originating from putative cerebellar nuclei neurons if they were recorded at a depth of at least 1700 µm from the cerebellar surface and if the recording contained only a single type of action potentials, what differentiated them from Purkinje cell recordings. Spike times were retrieved off-line using SpikeTrain (Neurasmus

BV, Rotterdam, The Netherlands). After automated spike detection and sorting, all traces were inspected manually and improper event classification was corrected.

**Coherence analysis.** The phase coherence analysis was computed using the Fieldtrip toolbox (2). For this, LFP snippets of 5 second pre- and 5 second post-stimulus were used to calculate the coherence spectrum per trial. If necessary, line noise at 50 Hz was removed first from the waveforms by fitting a PSD around the time of the peaks of the power spectrum and then filtering the signal with the inversed square root of this function. Next, the coherence in a frequency-dependent window (2 * 1/frequency) after stimulus onset was averaged per frequency to perform the further analysis on. The effect of optogenetic Purkinje cell activation on the sensory triggered wS1-wM1 coherence was determined by subtracting the averaged air puff induced coherence from the air puff with optogenetically evoked coherence. To test for differences between the conditions, the difference of coherence test was used, as described by Amjad et al. (3). In short, the Fisher transform ($\tanh^{-1}$) was applied on the coherence and this was compared to a $\chi^2$-distribution with $k - 1$ degrees of freedom, where $k$ is the number of conditions that were tested (in all cases $k = 2$). The 95% confidence limit was then determined using $\chi^2_{(0.05;1)} = 3.84$. The significant frequencies are indicated in the difference of coherence figures using lines and asterisks.

**Whisking behavior.** Whisker movements were tracked off-line using the BIOTACT Whisker Tracking Tool (BWTT) with the sdGeneric, stShapeSpaceKalman, ppBigExtractionAndFiltering, and wdIgorMeanAngle plugins (http://bwtt.sourceforge.net) (4). Briefly, we first determined

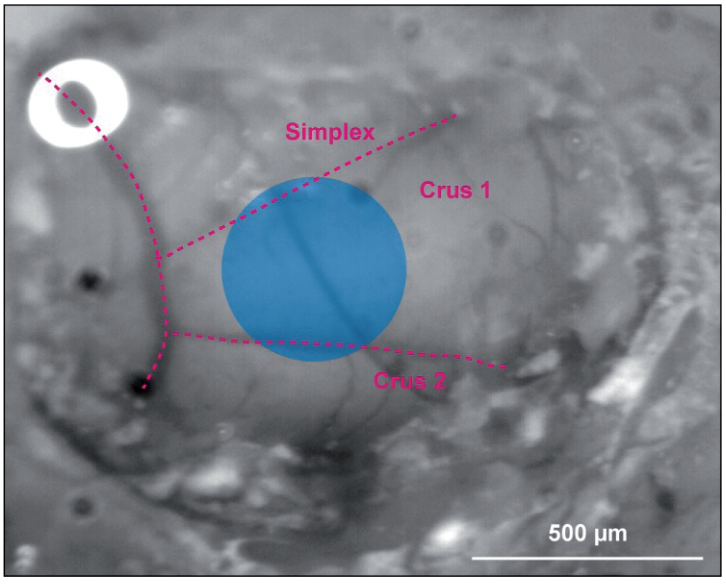


**Figure S1.** Location of optogenetic stimulation.
Approximate location of a 400 µm diameter optic fiber in the center of crus 1 as seen through the craniotomy.

the position of the snout in each frame semi-automatically by fitting a template to the snout. After masking the snout and subtracting the unmoved background from each frame, the whiskers were traced in a radial approach. The algorithm detected edges in the frame in consecutive concentric snout-shaped masks around the actual snout mask. Ultimately, we detected the start and end nodes of the fitted line segments, and calculated the angles of the whiskers from these values. The final BWTT result provided us with the angles of all detected whiskers per video frame. To relate the angles across frames to the tracks, we wrote an algorithm that predicts track values in consecutive frames based on the position and velocity in the angular value as well as the y-position of the last video frames (5, 6). The predicted track values for the next frame were compared with the detected values in the next frame and were assigned according to a minimum deviation approach between them. Finally, the mean angle per frame was calculated from the individual whisker traces.



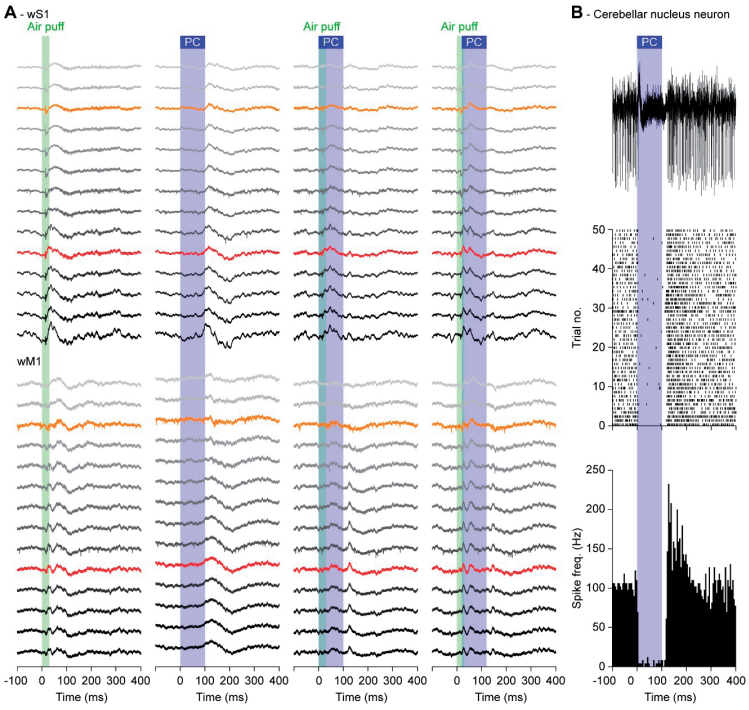


**Figure S2.** Purkinje cell stimulation reduces the impact of whisker stimulation on wS1 and wM1.
**A** Air puff stimulation of the large facial whiskers evoked sensory responses in contralateral wS1 and wM1, recorded here as deviations in the local field potential (LFP) of a randomly selected single trial (left column). The LFP recordings were made using linear silicon probes with 100 µm inter-electrode distances. The recordings are organized from superficial to deep (color code as in Fig. 1B). Electrodes 3 and 10, that were used for most analyses in this study, are marked with orange and red, respectively. Optogenetic stimulation of Purkinje cells (PC) was done with an optic fiber with a diameter of 400 µm placed on the center of crus 1 (see Fig. S1), leading to a delayed response in both wS1 and wM1 (2$^{nd}$ column). The other columns depict randomly selected trials from the same experiment, showing respectively the combined sensory and optogenetic Purkinje cell stimulation and the latter with a delay of 20 ms before the onset of the Purkinje cell stimulation. **B** Optogenetic Purkinje cell stimulation leads to a pause in firing of an exemplary neuron in the cerebellar nuclei, followed by rebound firing after the end of stimulation. Further analysis of cerebellar nuclear activity is presented in Figs. S8-S10.

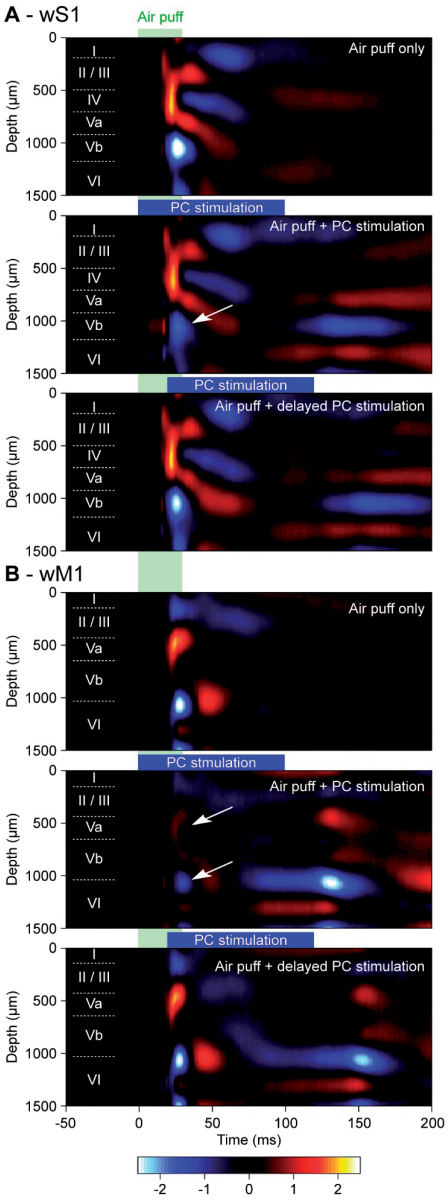


**Figure S3.** Purkinje cell stimulation reduces sensory responses in wS1 and wM1.

**A** Current source density analysis of the averaged local field potentials across the layers of the whisker area of S1 (see Fig. 1C-H) during whisker air puff stimulation alone or in combination with optogenetic stimulation of Purkinje cells using an optic fiber with a diameter of 400 µm placed on the center of crus 1 (see Fig. S1). Purkinje cell stimulation applied simultaneously with whisker stimulation suppressed predominantly the fast current sinks (blue; white arrow), but a 20 ms delay between air puff and whisker stimulation largely restores the impact of air puff stimulation. **B** The same was true for the whisker area of wM1. The heat maps indicate the averaged values of 8 mice with color scaling in arbitrary units. The layers of wS1 and wM1 are indicated by approximation.

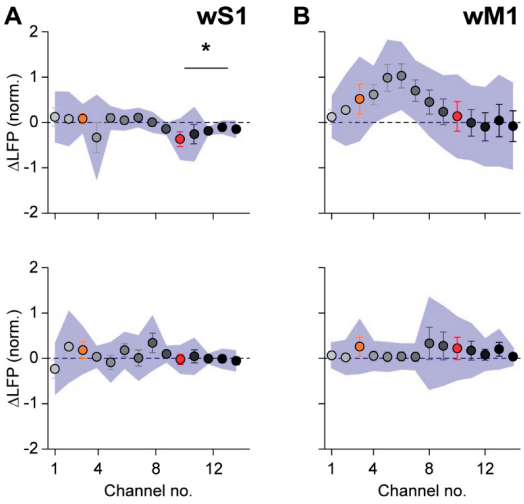


**Figure S4.** Optogenetic Purkinje cell stimulation increases the spread of excitation triggered by whisker stimulation.

**A** Air puff whisker stimulation triggers excitation in contralateral wS1 and wM1. In wS1, the amplitude of the first negative LFP peak (corresponding to excitatory activity) in the subgranular layers was enhanced ($p = 0.012$, $\chi^2 = 2.500$, Dunn's post-hoc test after Friedmann's ANOVA, Table S1). This effect was absent upon introducing a delay of 20 ms between whisker and Purkinje cell stimulation (bottom row). **B** The same for wM1. Plotted are the averaged differences in amplitude of the first positive LFP peaks. Error bars indicate SEM and shaded area sd. $n = 100$ trials each in $N = 8$ mice.

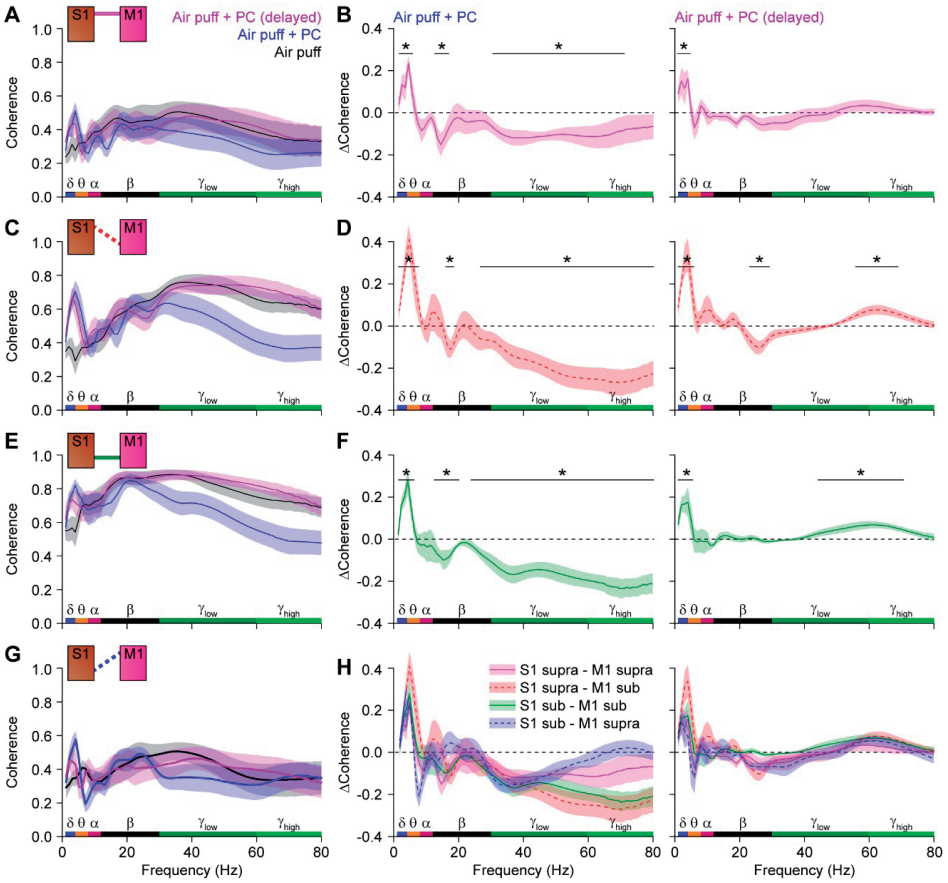


**Figure S5.** Cerebellar Purkinje cell stimulation suppresses sensory-induced gamma band coherence between wS1 and wM1.

**A** Averaged coherence between the supragranular layers of wS1 and wM1 following air puff stimulation of the contralateral facial whiskers in isolation or in combination with simultaneous or 20 ms delayed optogenetic stimulation of Purkinje cells using an optic fiber with a diameter of 400 µm placed on the center of crus 1 (see Fig. S1). Shaded areas indicate SEM. $n = 100$ trials per condition each in $N = 8$ mice. **B** Purkinje cell stimulation suppressed mainly the gamma band coherence induced by air puff sensory stimulation. This effect was largely abolished by introducing a 20 ms delay between the start of the sensory stimulation and that of the Purkinje cells. **C-H** The same for the coherence between different layers of wS1 and wM1 as indicated schematically in the upper left corners. Although the details varied to some extent, in all cases Purkinje cell stimulation suppressed sensory-induced gamma band coherence between wS1 and wM1. * $p < 0.05$ ($\chi^2 > 3.84$; difference of coherence test, see Methods).

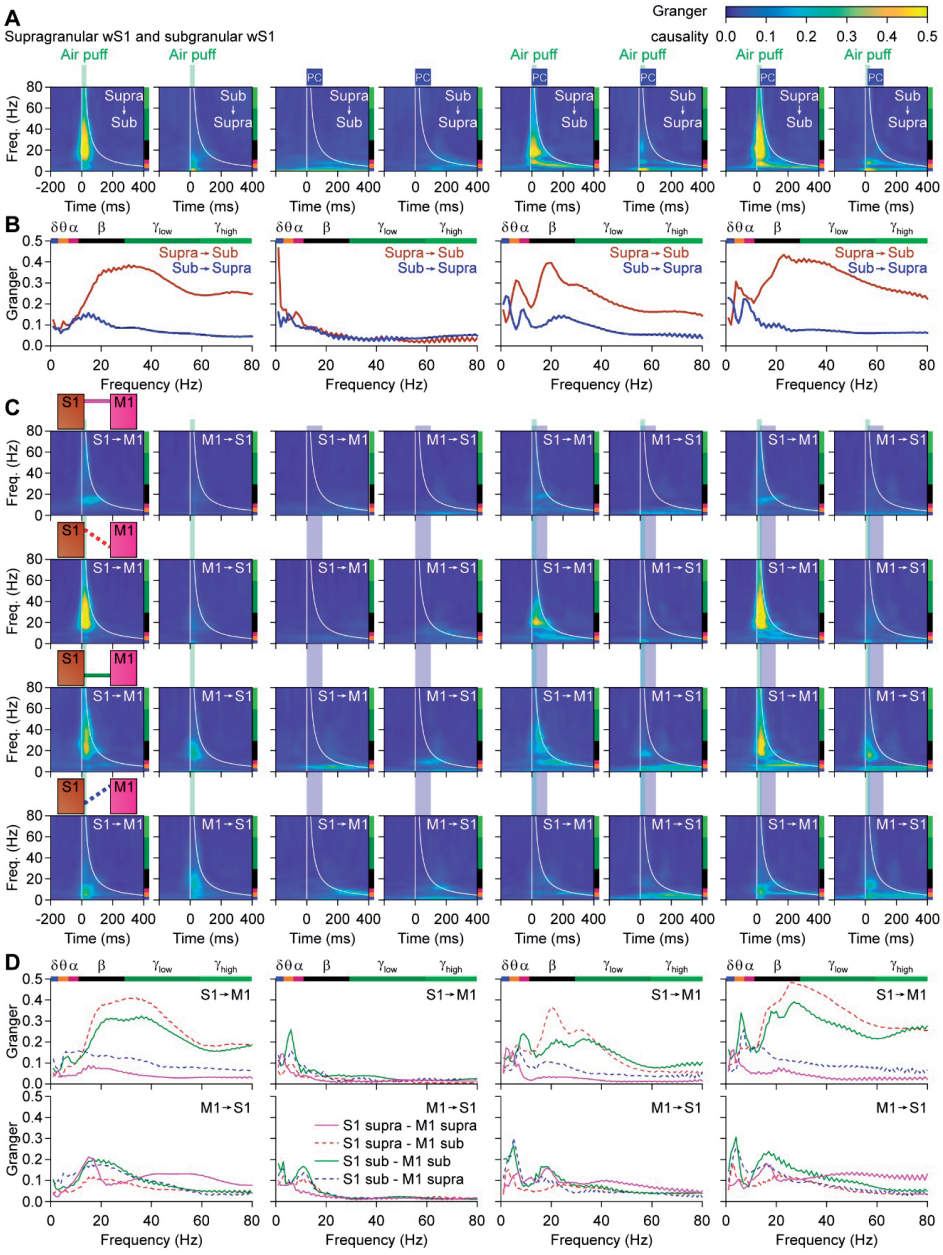


**Figure S6.** Granger causality analysis.

**A** Granger causality analysis revealed that the sensory-induced beta and gamma band coherence within wS1 was mainly caused by activity in the supragranular layers. The flow from the superficial to the deeper layers in the gamma, but not the beta, band was disrupted by simultaneous Purkinje cell stimulation. **B** The mean Granger causality values for the different conditions, comparing the flow from superficial to deep layers vs. the flow from deep to superficial layers. **C** Granger causality analysis of the coherence between wS1 and wM1, expanding on the analysis shown in Fig. 2C-D where the subgranular layers of wS1 were compared to the supragranular layers of wM1 (data copied in the fourth row to facilitate comparisons). This analysis suggest that the sensory-induced gamma band coherence is mainly caused by the superficial layers of wS1, and

from there spreads over wS1 and wM1. The strongest interconnections are found between subgranular layers of wS1 and the supragranular layers of wM1 (fourth row). Also here, wS1 drives wM1 stronger than vice versa, but also wM1 has a share in this coherence, stressing the importance of the connections between wS1 and wM1. **D** The mean Granger causality values for the different relations between wS1 and wM1.

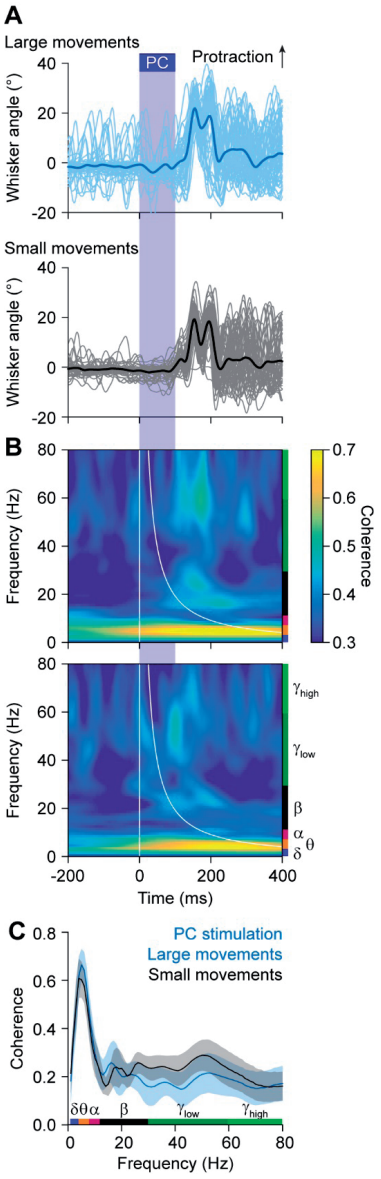


**Figure S7.** Optogenetic Purkinje cell stimulation induces delayed whisker protraction.
**A** Optogenetic stimulation of Purkinje cells, using a 400 µm diameter optic fiber placed on the center of crus 1, induced whisker protraction at the end of the stimulus. Shown are the 100 trials of a representative experiment, split into the 50% of the trials with the largest and the 50% with the smallest protraction. **B** Heat maps of the coherence over time, showing predominantly activity in the theta band, that was not different between the groups of trials (**C**). *N* = 8 mice. Shades indicate SEM.

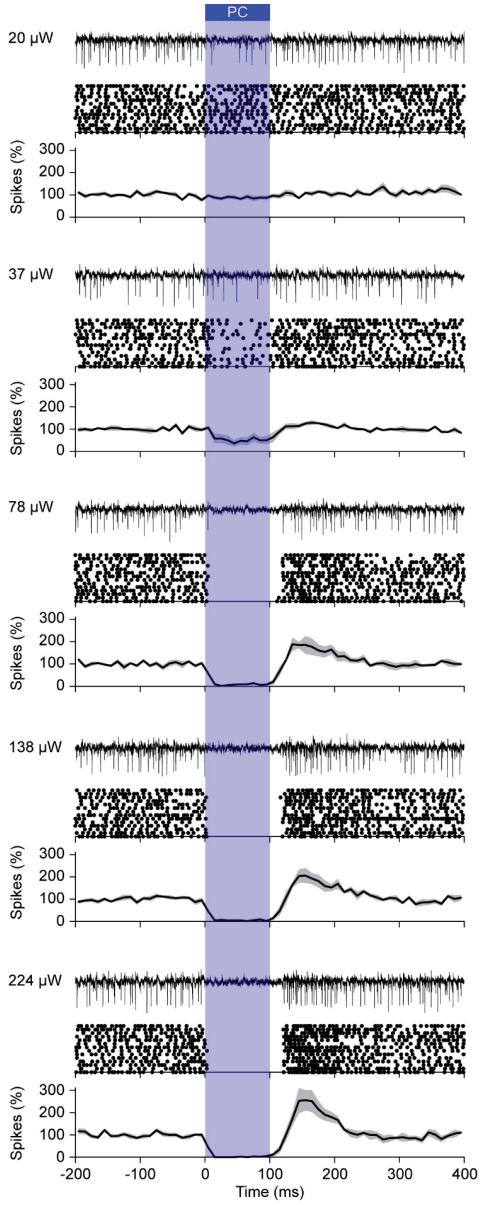


**Figure S8.** Optogenetic stimulation of Purkinje cells silences neurons of the cerebellar nuclei.
Using different illumination intensities and an optic fiber with a diameter of 105 µm, optogenetic stimulation of Purkinje cells induced a pause in firing of cerebellar nuclei neurons. At higher intensities, the pause was followed by rebound firing. For each intensity, an example trace is plotted, followed by a raster plot of the same experiment and the averaged peri-stimulus histogram of the spike rate (normalized to baseline = 100%) constructed from 6 responsive neurons in *N* = 2 mice. The shades indicate SEM.

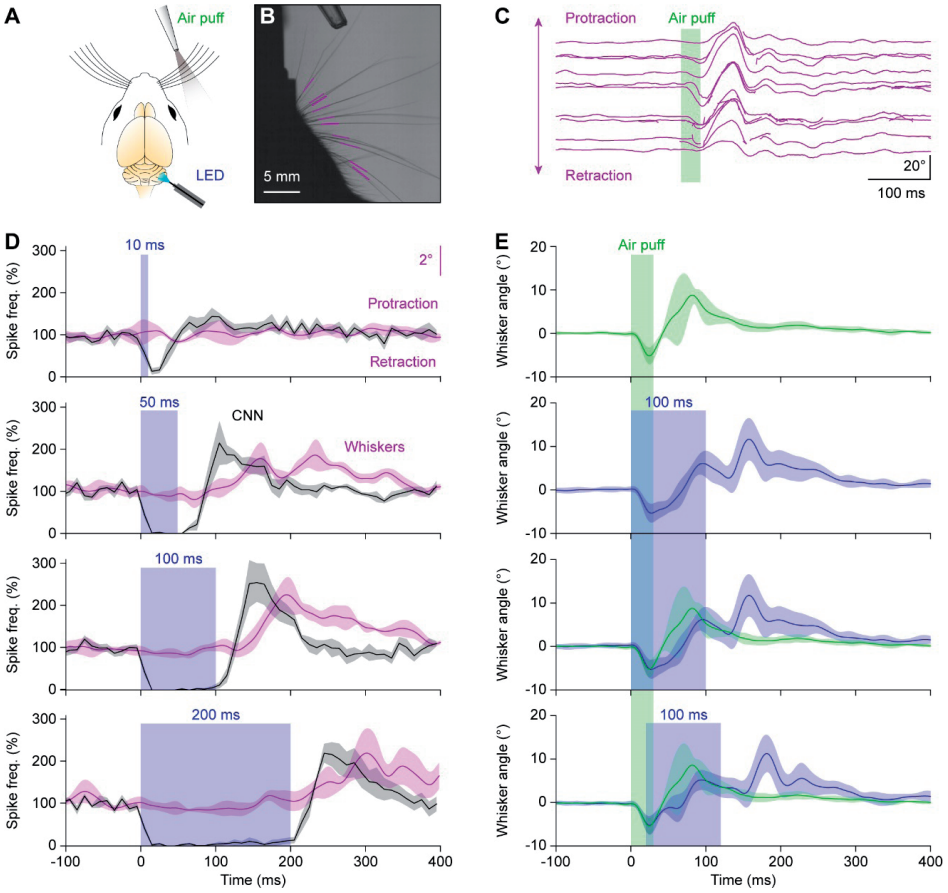


**Figure S9.** Rebound firing in the cerebellar nuclei is linked to whisker protraction.
**A** Experimental scheme. **B** The movements of the whiskers were tracked using video-analysis. The colored line fragments indicate the tracked part of the whiskers. **C** Raw output of the whisker tracking algorithm, showing for one trial how an air puff blew the whiskers backwards, after which an active protraction followed. **D** Optogenetic stimulation could also trigger whisker protraction, but not during the period of stimulation. By varying the stimulus duration, we observed that the rebound firing in the cerebellar nucleus neurons (CNN) varied in timing and amplitude and that the whisker protraction followed the rebound firing. *n* = 6 cerebellar nucleus neurons in *N* = 2 mice. E Whisker air puff stimulation induced a reflexive protraction. This protraction was reduced during the stimulus, but increased at the end of the stimulus. The whisker angle was normalized for each mouse at 0° before stimulus onset. *N* = 4 mice with each *n* = 100 trials per condition. Lines indicate average and shades SEM.

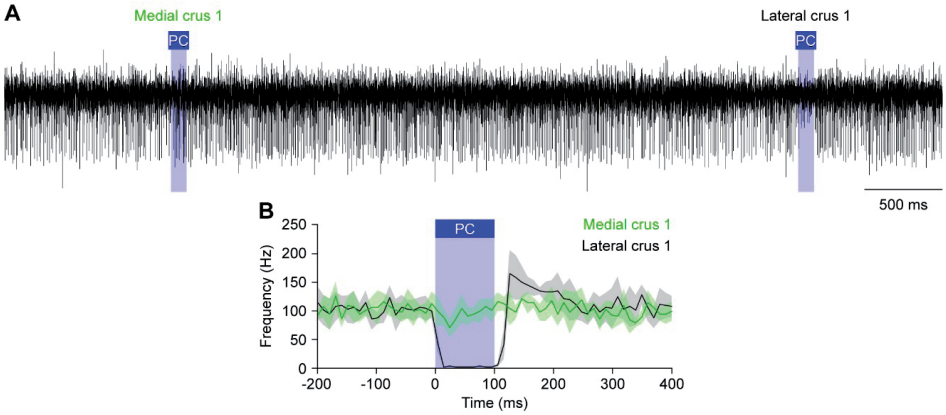


**Figure S10.** Optogenetic Purkinje cell stimulation acts locally.
**A** Extracellular recording of an exemplary cerebellar nucleus neuron displaying inhibition upon optogenetic stimulation of Purkinje cells in the lateral, but not the medial part of crus 1. For this experiment, an optic fiber with a diameter of 105 µm was used. **B** Averaged peri-stimulus histogram of two simultaneously recorded cerebellar nucleus neurons. The two neurons were separated laterally by 305 µm.

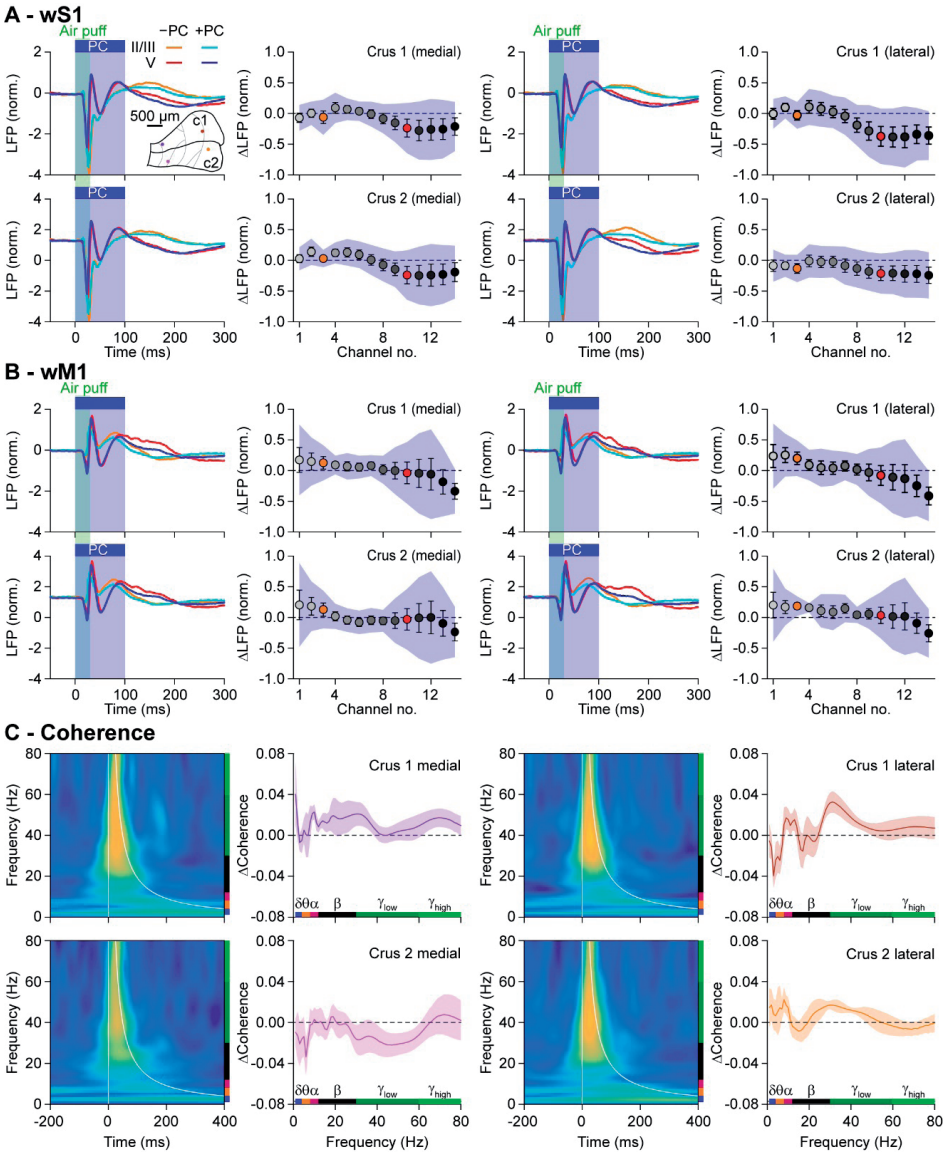


**Figure S11.** Regional differences in the impact of Purkinje cell stimulation on sensory-induced local field potentials in wS1 and wM1.

**A** Averaged local field potentials (LFP) of the supra- (light colors) and subgranular (dark colors) of wS1 upon either only air puff stimulation of the contralateral facial whiskers (red colors) or air puff stimulation in combination with optogenetic stimulation of Purkinje cells (PC; blue colors). Optogenetic Purkinje cell stimulation was performed using four optic fibers with 105 µm diameter placed at different locations in crus 1 (c1) and crus 2 (c2; inset). During each trial, one of the fibers was activated in a random sequence. The 2$^{nd}$ and 4$^{th}$ columns indicate the difference in the amplitudes of the first positive peaks following stimulation, using the same color codes as in Fig. 1. Error bars indicate SEM and shaded areas sd. **B** The same analysis, but now for wM1. **C** Combined air puff whisker stimulation and optogenetic Purkinje cell stimulation resulted in gamma band coherence between wS1 and wM1 (heat maps). The coherence was different from those trials in which only the whiskers were stimulated, as indicated by the ΔCoherence plots. The impact of Purkinje cell stimulation on sensory-induced coherence depended on the location of optogenetic stimulation, with the lateral part of crus 1 and the medial part of crus 2 having op-

posite impact on gamma (but not theta) band coherence and the other locations having more intermediate effects. Lines are averages and shaded areas indicate SEM. *N* = 7 mice.

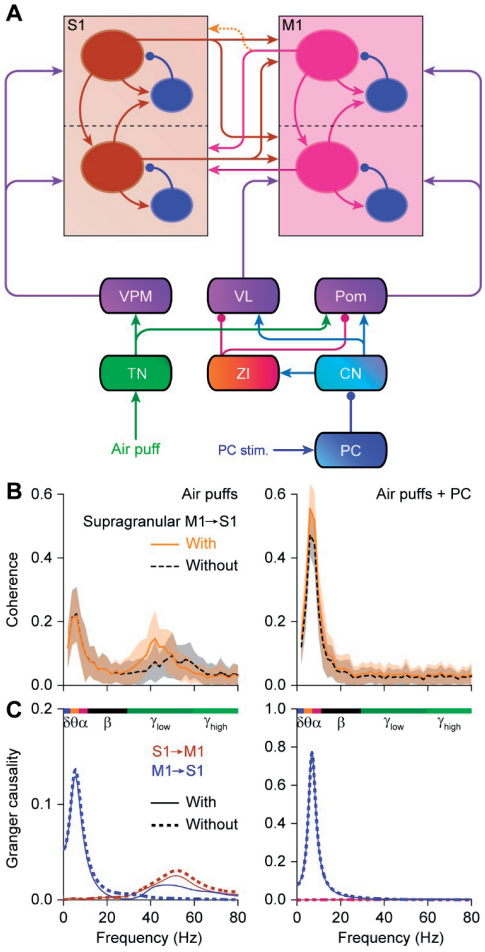


**Figure S12.** Laminar model: impact of a projection for the supragranular layers of M1 to the supragranular layers of S1.

**A** Here we compared the circuit with and without a direct connection between the supragranular layers of M1 and S1 (dashed orange arrow). **B** Removing the supragranular M1 to S1 connection resulted in a slightly less powerful gamma band coherence (black) upon simulation of the trigeminal nuclei (simulating sensory input of the whiskers) than the same simulation in the presence of the supragranular M1 to S1 connection (orange). The impact of this connection was less during the combined trigeminal + Purkinje cell stimulation. C Granger causality analysis revealed that deleting the supragranular M1 to S1 connection resulted in a virtually complete lack of the contribution of M1 to the sensory-induced gamma band coherence. Note that the situation with the supragranular M1 to S1 connection is the circuit that was used to generate the data of Fig. 5. These data are replicated here to facilitate comparison. Lines indicate averages and shaded areas sd.

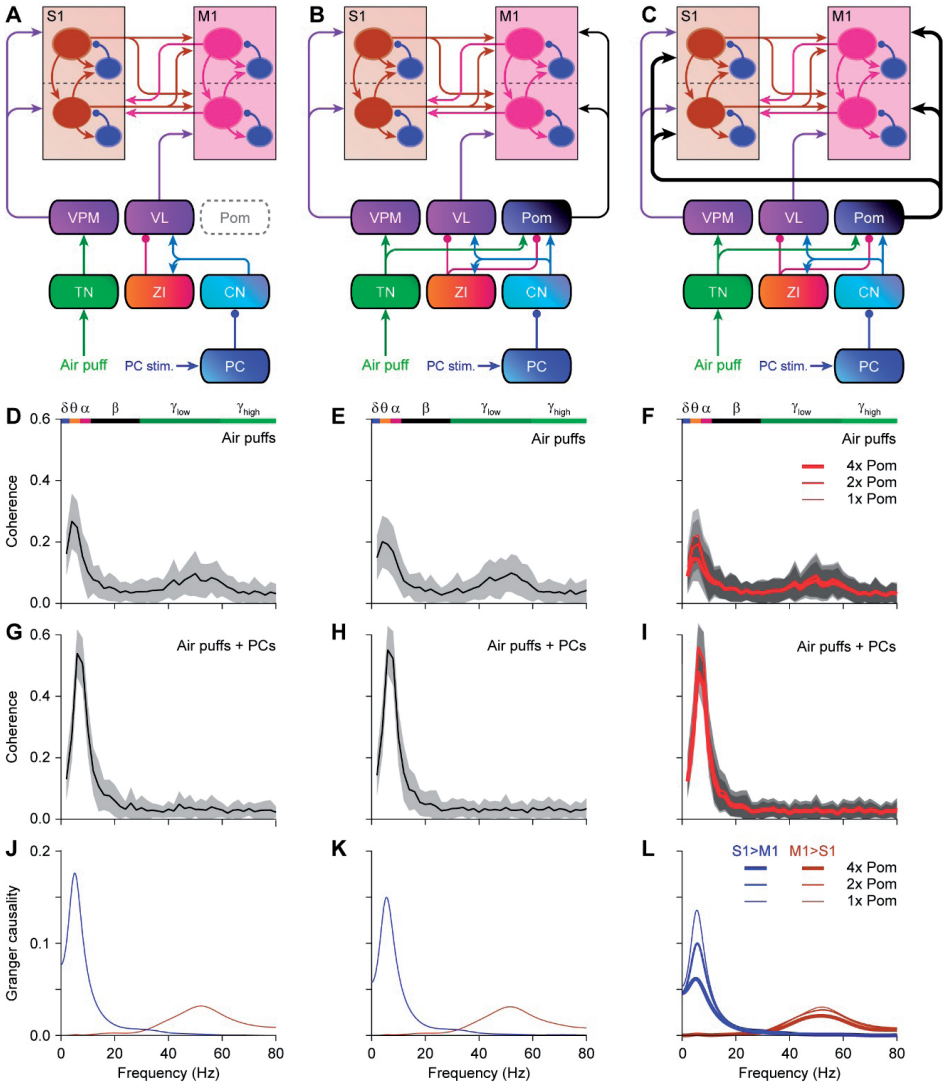


**Figure S13.** Impact of Pom connectivity on laminar model

To test whether the Pom could affect the flow between S1 and M1 during gamma band coherence, we used our computation model in the configuration without a supragranular connection between M1 and S1 (Fig. S12). In this configuration, S1 is dominant over M1 when generating gamma band coherence. To study the impact of the Pom, we compared three different configurations: without Pom (**A**), with Pom projecting only to M1 (**B**) and with Pom symmetrically projecting to S1 and M1 (**C**). Of the latter, we implemented the connectiivty strength as used for Pom to M1 connection in Fig. 5, double ("2x Pom") and quadruple strength ("4x Pom). **D-F** The different configurations did affect the amplitude of sensory-induced coherence between S1 and M1 (simulated by stimulation of the trigeminal nuclei), but did not affect the frequency characteristics. **G-I** A similar observation was made for the conjunctive trigeminal + Purkinje cell stimulation. **J-L** Granger causality analysis demonstrated that the Pom could not induce M1 to be causative for sensory-induced gamma band coherence (as the direct supragranular connection between M1 and S1 could; see Fig. S12). Lines indicate averages and shaded areas sd.

**Table S1.**

| | *p* | $\chi^2$ | Sign.? | Test |
|---|---|---|---|---|
| **First negative peak** | | | | |
| wS1 [supragranular layers] | 0.417 | 1.750 | | Friedman's |
| wS1 [layer IV] | 0.197 | 3.250 | | Friedman's |
| wS1 [subgranular layers] | **0.030** | 7.000 | | Friedman's |
| *Air puff vs. Air puff + simultaneous PC stimulation* | ***0.012*** | *2.500* | *yes* | *Dunn's* |
| *Air puff vs. Air puff + delayed PC stimulation* | *0.046* | *-2.000* | *no* | *Dunn's* |
| *Simultaneous vs. delayed stimulation* | *0.617* | *0.500* | *no* | *Dunn's* |
| wM1 [supragranular layers] | 0.093 | 4.750 | | Friedman's |
| wM1 [subgranular layers] | 0.417 | 1.750 | | Friedman's |
| **First positive peak** | | | | |
| wS1 [supragranular layers] | 0.607 | 1.000 | | Friedman's |
| wS1 [layer IV] | 0.325 | 2.250 | | Friedman's |
| wS1 [subgranular layers] | **0.008** | 9.750 | | Friedman's |
| *Air puff vs. Air puff + simultaneous PC stimulation* | ***0.024*** | *2.250* | *yes* | *Dunn's* |
| *Air puff vs. Air puff + delayed PC stimulation* | *0.453* | *-3.000* | *no* | *Dunn's* |
| *Simultaneous vs. delayed stimulation* | ***0.003*** | *-0.750* | *yes* | *Dunn's* |
| wM1 [subgranular layers] | **0.030** | 7.000 | | Friedman's |
| *Air puff vs. Air puff + simultaneous PC stimulation* | 0.617 | -0.500 | *no* | *Dunn's* |
| *Air puff vs. Air puff + delayed PC stimulation* | **0.012** | -2.500 | *yes* | *Dunn's* |
| *Simultaneous vs. delayed stimulation* | 0.046 | -2.000 | *no* | *Dunn's* |
| wM1 [subgranular layers] | 0.008 | 9.750 | | Friedman's |
| *Air puff vs. Air puff + simultaneous PC stimulation* | ***0.024*** | *2.250* | *no* | *Dunn's* |
| *Air puff vs. Air puff + delayed PC stimulation* | *0.453* | *-3.000* | *yes* | *Dunn's* |
| *Simultaneous vs. delayed stimulation* | ***0.003*** | *-0.750* | yes | *Dunn's* |

**Statistical evaluation of the data represented in Figs. 1 and S4.** For each mouse, the averages of the first negative and the first positive peak were compared between three conditions (only air puff stimulation of the whiskers, simultaneous air puff and optogenetic Purkinje cell (PC) stimulation and air puff stimulation combined with a 20 ms delayed PC stimulation. Averages were compared with Friedman's two-way ANOVA and, if significant, with pair-wise Dunn's post-tests. The *p* values of the post-tests were not corrected for multiple comparisons, but Benjamini-Hochberg correction was performed for multiple comparisons among post-tests and the outcomes are listed as statistically significant or not in the column "Sign.?".

## SI REFERENCES


1. J. Potworowski, W. Jakuczun, S. Leski, D. Wójcik, Kernel current source density method. *Neural Computation* **24**, 541-575 (2012).
2. R. Oostenveld, P. Fries, E. Maris, J. M. Schoffelen, FieldTrip: Open source software for advanced analysis of MEG, EEG, and invasive electrophysiological data. *Comput Intell Neurosci* **2011**, 156869 (2011).
3. A. M. Amjad, D. M. Halliday, J. R. Rosenberg, B. A. Conway, An extended difference of coherence test for comparing and combining several independent coherence estimates: theory and application to the study of motor units and physiological tremor. *J Neurosci Methods* **73**, 69-79 (1997).
4. I. Perkon, A. Kosir, P. M. Itskov, J. Tasic, M. E. Diamond, Unsupervised quantification of whisking and head movement in freely moving rodents. *J Neurophysiol* **105**, 1950-1962 (2011).
5. N. Rahmati et al., Cerebellar potentiation and learning a whisker-based object localization task with a time response window. *J Neurosci* **34**, 1949-1962 (2014).
6. V. Romano et al., Potentiation of cerebellar Purkinje cells facilitates whisker reflex adaptation through increased simple spike activity. *eLife* **7**, e38852 (2018).

# 7

# General discussion

The main results of this thesis revealed how the simple spike activity of Purkinje cells of Crus 1, Crus 2, and simplex lobule can affect whisker and respiratory movements. The simple spikes of Purkinje cells can accelerate the respiratory and whisker movements, mainly during training and/or adaptation. In Crus1, Crus2, and simplex lobule, simple spike facilitation was the primary neural correlate of the whisker movement adaptation, and Purkinje cell potentiation appears to be the crucial cellular mechanism sustaining the simple spike facilitation. Conversely, the fact that suppression of simple spike activity was observed only in a minority of cells suggests that the type of whisking and breathing adaptation that we examined in this thesis is unlikely to depend on Purkinje cell depression in this cerebellar area. In addition to the main results of this thesis, other considerations on the specific results of the various chapters will be discussed in the following paragraphs grouping the results relative to simple spikes, complex spikes, as well as Purkinje cell potentiation.

## THE ROLE OF SIMPLE SPIKES



In chapter 2, the simple spike activity of Purkinje cells lacking protein phosphatase 2B was more regular than in wild type mice, and the learning of a whisker-based object localization task was inefficient. In these mice, the lack of the protein phosphatase 2B, which impaired Purkinje cell potentiation, did not affect motor performance of the vestibular ocular reflex, but principally its adaptation (Schonewille et al., 2010). The learning deficits presented in chapter 2 increased depending on the level of challenge that the mice were presented with. This suggests that the unimpaired simple spike firing pattern is particularly important when mice have to learn to perform fast sensory-motor integration.

In chapter 3, we examined the ability of two Purkinje cell-specific knockout mouse lines (one for protein phosphatase 2B and one lacking the gene for AMPA receptor GluA3 subunit) to adapt their reflexive whisker protraction (i.e., a forward whisker sweep induced by sensory stimulation). The whisker adaptation was induced by applying a training paradigm consisting of 20 seconds of 4 Hz air-puff stimulation. In these mouse lines, the altered simple spike modulation did not result in any detectable deficit of the motor performance of the untrained reflexive whisker protraction. However, it impaired the capability of Purkinje cell-specific knockout mice to adapt their whisker reflexive protraction. When we compared the trial-by-trial variation in instantaneous simple spike firing with that of the whisker position, we noted that there was a positive correlation. This means that trials with relatively many simple spikes typically displayed stronger whisker protraction. We found that the correlation was maximal with a zero lag, implying that simple spike modulation neither preceded nor followed the whisker movement, but occurred at the same time. This result did not emerge in a previous study in which the correlation between simple spike modulation and whisker position had been calculated at a population level (Brown & Raman, 2018). Our result indicates that simple spikes were

unlikely to drive the untrained reflexive whisker protraction. After the training paradigm, the simple spikes correlated with the magnitude of the whisker movement with a lead of about 20 ms. This temporal relationship corresponded to what could be expected for the simple spike driving whisker movement via the cerebellar nuclei and the pre-motor whisker neurons in the brainstem (Bellavance et al., 2017; Deschenes et al., 2016; Moore et al., 2013; Teune, 2000). Thus, the result of chapter 3 indicates that the simple spikes represent the untrained reflexive whisker protraction, but they can anticipate and amplify the reflex execution under particular circumstances.

The findings of chapter 5 offer a new way of looking at simple spike modulation during the performance of simultaneous movements. After the investigation of how Purkinje cell activity could affect whisker movements, we have evaluated their impact on respiration. At rest, simple spikes encode but do not anticipate, the phase of the respiratory cycle. Instead, upon air puff sensory stimulation, an increase of simple spike activity preceded and potentially accelerated the subsequent respiration cycle. This facilitation was not only necessary for the anticipation of the subsequent cycle but also predicted the magnitude of the inhalation on a trial-by-trial base of about 20ms. Therefore, during the resting condition, the simple spikes were representing the phase of the ongoing respiratory cycle; then, in response to external environmental conditions, the simple spikes potentially contributed to the adaptation of respiration. In addition to these findings, another important aspect links chapter 3 and chapter 5. About half of the cells involved in the adaptation of respiration also exhibited neural correlates of whisker position. This result suggests that Purkinje cells are a suitable candidate not only for adjusting respiration upon sensory stimulation but also for the synergistic control of breathing and whisking. In fact, the optogenetic stimulation of the Purkinje cells correlating with whisking and breathing was able to affect both respiration and whisker movements. Therefore, Purkinje cells that are thought to control one single motor behavior could, in principle, coordinate that particular behavior with others that tend to occur simultaneously.

Besides the Purkinje cell contribution to behavior described, the results in chapter 6 indicate that the impact of simple spike burst on primary motor and sensory cortices depends on the state of the animal. We compared the impact of air puff and optogenetic Purkinje cell stimulation on the coherence between primary somatosensory and motor cortices. Purkinje cell optogenetic stimulation affected mainly the coherence between primary somatosensory and motor cortices within the gamma band. The effect of Purkinje stimulation was stronger in the trials with larger whisker movement than in those with smaller movements. This result suggests that similarly to what resulted from chapter 3 for whisking and chapter 5 for respiration, the extent to which the cerebellar output affects other brain areas, like the primary motor and sensory cortices, also depends on behavioral context: “stronger impact of the cerebellar activity during larger movements.” It would be interesting to test whether the theta sensory stimulation used (to induce plasticity in Purkinje cells and enhance whisker protraction) in chapter 3 could have an impact on the coherence between primary somatosensory and motor cortices. This because

it has been proposed that, during whisking, the transfer of information between the neocortex and other brain structures, such as the hippocampus, occurs in the theta rhythm (Grion et al., 2016; Kleinfeld et al., 2016). Considering that also the cerebellar activity is enhanced in the theta band (D'Angelo et al., 2009; Moscato et al., 2019; Ramakrishnan et al., 2016; Roggeri et al., 2008) it is likely that Purkinje cell stimulation at theta frequencies could be particularly effective to modulate the coherence between primary somatosensory and motor cortices in the gamma band (as described in chapter 5), but also in other ranges of frequencies.

In conclusion, during whisker movement, the simple spikes rate of Purkinje cells of Crus 1, Crus 2 mainly increases, and more simple spikes correlate with bigger whisker protraction (Brown & Raman, 2018; Chen et al., 2016). In addition to previous works, we propose that simple spikes of lobule simple Crus 1 and Crus 2, which always modulate during movements, can affect movement only when particular environmental circumstances intensify their activity. This was demonstrated for whisker movement in chapter 3 and respiration in chapter 5. In this respect, the cerebellum appears to monitor the ongoing movements, which is represented by the simple spike activity and boost this activity via external stimuli when the environment calls for adaptation and/or learning.



## THE ROLE OF COMPLEX SPIKES

In chapter 3, we used 4 Hz air-puff stimulation that increased the simple spike responses to the subsequent air-puff stimulation. The enhancement of the simple spike responses required intact Purkinje cell potentiation and depended on the low complex spike response probability of each Purkinje cell. Thus, the potentiation of simple spikes, described in chapter 3, was negatively correlated with the occurrence of complex spikes. This result was predicted by in vitro studies (Coesmans, Weber, De Zeeuw, & Hansel, 2004; Hirano, 1990; Linden & Ahn, 1999; Shibuki & Okada, 1992), but also suggested by in vivo studies on compensatory and saccade eye movements (Herzfeld, Kojima, Soetedjo, & Shadmehr, 2018; Koekkoek et al., 2003; Medina & Lisberger, 2008; ten Brinke et al., 2015; Ten Brinke et al., 2017; Voges, Wu, Post, Schonewille, & De Zeeuw, 2017). Indeed, in the long run complex spikes can control simple spike firing (De Zeeuw et al., 2011). However, also other mechanisms can contribute to the complementarity of simple spikes and complex spikes. It has been demonstrated that simple spike activity can control the discharges of their climbing fibers via disynaptic connection involving the cerebellar nuclei (Badura et al., 2013; Chaumont et al., 2013; X. Chen et al., 2010). In line with these studies, signs of reciprocal control between simple and complex spikes were detected in Purkinje cell-specific knockouts used in this thesis. In fact, the basic complex spike firing rate, as well as its modulation during the whisker-based object localization task and whiskers reflexive protraction of chapter 2 and chapter 3, were affected even when the mutation did not directly affect the olivary neurons. These results can then be explained by Chris Miall's theory in which

there is a reciprocal control between simple and complex spike activity. This reciprocal control is mediated by the disynaptic connection between Purkinje cell, cerebellar nuclei, and inferior olivary cells and serves as a mechanism to maintain the Purkinje cell homeostasis between potentiation and suppression (Miall, Keating, Malkmus, & Thach, 1998). Thus, there is converging evidence on the role of complex spikes in regulating Purkinje plasticity mechanisms (Gao, van Beugen, De Zeeuw, 2012).

More controversial is the impact of the complex spike on whisker reflexes and respiration. In chapter 3, the presence of air puff induced complex spike consistently predicted a bigger whisker reflexive protraction. In chapter 5, instead, the respiratory cycles associated with the occurrence of complex spikes were not different than the rest of the respiratory cycles. On the other hand, at rest, spontaneous complex spike activity was particularly high in a very specific phase of the respiratory cycle. The fact that the preferred complex spike phase was right after the phase of maximum simple spike increase fits again with Chris Miall's theory (Miall et al., 1998). According to this theory, a brief increase of simple spikes can trigger complex spikes, via disinhibition of the nucleo-olivary pathway. In turn, this reduces the simple spike activity to maintain the Purkinje cell homeostasis in a certain firing range. From these results, the role of the complex spike in shaping simple spike firing patterns seems clearer than its role in controlling behavior. Complex spikes may induce pauses in simple spike firing, and this could affect the behavior, but we couldn't see any sign of their effect on respiration. Different experiments, in which complex spike activity is optogenetically modulated, could indeed clarify the actual complex spike contribution to the actions. Manipulating complex spike activity using specific spatio-temporal patterns would be needed to be conclusive on the impact of the complex spike on motor actions. However, the fact that optogenetic activation of olivary neurons has not yet been reported indicates that these types of neurons are more difficult to manipulate. Considering that complex spikes can be triggered by external stimuli, in chapter 5, we investigated the extent to which we could manipulate the inferior olivary activity using particular temporal patterns of sensory stimulation. The fact that in chapter 5, the average olivary spiking rate (i.e., complex spike frequency) was not affected by any patterns of sensory stimulation confirmed that it is indeed difficult to increase the rate of the occurrence of the complex spike experimentally. Thus, while we manipulated the simple spikes activity to establish their contribution to the adaptation of respiration and whisker reflexes, manipulation to assess the impact of the complex spike on movement has not been performed yet, and this leave opens the possibility of an impact of complex spikes on behavior. From the result of chapter 3, we conclude that there is at least an indirect impact of complex spikes on behaviors, and it is mediated by a more long-term impact of complex spike on simple spikes.

## THE ROLE OF PURKINJE CELLS POTENTIATION

Although Purkinje cell depression as the sole mechanism underlying cerebellar learning has been extensively questioned in the past decade (De Zeeuw & Ten Brinke, 2015; Galliano et al., 2013; Galliano et al., 2018; Ke, Guo, & Raymond, 2009; Schonewille et al., 2011), whether Purkinje cell potentiation and suppression co-occur in different sub-population of Purkinje cells during specific types of learning is not yet understood. It has been proposed a predominance of potentiation or suppression mechanisms for memory formation in different cerebellar areas (De Zeeuw & Ten Brinke, 2015). One of the main results of this thesis is the demonstration that Purkinje cells potentiation is a key mechanism underlying whisker adaptation. In addition to the findings in chapter 3, the results of chapter 2 and chapter 5 demonstrate that Purkinje cell potentiation is essential for several forms of cerebellar learning, especially those requiring fast sensory-motor integration.

Originally, the object discrimination task, described in chapter 2, has been used to study neural correlates of associative learning in the cerebrum (Huber et al., 2012; O'Connor, Peron, Huber, & Svoboda, 2010). However, whether the cerebellum was involved at all, it was completely unknown. Showing that Purkinje cell potentiation was required for the acquisition of that object discrimination task, sheds light on the importance of the cerebellum and its plasticity for that type of associative learning. It has been discovered that cerebellar preparatory activity precedes the execution of a similar task (Gao et al., 2018), but what is the cerebellar neural correlate of this type of learning is still unknown. Our results in chapter 2 show that the contribution of Purkinje cell potentiation was particularly relevant when the task needs to be performed rapidly. Whether Purkinje cell depression is also required for the learning of the object discrimination task remains to be tested. However, in contrast with what hypothesized in James S. Albus's theory (Albus, 1971), Purkinje cell potentiation was required to learn the discrimination task of chapter 2 efficiently. Furthermore, I interpret the bigger impairment of potentiation-deficient mice when the response window was narrower, as Purkinje cell potentiation is particularly important in learning how to perform fast sensory-motor integration.

In chapter 3, we collected several independent pieces of evidence, all pointing towards an essential role of Purkinje cell potentiation as cellular mechanisms for the enhancement of the whisker reflexive protraction. This enhancement consisted of larger, but also faster, whisker forward sweeps in response to air-puff stimulation. The correlation between simple spike facilitation and occurrence of complex spike indicates that this type of potentiation follows the rule of parallel fiber to Purkinje cells LTP derived from slices physiology studies (Coesmans et al., 2004). However, upon 4 Hz air-puff stimulation, even the cells with the highest complex spike response probability did not exhibit significant depression of their simple spike responses. One reasonable possibility is that in this subgroup of cells, the complex spike responses do suppress the simple spike responses but not upon 4 Hz air-puff stimulation. Our protocol was meant to maximize the parallel fibers activity by exploiting the resonance property of the granular

layer (D'Angelo et al., 2009; Roggeri et al., 2008). Regardless of whether those cells, with high complex response probability, can also undergo Purkinje cells simple spike depression upon sensory stimulation, the majority of the cells (66%) exhibited facilitated simple spike responses. This form of Purkinje cell plasticity was prevented in Purkinje cell potentiation-deficient mice. The results that emerged under our experimental condition suggest that in lobules Crus1 and Crus2, Purkinje cells potentiation, rather than depression, is the main mechanism underlying the facilitation of the whisker reflexive protraction. Even in this case, the optogenetic modulation of the climbing fiber activity could reveal if long-lasting Purkinje cell depression can be induced and if this would result in suppressed whisker reflexive protraction. From the evidence collected so far, we propose Purkinje cell potentiation as a cellular mechanism to make faster and bigger whisker reflexive protraction.

In chapter 5, the sensory-induced adaptation of the respiration was tightly associated with simple spike facilitation. The fact that the mice with impaired Purkinje cell potentiation could not promptly adapt their respiration suggests that this cellular mechanism could be required for performing fast sensory-motor integration. Also, the fact that the simple spike facilitation is outstanding in the area between medial Crus 1 and simple lobule suggests that in this cerebellar area, potentiation could dominate on depression. Another alternative explanation could be that the area with a predominant simple spike increase receives more excitatory synaptic inputs from the parallel fibers. Even in this scenario, however, the massive activation of the parallel fibers would lead to potentiation of both intrinsic firing property and involved synapses. Potentiation could take place, especially because in that area, the climbing fibers activity was relatively low compared to the surrounding areas. Conversely, the area that received a lot of climbing fiber inputs, located in some lateral parts of the hemispheres, could be dominated by Purkinje cell depression. What would be the biological function of such segregation between areas dominated by one of the two competing plasticity mechanisms must be elucidated with further experiments. The results of our experiments, however, suggest that they do exist.

## CONCLUSION

In summary, cerebellar activity reflects a representation of multiple and diverse ongoing behaviors such as whisking and breathing, even at the level of individual Purkinje cells. This modulation does not affect movement during unperturbed conditions, because it does not precede it in time. When adaptation is required, the temporal relationship between simple spike and movements changes, and Purkinje cells lead the adapted movement. Thus, a conspicuous part of cerebellar activity does not have any direct impact on the execution of basic movements, such as breathing, but it just continually supervises them in case adaptation is required. From our results, Purkinje cells potentiation is an instrumental mechanism for achieving faster discrimination (chapter 2), faster and bigger whisker reflexive protractions (chapter 3), and

faster adaptation of respiration (chapter 4). The link between Purkinje potentiation and faster sensorimotor integration has not been established before and explains why the cerebellar patients are slower and why they need to supervise their actions consciously.

Furthermore, I believe that Purkinje cell depression, in adjacent cerebellar areas, is also important to take actions faster. To test this hypothesis, specific studies need to be done. Based on the findings collected so far, I propose that the cerebellum, as the Big Brother of Orwell's novel, continuously supervises us: it operates omnipresent surveillance of our actions and uses mechanisms, such as Purkinje cell potentiation, to facilitate the simple spike activity to achieve goals such as faster sensory-motor integration, when it is required. Indeed, our Small Brother is Watching us!

## REFERENCES

Albus, J. S. (1971). A theory of cerebellar function. *Mathematical Biosciences, 10*(1), 25-61. doi:https://doi.org/10.1016/0025-5564(71)90051-4

Badura, A., Schonewille, M., Voges, K., Galliano, E., Renier, N., Gao, Z., . . . De Zeeuw, C. I. (2013). Climbing fiber input shapes reciprocity of Purkinje cell firing. *Neuron, 78*(4), 700-713. doi:10.1016/j.neuron.2013.03.018

Bellavance, M. A., Takatoh, J., Lu, J., Demers, M., Kleinfeld, D., Wang, F., & Deschenes, M. (2017). Parallel Inhibitory and Excitatory Trigemino-Facial Feedback Circuitry for Reflexive Vibrissa Movement. *Neuron, 95*(3), 722-723. doi:10.1016/j.neuron.2017.07.022

Brown, S. T., & Raman, I. M. (2018). Sensorimotor Integration and Amplification of Reflexive Whisking by Well-Timed Spiking in the Cerebellar Corticonuclear Circuit. *Neuron, 99*(3), 564-575 e562. doi:10.1016/j.neuron.2018.06.028

Chaumont, J., Guyon, N., Valera, A. M., Dugue, G. P., Popa, D., Marcaggi, P., . . . Isope, P. (2013). Clusters of cerebellar Purkinje cells control their afferent climbing fiber discharge. *Proc Natl Acad Sci U S A, 110*(40), 16223-16228. doi:10.1073/pnas.1302310110

Chen, S., Augustine, G. J., & Chadderton, P. (2016). The cerebellum linearly encodes whisker position during voluntary movement. *Elife, 5*, e10509. doi:10.7554/eLife.10509

Chen, X., Kovalchuk, Y., Adelsberger, H., Henning, H. A., Sausbier, M., Wietzorrek, G., . . . Konnerth, A. (2010). Disruption of the olivo-cerebellar circuit by Purkinje neuron-specific ablation of BK channels. *Proc Natl Acad Sci U S A, 107*(27), 12323-12328. doi:10.1073/pnas.1001745107

Coesmans, M., Weber, J. T., De Zeeuw, C. I., & Hansel, C. (2004). Bidirectional parallel fiber plasticity in the cerebellum under climbing fiber control. *Neuron, 44*(4), 691-700. doi:10.1016/j.neuron.2004.10.031

D'Angelo, E., Koekkoek, S. K., Lombardo, P., Solinas, S., Ros, E., Garrido, J., . . . De Zeeuw, C. I. (2009). Timing in the cerebellum: oscillations and resonance in the granular layer. *Neuroscience, 162*(3), 805-815. doi:10.1016/j.neuroscience.2009.01.048

De Zeeuw, C. I., & Ten Brinke, M. M. (2015). Motor Learning and the Cerebellum. *Cold Spring Harb Perspect Biol, 7*(9), a021683. doi:10.1101/cshperspect.a021683

Deschenes, M., Takatoh, J., Kurnikova, A., Moore, J. D., Demers, M., Elbaz, M., . . . Kleinfeld, D. (2016). Inhibition, Not Excitation, Drives Rhythmic Whisking. *Neuron, 90*(2), 374-387. doi:10.1016/j.neuron.2016.03.007

Galliano, E., Gao, Z., Schonewille, M., Todorov, B., Simons, E., Pop, A. S., . . . De Zeeuw, C. I. (2013). Silencing the majority of cerebellar granule cells uncovers their essential role in motor learning and consolidation. *Cell Rep, 3*(4), 1239-1251. doi:10.1016/j.celrep.2013.03.023

Galliano, E., Schonewille, M., Peter, S., Rutteman, M., Houtman, S., Jaarsma, D., . . . De Zeeuw, C. I. (2018). Impact of NMDA Receptor Overexpression on Cerebellar Purkinje Cell Activity and Motor Learning. *eNeuro, 5*(1). doi:10.1523/ENEURO.0270-17.2018

Gao, Z., Davis, C., Thomas, A. M., Economo, M. N., Abrego, A. M., Svoboda, K., . . . Li, N. (2018). A cortico-cerebellar loop for motor planning. *Nature, 563*(7729), 113-116. doi:10.1038/s41586-018-0633-x

Grion, N., Akrami, A., Zuo, Y., Stella, F., & Diamond, M. E. (2016). Coherence between Rat Sensorimotor System and Hippocampus Is Enhanced during Tactile Discrimination. *PLoS Biol, 14*(2), e1002384. doi:10.1371/journal.pbio.1002384

Herzfeld, D. J., Kojima, Y., Soetedjo, R., & Shadmehr, R. (2018). Encoding of error and learning to correct that error by the Purkinje cells of the cerebellum. *Nat Neurosci, 21*(5), 736-743. doi:10.1038/s41593-018-0136-y

Hirano, T. (1990). Depression and potentiation of the synaptic transmission between a granule cell and a Purkinje cell in rat cerebellar culture. *Neurosci Lett, 119*(2), 141-144. doi:10.1016/0304-3940(90)90818-t

Huber, D., Gutnisky, D. A., Peron, S., O'Connor, D. H., Wiegert, J. S., Tian, L., . . . Svoboda, K. (2012). Multiple dynamic representations in the motor cortex during sensorimotor learning. *Nature, 484*(7395), 473-478. doi:10.1038/nature11039

Ke, M. C., Guo, C. C., & Raymond, J. L. (2009). Elimination of climbing fiber instructive signals during motor learning. *Nat Neurosci, 12*(9), 1171-1179. doi:10.1038/nn.2366

Kleinfeld, D., Deschenes, M., & Ulanovsky, N. (2016). Whisking, Sniffing, and the Hippocampal theta-Rhythm: A Tale of Two Oscillators. *PLoS Biol, 14*(2), e1002385. doi:10.1371/journal.pbio.1002385

Koekkoek, S. K., Hulscher, H. C., Dortland, B. R., Hensbroek, R. A., Elgersma, Y., Ruigrok, T. J., & De Zeeuw, C. I. (2003). Cerebellar LTD and learning-dependent timing of conditioned eyelid responses. *Science, 301*(5640), 1736-1739. doi:10.1126/science.1088383

Linden, D. J., & Ahn, S. (1999). Activation of presynaptic cAMP-dependent protein kinase is required for induction of cerebellar long-term potentiation. *J Neurosci, 19*(23), 10221-10227. Retrieved from https://www.ncbi.nlm.nih.gov/pubmed/10575019

Medina, J. F., & Lisberger, S. G. (2008). Links from complex spikes to local plasticity and motor learning in the cerebellum of awake-behaving monkeys. *Nat Neurosci, 11*(10), 1185-1192. doi:nn.2197 [pii] 10.1038/nn.2197

Miall, R. C., Keating, J. G., Malkmus, M., & Thach, W. T. (1998). Simple spike activity predicts occurrence of complex spikes in cerebellar Purkinje cells. *Nat Neurosci, 1*(1), 13-15. doi:10.1038/212

Moore, J. D., Deschenes, M., Furuta, T., Huber, D., Smear, M. C., Demers, M., & Kleinfeld, D. (2013). Hierarchy of orofacial rhythms revealed through whisking and breathing. *Nature, 497*(7448), 205-+. doi:10.1038/nature12076

Moscato, L., Montagna, I., De Propris, L., Tritto, S., Mapelli, L., & D'Angelo, E. (2019). Long-Lasting Response Changes in Deep Cerebellar Nuclei in vivo Correlate With Low-Frequency Oscillations. *Front Cell Neurosci, 13*, 84. doi:10.3389/fncel.2019.00084

O'Connor, D. H., Peron, S. P., Huber, D., & Svoboda, K. (2010). Neural activity in barrel cortex underlying vibrissa-based object localization in mice. *Neuron, 67*(6), 1048-1061. doi:10.1016/j.neuron.2010.08.026

Ramakrishnan, K. B., Voges, K., De Propris, L., De Zeeuw, C. I., & D'Angelo, E. (2016). Tactile Stimulation Evokes Long-Lasting Potentiation of Purkinje Cell Discharge In Vivo. *Front Cell Neurosci, 10*, 36. doi:10.3389/fncel.2016.00036

Roggeri, L., Rivieccio, B., Rossi, P., & D'Angelo, E. (2008). Tactile stimulation evokes long-term synaptic plasticity in the granular layer of cerebellum. *J Neurosci, 28*(25), 6354-6359. doi:10.1523/JNEUROSCI.5709-07.2008

Schonewille, M., Belmeguenai, A., Koekkoek, S. K., Houtman, S. H., Boele, H. J., van Beugen, B. J., . . . De Zeeuw, C. I. (2010). Purkinje cell-specific knockout of the protein phosphatase PP2B impairs potentiation and cerebellar motor learning. *Neuron, 67*(4), 618-628. doi:10.1016/j.neuron.2010.07.009

Schonewille, M., Gao, Z., Boele, H. J., Veloz, M. F., Amerika, W. E., Simek, A. A., . . . De Zeeuw, C. I. (2011). Reevaluating the role of LTD in cerebellar motor learning. *Neuron, 70*(1), 43-50. doi:10.1016/j.neuron.2011.02.044

Shibuki, K., & Okada, D. (1992). Cerebellar long-term potentiation under suppressed postsynaptic Ca2+ activity. *Neuroreport, 3*(3), 231-234. doi:10.1097/00001756-199203000-00003

ten Brinke, M. M., Boele, H. J., Spanke, J. K., Potters, J. W., Kornysheva, K., Wulff, P., . . . De Zeeuw, C. I. (2015). Evolving Models of Pavlovian Conditioning: Cerebellar Cortical Dynamics in Awake Behaving Mice. *Cell Rep, 13*(9), 1977-1988. doi:10.1016/j.celrep.2015.10.057

Ten Brinke, M. M., Heiney, S. A., Wang, X., Proietti-Onori, M., Boele, H. J., Bakermans, J., . . . De Zeeuw, C. I. (2017). Dynamic modulation of activity in cerebellar nuclei neurons during pavlovian eyeblink conditioning in mice. *Elife, 6*. doi:10.7554/eLife.28132

Teune, T. M., van der Burg, J., van der Moer, J., Voogd, J., & Ruigrok, T. J. (2000). Topography of cerebellar nuclear projections to the brain stem in the rat. *Prog Brain Res, 124*, 141-172. doi:10.1016/S0079-6123(00)24014-4

Voges, K., Wu, B., Post, L., Schonewille, M., & De Zeeuw, C. I. (2017). Mechanisms underlying vestibulocerebellar motor learning in mice depend on movement direction. *J Physiol, 595*(15), 5301-5326. doi:10.1113/JP274346

# A

# Appendices

## ABSTRACT NL

Van oudsher werd gedacht dat synaptische plasticiteit het belangrijkste mechanisme is waarmee zenuwcellen kunnen zorgen voor leren en geheugen. Aanvankelijk werd het vermogen van het cerebellum om bij te dragen aan motorisch leergedrag toegeschreven aan de verzwakking van de synapsen tussen parallelvezels en Purkinjecellen. Dit proefschrift laat, in samenspraak met andere resultaten van de laatste tien jaar, zien dat ook andere vormen van plasticiteit van belang zijn voor cerebellair leergedrag. Hierbij gaat het vooral om de versterking van Purkinjecellen. In het bijzonder ga ik hier in op het belang van deze vorm van plasticiteit voor aanpassingen in snorhaarbewegingen, likken en ademhaling. Gebaseerd op de resultaten, zoals samengevat in dit proefschrift, suggereer ik dat de intrinsieke prikkelbaarheid van Purkinjecellen samen met de versterking van de synapsen tussen parallelvezels en Purkinjecellen leidt tot een verhoogde activiteit van simple spikes. Dit leidt vervolgens tot een versnelde sensomotorische integratie. Deze resultaten geven reden om aan te nemen dat afwijkingen in zulke neuronale mechanismen bij kunnen dragen aan beperkingen in het aanleren en uitvoeren van snelle reflexen bij cerebellaire patiënten.

## BREVE RIASSUNTO

I neuroni sono collegati tra loro e comunicano attraverso delle connessioni chiamate sinapsi. La forza con cui due neuroni sono collegati può cambiare in risposta all'esperienza e tale processo si chiama plasticita sinaptica. I neuroscienziati pensano che la plasticità sinaptica sia il meccanismo attraverso il quale noi cambiamo il nostro comportamento in risposta all'esperienza, cioè apprendiamo e formiamo nuova memoria. Per esempio, esistono neuroni che si attivano in risposta a particolari suoni e neuroni che si attivano in risposta a stimoli dolorosi. Se questi due tipi di neuroni sono ripetutamente attivati in simultanea, il che accade quando un certo stimolo sonoro è associato ad uno doloroso, il circuito che li connette si rafforza. Ne consegue che, anche in assenza dello stimolo doloroso, lo stimolo sonoro, attiverà i neuroni del dolore. Questo è un classico esempio di apprendimento dovuto alla modificazione delle connessioni tra neuroni, in altre parole, di plasticità sinaptica. Nel mio lavoro di tesi ho dimostrato che un tipo di plasticità sinaptica, detto potenziamento delle cellule di Purkinje, è fondamentale per adattare diversi tipi di movimenti. Dai miei risultati emerge che il potenziamento dei neuroni di Purkinje induce un aumento del numero di segnali che essi mandano ai neuroni del movimento. In questo modo viene raggiunta una più veloce conversione degli stimoli sensoriali in risposte motorie, al pari di quando si rafforzano i propri riflessi.

Da questi risultati emerge che malfunzionamenti in questo meccanismo neuronale potrebbero essere alla base di alcune malattie in cui i riflessi sono rallentati.

## SUMMARY EN

This thesis aims to elucidate how the cerebellum contributes to spatio-temporal coordination of movements. It is investigated to what extent Purkinje cell potentiation can serve as a cellular mechanism to sustain the increase of simple spike activity that is essential for adaptation of movements. More specifically, we study the movements of the whiskers (the relatively big mystacial vibrissae that mice use to explore the surrounding) and the abdomen (which relates to the respiratory cycle) in relationship with the activity of the Purkinje cells of the lateral cerebellum. In **chapter 1**, I recapitulate the current state of the art about our anatomical and physiological comprehension of the systems that are investigated in the subsequent chapters. These systems are likely to undergo plastic changes during adaptation. In the past two decades it emerged that multiple forms of plasticity underlie motor learning and adaptation. For example, it was found that Purkinje cell potentiation, i.e., parallel fiber to Purkinje cell synapse long term potentiation (LTP) together with intrinsic excitability, is critical for adaptation of the vestibule-ocular reflex (Gutierrez-Castellanos et al., 2017; Voges et al., 2017). We continued along this line showing that Purkinje cell potentiation is also required for other learning tasks that cover a different domain, including active exploration and more autonomic functions.

In **chapter 2**, we show that learning of a whisker-based object localization task is inefficient in mice lacking protein phosphatase 2B, which is essential for the expression of Purkinje cell potentiation. The learning deficits of these mice are heavier when the localization must be performed rapidly. Thus, the normal acquisition of this type of fast sensorimotor integration requires intact Purkinje cell potentiation.

In **chapter 3**, we developed a paradigm that requires sensorimotor integration to enhance reflexive whisker protraction. This reflex consists of a forward whisker sweep with which mice react to sensory stimulation of their whiskers (e.g., by giving a brief air puff). We show that reflexive whisker protraction becomes faster and bigger in amplitude after 20 seconds of 4 Hz air puff stimulation. Using two independent mouse lines with impaired Purkinje cell potentiation, we demonstrate that the adaptation of the whisker reflex depends on an increased simple spike response to the air puff. Also, transiently mimicking the increased simple spike response (with the use of optogenetics) we were able to enhance the reflexive whisker protraction. Thus, we propose that Purkinje cell potentiation is a crucial cellular mechanism underlying whisker reflexive adaptation through increased simple spike responses. The complex spike activity, instead, determines which Purkinje cells undergo potentiation and its modulation is studied, in greater detail, in **chapter 4**.

In **chapter 4**, we first investigate the complex spike rhythmicity induced by applying air puff stimulation to the facial whiskers of the mouse and we subsequently investigate to what extent these experimental data can be explained by the mechanisms revealed in a realistic tissue-scale computational model of the inferior olive (the brainstem nucleus where the climbing fibers that trigger complex spikes originate from). We can explain the induction of rhythmic complex

spike activity, but not the prolonged activity following specific patterns of stimulation. Likewise, we can control the timing of the initial complex spikes using sensory stimulation, but not their overall rate. Elaborating on the possibility that the rhythmicity of complex spikes could relate to one or multiple rhythmic behaviours, next, we evaluated the Purkinje cell activity in relationship with whisking and breathing.

In **chapter 5**, we show that in the lateral cerebellum inputs coming from the whisker and respiratory systems are integrated for synergistic control of both behaviours. The sensory inputs, induced by applying air puffs to the whiskers, cause a simple spike increase in Purkinje cells that can control both whisking and breathing. In fact, when these Purkinje cells are optogenetically stimulated, a similar simple spike increase results in an anticipation of the subsequent respiratory cycle and in a whisker protraction. Instead, manipulation that prevents the increase of simple spike activity also impairs sensory-induced acceleration of the respiration. Thus, sensory inputs to the whisker system cause increased simple spike activity that affects the downstream brainstem nuclei controlling whisking and respiration. Because of other anatomical connections, similar increases in simple spike activity are likely to reach also upstream brain structures such as the neocortex.

In **chapter 6**, we studied the impact of optogenetically-induced simple spike increases on primary motor and somatosensory cortex during sensorimotor processing. We show that stimulation of Purkinje cells affects the coherence between primary somatosensory and motor cortices, mainly within the gamma band. This effect was stronger during larger reflexive whisker protraction. Thus, the Purkinje cell activity can affect both brainstem pre-motor neurons (related to whisking and respiration) and higher order brain structures like the neocortex.

The interpretation of our results in **chapter 7**, is in line with the view that behaviour emerges from an interplay between several parts of the central nervous systems. We conclude that the cerebellum receives a representation of ongoing movements and uses sensory inputs to adapt movements. In this respect, the cerebellum can be compared to the big brother of George Orwell's novel 1984. The cerebellum (our small brother), like the big brother, operates as an omnipresent surveillance of our actions. This surveillance enables our small brother to promptly adapt our movements when correction is required from internal or external circumstances.

## SAMENVATTING NL

Dit proefschrift heeft als doel te ontcijferen hoe het cerebellum bijdraagt aan de spatio-temporele coördinatie van de bewegingen. Er wordt onderzocht in hoeverre potentiatie van Purkinje cellen in het cerebellum kan dienen als een cellulair mechanisme voor de instandhouding van de simple spike activiteit die nodig is voor de aanpassing van bewegingen. In het bijzonder bestuderen we de bewegingen van de snorharen (de relatief grote vibrissae op de snuit van muizen die gebruikt worden om de omgeving te verkennen) en van ademhalings-gerelateerde bewegingen van de buik in relatie tot de activiteit van de Purkinje cellen van het laterale cerebellum. In **hoofdstuk 1** geef ik een overzicht van de huidige stand van zaken met betrekking tot ons anatomisch en fysiologisch begrip van de systemen die in de volgende hoofdstukken worden onderzocht. Het zijn deze systemen waarvan we aannemen dat zij veranderen ("plasticiteit vertonen") tijdens aanpassingen in bewegingen. In de afgelopen twee decennia is gebleken dat meerdere vormen van plasticiteit de basis vormen van motorische adaptatie en van het motorisch leervermogen. Zo werd bijvoorbeeld gevonden dat Purkinjecelpotentiatie, d.w.z. de combinatie van langetermijnpotentiatie (LTP) van de synapsen tussen parallelvezels en Purkinje cellen en intrinsieke plasticiteit van Purkinje cellen, cruciaal is voor de aanpassing van de vestibulo-oculaire reflex (Gutierrez-Castellanos et al., 2017; Voges et al., 2017). In dit proefschrift zijn we verdergegaan langs deze lijn en laten we zien dat Purkinjecelpotentiatie ook nodig is voor andere motorische leertaken, zoals diegene die betrokken zijn bij actieve exploratie en bij autonome functies.

In **hoofdstuk 2** laten we zien dat het voor muizen die een bepaald eiwit (proteïne fosfatase 2B) missen lastiger is om te leren hun snorharen te gebruiken om de precieze plaats van een object te koppelen aan de aanwezigheid van een beloning. Proteïne fosfatase 2B is onontbeerlijk voor Purkinjecelpotentiatie. De leerachterstand van deze muizen wordt verergerd wanneer de lokalisatie snel moet worden uitgevoerd. De normale verwerving van dit type snelle sensomotorische integratie vereist dus intacte Purkinjecelpotentiatie.

In **hoofdstuk 3** hebben we een paradigma ontwikkeld waarin we muizen sensomotorische integratie laten gebruiken om reflexmatige snorhaarbewegingen te versterken. Deze reflex bestaat uit een voorwaartse snorhaarbeweging die muizen maken na aanraking van hun snorharen (bijvoorbeeld door het geven van een kortdurend luchtpufje). We laten zien dat de reflexmatige snorhaarbeweging sneller en groter wordt na een periode van 20 seconden met 4 luchtpufjes per seconde. Met behulp van twee verschillende mutante muislijnen, die allebei verstoorde Purkinjecelpotentiatie vertonen, laten we zien dat de aanpassing van de snorhaarreflex afhankelijk is van een verhoogde eenvoudige simple spike reactie op het luchtpufje. Ook met het kortstondig nabootsen van de verhoogde simple spike reactie (met het gebruik van optogenetische sitmulatie), waren we in staat om de reflexmatige snorhaarbeweging te versterken. Om deze redenen veronderstellen we dat Purkinjecelpotentiatie een cruciaal cellulair mechanisme is voor de aanpassing van reflexmatige snorhaarbewegingen door middel

van verhoogde simple spike activiteit. De complex spike activiteit bepaalt daarentegen welke Purkinje cellen potentiatie ondergaan en de modulatie van de complex spike activiteit wordt in **hoofdstuk 4** nader bestudeerd.

In **hoofdstuk 4** onderzoeken we eerst hoe de stimulatie van de snorharen met luchtpufjes kan leiden tot het ritmisch vuren van complex spikes. Vervolgens onderzoeken we in hoeverre deze experimentele gegevens kunnen worden verklaard door de mechanismen die verklaard worden door een realistisch netwerkmodel van de onderste olijfkern. De onderste olijfkern bevindt zich in de hersenstam en is de oorsprong van de klimvezels wier activiteit complex spikes veroorzaken. Met behulp van dit computermodel kunnen we verklaren dat stimulatie leidt tot kortdurende periodes waarin complex spikes ritmisch voorkomen. Uit de experimentele data blijkt dat we weliswaar complex spikes kunnen triggeren door sensorische stimulatie, maar dat we uiteindelijk de totale vuurfrequentie over langere tijd niet kunnen beïnvloeden. Vervolgens zijn we verdergegaan met het onderzoeken in hoeverre de ritmiek van complex spikes gecorreleerd kan worden met één of meer ritmische gedragingen. Daartoe hebben we vervolgens de Purkinjecelactiviteit gerelateerd aan bewegingen van de snorharen en ademhaling.

In **hoofdstuk 5** laten we zien dat er in het laterale cerebellum integratie plaatsvindt van inputs van de snorharen en het ademhalingssysteem en dat deze informatie gebruikt kan worden om beide typen gedrag op elkaar af te stemmen. Sensorische input van de snorharen, uitgelokt door luchtpufjes te geven aan de snorharen, veroorzaakt een toename in simple spike activiteit van Purkinje cellen. Op hun beurt kunnen deze simple spikes zowel de bewegingen van de snorharen als de ademhaling beïnvloeden. Ook door de betrokken Purkinje cellen optogenetisch te stimuleren wordt een dergelijke toename in simple spike activiteit veroorzaakt. Deze toename blijkt inderdaad te kunnen leiden tot een versnelling van de volgende inademing en tot een voorwaartse beweging van de snorharen. In het omgekeerde geval, wanneer er als het gevolg van een mutatie geen toename in simple spike activiteit niet plaats kan vinden, vindt er ook geen versnelling van de ademhaling plaats. Samengevat zorgt stimulering van de snorharen voor een verhoging van de simple spike activiteit, welke op haar beurt de kernen beïnvloedt die in de hersenstam verantwoordelijk zijn voor de aansturen van snorhaarbewegingen en ademhaling. Het ligt in de lijn der verwachting dat, gezien de anatomische verbindingen, ook andere hersengebieden, zoals de neorcortex, bereikt worden door vergelijkbare toenamen in simple spike activiteit.

In **hoofdstuk 6** hebben we bestudeerd wat de impact is van optogenetische stimulatie van Purkinje cellen en de daardoor veroorzaakte toename in simple spikes op de activiteit van de primaire motorische en somatosensorische cortex tijdens de sensomotorische integratie. We laten zien dat stimulatie van Purkinje cellen coherente activiteit tussen de primaire somatosensorische en motorische cortex beïnvloedt, voornamelijk binnen de gamma band. Dit effect was sterker tijdens grotere reflexmatige snorhaarprotractie. Zo kan de Purkinje celactiviteit zowel de pre-motorische neuronen van de hersenstam (gerelateerd aan de beweging van de snorharen en de ademhaling) als de hogere hersenstructuren zoals de neocortex beïnvloeden.

De interpretatie van onze resultaten in **hoofdstuk 7** is in lijn met de opvatting dat gedrag voortkomt uit een wisselwerking tussen verschillende delen van het centrale zenuwstelsel. We concluderen dat het cerebellum informatie krijgt over op dat moment uitgevoerde bewegingen en dat het sensorische input gebruikt om bewegingen aan te passen. In dit opzicht kan het cerebellum worden vergeleken met de grote broer van George Orwell's roman 1984. Het cerebellum (ons kleine broertje) werkt, net als de grote broer, als een alomtegenwoordige bewaker van onze handelingen. Deze bewaker stelt onze kleine broer in staat om onze bewegingen snel aan te passen wanneer er correctie nodig is door interne of externe omstandigheden.

## CURRICULUM VITAE

**Name:** Vincenzo Romano

**Date of Birth**: 17 April 1985

**Place of Birth**: Cariati, Italy
Education and Experience:
**2016- Present**: PhD program in Neuroscience, Department of Neuroscience, Erasmus MC, Erasmus University, Rotterdam, The Netherlands
**2013- 2016**: Research analyst, Department of Neuroscience, Erasmus MC, Erasmus University, Rotterdam, The Netherlands
**2012- 2013**: Erasmus programme, Department of Neuroscience, Erasmus MC, Erasmus University, Rotterdam, The Netherlands
**2009-2013**: Neurobiology (MSc), Department of Biology and Biotechnology, University of Pavia, Pavia, Italy
**2004-2009**: Biotechnology (BSc), Department of Biology and Biotechnology, University of Pavia, Pavia, Italy

# PhD PORTFOLIO

## List of publications

Rahmati, N., Owens, C. B., Bosman, L. W., Spanke, J. K., Lindeman, S., Gong, W., Potters, J. W., Romano, V., Voges, K., Moscato, L., Koekkoek, S. K., Negrello, M., & De Zeeuw, C. I. (2014). Cerebellar potentiation and learning a whisker-based object localization task with a time response window. *The Journal of neuroscience : the official journal of the Society for Neuroscience*, *34*(5), 1949–1962. https://doi.org/10.1523/JNEUROSCI.2966-13.2014

Romano, V., De Propris, L., Bosman, L. W., Warnaar, P., Ten Brinke, M. M., Lindeman, S., Ju, C., Velauthapillai, A., Spanke, J. K., Middendorp Guerra, E., Hoogland, T. M., Negrello, M., D'Angelo, E., & De Zeeuw, C. I. (2018). Potentiation of cerebellar Purkinje cells facilitates whisker reflex adaptation through increased simple spike activity. *eLife*, *7*, e38852.

Negrello, M., Warnaar, P., Romano, V., Owens, C. B., Lindeman, S., Iavarone, E., Spanke, J. K., Bosman, L., & De Zeeuw, C. I. (2019). Quasiperiodic rhythms of the inferior olive. *PLoS computational biology*, *15*(5), e1006475.

Yang Ma, Prajith Ramakrishnan Geethakumari, Georgios Smaragdos, Sander Lindeman, Vincenzo Romano, Mario Negrello, Ioannis Sourdis, Laurens W.J. Bosman, Chris I. De Zeeuw, Zaid Al-Ars and Christos Strydis. "Towards real-time whisker tracking in rodents for studying sensorimotor disorders," *2017 International Conference on Embedded Computer Systems: Architectures, Modeling, and Simulation (SAMOS)*, Pythagorion, 2017, pp. 137-145.

Vincenzo Romano, Aoibhinn L. Reddington, Silvia Cazzanelli, Roberta Mazza, Yang Ma, Christos Strydis, Mario Negrello, Laurens W.J. Bosman and Chris I. De Zeeuw. Functional convergence of autonomic and sensorimotor processing in the lateral cerebellum. (Submitted).

Sander Lindeman, Lieke Kros, Sungho Hong, Jorge F. Mejias, Vincenzo Romano, Mario Negrello, Laurens W.J. Bosman and Chris I. De Zeeuw. Cerebellar Purkinje cells can differentially modulate coherence between sensory and motor cortex depending on region and behavior. (Submitted).

## ACKNOWLEDGMENTS

Finally, after many years of effort, sacrifice, and hard work, I made it!

I made it thanks to all the beautiful people I had the luck of meeting during this journey, but I made it also despite some less beautiful people (just joking :p).

I want to thank the people that helped me. I received help from so many people that I will, for sure, forget some of them. So big thanks to the people that I am forgetting, even if your name doesn't appear here. If you helped me once, I might forget to write your name here today, but I will always remember that you helped me, when I see you around.

Then I want to thank the Italians that welcomed me in the department. Elisa Galliano inspired and guided me, giving me the right tips to succeed in our field/group. Paolo Bazzicalupi, who was hiding from me during the day and secretly calling me at night to keep him company at Vibes. The "mitico" Marco Baratella alias Schettino. You taught me that everything in life is possible. After I saw you with that girl in the park, I realized that all kinds of miracles can indeed happen.

Then I want to thank the Dutch people in the department that welcomed me. Loes, from the first day, you have been so kind to me that I have always seen you as a relative (zia Loes). It helped me so much knowing that I could count on you, and you would always be there for me, being so lovely. Then I want to thank Kees. You taught me so many things (more English than Dutch, though). We had so much fun together. Unfortunately, I cannot write any of our anecdotes here (actually its better if they're not written anywhere). Mohamed, who helped me so much, we also had so much fun with that pink bike. Then I want to thank Cullen, who accepted me in the lab despite my English not being good enough and who was also very kind to me. Without you, Cullen, I wouldn't be here today. And Cullen was also a good friend, together with Kai, Jochen, Sander and Mario. I have learned so much from each of you that I will write an entire book on that, seriously. Of course, I have to thank Froukje; she has taught me all I need to know in order to run the experiments. There are no words to express how grateful I am to you for teaching me this job and also for the fun we had in the office! Thank you!

Then I want to thank other people from the department that helped me a lot. Elise, who helped me with all the questions about my Ph.D. graduation. I think all Ph.D. students in our department are fortunate that you are there. Elize, there are no words to thank you for the histology you did for us. So, I'll just thank you for the excellent company during lunch break and for the delicious cookies that you prepared for your birthday. Thanks also for organizing the the department's social events, they create a friendly social environment in the department, which is very important, especially for foreigners, thank you very much! Then I want to thank Dick for all the funny jokes and the strange names that he gives to people. Dick, you are also a lovely person, always available and also for serious things, thanks! Talking about beautiful people, I want to thank Tom, who is the nicest. I came so many times to disturb you with silly questions, and thanks to you, I understood how complicated anatomy is and how much I need to learn.

Thank you very much for the lovely scientific discussions. I want to thank also Gerard, who recently started to talk Italian to me. I wonder if, for the past seven years, he was preparing for that, or he could already speak some Italian, but he was a bit shy.

Then I want to thank Bas Koekkoek; you helped me solve so many technical issues in the lab. Thank you for making me confident that if a new problem were to arise, you would find a solution for it. Thanks also to Pieter Kruizinka. You also helped me with some technical issues and lending me your stuff; thanks a lot for that and for teaching me that nothing is ever ok. Thanks also to Peter Bremen! I came to ask tips for new analyses to you so many times, and you were always friendly and helpful! Thank you! Thanks to Marcel de Jeu for the inspiration for further experiments and the conversation during our lunch. Thanks to Gao for our Sunday discussions, if there is one thing that I miss from my previous office, it is seeing you passing and stopping by! Wow, so many people still I have to thank, and I'm two weeks late with printing the thesis; I have to speed it up. Thanks to Lieke, Ritobrata, Dagmar, Bas Hoogstraten, Michiel, Aleksandra, Carmen, Martina, Geeske, Lisanne, Stephanie, Nina, Nikki, Lucas, Ines, Joshua, Catarina, Gerco, Francois, Xiaolu, Si-yang, Bin, Zong, Farnaz, Sadaf, Mandy, Erica, Laura, Bastiaan, Hana, Christos, Aaron, Henk-Jan, George, Angelos and, Bastian Generowicz. You all helped me in some way, sometimes with tiny things, it seems unbelievable, but it is true. So, thank you very much for that.

Of course, I want to thank the members of the Whisker lab that I have not mentioned before. In particular, I want to thank Teun that made the cover of this thesis. My thanks go to the people that left: Pascal, Silvia, Aoibhinn, Negah, Brian, Letizia, Licia, Marco, Maurizio, Bram, Ester, Sander van Gulp, Stan, Samuel. Thank you all for the work we did together, the scientific discussions and the excellent company! For the same reason, I want to thank Manuele, Lucas, Friedrich and Sanne. A special thanks I want to give to the members of my new group. Thanks to Nathalie, Roberta, Pei Pei and Annabel; we are doing a great job together, and I hope with can keep doing science together for a long time! Thanks!

Of course, I want to thank my paranymphs. Thanks to Lorenzo and Francesca. With you, we share way more than our job. We enjoy a lot of stupid-funny jokes, but also serious, scientific gossips. Let's make it very funny again! Thanks for all the company during the coffee breaks, you two good friends! Then I want to thank my friends that do not work at the Erasmus MC, thanks to Eirini, Douglas, David, Bea, Derk, Alessandro, Cathi, Bang, Iveta and Tobia. I thank you for listening to me talking about my job, especially when you couldn't care less. A big thanks to Dennis and Alison for helping me with this thesis. Thanks for being there when I needed it!

A big thanks also to my compare "Jimi" for helping me with English writing (of this acknowledgment) and to "compare" Greg for the English certificate that he gave to me :p

Thanks also to my friend Davide for the statistical guidance and in general for being such a lovely person.

Finally, a special thank goes to the members of the defence committee. Thank you for making time to be part of my defence committee. Thank you very much for accepting my invitation!

In particular, I want to thank the secretary of the small committee, Dr. Martijn Schonewille, for the constructive feedback on the thesis and for being so kind in general. I also came to your office so many times with many scientific questions (actually even for materials and devices). You were always available, kind and helpful. Thank you. I'm so happy that you accepted our invitation!

Another special thank goes to my co-promoter, Dr. Laurens Bosman. Dear Laurens, we did so much together, we worked and succeeded together. It was a long journey, and it was not always easy. I want to thank you for everything I have learned from you. Thanks to you, I grew so much, and I will never forget this!

Last but not least, of course, is my promoter, grande capo, Prof., dr., Chris de Zeeuw. Dear Chris, you gave me an opportunity that I took on as my mission. You have been the driving force that pushed me to express my full potential. You motivated me to give to science as much as possible, and thanks to you, I was able to reach objectives that seemed impossible. I'm just thanking you with words here, but I hope I will also show my gratitude with actions too, by doing great science and bringing spectacular results to you in the coming years.

And now that I'm getting emotional, I want to give the biggest thanks to my family and Daria.

I wanted to thank my sisters that guided me in the early years of my studies. Assunta, for me, you have been the star to follow. You still are an example of success, and I will keep getting inspired by you. Thanks for showing me how things should be done to succeed in life! Thanks!

Bina, you were guiding me when I just started university studies. You gave me all the material and moral support to pass the most challenging period of all my studies. Thanks for helping me when I need it, and for insulting me (as a joke, I hope) all the rest of the time.

Most important of all, I thank my parents because giving me (and to my sisters) a good education has always been the main objective of their life. Mamma e papà you have succeeded! I'm here because of you and for you! Today you have to be proud of yourself and not of me. You gave me all the opportunities that you never had in your life, and if I get a Ph.D. in Neuroscience today, you get a Ph.D. in being the best parents!

At the very end, I want to thank my love, Daria. You were next to me during the most challenging part of this Ph.D. You gave me the right support that I needed to overcome all the difficulties. You have been my biggest joy in this difficult period. I want to thank you for this, but most of all I want to thank you in advance for the future, because you will always be the biggest joy of my life!

# TRANSLATION FOR MY PARENTS

## Ringraziamenti ai miei genitori

Al primo posto in ordine d'importanza ci sono i ringraziamenti ai miei genitori. Vi ringrazio perché per voi, dare un'ottima istruzione a me, a Bina ed ad Assunta, è stato sempre l'obiettivo principale della vostra vita. Mamma e papà ce l'avete fatta! Io sono qui grazie a voi e per voi! Oggi voi dovete essere orgogliosi di voi stessi e non di me. Voi mi avete dato tutte le opportunità che la voi non avete mai potuto avere nella vostra vita e se oggi io prendo un dottorato in neuroscience, voi prendete un dottorato come migliori genitori.